

HETEROPOLY OXOMETALATES OF 1B AND 3B CATIONS,
THEIR MORPHOLOGICAL AND CATALYTIC PROPERTIES.

by

Michelle Antoinette Parent

A thesis
presented to the University of Waterloo
in fulfilment of the
thesis requirement for the degree of
Doctor of Philosophy
in
Chemistry

Waterloo, Ontario, Canada, 1997

© Michelle Antoinette Parent 1997



National Library
of Canada

Acquisitions and
Bibliographic Services

395 Wellington Street
Ottawa ON K1A 0N4
Canada

Bibliothèque nationale
du Canada

Acquisitions et
services bibliographiques

395, rue Wellington
Ottawa ON K1A 0N4
Canada

Your file Votre référence

Our file Notre référence

The author has granted a non-exclusive licence allowing the National Library of Canada to reproduce, loan, distribute or sell copies of this thesis in microform, paper or electronic formats.

The author retains ownership of the copyright in this thesis. Neither the thesis nor substantial extracts from it may be printed or otherwise reproduced without the author's permission.

L'auteur a accordé une licence non exclusive permettant à la Bibliothèque nationale du Canada de reproduire, prêter, distribuer ou vendre des copies de cette thèse sous la forme de microfiche/film, de reproduction sur papier ou sur format électronique.

L'auteur conserve la propriété du droit d'auteur qui protège cette thèse. Ni la thèse ni des extraits substantiels de celle-ci ne doivent être imprimés ou autrement reproduits sans son autorisation.

0-612-22226-8

The University of Waterloo requires the signatures of all persons using or photocopying this thesis. Please sign below, and give address and date.

Abstract

Heteropoly Oxometalates of 1B and 3B Cations, Their Morphological and Catalytic Properties.

Heteropoly oxometalates are ionic solids with discrete cations and anions. Although a wide variety of these exist, those with the Keggin anion, $\text{XM}_{12}\text{O}_{40}^{n-}$ ($\text{X} = \text{P}, \text{Si}; \text{M} = \text{W}, \text{Mo}$), are among those which are most thermally stable. When protons serve as the cations, superacids with an overall chemical formula of $\text{H}_n\text{XM}_{12}\text{O}_{40}$ result. Heteropoly acids (HPA's) are multifunctional, being capable of acting catalytically in oxidation processes or, alternatively as acid catalysts, depending on their elemental composition.

Salts of 12-tungstophosphoric, 12-tungstosilicic and 12-molybdophosphoric acids were prepared with stoichiometric and nonstoichiometric quantities of silver(I) and thallium(I) cations. All of the salts except silver 12-molybdophosphate have high surface areas (with at least a 10-fold increase over that observed with the pure HPA) and microporous structures, as shown by analysis of nitrogen adsorption-desorption isotherms, obtained at 77 K. A microporous structure could not be obtained for silver(I) 12-molybdophosphate. Powder X-ray diffraction and infrared spectroscopy confirm that the Keggin anions retain their structure and the substituted cations reside in positions previously occupied by the protons in the heteropoly acid.

In contrast, attempts to prepare salts containing the divalent copper(II) cation proved unsuccessful in forming solids with a microporous structure. Studies of the surface and bulk properties revealed that the isolated solids were a mixture of the copper cation and the 12-heteropoly acid. Solid state ion exchange with the monovalent copper(I) cation and the 12-tungstophosphoric acid was also unsuccessful in forming a high surface area solid, although powder XRD patterns indicated that there may be favourable orientation of the anions to facilitate a microporous structure. Solid state ion exchange of the copper(I) ion and the ammonium 12-tungstophosphate salt indicated that migration of the copper(I) cation into the bulk had occurred although this resulted in a lower surface area and smaller microporous structure than present in the ammonium salt.

The Brunauer/Emmett/Teller (BET), MP, Dubinin-Radushkevich (DR) and Horvath-Kawazoe-Satio-Foley (HKSF) methods were used in the analysis of the N₂ adsorption-desorption isotherms of the stoichiometric thallium salts of 12-tungstosilicic and 12-molybdophosphoric acids. A comparative study regarding the advantages and disadvantages of each method is discussed with respect to obtaining information on the surface areas, micropore volumes and pore size distributions.

Solid-state ¹H NMR studies showed that protons remained in the stoichiometric and nonstoichiometric cesium(I), silver(I) and thallium(I) 12-heteropoly salts, although the numbers decreased as the preparative cation to proton ratio increased. As shown from NH₃ TPD studies the distribution of acid strengths shifts as the nature of the cation and stoichiometry of the salt are altered.

The cesium(I), silver(I) and thallium(I) 12-heteropoly salts of various stoichiometries were examined as heterogeneous catalysts in the acid catalyzed processes of the isomerization of 1-butene and the dehydration of primary, secondary, and tertiary butanols. In comparison to HPA's, the creation of a microporous structure in the salts increases the accessibility to the protons in the solid lattice; however there is a decrease in the number of available acid sites as the amount of cation substituted into the salt is increased. In addition, the incorporation of a nonprotonic cation causes a shift in the distribution of acidic strengths of the salt, with the disappearance of the strongest acid sites as the cation:proton ratio is increased. Further analysis of the catalytic data indicated that the acidic strength may be the result of a perturbation in the chemical environment by interaction of the nonprotonic cations with the oxygen atoms of the Keggin anions.

Acknowledgements

I wish to thank Professor J.B. Moffat for his guidance throughout this project. His expertise and eagerness to discuss the research project were greatly appreciated.

Many thanks are extended to past and present members of Professor Moffat's research group, who have provided advice and valuable information regarding experimental techniques.

The following people have provided valuable technical assistance in this research: Christopher Kirby and Dr. Sandra Mooibroek for obtaining ^1H MAS NMR spectra; Christopher Kirby for the analysis of the ^1H MAS NMR data; members of Professor Nazar's research group for their assistance in obtaining powder XRD patterns; and Dr. Jake Fisher, whose computing skills and knowledge were indispensable.

Financial support from the Province of Ontario, in the form of an Ontario Graduate Scholarship, the University of Waterloo, and the Department of Chemistry are gratefully acknowledged. Project funding was provided by the Natural Sciences and Engineering Research Council (NSERC).

Finally, and most importantly, I would like to thank Scott Parent for his unconditional love, encouragement and support of my decisions; and my family, particularly my parents, Carole and Richard Seay, and Laura and Reg Parent for their continual support throughout this period of study.

To my husband,
J. Scott Parent.

Table of Contents

| | |
|----------------------------------------------------------------------------------------------------------|-----------|
| Author's Declaration | ii |
| Borrower's Page | iii |
| Abstract | iv |
| Acknowledgements | vi |
| Dedication | vii |
| Table of Contents | viii |
| List of Tables | xi |
| List of Figures | xiv |
| | |
| CHAPTER 1 Introduction | 1 |
| 1.1 Anion Composition and Structure | 1 |
| 1.2 Properties of 12-Heteropoly Oxometalates | 7 |
| 1.3 Scope of Research | 10 |
| 1.4 References | 12 |
| | |
| CHAPTER 2 Synthesis and Characterization of Monovalent Salts | 17 |
| 2.1 Introduction | 17 |
| 2.2 Experimental | 20 |
| 2.2.1 <i>Synthesis</i> | 20 |
| 2.2.2 <i>Characterization Techniques</i> | 21 |
| 2.3 Results | 24 |
| 2.3.1 <i>Characterization of Surface and Bulk Properties of Pure Silver and Thallium Salts</i> | 24 |
| 2.3.2 <i>Reproducibility of Surface Area and Mean Micropore Radii Measurements.</i> | 33 |
| 2.3.3 <i>Effects of Reaction Parameters on the Resulting Surface and Bulk Properties.</i> | 34 |
| 2.3.4 <i>Characterization of Surface and Bulk Properties of Mixed Salts.</i> | 43 |
| 2.3.5 <i>Characterization of Surface and Bulk Properties of Cesium Salts.</i> | 46 |

| | |
|---------------------------------------------------------------------------------------------------------------|------------|
| 2.4 Discussion | 50 |
| 2.5 References | 58 |
| CHAPTER 3 Synthesis and Characterization of Copper(II) and Copper(I) Salts | 61 |
| 3.1 Introduction | 61 |
| 3.2 Experimental | 63 |
| 3.2.1 <i>Synthesis</i> | 63 |
| 3.2.2 <i>Characterization Techniques</i> | 65 |
| 3.3 Results | 65 |
| 3.3.1 <i>Characterization of Surface and Bulk Properties of Copper(II) Salts</i> . | 65 |
| 3.3.2 <i>Characterization of Surface and Bulk Properties of Copper(I) Salts</i> .. | 71 |
| 3.4 Discussion | 76 |
| 3.5 References | 80 |
| CHAPTER 4 A Comparison of Methods for the Characterization of the Microporous Structure in Solids. | 83 |
| 4.1 Introduction | 83 |
| 4.2 Experimental | 85 |
| 4.2.1 <i>Experimental</i> | 85 |
| 4.2.2 <i>Calculations</i> | 86 |
| 4.3 Results | 86 |
| 4.4 Discussion | 100 |
| 4.5 References | 103 |
| CHAPTER 5 Isomerization of 1-Butene | 106 |
| 5.1 Introduction | 106 |
| 5.2 Experimental | 109 |
| 5.2.1 <i>Materials</i> | 109 |
| 5.2.2 <i>Characterization Techniques</i> | 110 |
| 5.2.3 <i>Apparatus and Procedure</i> | 111 |

| | |
|------------------------------------------------------------------|------------|
| 5.2.4 <i>Definitions</i> | 113 |
| 5.3 Results | 113 |
| 5.3.1 <i>Distribution of Acid sites and Strengths</i> | 113 |
| 5.3.2 <i>Isomerization of 1-Butene</i> | 128 |
| 5.4 Discussion | 135 |
| 5.5 References | 146 |
| | |
| CHAPTER 6 Dehydration of Butyl Alcohols | 152 |
| 6.1 Introduction | 152 |
| 6.2 Experimental | 156 |
| 6.2.1 <i>Materials</i> | 156 |
| 6.2.2 <i>Apparatus and Procedure</i> | 156 |
| 6.2.3 <i>Definitions</i> | 158 |
| 6.3 Results | 159 |
| 6.3.1 <i>Dehydration of tert-Butanol.</i> | 159 |
| 6.3.2 <i>Dehydration of 2-Butanol.</i> | 163 |
| 6.3.3 <i>Dehydration of 1-Butanol.</i> | 174 |
| 6.4 Discussion | 183 |
| 6.5 References | 195 |
| | |
| CHAPTER 7 Conclusions | 198 |
| 7.1 Summary | 198 |
| 7.2 Future work | 202 |
| | |
| APPENDIX A Sample Calculations for the HKSF Methods | 203 |

List of Tables

| | | |
|--------------|--------------------------------------------------------------------------------------------------------------------------------|----|
| Table 2.1 - | Characteristic frequencies from infrared spectra of parent acids and salts. | 25 |
| Table 2.2 - | Characteristic frequencies for infrared spectrum of silver 12-molybdophosphate. | 25 |
| Table 2.3 - | Data from indexed powder XRD patterns for parent acids and stoichiometric salts. | 27 |
| Table 2.4 - | Summary of surface area and C_{BET} parameters for parent acids and stoichiometric salts | 30 |
| Table 2.5 - | Replicate trials in measuring the surface areas and mean micropore radii of $\text{Tl}_3\text{PW}_{12}\text{O}_{40}$ | 34 |
| Table 2.6 - | Characterization of the microporous structure of $\text{Ag}_3\text{PW}_{12}\text{O}_{40}$ | 35 |
| Table 2.7 - | Characterization of the microporous structure of $\text{Tl}_3\text{PW}_{12}\text{O}_{40}$ | 35 |
| Table 2.8 - | Yields (%) in the synthesis of the stoichiometric and nonstoichiometric salts. | 36 |
| Table 2.9 - | Surface areas (S_{BET}) of the stoichiometric and nonstoichiometric salts. | 38 |
| Table 2.10 - | Characterization of mixed stoichiometric salts of 12-tungstophosphoric acid. | 44 |
| Table 2.11 - | Characterization of the mixed stoichiometric salts of 12-tungstosilicic acid. | 45 |
| Table 2.12 - | Characterization of the stoichiometric cesium salts | 46 |
| Table 2.13 - | Characterization of cesium salts of 12-tungstophosphoric acid. | 47 |
| Table 2.14 - | Characterization of cesium salts of 12-tungstosilicic acid. | 48 |
| | | |
| Table 3.1 - | Characteristic frequencies from infrared spectra of parent acids and copper(II) salts. | 68 |
| Table 3.2 - | Summary of surface areas for parent acids and stoichiometric copper(I) salts. | 69 |
| Table 3.3 - | Data from indexed powder XRD patterns for parent acids and stoichiometric copper(II) salts. | 70 |
| Table 3.4 - | Surface areas and data from indexed powder XRD patterns for copper(I) salts of 12-tungstophosphoric acid. | 71 |
| Table 3.5 - | Surface areas and data from indexed powder XRD patterns for copper(I) salts of ammonium 12-tungstophosphate. | 74 |
| | | |
| Table 4.1 - | Calculated surface areas and C_{BET} constants for the thalious salts, TlSiW and TlPMo | 89 |
| Table 4.2 - | Calculated micropore volumes and sizes for the thalious salts, TlSiW and TlPMo | 92 |
| Table 4.3 - | Parameters used for the adsorbent and adsorbate components. | 95 |
| Table 4.4 - | Summary of effective pore diameter calculated for the thalious salts, TlSiW and TlPMo | 97 |

| | | |
|--------------|--------------------------------------------------------------------------------------------------------------------------------|-----|
| Table 5.1 - | Chemical shifts (ppm) of residual protons for the stoichiometric and nonstoichiometric salts. | 114 |
| Table 5.2 - | Composition of 12-tungstophosphate salts containing residual protons. | 116 |
| Table 5.3 - | Composition of 12-tungstosilicate and 12-molybdophosphate salts containing residual protons. | 117 |
| Table 5.4 - | Distribution of acid strengths and total acidity of 12-tungstophosphate salts. | 118 |
| Table 5.5 - | Distribution of acid strengths and total acidity for 12-tungstosilicate and 12-molybdophosphate salts. | 126 |
| Table 5.6 - | Isomerization of 1-butene at 100 °C with salts of $H_3PW_{12}O_{40}$ | 128 |
| Table 5.7 - | Isomerization of 1-butene at 200 °C with salts of $H_3PW_{12}O_{40}$ | 129 |
| Table 5.8 - | Isomerization of 1-butene at 300 °C with salts of $H_3PW_{12}O_{40}$ | 130 |
| Table 5.9 - | Isomerization of 1-butene at 100 °C with salts of $H_4SiW_{12}O_{40}$ | 131 |
| Table 5.10 - | Isomerization of 1-butene at 200 °C with salts of $H_4SiW_{12}O_{40}$ | 132 |
| Table 5.11 - | Isomerization of 1-butene at 300 °C with salts of $H_4SiW_{12}O_{40}$ | 133 |
| Table 5.12 - | Isomerization of 1-butene at 100 °C with $H_3PMo_{12}O_{40}$ and $Tl_3PMo_{12}O_{40}$ | 134 |
| Table 5.13 - | Isomerization of 1-butene at 200 °C with $H_3PMo_{12}O_{40}$ and $Tl_3PMo_{12}O_{40}$ | 134 |
| Table 5.14 - | Isomerization of 1-butene at 300 °C with $H_3PMo_{12}O_{40}$ and $Tl_3PMo_{12}O_{40}$ | 135 |
| Table 5.15 - | Conversion of 1-butene at 10 minutes with salts of $H_3PW_{12}O_{40}$ and $Tl_3PMo_{12}O_{40}$ | 144 |
| Table 5.16 - | Conversion of 1-butene at 10 minutes with salts of $H_4SiW_{12}O_{40}$ | 145 |
| | | |
| Table 6.1 - | Distribution of products in dehydration of 2-butanol with salts of 12-tungstophosphoric acid for initial measurements. | 166 |
| Table 6.2 - | Distribution of products in dehydration of 2-butanol with salts of 12-tungstophosphoric acid at higher time-on-stream. | 167 |
| Table 6.3 - | Distribution of products in dehydration of 2-butanol with salts of 12-tungstosilicic acid for initial measurements. | 170 |
| Table 6.4 - | Distribution of products in dehydration of 2-butanol with salts of 12-tungstosilicic acid at higher time-on-stream. | 171 |
| Table 6.5 - | Distribution of products in dehydration of 2-butanol with salts of 12-molybdophosphoric acid for initial measurements. | 173 |
| Table 6.6 - | Distribution of products in dehydration of 2-butanol with salts of 12-molybdophosphoric acid at higher time-on-stream. | 173 |
| Table 6.7 - | Distribution of products in dehydration of 1-butanol with salts of 12-tungstophosphoric acid for initial measurements. | 176 |
| Table 6.8 - | Distribution of products in dehydration of 1-butanol with salts of 12-tungstophosphoric acid at higher time-on-stream. | 177 |

| | | |
|--------------|--------------------------------------------------------------------------------------------------------------------------------|-----|
| Table 6.9 - | Distribution of products in dehydration of 1-butanol with salts of 12-tungstosilicic acid for initial measurements. | 180 |
| Table 6.10 - | Distribution of products in dehydration of 1-butanol with salts of 12-tungstosilicic acid at higher time-on-stream. | 181 |
| Table 6.11 - | Distribution of products in dehydration of 1-butanol with salts of 12-molybdophosphoric acid for initial measurements. | 183 |
| Table 6.12 - | Distribution of products in dehydration of 1-butanol with salts of 12-molybdophosphoric acid at higher time-on-stream. | 183 |
| Table 6.13 - | Conversions of the 1-, 2- and <i>tert</i> -butanols with salts of $H_3PW_{12}O_{40}$ | 191 |
| Table 6.14 - | Conversions of the 1-, 2- and <i>tert</i> -butanols with salts of $H_4SiW_{12}O_{40}$ and $Tl_3PMo_{12}O_{40}$ salts. | 192 |

List of Figures

| | |
|---------------------------------------------------------------------------------------------------------------------------------------------------------------------------------------------------|----|
| Figure 1.1 - Structural representation of the Keggin anion, $(XM_{12}O_{40})^{n-}$ | 3 |
| Figure 1.2 - Octahedral representation of the (a) trimetalate unit M_3O_{13} and central tetrahedron XO_4 and (b) Keggin anion. | 4 |
| Figure 1.3 - Representation of $H_3PW_{12}O_{40} \cdot 6H_2O$ | 5 |
| Figure 2.1 - Volumetric nitrogen adsorption system. | 23 |
| Figure 2.2 - Infrared spectra of silver and thallium 12-tungstophosphate. | 26 |
| Figure 2.3 - N_2 adsorption-desorption isotherms for $Ag_3PW_{12}O_{40}$ and $Tl_3PW_{12}O_{40}$ | 29 |
| Figure 2.4 - Pore size distribution for thallium 12-tungstophosphate for various preparative stoichiometries. | 32 |
| Figure 2.5 - Surfaces areas (S_{BET}) of the (a) silver and (b) thallium salts for various preparative stoichiometries. | 37 |
| Figure 2.6 - 1H MAS NMR spectrum of $Tl_3PW_{12}O_{40}$ for various preparative stoichiometries. | 40 |
| Figure 2.7 - 1H MAS NMR spectra of $Ag_4SiW_{12}O_{40}$ and $Tl_4SiW_{12}O_{40}$ for various preparative stoichiometries. | 41 |
| Figure 2.8 - 1H MAS NMR spectra of $Ag_3PW_{12}O_{40}$ and $Tl_3PMo_{12}O_{40}$ for various preparative stoichiometries. | 42 |
| Figure 2.9 - 1H MAS NMR spectra of $Cs_3PW_{12}O_{40}$ and $Cs_4SiW_{12}O_{40}$ for various preparative stoichiometries. | 49 |
| Figure 2.10 - Micropore volumes and XRD $I[110]/I[222]$ ratios for stoichiometric silver and thallium salts of HPW together with values reported earlier for other cations. | 51 |
| Figure 2.11 - Surface areas and cation diameters for the silver and thallium salts of the three heteropoly acids. | 53 |
| Figure 2.12 - Mean micropore radii versus number of layers (n) from the finite layer BET equation for silver and thallium salts of the three acids with comparison to earlier values. | 54 |
| Figure 3.1 - Infrared spectra of copper(II) 12-tungstophosphate. | 67 |
| Figure 3.2 - Powder XRD patterns of copper(I) 12-tungstophosphate salts. | 72 |
| Figure 3.3 - Powder XRD patterns of ammonium and copper(I) 12-tungstophosphate salts. | 75 |
| Figure 4.1 - N_2 adsorption-desorption isotherms for $Tl_4SiW_{12}O_{40}$ and $Tl_3PMo_{12}O_{40}$ | 87 |
| Figure 4.2 - Pore size distribution of $Tl_4SiW_{12}O_{40}$ and $Tl_3PMo_{12}O_{40}$ by the MP method. | 91 |
| Figure 4.3 - Dubinin-Radushkevich plots for $Tl_4SiW_{12}O_{40}$ and $Tl_3PMo_{12}O_{40}$ | 93 |
| Figure 4.4 - Pore size distribution of $Tl_4SiW_{12}O_{40}$ by HKSF methods. | 98 |
| Figure 4.5 - Pore size distribution of $Tl_3PMo_{12}O_{40}$ by HKSF methods. | 99 |

| | |
|---------------------------------------------------------------------------------------------------------------------------|-----|
| Figure 5.1 - Mechanistic scheme for the isomerization of 1-butene. | 107 |
| Figure 5.2 - Catalytic reactor system.. . . . | 112 |
| Figure 5.3 - TPD of ammonia with $\text{Ag}_3\text{PW}_{12}\text{O}_{40}$ | 119 |
| Figure 5.4 - TPD of ammonia with $\text{Tl}_3\text{PW}_{12}\text{O}_{40}$ | 120 |
| Figure 5.5 - TPD of ammonia with $\text{Cs}_3\text{PW}_{12}\text{O}_{40}$ | 121 |
| Figure 5.6 - TPD of ammonia with $\text{Ag}_4\text{SiW}_{12}\text{O}_{40}$ | 123 |
| Figure 5.7 - TPD of ammonia with $\text{Tl}_4\text{SiW}_{12}\text{O}_{40}$ | 124 |
| Figure 5.8 - TPD of ammonia with $\text{Cs}_4\text{SiW}_{12}\text{O}_{40}$ | 125 |
| Figure 5.9 - TPD of ammonia with $\text{Tl}_3\text{PMo}_{12}\text{O}_{40}$ | 127 |
| | |
| Figure 6.1 - Catalytic reactor system. | 157 |
| Figure 6.2 - Conversion of <i>tert</i> -butanol at 46 °C with salts of $\text{H}_3\text{PW}_{12}\text{O}_{40}$ | 160 |
| Figure 6.3 - Conversion of <i>tert</i> -butanol at 46 °C with salts of $\text{H}_4\text{SiW}_{12}\text{O}_{40}$ | 161 |
| Figure 6.4 - Conversion of <i>tert</i> -butanol at 46 °C with $\text{Tl}_3\text{PMo}_{12}\text{O}_{40}$ salts. | 162 |
| Figure 6.5 - Conversion of 2-butanol at 108 °C with salts of $\text{H}_3\text{PW}_{12}\text{O}_{40}$ | 165 |
| Figure 6.6 - Conversion of 2-butanol at 108 °C with salts of $\text{H}_4\text{SiW}_{12}\text{O}_{40}$ | 168 |
| Figure 6.7 - Conversion of 2-butanol at 108 °C with $\text{Tl}_3\text{PMo}_{12}\text{O}_{40}$ salts. | 172 |
| Figure 6.8 - Conversion of 1-butanol at 108 °C with salts of $\text{H}_3\text{PW}_{12}\text{O}_{40}$ | 175 |
| Figure 6.9 - Conversion of 1-butanol at 108 °C with salts of $\text{H}_4\text{SiW}_{12}\text{O}_{40}$ | 179 |
| Figure 6.10 - Conversion of 1-butanol at 108 °C with $\text{Tl}_3\text{PMo}_{12}\text{O}_{40}$ salts. | 182 |
| Figure 6.11 - Mechanistic scheme for the dehydration of 1-butanol. | 187 |

CHAPTER 1

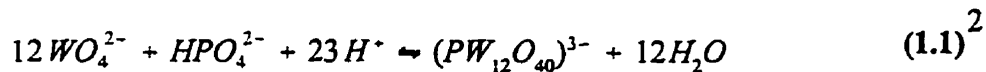
Introduction

Heteropoly oxometalates, commonly referred to as metal-oxygen cluster compounds (MOCC), are oxide cluster ions, often of a high molecular weight. While isopolyanions, $[M_mO_y]^{p-}$, consist of only oxygen and a second element, the heteropoly ions, $[X_xM_mO_y]^{q-}$ ($x \leq m$), contain a minimum of two different elements in addition to oxygen. They have been known for more than 150 years.¹ These inorganic anions form a unique family of materials in which the structural form and integrity of the anion is maintained when selective substitution of atoms occurs.¹ Modifications in the elemental composition of these compounds have made them suitable for many applications. A number of reviews have been published in the literature summarizing the synthesis, characterization, and applications of the various heteropoly oxometalates.¹⁻¹²

1.1 Anion Composition and Structure

While the stoichiometry of heteropoly oxometalates, $[X_xM_mO_y]^{q-}$ ($x \leq m$), suggests that a wide variety of compounds may be synthesized from various elements in the periodic table, Pope has noted that for a metal element to occupy the peripheral position in the heteropoly anion, denoted as M, specific ionic radii and charges and the capability of forming $d\pi-p\pi$ metal-oxygen bonds (M-O) are required.¹ Due to these restrictions, molybdenum or tungsten are usually considered suitable elements to occupy the peripheral metal positions, although in some cases vanadium, niobium or tantalum have been used.¹ Requirements for the central atom X appear to be less stringent than those of the peripheral metal atom, and as many as 65 elements in the periodic table have been incorporated.¹

Heteropoly anions are generally formed by the condensation of two or more different oxoanions containing the desired elements in an acidic aqueous solution. Equation 1.1 illustrates the apparent simplicity of the method in forming the 12-tungstophosphate anion. While many structures of the heteropoly oxometalates are still possible with the restrictions of the peripheral metals (M), the nature of the species



isolated is also dependent upon the proportional quantities of the oxides used in the synthesis, determining the (x/m) ratio, and the pH of the solution. In comparison with other heteropoly anions, the 12-heteropoly oxometalates, also referred to as Keggin anions, $[\text{X}^{n+}\text{M}_{12}^{\text{m}+}\text{O}_{40}]^{[80-n-12m]-}$, are easily obtained and are among the most stable.¹² This has resulted in these anions' being the most extensively studied. The resulting charge on the Keggin anion, $(\text{XM}_{12}\text{O}_{40})^n$, is dictated by the oxidation states of the central and peripheral metals. A solid acid is formed when hydrogen atoms are added to the Keggin anion, forming a neutral species, $\text{H}_n\text{XM}_{12}\text{O}_{40}$. General properties of the Keggin anion, such as the structure, electronic states and reactivities are found in the literature.^{1,6}

The first published record of a 12-heteropoly oxometalate synthesis was in 1826 by the Swedish chemist Jöns Jakob Berzelius.¹³ The compound was what is now known as ammonium 12-molybdophosphate $((\text{NH}_4)_3\text{PMo}_{12}\text{O}_{40})$. However, it was not until 1933, that J.D.F. Keggin, an x-ray crystallographer, was able to determine the structure of the 12-heteropoly anion in 12-tungstophosphoric acid, $\text{H}_3\text{PW}_{12}\text{O}_{40} \cdot 5\text{H}_2\text{O}$.¹⁴ This finding confirmed the structure originally proposed by Pauling.¹⁵ The class of 12-heteropoly anions was subsequently named Keggin ion systems.

The approximately spherical structure of the Keggin anion, as depicted in Figure 1.1, can be described as a central atom (X), typically phosphorus or silicon, bonded to four oxygen atoms arranged tetrahedrally. Each of the twelve peripheral metal atoms (M) forms a slightly distorted octahedron with the peripheral metal located at the approximate centre and six oxygen atoms at its vertices.¹⁶⁻¹⁸ The twelve octahedra are arranged in four groups of three edge-shared octahedra, M_3O_{13} , which are linked by shared corners to each other and to the central XO_4 tetrahedron. (Figure 1.2) Despite the arrangement of the peripheral metal atoms in the Keggin anion, they are considered to be equivalent to one another. ¹⁸³W and ⁹⁵Mo NMR spectra of these anions contain only a single resonance for the peripheral metal atoms, indicating that the twelve metal atoms reside in identical chemical environments, and independent of the nature of the central atom (phosphorus, silicon or boron).^{19,20} The only exception to this is the appearance of a narrow doublet in the ¹⁸³W NMR spectra of $\text{PW}_{12}\text{O}_{40}^{3-}$, resulting from the two bond coupling of the ¹⁸³W and

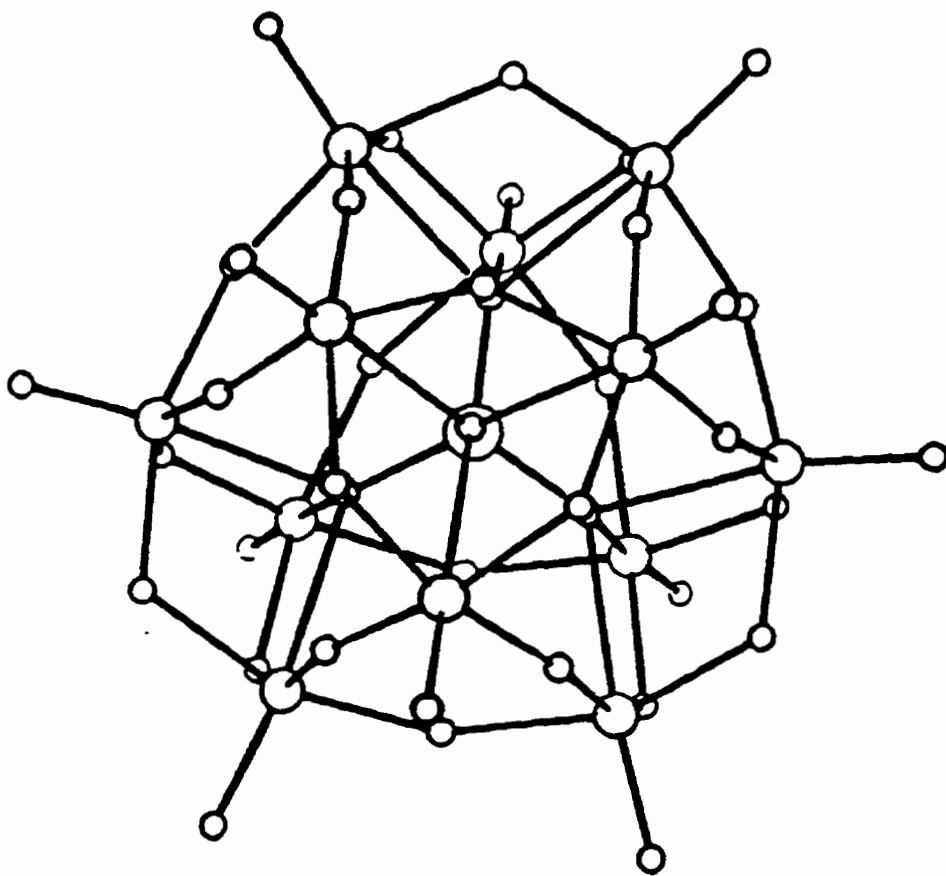


Figure 1.1 - Structural representation of the Keggin anion, $(XM_{12}O_{40})^{n-}$.

^{31}P nuclei.¹⁹ Due to the arrangement of the twelve octahedra and the central tetrahedron, three types of oxygen atoms exist in the Keggin anion: those which bridge two peripheral metal atoms, interconnecting the octahedra; those which bridge the peripheral metal atom with the central atom; and the oxygen atoms which project radially from each of the octahedra, often referred to as the terminal oxygen atoms.

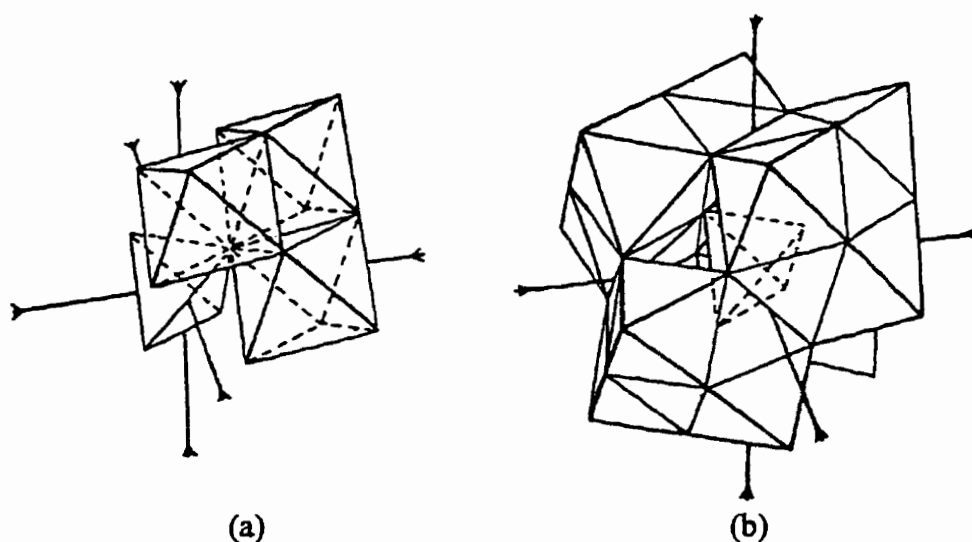


Figure 1.2 - Octahedral representations of the (a) trimetalate unit M_3O_{13} and central tetrahedron XO_4 and (b) Keggin anion.¹⁴

In spite of its cagelike appearance (Figure 1.1) the atoms in the Keggin anion are in close proximity to one another, due to the bridging oxygen atoms. This arrangement of atoms prevents the migration of small gaseous species into the anion structure. The 12-heteropoly oxometalates are ionic solids consisting of discrete anions and cations, forming a solid lattice. The data from a combination of x-ray and neutron diffraction techniques allowed Brown *et al.*¹⁷ to provide a detailed picture of the lattice structure for the hexahydrate of 12-tungstophosphoric acid, $\text{H}_3\text{PW}_{12}\text{O}_{40}\cdot 6\text{H}_2\text{O}$. (Figure 1.3) Hydrated protons, $(\text{H}_3\text{O})_2^+$, link four Keggin anions through hydrogen bonds with the terminal oxygen atoms of the anion, creating interstitial voids within the lattice framework. In Figure 1.3 a two-fold thermal disorder exists for the water molecules hydrogen bonded to the proton in a quasi-planar arrangement. For 12-tungstophosphoric acid hexahydrate the protons and anions are arranged in a cubic $\text{Pn}3\text{m}$ structure.¹⁷ The degree of hydration

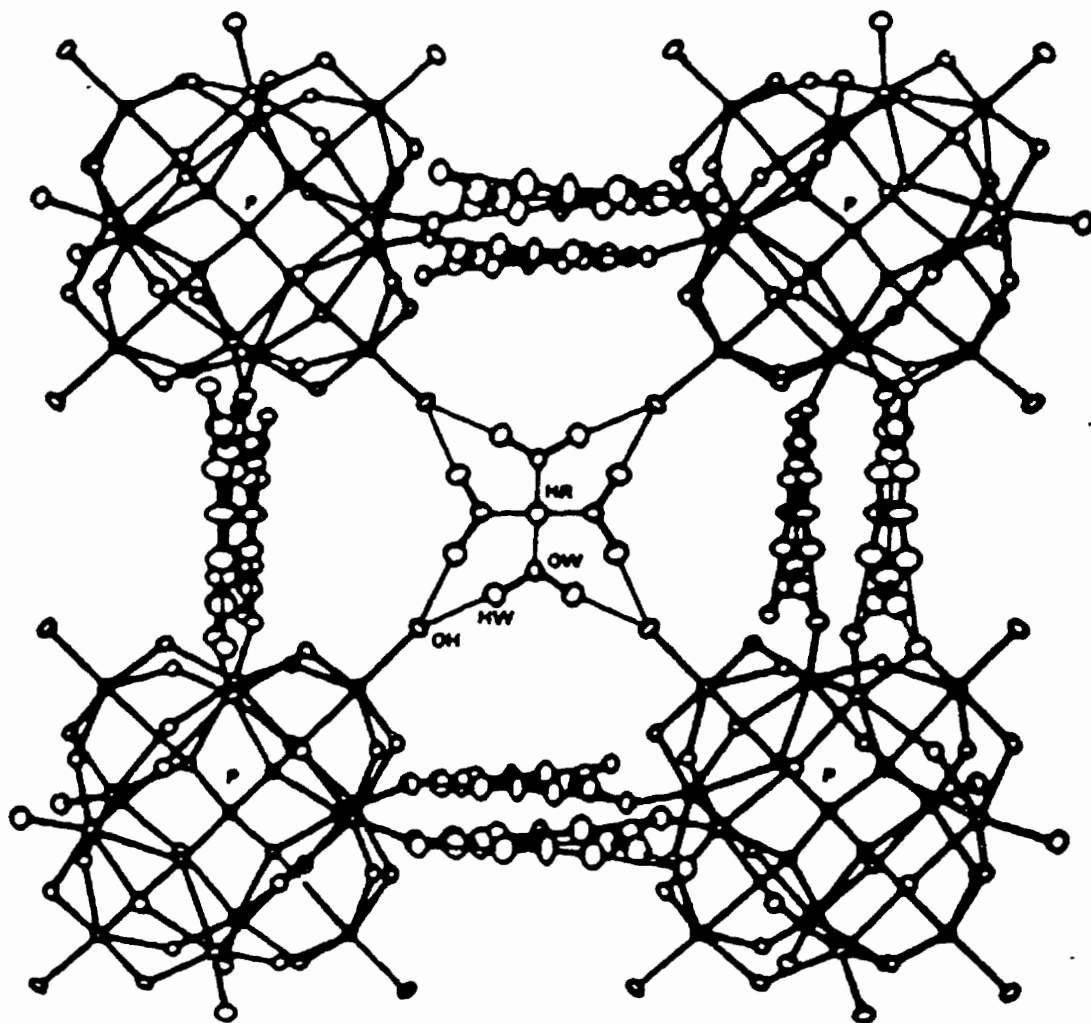


Figure 1.3 - Representation of $\text{H}_3\text{PW}_{12}\text{O}_{40} \cdot 6\text{H}_2\text{O}$.¹⁷

does alter the space group assigned to the crystal structure, as determined for the structures of $\text{H}_3\text{PW}_{12}\text{O}_{40}\cdot 21\text{H}_2\text{O}$ ²¹ and $\text{H}_3\text{PW}_{12}\text{O}_{40}\cdot 29\text{H}_2\text{O}$,²² although the general cubic arrangement is maintained. Brown *et al.* also noted that the original structure determined by Keggin¹⁴ was actually the hexahydrate form of the acid rather than the pentahydrate as stated.¹⁷

With respect to the molybdenum derivative of the 12-heteropoly oxometalate, $\text{H}_3\text{PMo}_{12}\text{O}_{40}$, a similar arrangement for the protons and anions was determined. Strandberg had originally classified the $\text{H}_3\text{PMo}_{12}\text{O}_{40}\cdot 29\text{-}31\text{H}_2\text{O}$ as having T_d symmetry, and assigned the space group of $I4_1/amd$.²³ However, in the analysis of the same data, Allmann concluded that this acid actually belonged to the $Fd3m$ space group.²⁴ This was also concluded by Clark and Hall.¹⁶ The removal of hydrating water molecules changes the space group classification from cubic to triclinic for $\text{H}_3\text{PMo}_{12}\text{O}_{40}\cdot 13\text{-}14\text{H}_2\text{O}$.²⁵

Preliminary solid state ^1H and ^{31}P NMR studies carried out by Misono and coworkers indicated that the protons may be migrating to the bridging oxygen atoms (W-O-W) when $\text{H}_3\text{PW}_{12}\text{O}_{40}\cdot n\text{H}_2\text{O}$ was dehydrated from $n=17$ to $n=0.5$.²⁶ However, powder x-ray diffraction patterns did not change as the number of hydrating water molecules was decreased from $n=6$ to $n=0.5$, indicating that the secondary structure of $\text{H}_3\text{PW}_{12}\text{O}_{40}\cdot 0.5\text{H}_2\text{O}$ may be identical to that of $\text{H}_3\text{PW}_{12}\text{O}_{40}\cdot 6\text{H}_2\text{O}$, as proposed by Brown *et al.*¹⁷ On the basis of FTIR band broadening Misono *et al.* concluded that the protonation of the bridging oxygen atoms occurred in the dehydrated acid.²⁷ Kozhevnikov *et al.* believed that these IR studies failed to establish unambiguously the protonation sites in the 12-tungstophosphoric acid.^{28(b)} The application of ^{17}O MAS NMR by this latter group to the dehydrated acids of 12-tungstophosphoric and 12-tungstosilicic acid ($\text{H}_4\text{SiW}_{12}\text{O}_{40}$) confirmed that the protons remain predominately localized on the terminal oxygen atoms.²⁸ All of the terminal oxygen atoms appear equivalent in the NMR spectrum, suggesting that the protons migrate between the four terminal oxygen atoms, linking the Keggin anions similar to the role of the hydrated protons, $(\text{H}_5\text{O})_2^+$, in $\text{H}_3\text{PW}_{12}\text{O}_{40}\cdot 6\text{H}_2\text{O}$ as proposed by Brown *et al.*¹⁷ This accounts for the cubic arrangement of the anions being maintained during the dehydration of the acid.

Heteropoly oxometalate salts containing monovalent cations, other than protons, were first characterized by Santos, who concluded that the cations occupied the positions previously occupied by the protons, maintaining the symmetry of the $Pn3m$ space group.²⁹ Direct evidence was provided by Boeyens *et al.*³⁰ who performed single crystal studies on the potassium and ammonium salts of 12-molybdophosphoric acid. This was reiterated by Brown *et al.* with the examination of the cesium salt of 12-tungstophosphoric acid, $Cs_3PW_{12}O_{40}$.¹⁷ Several of the crystallographic space groups have been determined for various heteropoly oxometalate salts by single crystal studies and are tabulated in the literature.^{31,32} The properties of the 12-heteropoly oxometalates are significantly influenced by the nature of the cation. The following section will discuss some aspects of these while more specific details will be explored in later chapters.

1.2 Properties of 12-Heteropoly Oxometalates

Catalysis by heteropoly oxometalates is a field of growing importance, attracting increasing attention worldwide. This is in part due to the catalytic functionality's being modified by varying the elemental composition of the anion while its structural integrity is maintained.^{8(a),(c)} The properties playing the largest role in the 12-heteropoly oxometalates include electrochemical and acid-base properties, redox properties, and well defined primary (the Keggin anion) and secondary (the lattice) structures in the solid state. Recent reviews in the literature^{8,10-12} tabulate many of the reactions for which 12-heteropoly oxometalates have been used as homogeneous and heterogeneous catalysts. The catalytic activity is affected by the choice of central and peripheral atoms, the ratio in mixed peripheral atoms and the choice of accompanying cation. In the solid state, the acid strength, redox properties, and physical properties are also strongly dependent on the counteranion.

12-Heteropoly acids are considered to be superacids, possessing predominantly Brønsted acidity and are stronger than the conventional solid acids such as $SiO_2-Al_2O_3$, H_3PO_4/SiO_2 and HX and HY zeolites, indicated by Hammett indicators when titrated with *n*-butylamine.^{33,34} A superacid is an acid that exhibits acid strength greater than 100% H_2SO_4 .³⁵ Recent microcalorimetric measurements of the differential heat of adsorption of

ammonia have provided the first direct evidence of the superacid properties in heteropoly acids.³⁶ Semiempirical quantum mechanical (Extended Hückel) calculations have predicted that the solid heteropoly acids with anions containing tungsten should have higher acid strengths than those with molybdenum, while the latter materials are expected to have more labile oxygen atoms than the former.³⁷ Experimental work has provided support for these predictions with the $\text{H}_3\text{PW}_{12}\text{O}_{40}$ acid active in the conversion of methanol to hydrocarbons³⁸ while the partial oxidation of methane to methanol was more effective with the molybdenum analogue.³⁹ Recent microcalorimetric experiments of the differential heat of adsorption of ammonia have confirmed the sequence of acidic strengths for the heteropoly acids: $\text{H}_3\text{PW}_{12}\text{O}_{40} > \text{H}_4\text{SiW}_{12}\text{O}_{40} \gg \text{H}_3\text{PMo}_{12}\text{O}_{40} > \text{H}_4\text{SiMo}_{12}\text{O}_{40}$.³⁶ This is in agreement with conclusions made by other research groups, in which the relative catalytic activities of the heteropoly acids are consistent with this ordering, in both homogeneous and heterogeneous systems.^{12,40} Other heterogeneous reactions which are catalyzed more effectively by tungsten-containing Keggin anions include alcohol dehydration and hydrocarbon reactions such as isomerizations, alkylations, and cracking processes. In addition to the acid properties, the Keggin anions can undergo reversible reduction reactions without loss of structural integrity, which is common for heteropoly oxometalates possessing one terminal oxygen atom per MO_6 unit.¹ The electrons add to the largely nonbonding orbital of the metal with small changes in bond lengths.

The thermal stability of the 12-heteropoly oxometalates in the solid state is dependent both on the composition of the anion and the nature of the accompanying cation.⁴¹⁻⁴³ Although the nature of the central atom is critical for the stabilization of the primary structure,¹¹ the tungsten based anions are more stable than those containing molybdenum and anions consisting of only one peripheral metal element are generally more stable than those containing two types of peripheral metals.⁴³ Differential thermal analysis (DTA) of 12-heteropoly acids by West and Audrieth indicated that the decomposition of $\text{H}_3\text{PW}_{12}\text{O}_{40}$, $\text{H}_4\text{SiW}_{12}\text{O}_{40}$, $\text{H}_3\text{PMo}_{12}\text{O}_{40}$, and $\text{H}_4\text{SiMo}_{12}\text{O}_{40}$ occurred at 573 °C, 487 °C, 397 °C, and 340 °C, respectively, producing mainly oxides of W(VI) and Mo(VI).⁴⁴ Salts are generally more stable than the parent acids.⁴³

Although interstitial voids are created by the terminal oxygen atoms linking the hydrated protons, since these are not interconnected the resulting solid acids have low surface areas. The surface areas, determined by BET (N_2), of 12-tungstophosphoric, 12-tungstosilicic, and 12-molybdophosphoric acids are 8, 4, and 4 m^2/g , respectively.⁴⁵ Despite these values, photoacoustic FTIR studies have demonstrated that polar molecules such as ammonia, pyridine, and methanol are capable of penetrating from the vapour phase into the bulk structure, that is between the cation and anions, where interaction with the protons may occur.⁴⁶ The protons are considered to possess some degree of mobility in the solid structure. Temperature programmed hydrogen-deuterium exchange (TPE) revealed that all of the original protons in 12-tungstophosphoric and 12-tungstosilicic acids can be exchanged, producing HD(g) as the principal product.⁴⁷ Although no exchange was observed for 12-molybdophosphoric acid, consumption of deuterium and reduction of the acid was noted.⁴⁷

As mentioned in Section 1.1, with the substitution of various monovalent cations for protons in 12-heteropoly oxometalates, the crystallographic structure is generally maintained. However, it was first noticed with the ammonium salt of 12-molybdophosphoric acid, $(NH_4)_3PMo_{12}O_{40}$, that the BET (N_2) surface area was calculated to be greater than 140 m^2/g , 35 times the value recorded for the parent acid, $H_3PMo_{12}O_{40}$.⁴⁸ The ammonium 12-tungstophosphate salt produced a higher conversion of methanol than the parent acid, and this increase could not be solely accounted for by the increased surface area of the ammonium salt.^{41(b)} A difference in the distribution of products was also noted with the ammonium salt producing mainly paraffins rather than olefins as observed with the parent acid.^{38,41(b)} Further research in this laboratory has shown, in part from the analysis of nitrogen adsorption-desorption isotherms, that certain salts of the 12-heteropoly oxometalates prepared with monovalent cations have relatively high surface areas and porous structures.^{45,49-63} This is a result of accommodating the larger cations in the lattice by the rotation and translation of the Keggin anions, removing the barriers between the interstitial voids and creating channels throughout the structure. A comprehensive review of this work has also been published.⁶⁴ It was determined that the pore structure is dependent on both the nature of the cations and the elemental

compositions of the anions.^{45,49(b),50,53} The preparative stoichiometry and temperature as well as the pretreatment temperature have been shown to influence the morphology of these solids.^{59,60}

The synthesis of porous solids is of continuing interest in catalysis⁶⁵ and it is generally accepted that the presence of microporous channels is one of the most significant factors influencing the reactions in zeolites.⁶⁶ The small pore catalysts of the zeolite family, particularly ZSM-5, are important in shape-selectivity processes,⁶⁷ with increasing emphasis placed on large pore materials.⁶⁸ The benefits from creating a micropore structure for a heterogeneous catalyst include increasing the contact area of the catalyst, providing shape-selectivity, and trapping unwanted materials from the feed stream. Corma concluded that considering textural results of 12-heteropoly oxometalates^{45,58(b)} one should not expect to control the pore size to the same extent as with zeolites.¹² His reasoning was based on the fact that the pore size distributions of the heteropoly salts are relatively broad so that the fraction of the surface area with the potential shape selective effects will be considerably smaller than expected in a solid with pores of similar and uniform section. However, more recent work by Bonardet *et al.*⁶³ has confirmed that for the ammonium, potassium and cesium salts of 12-tungstophosphoric acid the presence of a microporous structure was found to be homogenous and well organized by ¹²⁹Xe NMR methods.

1.3 Scope of Research

The objective of this research is to establish the existence of a micropore structure in salts of 12-heteropoly oxometalate containing representative cations of the 1B and 3B groups of the periodic table. Factors such as the nature of the cation and anion, the preparative stoichiometry and the resulting morphology of the salts will be investigated with respect to the catalytic properties of the salt, in order to provide further insight into the perturbations of acidic strength when nonprotonic cations are introduced into the solid.

In Chapter Two the characterization of the silver(I) and thallium(I) salts of the three heteropoly acids: 12-tungstophosphoric, 12-tungstosilicic and 12-molybdophosphoric

acids is discussed. A variety of techniques were employed to establish and characterize the existence of a microporous structure, with the observations compared to the analogous cesium-containing salts. This will help to determine if the trends apparent with the some of the salts containing alkali metals with respect to the nature and size of the cation and the anion composition are maintained for the transition metal salts. The preparative techniques used in the synthesis of the salt are examined as a third factor.

The work reported in Chapter Three had as its objective the preparation of a high surface area, microporous solid from the monovalent cation of an element capable of existing in two or more oxidation states and subsequently to determine the morphological effect of conversion of that cation to a higher oxidation state.

In Chapters 2 and 3 a variety of techniques are described which characterize the pore structure in the 12-heteropoly oxometalate salts synthesized. In Chapter Four, four methods of analysis, specifically Brunauer/Emmett/Teller (BET), MP, Dubinin-Radushkevich (DR), and Horvath-Kawazoe-Satio-Foley (HKSF), are described for the N_2 adsorption-desorption isotherms of the stoichiometric salts of $Tl_4SiW_{12}O_{40}$ and $Tl_3PMo_{12}O_{40}$ in order to compare and contrast the aforementioned methods and the results obtained therefrom.

In Chapter Five the number and nature of acid sites available in each 12-heteropoly salt are characterized by data from 1H MAS NMR and ammonia temperature programmed desorption. Chapters Five and Six provide a discussion of the results for the catalytic behaviour of the synthesized salts in terms of pore structure and cation composition. Isomerization of 1-butene with the stoichiometric and nonstoichiometric silver(I) and thallium(I) salts is discussed in Chapter Five.

The catalytic properties of the stoichiometric and nonstoichiometric salts containing the monovalent cations of cesium, silver, and thallium in the dehydration of a series of butyl alcohols: *tert*-butanol, 2-butanol, and 1-butanol are discussed in Chapter Six. From these catalytic experiments, it is hoped to gain an understanding of the dependence of the catalytic properties on the nature of the cation, stoichiometry of the salts, and the micropore structure.

1.4 References

1. (a) M.T. Pope. "Heteropoly and Isopoly Oxometalates." Springer-Verlag: Berlin, 1983.
(b) M.T. Pope; A. Müller. *Angew. Chem. Int. Ed. Engl.*, **30**, 34 (1991).
2. P. Souchay. "Polyanions and Polycations." Gaultier-Villars: Paris, 1963.
3. P. Souchay. *Pure Appl. Chem.*, **6**, 61 (1963).
4. D.L. Kepert. "The Early Transition Metals." Academic Press: New York, 1972, pp. 46-60, 288-304.
5. T.J.R. Weakley. *Structure and Bonding*, **18**, 131 (1974).
6. G. Tsigdinos. *Ind. Eng. Chem., Prod. Res. Devel.*, **13**, 267 (1974).
7. V.W. Day and W.G. Klemperer. *Science*, **228**, 533 (1985).
8. (a) M. Misono. *Catal. Rev.-Sci. Eng.*, **29**, 269 (1987).
(b) M. Misono. *Catal. Rev.-Sci. Eng.*, **30**, 339 (1988).
(c) K. Tanabe, M. Misono, Y. Ono. *Stud. Surf. Sci. Catal.*, **51**, 163 (1989).
9. Y. Ono in "Perspectives in Catalysis." (J.M. Thomas; K.I. Zamaraev, Eds.) Blackwell Scientific Publications: Oxford, 1992, p. 431.
10. R.J.J. Jansen; H.M. van Veldhuizen; M.A. Schwegler; H. van Bekkum. *Recl. Trav. Chem. Pays-Bas.*, **113**, 115 (1994).
11. A. Corma. *Chem. Rev.*, **95**, 559 (1995).
12. I.V. Kozhevnikov. *Catal. Rev.-Sci. Eng.*, **37**, 311 (1995).
13. J.J. Berzelius. *Pogg. Ann. Phys. Chem.*, **6** 369, 380 (1826).
14. J.F. Keggin. *Proc. Roy. Soc.*, **A144**, 75 (1934).
15. L.C. Pauling. *J. Am. Chem. Soc.*, **51**, 2868 (1929).
16. C.J. Clark and D. Hall. *Acta Cryst.*, **B32**, 1545 (1976).
17. G.M. Brown; M.-R. Noe-Spirlet; W.R. Busing; H.A. Levy. *Acta Cryst.*, **B33**, 1038 (1977).

18. R. Strandberg. *Acta Cryst.*, **B33**, 3090 (1977).
19. R. Acerete; C.F. Hammer; L.C.W. Baker. *J. Am. Chem. Soc.*, **101**, 267 (1979).
20. (a) M. Minelli; J.H. Enemark; R.T.C. Brownlee; M.J. O'Connor; A.G. Wedd. *Coord. Chem. Rev.*, **68**, 169 (1985).
(b) S.F. Gheller; M. Sidney; A.F. Masters; R.T.C. Brownlee; M.J. O'Connor; A.G. Wedd. *Aust. J. Chem.*, **37**, 1825 (1984).
(c) W.-C. Cheng; N.P. Luthra. *J. Catal.*, **109**, 163 (1988).
21. M.R. Noe-Spirlet and W.R. Busing. *Acta Cryst.*, **B34**, 907 (1978).
22. M.R. Noe-Spirlet; G.M. Brown; W.R. Busing; H.A. Levy. *Acta Cryst.*, **B31**, S80 (1975).
23. R. Strandberg. *Acta Chem. Scand.*, **A29**, 359 (1975).
24. R. Allmann. *Acta Chem. Scand.*, **A30**, 152 (1976).
25. R. Allmann. *Z. Kristallog.*, **143**, 1 (1976).
26. Y. Kanda; K.Y. Lee; S. Nakata; S. Asaoka; M. Misono. *Chem. Lett.*, 139 (1988).
27. K.Y. Lee; N. Mizuno; T. Okuhara; M. Misono. *Bull. Chem. Soc. Jpn.*, **62** 1731 (1989).
28. (a) I.V. Kozhevnikov; A. Sinnema; R.J.J. Jansen; H. van Bekkum. *Catal. Lett.*, **27**, 187 (1994).
(b) I.V. Kozhevnikov; A. Sinnema; H. van Bekkum. *Catal. Lett.*, **34**, 213 (1995).
29. J.A. Santos. *Proc. Roy. Soc.*, **A 150**, 309 (1935).
30. J.C.A. Boeyens; G.J McDougall; J. Van R. Smit. *J. Solid State Chem.* **18**, 91 (1976).
31. R.G.W. Wyckoff. "Crystal Structures." Interscience: New York, 1960, Vol. 3, p.887.
32. H.T. Evans in "Perspectives in Structural Chemistry." (J.D. Dunitz and J.A. Ibers, Eds) Wiley: New York, 1971, Vol.4, p.12.
33. M. Misono; N. Mizuno; K. Katamura; A. Kasai; Y. Konishi; K.Sakata; T. Okuhara; Y. Yoneda. *Bull. Chem. Soc. Jpn.*, **55**, 400 (1982).

34. M. Furuta; K. Sakata; M. Misono; Y. Yoneda. *Chem. Lett.*, 31 (1979).
35. (a) R.J. Gillespie. *J. Acc. Chem. Res.*, 1, 202 (1968).
(b) R.J. Gillespie and T.E. Peel. *Adv. Phys. Org. Chem.*, 9, 1 (1971).
(c) R.J. Gillespie; T.E. Peel; E. Robinson. *J. Am. Chem. Soc.*, 93, 5083 (1971).
(d) R.J. Gillespie and T.E. Peel. *J. Am. Chem. Soc.*, 95, 5173 (1973).
36. L.C. Jozefowicz; H.G. Karge; E. Vasilyeva; J.B. Moffat. *Microporous Materials*, 1, 313 (1993).
37. J.B. Moffat. *J. Mol. Catal.*, 26, 385 (1985).
38. H. Hayashi and J.B. Moffat. *J. Catal.*, 77, 473 (1982).
39. (a) S. Kasztelan and J.B. Moffat. *J. Catal.*, 106, 512 (1987).
(b) J.B. Moffat and S. Kasztelan. *J. Catal.*, 109, 206 (1988).
(c) S. Kasztelan; E. Payen; J.B. Moffat. *J. Catal.*, 125, 45 (1990).
40. I.V. Kozhevnikov. *Russ. Chem. Rev.*, 56, 811 (1987).
41. (a) H. Hayashi and J.B. Moffat. *J. Catal.*, 81, 61 (1983).
(b) H. Hayashi and J.B. Moffat. *J. Catal.*, 83, 192 (1983).
42. B.K. Hodnett and J.B. Moffat. *J. Catal.*, 88, 253 (1984).
43. J.B. McMonagle and J.B. Moffat. *J. Catal.*, 91, 132 (1985).
44. S.F. West and L.F. Audrieth. *J. Phys. Chem.*, 159, 1069 (1955).
45. J.B. Moffat. *J. Mol. Catal.*, 52, 169 (1989).
46. (a) J.G. Highfield and J.B. Moffat. *J. Catal.*, 88, 177 (1984).
(b) J.G. Highfield and J.B. Moffat. *J. Catal.*, 89, 185 (1984).
(c) J.G. Highfield and J.B. Moffat. *J. Catal.*, 95, 108 (1985).
47. B.K. Hodnett and J.B. Moffat. *J. Catal.*, 91, 93 (1985).
48. S.J. Gregg and R. Stock. *J. Chem. Soc. Faraday Trans.*, 53, 1355 (1957).
49. (a) J.B. McMonagle and J.B. Moffat. *J. Colloid Interface Sci.*, 101, 479 (1984).
(b) D.B. Taylor; J.B. McMonagle; J.B. Moffat. *J. Colloid Interface Sci.*, 108, 278 (1985).
(c) J.B. Moffat; J.B. McMonagle; D. Taylor. *Solid State Ionics*, 26, 101 (1988).

50. J.B. Moffat. *Polyhedron*, **5**, 261 (1986).
51. V.S. Nayak and J.B. Moffat. *J. Colloid Interface Sci.*, **120**, 301 (1987).
52. J.B. Moffat. *Stud. Surf. Sci. Catal.*, **30**, (1987).
53. G.B. McGarvey and J.B. Moffat. *J. Colloid Interface Sci.*, **125**, 51 (1988).
54. J.B. Moffat. *Stud. Surf. Sci. Catal.*, (1988).
55. (a) V.S. Nayak and J.B. Moffat. *J. Phys. Chem.*, **92**, 7097 (1988).
(b) V.S. Nayak and J.B. Moffat. *J. Phys. Chem.*, **92**, 2256 (1988).
(c) V.S. Nayak and J.B. Moffat. *J. Colloid Interface Sci.*, **122**, 475 (1988).
56. H. Nishi; K. Nowinska; J.B. Moffat. *J. Catal.*, **116**, 480 (1989).
57. J.B. Moffat. *Chem. Eng. Commun.*, **83**, 9 (1989).
58. (a) G.B. McGarvey and J.B. Moffat. *J. Catal.*, **128**, 69 (1991).
(b) G.B. McGarvey and J.B. Moffat. *J. Catal.*, **130**, 483 (1991).
59. D. Lapham and J.B. Moffat. *Langmuir*, **7**, 2273 (1991).
60. D. Lapham; G.B. McGarvey; J.B. Moffat. *Stud. Surf. Sci. Catal.*, **73**, 261 (1992).
61. G.B. McGarvey and J.B. Moffat in "Multifunctional Mesoporous Inorganic Solids." (C.A.C. Sequeira, Ed.) Kluwer: Dordrecht, 1993, p.451.
62. G.B. McGarvey; N.J. Taylor; J.B. Moffat. *J. Mol. Catal.*, **80**, 59 (1993).
63. J.L. Bonardet; J. Fraissard; G.B. McGarvey; J.B. Moffat. *J. Catal.*, **151**, 147 (1995).
64. J. Bonardet; K. Carr; J. Fraissard; G.B. McGarvey; J.B. McMonagle; M.Seay; J.B. Moffat, in "Advanced Catalysis and Nanostructured Materials." (W.R. Moser, Ed.) Academic Press: California, San Diego, 1996, p.395.
65. M.L. Occelli. "Synthesis of Microporous Materials." Van Nostrand-Reinhold: New York, 1992.
66. (a) N.Y. Chen and W.E. Garwood. *Catal. Rev.-Sci. Eng.*, **28**, 185 (1986).
(b) M.E. Davis. *Ind. Chem. Eng. Res.*, **30**, 1675 (1991).

67. See for example "Selectivity in Catalysis." (M.E. Davis and S.L. Suib, Eds.) ACS Symposium Series, 517, ACS: Washington, D.C., 1993.
68. R.F. Lobo; M. Pan; I. Chan; H.-X. Li; R.C. Medrud; S.J. Zones; P.A. Crozier; M.E. Davis. *Science*, **262**, 1543 (1993).

CHAPTER 2

Synthesis and Characterization of Monovalent Salts

2.1 Introduction

The structure of the heteropoly acid, 12-tungstophosphoric acid ($\text{H}_3\text{PW}_{12}\text{O}_{40}\cdot 6\text{H}_2\text{O}$) in the solid state, determined by Brown *et. al.*,¹ was discussed in detail in Chapter 1. With changes in the elemental composition to form the 12-tungstosilicic ($\text{H}_4\text{SiW}_{12}\text{O}_{40}$) and 12-molybdophosphoric ($\text{H}_3\text{PMo}_{12}\text{O}_{40}$) acids, a cubic arrangement of the Keggin anions and the hydrated protons in the solid state is maintained, although the $\text{H}_3\text{PMo}_{12}\text{O}_{40}$ is found to belong to the face-centred (Fd3m),^{2,3} not primitive (Pn3m) space group as with $\text{H}_3\text{PW}_{12}\text{O}_{40}$ and $\text{H}_4\text{SiW}_{12}\text{O}_{40}$.^{1,4(b)} All three heteropoly acids have small surface areas, typically less than $10 \text{ m}^2/\text{g}$.⁵ This is a result of the interstitial voids present in the lattice, separated from one other by the linking of the terminal oxygen atoms to the hydrated protons.

Tourneaux and Devin^{6,7} first demonstrated that the salts of 12-heteropoly acids were capable of adsorbing vapours of alcohols, acids, and hydrocarbons. Gregg and Stock later investigated the adsorption of hydrocarbon vapours, ammonia, water, and nitrogen on the ammonium salt of 12-molybdophosphoric acid, $(\text{NH}_4)_3\text{PMo}_{12}\text{O}_{40}$.⁸ The resulting adsorption isotherms were considered to be Type I, according to the Brunauer, Demming, Demming and Teller classification,⁹ and the BET surface area was calculated to be greater than $140 \text{ m}^2/\text{g}$.⁸ Monomolecular adsorption in micropores, defined as pores with diameters of less than 20 angstroms (2.0 nm),¹⁰ is associated with Type I isotherms. Gregg and Tayyab used the preadsorption of n-nonane to study the micropore structure of the ammonium salts $(\text{NH}_4)_3\text{PW}_{12}\text{O}_{40}$ and $(\text{NH}_4)_4\text{SiMo}_{12}\text{O}_{40}$ ¹¹ and concluded that micropores contributed significantly to the surface area of the heteropoly salts and that the microporosity was structural in nature. Work in this laboratory has continued to provide evidence that a microporous structure results with the substitution of the protons by monovalent cations of group 1A elements, accompanied by relatively high surface areas.⁴ Despite the evidence supporting the existence of a micropore structure, Misono attributes the higher surface area of the 12-heteropoly oxometalate salts to the very small size of the particles and not to the presence of intrinsic micropores in the crystal structure.^{12,13}

Microporous structures are absent in the sodium salts of 12-tungstophosphoric and 12-molybdophosphoric acids^{4(a)} and the sodium and potassium salts of 12-tungstosilicic acid.^{4(b)} More recently, ¹²⁹Xe NMR studies have confirmed the existence of the micropore structures of several heteropoly oxometalate salts prepared from the monovalent cations of group 1A alkali metals.¹⁴

Santos concluded that the 12-heteropoly salts containing monovalent cations belonged to the $Pn\bar{3}m$ space group, with the cations occupying the positions previously occupied by the protons.¹⁵ Direct evidence was provided by Boeyens *et al.*¹⁶ who performed single crystal studies on the potassium and ammonium salts of 12-molybdophosphoric acid. This was reiterated by Brown *et al.* with the examination of the cesium salt of 12-tungstophosphoric acid, $Cs_3PW_{12}O_{40}$.¹ It has been suggested that the microporous structure results from the distortion of the terminal oxygen atoms in the adjacent Keggin anions to accommodate the larger cation.⁴ The distortion can be described as the translation and rotation of the Keggin anions, which remove, at least partially, the barriers separating the interstitial voids from one another.

McMonagle and Moffat provided further evidence for the distortion of the terminal oxygen atoms by noting microporous salts share a common feature in the diffraction patterns obtained by powder XRD methods.^{4(a),(b)} The ratio of intensities of two indexed peaks in the powder XRD spectrum ($I[110]/I[222]$) decreases for a microporous solid. The [222] peak is the most intense in the spectrum and the decreased intensity of [110] is a result of a distortion interaction of the cation with the terminal oxygen atom reducing the electron density in the 110 plane. It was also noted that there is a strong inverse relationship between $I[110]/I[222]$ and the micropore volume as a function of the cation radius of the monovalent salts of HPW, HSiW, and HPMo.⁴

With the establishment of a microporous structure in heteropoly salts containing the monovalent cations of the alkali metals and ammonium, with the exception of sodium and in some cases potassium, the natural extension of this research was to form salts containing 12-heteropoly oxometalates with the divalent cations of the alkaline earths.¹⁷⁻²¹ Although an increase in catalytic activity had been noted for these salts containing the divalent cation, little was reported on the characterization of the surface and bulk

properties of these solids. Investigations showed that microporous structures were not formed.^{2,22} Single crystal x-ray diffraction studies of $\text{Ba}_3(\text{PW}_{12}\text{O}_{40})_2$ revealed that the barium cation did not occupy the proton's position and, in fact, there was no evidence of the divalent cation in the lattice network.² It was concluded by McGarvey and Moffat^{2,22} that the solids were mixtures of the 12-heteropoly acid and the divalent cations of the alkaline earth metals and that any differences in the catalytic behaviour was a result of the divalent cation present in the mixture with the acid, rather than the formation of a salt of the 12-heteropoly acid.

In addition to those containing alkaline earths, salts of the 12-heteropoly acids were formed with various transition metal cations.^{18,23-28} In particular, monovalent silver(I) and thallium(I) derivatives of the 12-heteropoly acids have been shown to have high catalytic activities in the dehydration of methanol²⁴ and 2-propanol,²⁵ the isomerization of hexane,²⁶ and the oxidation of various hydrocarbons.²⁷ Although the surface areas of the salts were reported,^{25(c),28} little or no characterization of the surface and bulk properties was carried out in order to explain the increased catalytic activity. However, due to the differences observed with the salts containing the alkali metals and alkaline earths, this type of characterization is essential in understanding the morphology of the salts and optimizing the synthetic conditions to facilitate their use in catalysis.

The present chapter provides the results of characterization of the silver(I) and thallium(I) salts of the three heteropoly acids: 12-tungstophosphoric acid, 12-tungstosilicic acid and 12-molybdophosphoric acid. Nitrogen adsorption-desorption isotherms and spectroscopic techniques were used to establish and characterize the existence of a microporous structure. The use of silver and thallium, as representative monovalent cations from each of the 1B and 3B groups of the periodic table, and the three types of Keggin anions provides information on the effect of (1) the nature and size of cation and (2) the anion composition on the microporous structure. Despite changes in the central and peripheral atoms, the structure of the Keggin anion is maintained. However, the charge carried by the anion is dependent upon the oxidation states of the atoms used. The preparative techniques used to synthesize the salts are considered as a third factor. These included a variation of the temperature at which the synthesis was carried out and the use

of nonstoichiometric amounts for the ratio of cation to proton in the synthesis of the salt.

As mentioned previously, $\text{Cs}_3\text{PW}_{12}\text{O}_{40}$ is a close structural analogue to $\text{H}_3\text{PW}_{12}\text{O}_{40}\cdot 6\text{H}_2\text{O}$ with the monovalent cation occupying the position previously held by the proton, as indicated by both x-ray diffraction¹ and ^{17}O MAS NMR data.²⁹ The microporous structures of the cesium salts of 12-tungstophosphoric and 12-tungstosilicic acids are well established and have been reported in the literature.^{4(a),(b)} The cesium salts have increasingly been recognized for their use as solid acid catalysts.¹³ As a result, the cesium salts $\text{Cs}_3\text{PW}_{12}\text{O}_{40}$ and $\text{Cs}_4\text{SiW}_{12}\text{O}_{40}$ were considered to be suitable standards with which to compare the characterization of the micropore structures in the salts of heteropoly oxometalates containing the silver and thallium monovalent cations.

2.2 Experimental

2.2.1 Synthesis

12-Tungstophosphoric acid ($\text{H}_3\text{PW}_{12}\text{O}_{40}$) and 12-tungstosilicic acid ($\text{H}_4\text{SiW}_{12}\text{O}_{40}$) were obtained from BDH (Anala R Grade) while 12-molybdophosphoric acid ($\text{H}_3\text{PMo}_{12}\text{O}_{40}$) was purchased from Aldrich. Silver nitrate (AgNO_3) and thalious nitrate (TlNO_3) were obtained from BDH and cesium nitrate (CsNO_3) from Aldrich and all three nitrate salts were used as received. All three acids were recrystallized prior to use. Helium and nitrogen were purchased from Praxair.

Eight different salts were synthesized from each 12-heteropoly acid with the nitrate salt of either cesium(I), silver(I) or thallium(I). To examine the effect of stoichiometry on the properties of the salts three molar ratios of the cation to the protons of the acid (0.85, 1.00, and 1.15) were employed in the preparation of each salt.

The silver salts of $\text{Ag}_3\text{PW}_{12}\text{O}_{40}$, $\text{Ag}_4\text{SiW}_{12}\text{O}_{40}$ and $\text{Ag}_3\text{PMo}_{12}\text{O}_{40}$ (abbreviated as AgPW, AgSiW and AgPMo, respectively), were obtained by precipitation when the desired amount of the AgNO_3 , dissolved in 2.0 mL of distilled deionized water, was added dropwise to an aqueous solution of the appropriate acid ($\approx 3\text{g}$ or $\approx 1 \times 10^{-3}$ mol) dissolved in 4.0 mL of distilled deionized water. After allowing the reaction mixture to stir for ten minutes, at room temperature, the mixture was filtered gravimetrically, transferring with a minimum amount of water (3×2.0 mL). The salt was then dried overnight under a low

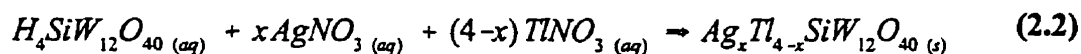
vacuum at room temperature.

The cesium salts of $\text{Cs}_3\text{PW}_{12}\text{O}_{40}$ and $\text{Cs}_4\text{SiW}_{12}\text{O}_{40}$ (abbreviated as CsPW and CsSiW, respectively) were obtained by the method employed for the silver salts. Since cesium nitrate is less soluble, a larger amount of water (4 mL) was employed for its solution.

The thallium salts of $\text{Tl}_3\text{PW}_{12}\text{O}_{40}$, $\text{Tl}_4\text{SiW}_{12}\text{O}_{40}$, and $\text{Tl}_3\text{PMo}_{12}\text{O}_{40}$ (abbreviated as TIPW, TlSiW and TIPMo, respectively), were obtained by a similar procedure but with a reaction temperature of 60 °C and the covered reaction mixture was stirred at 60 °C for one hour, prior to filtration. The decreased solubility of the thallium nitrate salt necessitated the dissolution of both the cation and acids in 6 mL of distilled deionized water. This synthesis is based on the method previously used by Thistlethwaite *et al.*³⁰

All the salts were stored in a desiccator after drying. For the AgPW and TIPW salts, the cation to proton ratios of 0.5 and 1.5 were also investigated.

The mixed salts of 12-tungstophosphoric and 12-tungstosilicic acids were synthesized by varying the ratio silver(I) and thallium(I) cations while still maintaining a stoichiometric (1.0) molar ratio for the total cations to the protons in the acid. The synthetic procedure was identical to that outlined for the thallium salts. Both cations were dissolved together in 6 mL of water prior to their addition to the solution of acid at 60 °C. The stoichiometric equations for the mixed salts of 12-tungstophosphoric and 12-tungstosilicic acids are as follows:



2.2.2 Characterization Techniques

Infrared spectra were recorded, from either nujol mulls or KBr disks of the salts, of the fingerprint region of the 12-heteropoly anions (2000 - 400 cm^{-1}) on a Bomem MB-100 FT-IR spectrometer. Powder X-ray diffraction patterns were recorded on a Siemens

D500 diffractometer using $\text{CuK}\alpha$ radiation and a graphite monochromator, at 30 mA and 40 kV. The samples were taken directly from the desiccator and the spectrum recorded at room temperature. ^1H MAS NMR spectra were obtained on a Bruker AMX-500, with an external reference of benzene, at room temperature. The spinning rate ranged between 6.5 - 8 kHz, depending upon the sample.

Nitrogen adsorption-desorption isotherms were measured on a standard volumetric glass system (Figure 2.1) fitted with an MKS Baratron type 590HA Capacitance Manometer. The vacuum system consisted of a Balzers rotary pump and two water cooled mercury diffusion pumps in series, which were capable of achieving a pressure of 10^{-6} torr. Samples, consisting of approximately 0.5 g, were outgassed at 10^{-5} torr at 473 K for two hours prior to the analysis, at 77 K. Calibration of the volumes at room temperature (278 K) was carried out with helium gas. With the sample holder isolated, the pressure of an aliquot of gas is measured in the closed system by the capacitance manometer. The stopcock to the sample holder is then opened and the pressure is recorded once equilibrium has been established. The level of mercury in the gas burette remained fixed for a given sample. The pressure was measured to ± 0.001 torr to a maximum pressure of 100 torr and ± 0.01 torr for the remainder of the adsorption-desorption isotherm. Equilibrium required durations of time which varied from sample to sample but was assumed to have been attained when no measurable changes were apparent. To complete the isotherm, the pressure of the aliquots of gas are increased from 2 to 760 torr. Approximately 25 and 10 data points were obtained for the adsorption and desorption sections of the isotherm, respectively.

Temperature-programmed desorption experiments were performed with a Shimadzu gas chromatograph (GC-9A) equipped with an empty brass tube (0.30 m x 1/4") and a CR32A Chromatopac Integrator. The samples, approximately 0.150 g, were placed in a glass tube inserted into a heater and were pretreated at 30 °C with a stream of pure helium for 20 minutes. The experiment consisted of ramping the temperature from 30 °C to 600 °C at 41 °C/min, while maintaining a flow of helium at 46 mL/min. Slower ramping temperature rates were not suitable in distinguishing a peak for the residual protons.

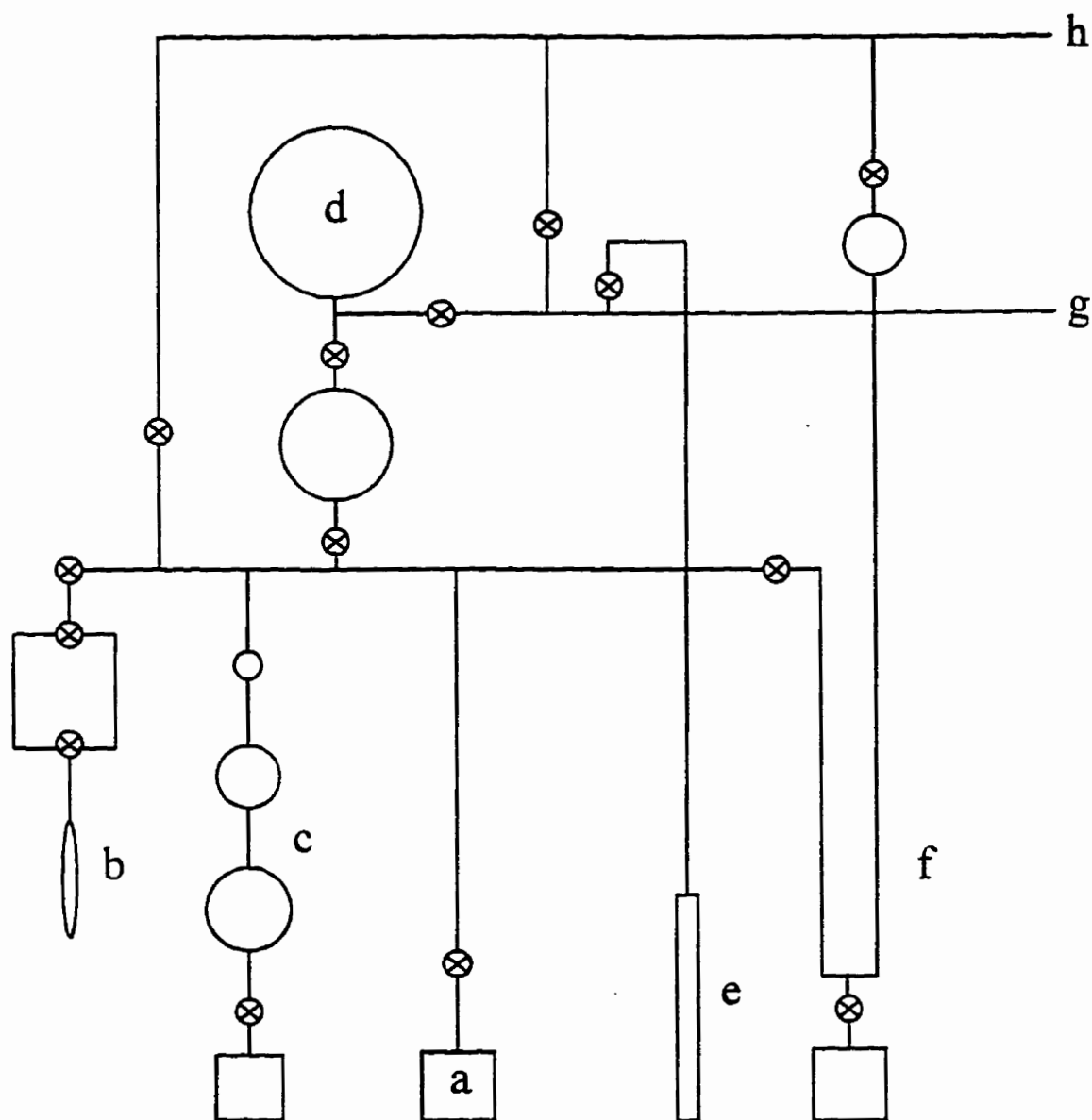


Figure 2.1 - Volumetric nitrogen adsorption system. (a) capacitance manometer; (b) sample holder; (c) gas burette; (d) nitrogen storage; (e) nitrogen blow-off tube; (f) U-tube manometer; (g) to nitrogen cylinder; (h) to vacuum pumps.

2.3 Results

2.3.1 Characterization of Surface and Bulk Properties of Pure Silver and Thallium Salts

As mentioned earlier, the structural arrangement of the Keggin anion is maintained with the interchangeability of various central and peripheral atoms. Infrared spectroscopy provides five characteristic bands for the Keggin anion in the region of 2000 to 400 cm^{-1} .³¹ The first is the triply degenerate asymmetric stretch of the central atom-oxygen bond of the central tetrahedron (denoted as $\nu_{\text{as}}(\text{X-O})$). Second is the asymmetric stretch of the peripheral atom and the terminal oxygen atom bond (denoted as $\nu_{\text{as}}(\text{M-O})$). Two bands are associated with the peripheral metal-oxygen-peripheral metal bonds, accompanied by some bending character.³¹ The higher frequency, denoted as $\nu_{\text{as}}(\text{M-O-M})_{\text{inter}}$ involves the peripheral atom-oxygen atom bridge between the octahedra in adjacent M_3O_{13} trimetalate units while the lower frequency, $\nu_{\text{as}}(\text{M-O-M})_{\text{intra}}$, results from the vibration of the metal-oxygen-metal bridge between octahedra which share edges with one another within the same M_3O_{13} unit. Completing the set is a band, denoted as $\delta(\text{O-X-O})$, resulting from a combination of stretches of the central atom-oxygen bonds, causing deformation in the central tetrahedral unit.

Of the six salts synthesized (AgPW, AgPMo, AgSiW, TIPW, TIPMo and TlSiW), the structure of the Keggin anion and its orientation in the lattice structure was maintained with the substitution of the cations except for the AgPMo salt. The five characteristic bands for the Keggin anion are present in the infrared spectra for all the salts except the AgPMo salt. Table 2.1 summarizes these five bands for the three parent acids and the salts while Figure 2.2 contains the spectra observed for the silver and thallium salts of 12-tungstophosphoric acid.

The presence of additional bands for the $\text{Ag}_3\text{PMo}_{12}\text{O}_{40}$ salt indicates that the "defect" Keggin structure may have been formed.³² This "defect" structure has lost one heavy atom and a terminal oxygen, giving the molecular formula of $\text{PMo}_{11}\text{O}_{39}^{7-}$. The resulting hole in the structure decreases the symmetry of the anion from T_d to C_3 , and is reflected in the infrared spectrum by the splitting of the $\nu(\text{P-O})$ and $\nu_{\text{as}}(\text{M-O})$ bands as well as the $\nu_{\text{as}}(\text{M-O-M})_{\text{intra}}$ bands. These first two characteristics were observed in the IR spectrum of AgPMo with a definite broadening of the bridging bands. (Table 2.2)

Table 2.1 - Characteristic frequencies from infrared spectra of parent acids and salts.

| | $\nu(\text{X-O})$ | $\nu_{\text{as}}(\text{M-O})$ | $\nu(\text{M-O-M})$ inter | $\nu(\text{M-O-M})$ intra | $\delta(\text{O-X-O})$ |
|-------------------|-------------------|-------------------------------|------------------------------|------------------------------|------------------------|
| HPW ^a | 1080 | 985 | 887 | 807 | 598 |
| HSiW ^a | 1020/930 | 982 | 885 | 792 | 558 |
| HPMo ^a | 1070 | 965 | 870 | 790 | 598 |
| AgPW | 1078 | 980 | 888 | 798 | 599 |
| TIPW | 1078 | 982 | 887 | 801 | 596 |
| AgSiW | 922 | 978 | 891 | 784 | 522 |
| TlSiW | 1014/924 | 974 | 877 | 786 | 537 |
| TIPMo | 1063 | 964 | 866 | 790 | 595 |

^a Reference 31(a).**Table 2.2** - Characteristic frequencies for infrared spectrum of silver 12-molybdophosphate.

| | $\text{PMo}_{11}\text{O}_{39}^{7-}$ ^a | $\text{Ag}_3\text{PMo}_{12}\text{O}_{40}$ | $\text{PMo}_{12}\text{O}_{40}^{3-}$ ^b |
|--------------------------------------|--------------------------------------------------|-------------------------------------------|--------------------------------------------------|
| $\nu(\text{P-O})$ | 1060 1010 | 1065 1006 | 1070 |
| $\nu_{\text{as}}(\text{Mo-O})$ | 930 900 | 958 926 | 965 |
| $\nu(\text{Mo-O-Mo})_{\text{inter}}$ | 860 | 868 | 870 |
| $\nu(\text{Mo-O-Mo})_{\text{intra}}$ | 790 742 | 780 | 790 |
| $\delta(\text{O-P-O})$ | 600 | 595 | 598 |

^a Reference 32.^b Reference 31(a)

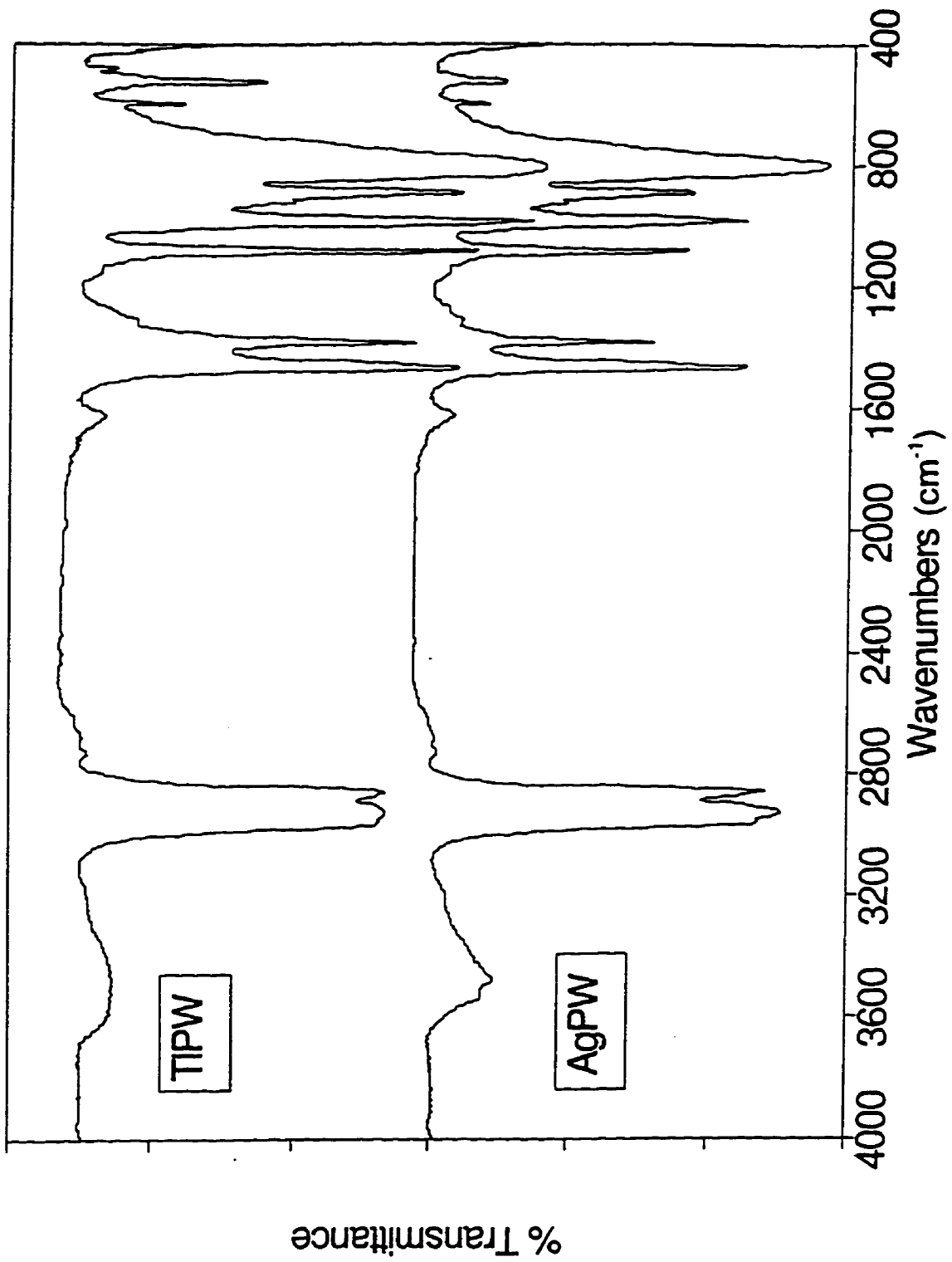


Figure 2.2 - Infrared spectra of silver and thallium 12-tungstophosphate.

Powder x-ray diffraction (XRD) patterns of the salts provides information on the orientation of the Keggin anions in the lattice now containing the substituted cations. The powder XRD patterns of all the salts, except AgPMo, were indexed according to the cubic Pn3m space group. This indicated the retention of the lattice framework initially present in the solid acids containing the Keggin anions, as depicted in Figure 1.3. The XRD spectrum for the AgPMo salt could not be indexed according to the cubic Pn3m space group and it is doubtful that the anticipated lattice structure was maintained.

Table 2.3 - Data from indexed powder XRD patterns for parent acids and stoichiometric salts.

| Sample | Lattice Parameter a_0 (Å) | I[110] / I[222] |
|-----------------------------------------------|--------------------------------|-----------------|
| $H_3PW_{12}O_{40} \cdot 6H_2O$ ^a | 12.5 | 1.22 |
| $H_3PMo_{12}O_{40} \cdot 30H_2O$ ^b | 23.2 | 0.84 |
| $H_4SiW_{12}O_{40}$ ^c | 12.2 | 1.49 |
| $Ag_3PW_{12}O_{40}$ | 11.8 | 0.40 |
| $Ag_3PMo_{12}O_{40}$ | - | - |
| $Ag_4SiW_{12}O_{40}$ | 11.8 | 0.41 |
| $Tl_3PW_{12}O_{40}$ | 11.6 | 0.13 |
| $Tl_3PMo_{12}O_{40}$ | 11.6 | 0.08 |
| $Tl_4SiW_{12}O_{40}$ | 11.6 | 0.06 |

^a Reference 4(a).

^b References 2,3.

^c Reference 4(b)

Indexing of the XRD patterns permitted the lattice parameters (a_0) to be calculated. (Table 2.3) Despite the thallium(I) cation having a larger diameter than the silver(I) cation, the lattice parameter was consistently smaller for the thallium salts than the silver salts of the corresponding acid. The lattice parameter appeared to be unaffected by the nature of the anion. Both these lattice parameters are smaller than those reported for the

pure heteropoly acids,^{2,3,4(a),(b)} although the degree of hydration has been noted to have an effect on these values. It was assumed that less water is associated with the salts, compared to the parent acid, due to the replacement of the protons by nonhydrated cations.

It has been previously noted that the ratio of the intensity of two indexed peaks in the XRD spectrum, ($I[110]/I[222]$), decreases with the presence of micropores.^{4,5} The peak indexed as [110] refers to the plane containing the terminal oxygen atoms of the Keggin anion while the peak indexed as [222] is the most intense peak in the spectrum. As discussed in Chapter 1, in the solid state the terminal oxygen atoms of the Keggin anions are hydrogen-bonded to the hydrated proton of the heteropoly acid. Substitution of a larger cation for the proton in the solid form of the salt causes the Keggin anions to be forced further apart from one another by rotation and translation, opening up the interstitial voids to form a microporous structure. As a result, fewer terminal oxygen atoms reside in the [110] plane, therefore decreasing the intensity of this peak in the XRD spectrum. As summarized in Table 2.3, the ratios of peak intensities have decreased significantly with the incorporation of the cations into the salts. The smaller ratio observed for the thallium salts indicates that the size of the cation may be an important factor in establishing the microporous structure.^{4(a),(b),(c)} In contrast, the elemental composition of the anion appears to play a less significant role.^{4(e)}

Figure 2.3 contains the N_2 adsorption-desorption isotherms for the stoichiometric AgPW and TIPW salts. The nitrogen adsorption-desorption isotherms of all of the salts, except that of the AgPMo salt, depict the sharp initial rise at low relative pressures, indicative of the presence of micropores. The absence of a hysteresis loop at the higher relative pressures serves as an indication that few, if any, mesopores are present. The surface area for these salts, as determined by application of the Brunauer/Emmett/Teller (BET) theory³³ to the adsorption isotherm, are summarized in Table 2.4. A detailed discussion of the analysis of an adsorption isotherm by the BET method is provided in Chapter 4 (Section 4.3). As noted in Table 2.4, the relatively large values for the C_{BET} parameters and reduced range of linearity of the fit to the BET equation differ from those which are typically observed,³⁴ and are indicative of the presence of micropores. All the

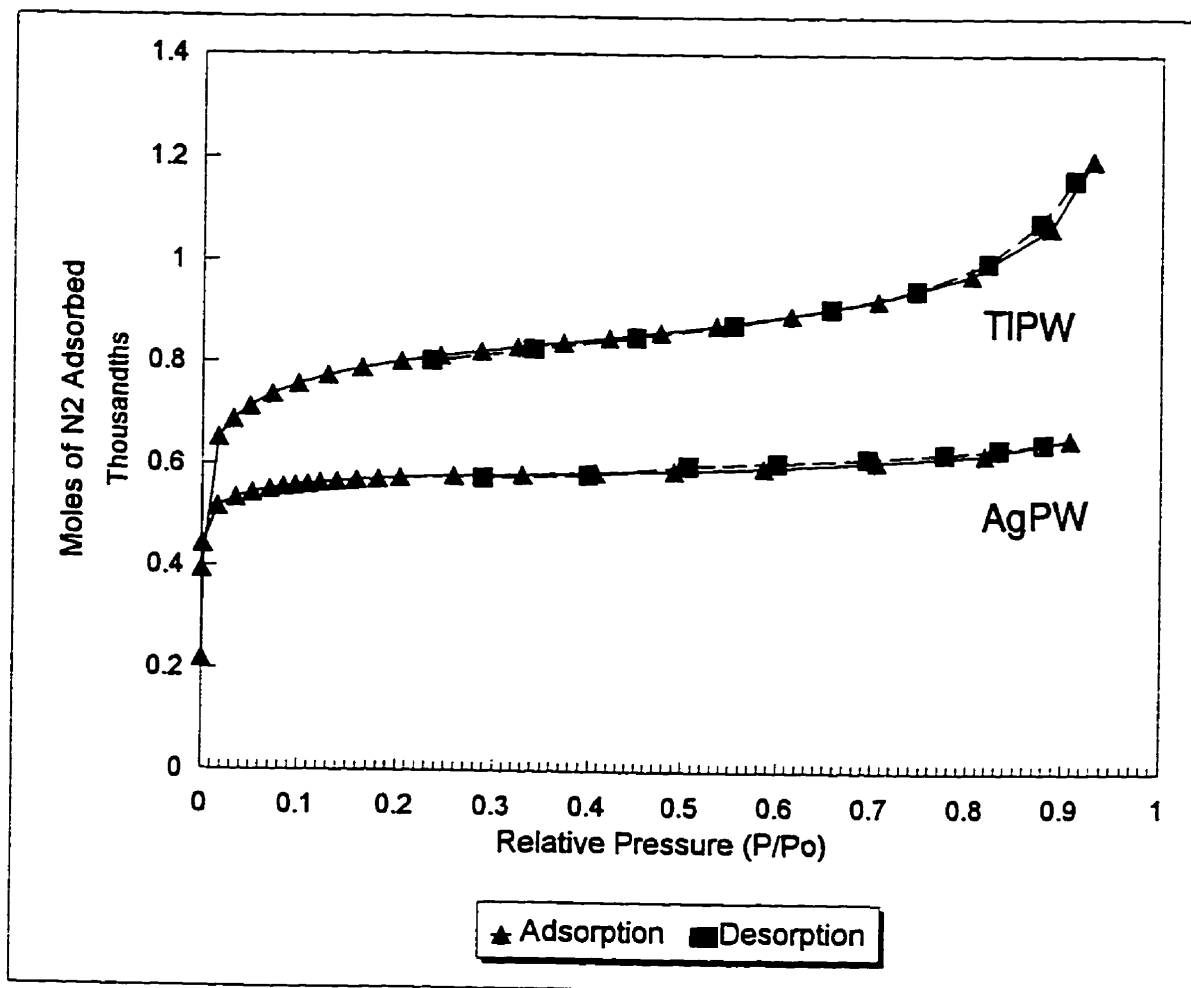


Figure 2.3 - N_2 adsorption-desorption isotherms for $Ag_3PW_{12}O_{40}$ and $Tl_3PW_{12}O_{40}$.

Table 2.4 - Summary of surface areas and C_{BET} parameters for parent acids and stoichiometric salts

| Sample | Range of P / P_0 ^a | n^b | C_{BET}^c | S_{BET}^d | S_t^e | V_{MP}^f | r_{MP}^g |
|-------------------|---------------------------------|-------|--------------------|--------------------|---------|-------------------|-------------------|
| HPW ^h | - | - | - | 8.0 | - | - | - |
| HPMo ^h | - | - | - | 8.0 | - | - | - |
| HSiW ^h | - | - | 100 | 4.0 | - | - | - |
| AgPW | 0.00 - 0.05 | 1.46 | 7400 | 100.9 | 104.4 | 0.037 | 7.9 |
| AgPMo | 0.00 - 0.10 | - | 14000 | 1.5 | - | - | - |
| AgSiW | 0.00 - 0.04 | 1.38 | 35600 | 106.0 | 108.8 | 0.040 | 7.6 |
| TIPW | 0.00 - 0.13 | 2.08 | 2700 | 131.6 | 131.4 | 0.045 | 8.2 |
| TIPMo | 0.00 - 0.17 | 2.68 | 900 | 157.0 | 149.8 | 0.046 | 8.4 |
| TISiW | 0.00 - 0.08 | 1.50 | 5000 | 97.5 | 96.2 | 0.036 | 8.0 |

^a Range of linearity for fit of the infinite layer BET equation.

^b Number of adsorbate layers from finite layer BET relationship (Equation 2.3).

^c Constant from the infinite layer BET equation.

^d Surface area determined from the infinite layer BET equation. (m^2/g)

^e Surface area determined from t-plots. (m^2/g)

^f Micropore volume. (mL/g)

^g Mean micropore radius. (\AA)

^h Reference 5.

salts, except AgPMo, have high surface areas, increasing at least an order of magnitude from the surface areas recorded for the pure acids.⁵

The surface areas (S_t) were also calculated from t-plots, using the method of Lecloux and Pirard³⁵ for calibration purposes, (Table 2.4) and are in good agreement with the values obtained by the BET method. The thallium salts of 12-tungstophosphoric and 12-molybdophosphoric acids have greater surface areas than the analogous silver salts while the salts of 12-tungstosilicic acid show the reverse trend. This difference may be attributed to the requirement of four equivalents of the cation in the 12-tungstosilicic acid as contrasted with three equivalents for the remaining two acids. The incorporation of the

extra cations into the lattice may be affected by the larger size of the thallium cation in the case of the 12-tungstosilicic acid, counteracting the creation of the microporous structure.

The finite layer BET relationship (Equation 2.3) was fitted to the adsorption data.

$$N = \frac{N_m C_{BET} x [1 - (n+1)x^n + nx^{n+1}]}{(1+x)[1 + (C_{BET} - 1)x - C_{BET} x^{n+1}]} \quad (2.3)$$

The values of N_m , the moles of nitrogen which form the monolayer, and C_{BET} were determined by the infinite layer BET relationship while x and N refer to the relative pressure (P/P_0) and moles of nitrogen adsorbed, respectively, in the N_2 adsorption isotherm. A nonlinear regression was performed to determine n , the maximum attainable number of adsorbate layers, summarized in Table 2.4. The values reported for n were less than 3, and are consistent with the presence of a microporous structure. It has been noted previously,^{4(a),(b)} that within a series for a specific solid acid, the value of n increases with the increase of the cation diameter. Our data are consistent with this observation.

The MP method³⁶ was employed to generate the micropore size distribution from the data plotted in the t-plots. Values for the micropore volume and pore size distributions are a function of the hydraulic radius; however, with heteropoly oxometalates, the assumption is made that the pores are cylindrically shaped and the hydraulic radius (r_h) is equal to one half of the cylindrical radius.³⁷ The calculations and construction of the t-plots and pore size distributions reflect this assumption. The volume of the micropores (V_{MP}) can be estimated from the t-plots by extrapolating from the linear pressure region of $0.4 < P/P_0 < 0.6$ to obtain the y-intercept while the mean micropore radius (r_{MP}) was calculated by the MP method. (Table 2.4) Chapter 4 provides an explanation how r_{MP} is calculated (Section 4.3).

The pore size distribution plots (Figure 2.4 shows TIPW as an example) generally consisted of one major peak and are typical of the distributions previously observed for microporous salts of the heteropoly acids.^{4,5} Consistent with the larger surface area, the thallium salts have a slightly larger pore diameter and larger micropore volumes than the

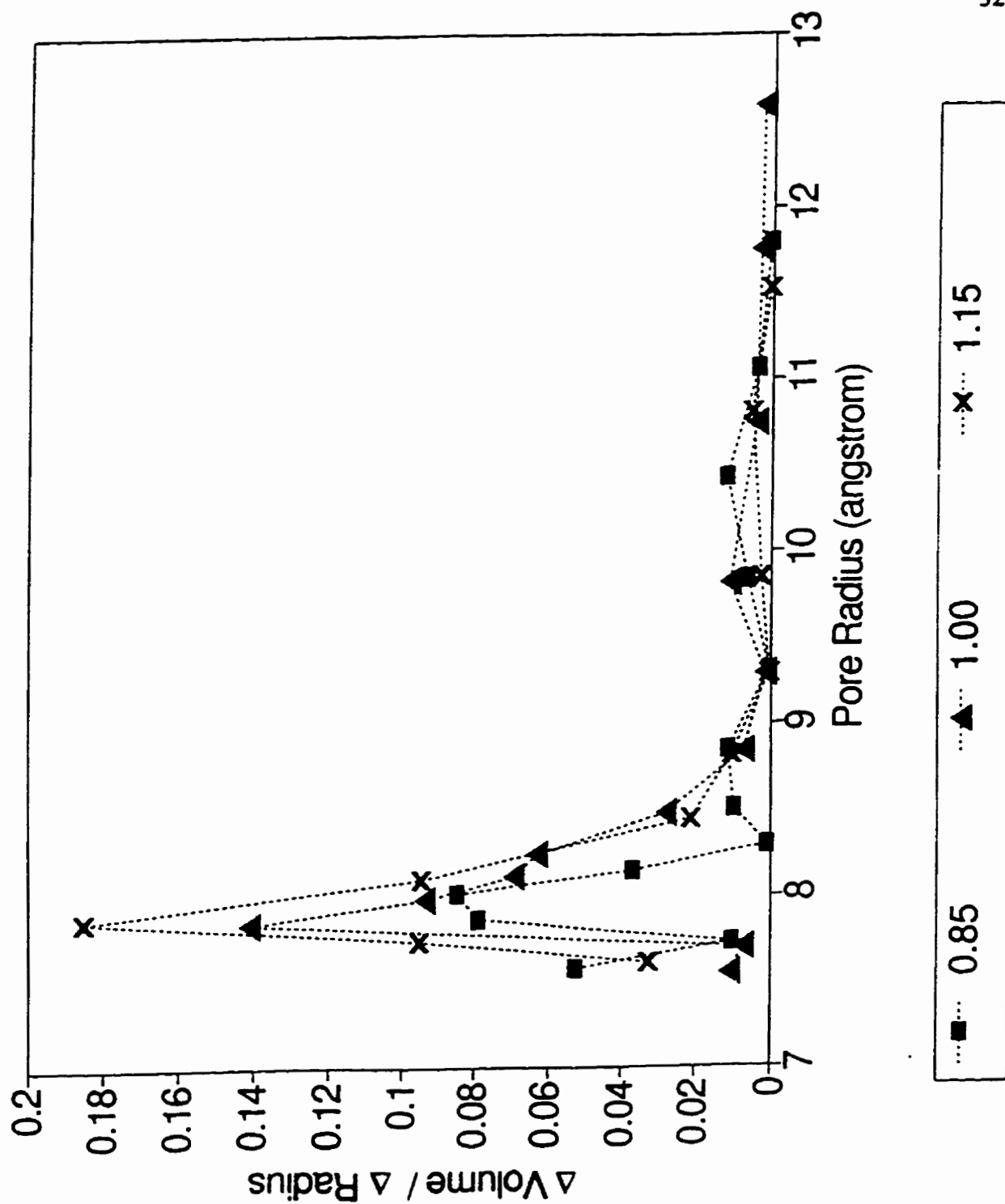


Figure 2.4 - Pore size distribution for thallium 12-tungstophosphate for various preparative stoichiometries.

analogous silver salts for the 12-tungstophosphoric and 12-molybdophosphoric acids. (Table 2.4) This correlates with the lower ratios of the XRD peak intensities of $I[110]/I[222]$ for the thallium salts in comparison to the silver salts. In contrast, the thallium and silver salts containing the 12-tungstosilicate anion have similar values.

The microporous structure and surface areas are consistent with those previously reported in the literature, except for AgPW. The surface area for this salt has been previously reported in the literature as $2^{25(c)} - 3^{4(a)}$ m^2/g . The significant difference between these and the values obtained in the present work could be attributed to the method of synthesis used. Previous procedures for synthesizing the salts of the heteropoly acids involved mixing aqueous solutions of the acid and the carbonate salt of the cation, forming the precipitate of the insoluble salt, followed by evaporation to dryness.³⁸ The present method isolates the precipitate by gravimetric filtration rather than evaporation. This is believed to minimize the presence of peripheral impurities on the solid by washing away excess reagents.

2.3.2 Reproducibility of Surface Area and Mean Micropore Radii Measurements.

To verify the reproducibility of the surface area calculated by the BET method³³ and from the t-plots, using the method of Lecloux and Pirard³⁵ for calibration purposes, two samples of the thallium salt of 12-tungstophosphoric acid (TIPW) were synthesized according to the procedure outlined in Section 2.2.1. Nitrogen adsorption isotherms were obtained for five independent aliquots of each of the two samples and the resulting surface areas are summarized in Table 2.5. The mean micropore radii are included, calculated by the MP method.³⁶

The standard deviation associated with each average surface area value indicates the two samples are within experimental error of one another. A t-test³⁹ performed on the data revealed that there is no significant difference between the average values of S_{BET} , S_t , and r_{MP} obtained for each of the two samples. More notably, there was no statistical difference between the average values of the surface areas calculated by the BET method and from the t-plots.

It can be concluded that the microporous structure created in the TIPW salt is

Table 2.5 - Replicate trials in measuring the surface areas and mean micropore radii of $Tl_3PW_{12}O_{40}$.

| Trial | Sample #1 | | | Sample #2 | | |
|-----------|--------------------------|----------------------|------------------------------|--------------------------|----------------------|------------------------------|
| | S_{BET} (m^2/g) | S_t (m^2/g) | r_{MP} (\AA) | S_{BET} (m^2/g) | S_t (m^2/g) | r_{MP} (\AA) |
| 1 | 130.2 | 131.5 | 8.1 | 127.1 | 126.1 | 8.2 |
| 2 | 128.6 | 129.6 | 7.8 | 128.8 | 127.6 | 7.8 |
| 3 | 128.1 | 128.6 | 7.9 | 130.6 | 130.0 | 7.9 |
| 4 | 129.1 | 128.7 | 7.8 | 130.3 | 130.4 | 7.9 |
| 5 | 128.7 | 127.9 | 7.9 | 128.8 | 127.8 | 8.0 |
| Average | 128.9 | 129.3 | 7.9 | 129.1 | 128.4 | 8.0 |
| Std. Dev. | 0.8 | 1.4 | 0.1 | 1.4 | 1.8 | 0.1 |

reproducible by the preparative method employed and data obtained from nitrogen adsorption isotherms, used to characterize the microporous structure, are consistent between replicate trials.

2.3.3 Effects of Reaction Parameters on the Resulting Surface and Bulk Properties.

Preparations of the AgPW and TIPW salts at various temperatures were also carried out to evaluate the effect of temperature on the salt's resulting structure. (Tables 2.6 and 2.7) The same synthetic technique and mixing times were maintained, with only the temperature being varied between 0 °C, room temperature (25 °C), and 60 °C. The three temperatures examined for the AgPW salt produced marked changes in surface area and micropore volume; a maximum value was obtained for the salt synthesized at room temperature. The relatively low surface area and micropore volume at 0 °C could be attributed to the low solubility of the salt, causing it to precipitate quickly out of solution, thus trapping impurities, a rationalization consistent with the lack of dependence of mean micropore radii (r_{MP}) on the preparative temperature in contrast with the micropore volume (V_{MP}). The higher temperature of 60 °C may contribute to the degradation of the salt,

but to a lesser extent than the higher temperature used for evaporation (100 °C). The TIPW salts prepared at the three different temperatures appear to be relatively unaltered by the temperature variation. For both types of salts prepared at various temperatures, no variations in the powder XRD pattern (with the measured lattice parameter, a_0 , or $I[110]/I[222]$) are evident.

Table 2.6 - Characterization of the microporous structure of $\text{Ag}_3\text{PW}_{12}\text{O}_{40}$.

| Temperature of Preparation (°C) | S_{BET} (m ² /g) | C_{BET} | V_{MP} (mL/g) | r_{MP} (Å) |
|---------------------------------|--------------------------------------|------------------|------------------------|---------------------|
| 0 | 42.8 | 3900 | 0.012 | 7.7 |
| 25 | 100.9 | 7400 | 0.037 | 7.9 |
| 60 | 44.1 | 7300 | 0.014 | 7.6 |
| 100 ^a | 3.0 ^b | | | |

^a Salt isolated by evaporation.

^b Reference 4(a).

Table 2.7 - Characterization of the microporous structure of $\text{Tl}_3\text{PW}_{12}\text{O}_{40}$.

| Temperature of Preparation (°C) | S_{BET} (m ² /g) | C_{BET} | V_{MP} (mL/g) | r_{MP} (Å) |
|---------------------------------|--------------------------------------|------------------|------------------------|---------------------|
| 0 | 135.7 | 2100 | 0.042 | 8.0 |
| 25 | 132.0 | 2600 | 0.043 | 8.1 |
| 60 | 132.2 | 2700 | 0.045 | 8.2 |
| 100 ^a | 140.9 ^b | | | |

^a Salt isolated by evaporation.

^b Reference 40.

Three ratios of the amount of cation to acid (0.85, 1.00, 1.15) were used in the synthesis of each salt except with AgPW and TlPW where five values were employed (0.50, 0.85, 1.00, 1.15, 1.50). The preparative reagents were employed in stoichiometric

Table 2.8 - Yields (%)^a in the synthesis of the stoichiometric and nonstoichiometric salts.

| Salt | Preparative Stoichiometry ^b | | | | |
|---------------------------------------------------|----------------------------------------|------|------|------|------|
| | 0.50 | 0.85 | 1.00 | 1.15 | 1.50 |
| Ag ₃ PW ₁₂ O ₄₀ | 50 | 86 | 95 | 98 | 100 |
| Ag ₃ PMo ₁₂ O ₄₀ | | 62 | 75 | 81 | |
| Ag ₄ SiW ₁₂ O ₄₀ | | 47 | 59 | 73 | |
| Tl ₃ PW ₁₂ O ₄₀ | 71 | 82 | 98 | 99 | 102 |
| Tl ₃ PMo ₁₂ O ₄₀ | | 63 | 103 | 108 | |
| Tl ₄ SiW ₁₂ O ₄₀ | | 90 | 93 | 101 | |

^a Based on the initial amount of 12-heteropoly acid used.

^b Cation:Proton ratio.

amounts or with an excess or deficit of the reagent supplying the cation, while keeping the amount of water and acid constant. As expected, the yields by mass (based on the amount of acid initially used in the synthesis) increased with the increase in the amount of cation used in the synthesis. (Table 2.8) Filtration, in contrast to evaporation, is believed to remove a portion of the unreacted reagents (either the excess acid or cation, depending upon the ratios used), in particular those on the surface of the precipitated particles.

The thallium salts are generally produced in a greater yield than the analogous silver salts of a particular acid, probably due to the lower solubility of the former salts. Some of the yields for the thallium salts were slightly larger than 100%, when an excess of the cation was used. These values are within experimental error, although the viscous nature of the mixture containing the precipitated salt may have prevented all of the unreacted reagents from being removed by filtration.

The changes in surface area (S_{BET}) of the salts, with relative amounts of a given cation, were smaller than those previously reported for ammonium salts.⁴¹ (Table 2.9 and Figure 2.5) The thallium salts generally have a larger surface area and the maximum S_{BET} obtained with a stoichiometric amount of cation could be attributed to the presence of

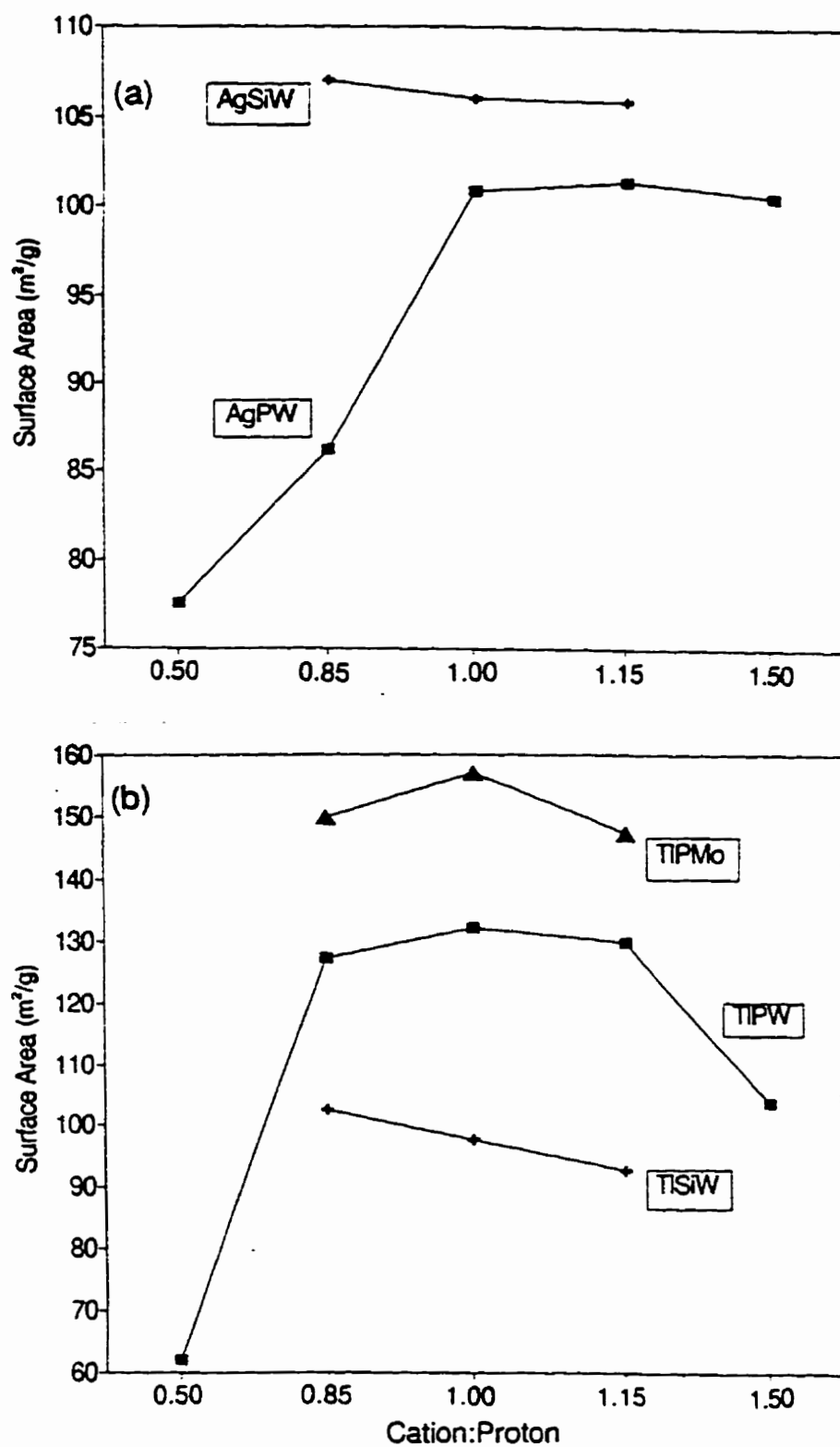


Figure 2.5 - Surfaces areas (S_{BET}) of the (a) silver and (b) thallium salts for various preparative stoichiometries.

Table 2.9 - Surface areas (S_{BET}) of the stoichiometric and nonstoichiometric salts.

| Salt | Preparative Stoichiometry ^a | | | | |
|-------------------------------------------|----------------------------------------|-------|-------|-------|-------|
| | 0.50 | 0.85 | 1.00 | 1.15 | 1.50 |
| $\text{Ag}_3\text{PW}_{12}\text{O}_{40}$ | 77.6 | 86.2 | 100.9 | 101.4 | 100.5 |
| $\text{Ag}_3\text{PMo}_{12}\text{O}_{40}$ | | 1.3 | 1.5 | 0.9 | |
| $\text{Ag}_4\text{SiW}_{12}\text{O}_{40}$ | | 107.1 | 106.0 | 105.9 | |
| $\text{Tl}_3\text{PW}_{12}\text{O}_{40}$ | 62.0 | 126.9 | 131.6 | 128.6 | 103.6 |
| $\text{Tl}_3\text{PMo}_{12}\text{O}_{40}$ | | 149.7 | 157.0 | 147.2 | |
| $\text{Tl}_4\text{SiW}_{12}\text{O}_{40}$ | | 102.5 | 97.5 | 92.7 | |

^a Cation:Proton ratio.

impurities trapped in the precipitate during the filtration due to its viscous nature. With the 50% deficit of the cation, a marked decrease now appeared for both the silver and thallium salts of the 12-tungstophosphoric acid. With a 50% excess of the cation, the AgPW salt maintained a consistent surface area while the analogous thallium salt showed a significant decrease in the surface area.

As illustrated in Figure 2.4, the pore size distribution for the salts remain virtually unchanged, despite the variation of the cation:proton ratio in the synthesis. The mean micropore radii (r_{MP}) and the powder XRD patterns (the lattice parameter (a_0) or $I[110]/I[222]$) remain similar with the relative amount of the cation employed in the preparation of the salt. However, the micropore volume (V_{MP}) follows the same trend as previously discussed with the S_{BET} observed for the various salts. In general, the largest micropore volumes for a given salt are obtained with stoichiometric quantities of the preparative reagents.

Temperature-programmed desorption (TPD) experiments were performed on the salts to confirm the presence of residual protons. Previous TPD experiments in this laboratory have shown that the 12-heteropoly acids desorb water in two temperature ranges. Water held in the solid structure by hydrogen bonding desorbs between 423K and

473K. The higher temperature peak (between 623 and 773 K) results for the associative desorption of H_2O formed from the extraction of anionic oxygen atoms by the protons.⁴² Initial results indicated that the relative amounts of the residual protons decreased with the increase of the cation ratio for the silver and thallium salts examined.

1H MAS NMR spectra were obtained for the TIPW salt series. (Figure 2.6) With an increase in the amount of cation used in the synthesis, the relative peak area attributed to the residual protons decreased. The chemical shift for the protons in the pure 12-tungstophosphoric acid has been reported at $\delta = 9.6$ ppm.⁴³ With an increase in the amount of thallium cation used in the synthesis, this resonance shifts upfield, reflecting a change in the chemical environment of the residual protons. From the spectra, it was concluded that only one type of salt was being formed. It should be noted that peaks were overlapped with a very broad peak attributed to the presence of water. This is not evident in the small chemical shift range presented in the Figure 2.6.

The chemical shift for the protons in the pure 12-tungstosilicic acid, HSiW, has been reported at $\delta = 10.9$ ppm.⁴³ For each of the two salts of the 12-tungstosilicic acid, AgSiW and TlSiW, two peaks upfield of the pure acid resonance are present in the spectrum; they appear to change in relative intensities as the amount of the cation is increased for the salt synthesis. (Figure 2.7) At this time it is not possible to determine whether the two peaks maintain their relative intensities while interchanging positions, so that the resonance further upfield shifts downfield with an increase in the cation ratio and the resonance furthest downfield shifts upfield, or a change in the product distribution is occurring. The spectrum of the AgPW salt has two resonances (Figure 2.8), a small broad resonance which appears to move downfield with the increase in the cation ratio, and a larger, more intense peak shifting upfield with the change in the cation ratio. Again, the change in the chemical shifts is not sufficiently large to determine whether the two peaks in the spectra of the 12-tungstosilicate salts are changing positions or a change in the product distribution as the cation to acid ratio is varied has occurred. Only the TIPMo salt reflected the same trend as the TIPW salt, with the chemical shift of a single resonance shifting upfield with the increase in the cation to acid ratio. (Figure 2.8) The chemical shifts for these resonances are also upfield of those reported for the protons in

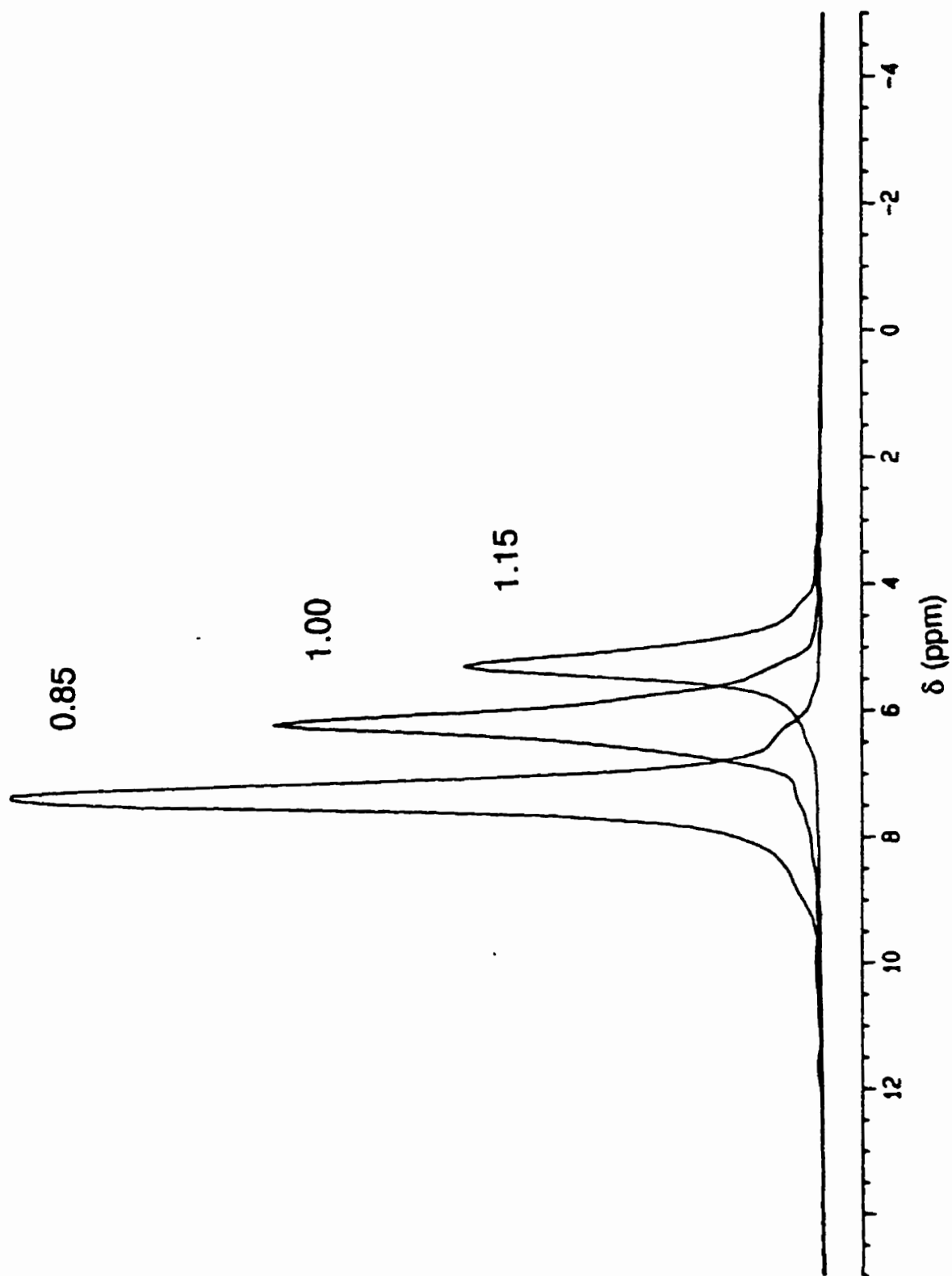


Figure 2.6 - ^1H MAS NMR spectrum of $\text{Tl}_3\text{PW}_{12}\text{O}_{40}$ for various preparative stoichiometries.

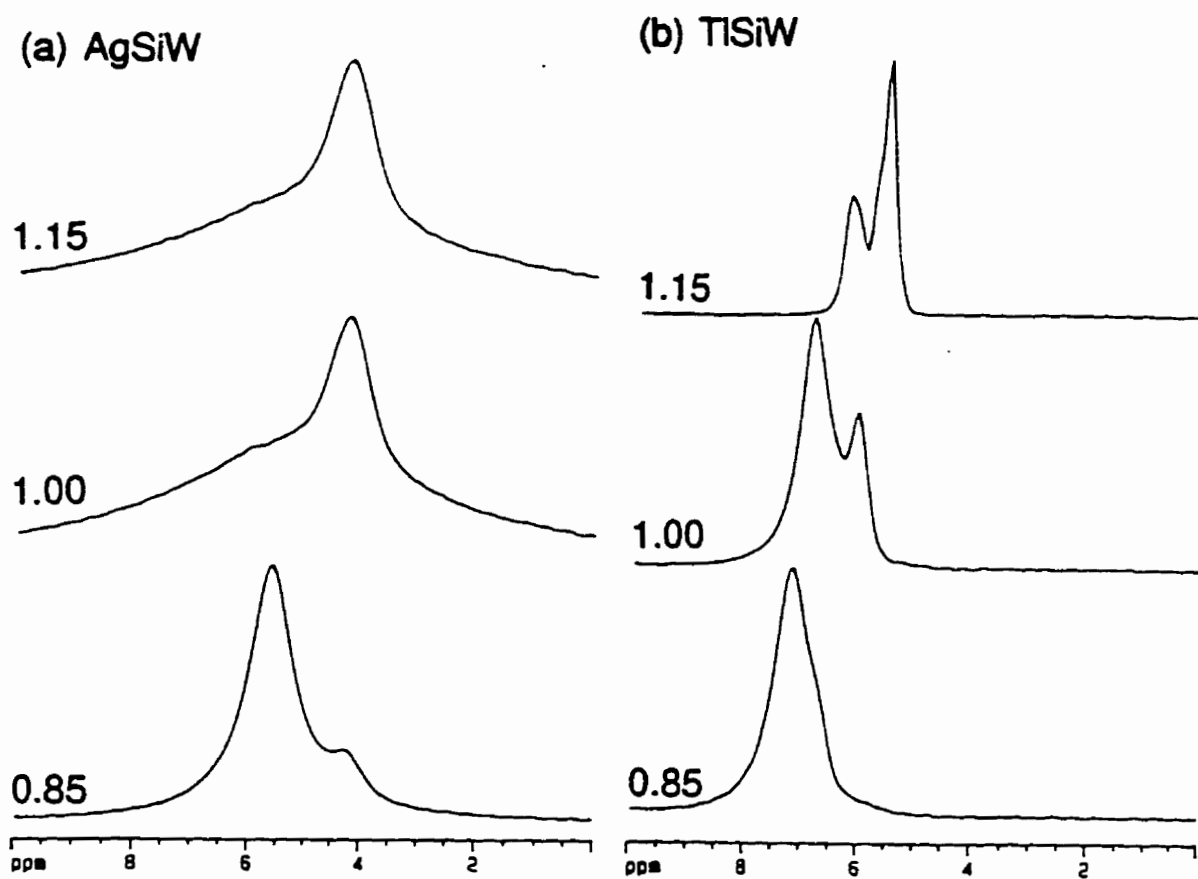


Figure 2.7 - ^1H MAS NMR spectra of $\text{Ag}_4\text{SiW}_{12}\text{O}_{40}$ and $\text{Tl}_4\text{SiW}_{12}\text{O}_{40}$ for various preparative stoichiometries.

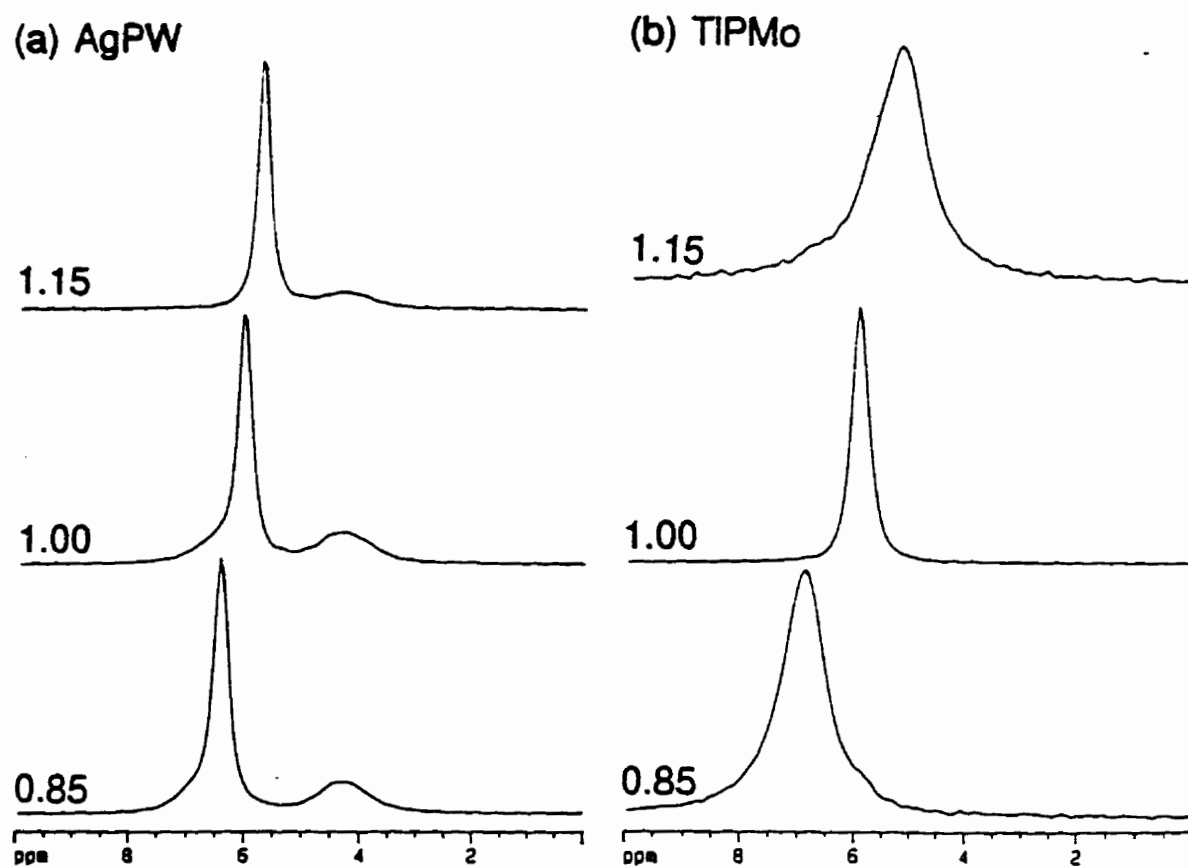


Figure 2.8 - ^1H MAS NMR spectra of $\text{Ag}_3\text{PW}_{12}\text{O}_{40}$ and $\text{Tl}_3\text{PMo}_{12}\text{O}_{40}$ for various preparative stoichiometries.

HPMo, $\delta = 7.4$ ppm.⁴⁴

2.3.4 Characterization of Surface and Bulk Properties of Mixed Salts.

In Section 2.3.1 the observation was made that the salts of 12-tungstophosphoric and 12-molybdophosphoric acids containing thallium had larger surface areas than the analogous silver salts while the salts of 12-tungstosilicic acid showed the reverse trend. However, it was observed in Section 2.3.3 that the microporous structure of the AgPW salt was dependent on the temperature at which the synthesis was carried out. As a result, a direct comparison between the surface areas could not be made for the silver and thallium salts of either acid. To obtain a correlation of the cation diameter and the resulting microporous structure, mixed stoichiometric salts were synthesized, containing different molar ratios of the silver and thallium cations.

The mixed salts of 12-tungstophosphoric acid were synthesized under identical reaction conditions used for the pure thallium salts. Table 2.10 contains a summary of the data characterizing these salts. Subscripts in the mixed salts indicate the relative amounts of the silver and thallium cations used in the preparation. (Equation 2.1) For comparison purposes, data for the AgPW salt synthesized at room temperature are also provided.

The solubility of the salts appear to be unaffected by the amount of thallium used in the synthesis. With the gradual increase in the thallium content of the salt, both the lattice parameter and the ratio of I[110]/I[222] peaks decrease. In contrast, the surface area appears to nearly double with each incremental increase of the thallium until a ratio of 1:2 for Ag:Tl is used to synthesize the salt. This value is similar to the measured surface area of TlPW.

The salts of 12-tungstosilicic acid required four equivalents of the cation (Equation 2.2) so that the mixed salts were synthesized under the identical conditions as the mixed salts of 12-tungstophosphoric acid. It should be noted that the pure AgSiW salt was not synthesized at 60 °C, but data for the salt synthesized at 25 °C was included for a comparison. (Table 2.11)

In contrast to the mixed salts of 12-tungstophosphoric acid, the yield of the mixed salts of 12-tungstosilicic acid appeared to be affected by the ratio of silver and thallium

Table 2.10 - Characterization of mixed stoichiometric salts of 12-tungstophosphoric acid.^a

| | AgPW | Ag ₂ TlPW ^b | AgTl ₂ PW ^b | TlPW |
|--------------------------------------|-------------------------|-----------------------------------|-----------------------------------|-------|
| Yield (%) | 93 (95) ^c | 91 | 88 | 98 |
| I[110]/I[222] | 0.35 (0.40) | 0.17 | 0.13 | 0.13 |
| a ₀ (Å) | 11.9 (11.8) | 11.8 | 11.7 | 11.6 |
| S _{BET} (m ² /g) | 44.1 (100.9) | 77.9 | 135.8 | 131.6 |
| S _t (m ² /g) | 45.8 (104.4) | 81.4 | 131.8 | 131.3 |
| C _{BET} | 7300 (7400) | 4400 | 1100 | 2700 |
| V _{MP} (mL/g) | 0.014 (0.037) | 0.023 | 0.049 | 0.045 |
| r _{MP} (Å) | 7.6 (7.9) | 7.7 | 8.4 | 8.2 |
| n | 1.5 (1.5) | 1.9 | 2.2 | 2.1 |

^a Preparative temperature of 60 °C.

^b Subscripts denote the relative amounts of cations used in the synthesis.

^c Values in parentheses are for salts synthesized at 25 °C.

cations, becoming more insoluble as the thallium content increased. The ratios of the indexed peaks in the powdered XRD patterns (I[110]/I[222]) indicate a microporous structure present in all of the salts and, similar to the mixed salts of HPW, there is a decrease in this peak ratio and lattice parameter with the increased relative amount of thallium used to make the salt.

It is apparent that the microporous structures of the silver salts of HSiW are more sensitive to the reaction temperature than the analogous salts of HPW. Although the

Table 2.11 - Characterization of the mixed stoichiometric salts of 12-tungstosilicic acid.^a

| | AgSiW | Ag ₃ TlSiW ^b | Ag ₂ Tl ₂ SiW ^b | AgTl ₃ SiW ^b | TlSiW |
|--------------------------------------|-------------------------|------------------------------------|--------------------------------------------------|------------------------------------|-------|
| Yield (%) | 22 (59) ^c | 66 | 88 | 95 | 93 |
| I[110]/I[222] | 0.33 (0.41) | 0.13 | 0.13 | 0.10 | 0.06 |
| a _o (Å) | 11.9 (11.8) | 11.8 | 11.7 | 11.7 | 11.6 |
| S _{BET} (m ² /g) | 0.4 (106.0) | 3.5 | 35.8 | 82.2 | 97.5 |
| S _t (m ² /g) | (108.1) | - | 36.7 | 85.7 | 96.2 |
| C _{BET} | (35600) | 3300 | 3300 | 6600 | 5000 |
| V _{MP} (mL/g) | (0.038) | - | 0.013 | 0.028 | 0.036 |
| r _{MP} (Å) | (7.6) | - | 7.7 | 7.5 | 8.0 |
| n | (1.4) | - | 1.8 | 1.6 | 1.5 |

^a Preparative temperature of 60 °C.

^b Subscripts denote the relative amounts of cations used in the synthesis.

^c Values in parentheses are for salts synthesized at 25 °C.

effects of the preparative temperature were not investigated with the stoichiometric AgSiW salt, the very low surface area for Ag₃TlSiW indicates that a similar value would most likely be obtained for the pure AgSiW salts synthesized at 60 °C. An increase in the thallium content is reflected by the increase in the measured surface area of the salt.

For all of the mixed salts, the IR spectra confirmed the presence of intact Keggin anions. Since the salts are all made at an identical reaction temperature, the effect of the increase in the average cation size directly related to increases in the surface area and micropore volume of the salts is confirmed.

2.3.5 Characterization of Surface and Bulk Properties of Cesium Salts.

In the synthesis of the salts containing the monovalent alkali metal cesium, $\text{Cs}_3\text{PW}_{12}\text{O}_{40}$ (CsPW) and $\text{Cs}_4\text{SiW}_{12}\text{O}_{40}$ (CsSiW), the structure of the Keggin anion and its orientation in the lattice structure were maintained. This was confirmed by infrared spectroscopy and powder XRD techniques. The microporous structure formed in the stoichiometric CsPW and CsSiW salts has been well characterized and reported in the literature.^{4(a),(b)} However, these salts had been isolated by evaporation of the aqueous phase. As observed with the analogous thallium salts (Section 2.3.3), isolation of the CsPW and CsSiW salts by filtration had a minimal effect on the micropore structure; similar values were obtained in the measurements of surface and bulk characteristics. (Table 2.12)

Table 2.12 - Characterization of the stoichiometric cesium salts.

| Sample | $I_{[110]}/I_{[222]}$ | a_o (Å) | n | C_{BET} | S_{BET} (m^2/g) | S_i (m^2/g) | V_{MP} (mL/g) | r_{MP} (Å) |
|------------------------------------------------------|-----------------------|--------------|-----|------------------|-----------------------------------------------|------------------------------------|---------------------------------------------|------------------------|
| $\text{Cs}_3\text{PW}_{12}\text{O}_{40}$ | 0.27 | 11.8 | 2.0 | 1700 | 147.9 | 147.1 | 0.045 | 8.3 |
| $\text{Cs}_3\text{PW}_{12}\text{O}_{40}^{\text{a}}$ | 0.27 | 11.8 | 3 | 1720 | 162.9 | 160.5 | 0.034 | 13.9 |
| $\text{Cs}_4\text{SiW}_{12}\text{O}_{40}$ | 0.22 | 11.7 | 1.8 | 2800 | 168.0 | 169.6 | 0.066 | 8.3 |
| $\text{Cs}_4\text{SiW}_{12}\text{O}_{40}^{\text{b}}$ | 0.16 | 11.8 | 2.1 | - | 150.4 | 152.7 | 0.052 | 10.5 |

^a Reference 4(a).

^b Reference 4(b).

A marked decrease in the $I_{[110]}/I_{[222]}$ peak ratio from that observed with the pure acids (Table 2.3) and an increase in the surface areas were the first indication of the microporous structure. Of the silver(I), thallium(I) and cesium(I) cations, cesium has the largest diameter. This is reflected in both types of cesium salts having the largest surface area and mean micropore radii for a series of cations with a given acid. (Tables 2.4 and 2.12)

Three cation-to-proton ratios were used in the synthesis of each cesium salt (0.85, 1.00, 1.15). As expected, the yields (based on the amount of acid initially used in the

Table 2.13 - Characterization of cesium salts of 12-tungstophosphoric acid.

| | Preparative Stoichiometry ^a | | |
|--------------------------------------|----------------------------------------|-------|-------|
| | 0.85 | 1.00 | 1.15 |
| Yield (%) | 98 | 99 | 100 |
| I[110]/I[222] | 0.25 | 0.27 | 0.24 |
| a_0 (Å) | 11.9 | 11.8 | 11.8 |
| S_{BET} (m ² /g) | 137.3 | 147.9 | 148.5 |
| C_{BET} | 1500 | 1700 | 1800 |
| V_{MP} (mL/g) | 0.043 | 0.045 | 0.043 |
| r_{MP} (Å) | 8.2 | 8.3 | 8.3 |
| n | 2.2 | 2.0 | 2.2 |

^a Cation:Proton ratio.

synthesis) increased with an increase in the amount of cation used in the synthesis. (Tables 2.13 and 2.14) The changes in the surface area (S_{BET}) in the two series with the relative amounts of cesium were again smaller than those previously reported for the ammonium salts⁴¹ with the maximum surface area obtained with the salts synthesized with an excess of the cation, although the differences between the three preparative stoichiometries are relatively small. However, the surface areas for the salts made with a stoichiometric amount and an excess of the cesium cation are very similar. Similar surface areas of two of the CsPW salts have been reported.⁴⁵ The mean micropore radii (r_{MP}) and the powder XRD patterns (the lattice parameter a_0 and I[110]/I[222]) remain virtually unchanged with the amount of the cation employed in the preparation of the salt, although there is a slight decrease in the mean micropore radius as the cation:proton ratio increases for the CsSiW series. (Tables 2.13 and 2.14) As noted with the silver and thallium salts, the micropore volume (V_{MP}) follows the same trend as discussed with the S_{BET} observed for the various salts.

¹H MAS NMR spectra were obtained for the three stoichiometries (0.85, 1.00,

Table 2.14 - Characterization of cesium salts of 12-tungstosilicic acid.

| | Preparative Stoichiometry ^a | | |
|--------------------------------------|----------------------------------------|-------|-------|
| | 0.85 | 1.00 | 1.15 |
| Yield (%) | 91 | 100 | 101 |
| I[110]/I[222] | 0.21 | 0.22 | 0.17 |
| a ₀ (Å) | 11.7 | 11.7 | 11.7 |
| S _{BET} (m ² /g) | 161.5 | 168.0 | 172.3 |
| C _{BET} | 2900 | 2800 | 2700 |
| V _{MP} (mL/g) | 0.065 | 0.066 | 0.070 |
| r _{MP} (Å) | 8.6 | 8.3 | 8.0 |
| n | 1.9 | 1.8 | 1.8 |

^a Cation:Proton ratio.

1.15) of the CsPW and CsSiW salts. (Figure 2.9) For both salts, the resonance for the residual protons is shifted upfield from that which is observed for the pure acids ($\delta = 9.6$ ppm for HPW and $\delta = 10.9$ ppm for HSiW).⁴³ The resonance continues to shift upfield with the increase in the amount of cesium used in the synthesis. As observed with the TIPW series (Section 2.3.3), with the increase in the amount of cesium cation used in the synthesis, the relative area attributed to the residual protons decreased for both cesium salts.

Consistent with the TlSiW and AgSiW salts, two peaks are present for all three ratios of the CsSiW salt examined, although the relative intensities within each spectrum do not change with the increase of the cesium content. In contrast, the 0.85 CsPW salt has a shoulder present which disappears and the resonance becomes sharper when a stoichiometric or excess amount of the cation is used. The relative area calculated for the stoichiometric salt is less than that calculated for the salt with a cation to proton ratio of 0.85, due to the broadness of the latter peak. In all spectra the peaks observed were overlapped with a very broad peak attributed to the presence of water, which is not

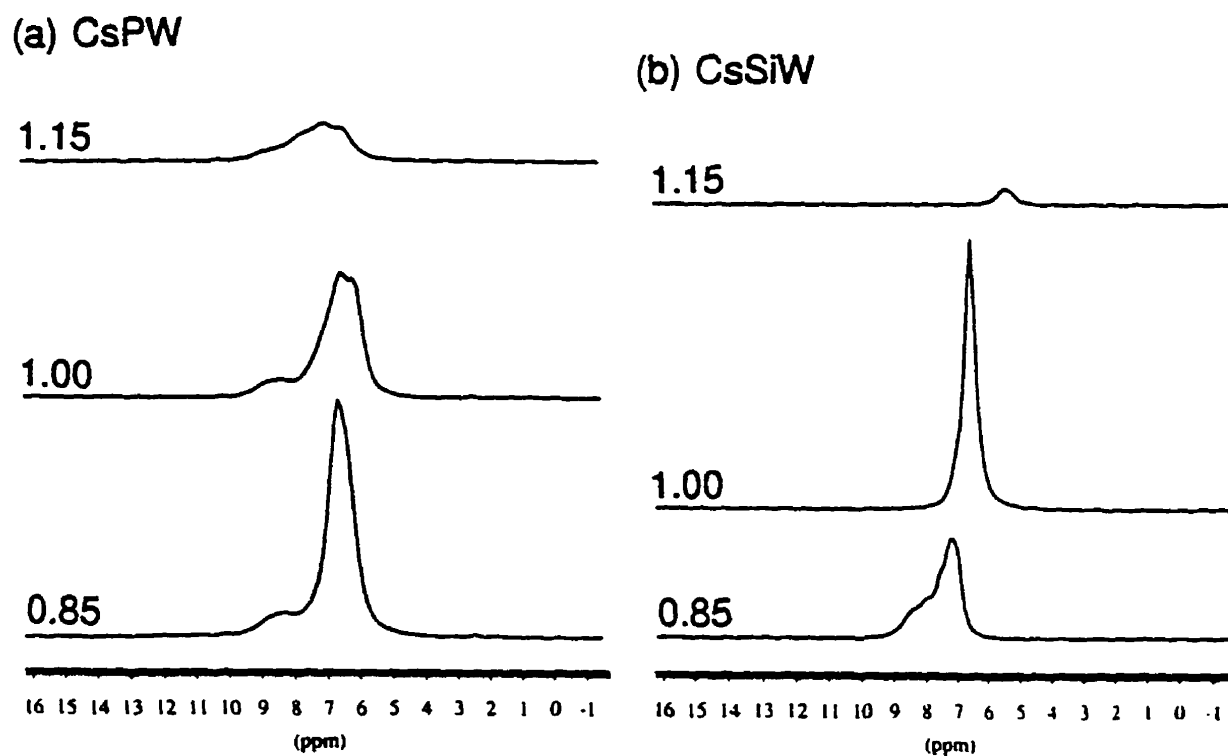


Figure 2.9 - ^1H MAS NMR spectra of $\text{Cs}_3\text{PW}_{12}\text{O}_{40}$ and $\text{Cs}_4\text{SiW}_{12}\text{O}_{40}$ for various preparative stoichiometries.

evident in the small chemical shift range present in Figure 2.9.

2.4 Discussion

Characterization of the salts provides evidence for the presence of micropores in all of the salts synthesized, except for AgPMo. This was not unexpected since it has been previously reported that the silver cation has a tendency to degrade the 12-molybdophosphoric Keggin unit,³⁸ which is consistent with the loss of integrity of the Keggin anion indicated by the infrared spectrum and the absence of the characteristic Pn3m pattern in the powder XRD pattern.

From the powder XRD patterns of the remaining five salts, it is postulated that the cations are occupying the positions in the solid structure previously occupied by the protons, as depicted in Figure 1.3. The smaller lattice parameter (a_0) measured for these substituted salts, in comparison with the pure acids, can be attributed to the fact that the cations substituted into the structure may not be hydrated, as the protons are, so that the repeating unit in the structure is smaller due to the loss of water.

It can be concluded that microporous structure can be created with both silver and thallium cations and, by extrapolation, from any cations of 1B and 3B groups and therefore is not restricted to salts of the alkali metals. The larger thallium cation presumably permits the Keggin anions to rotate and translate within the lattice structure, removing the barriers between the interstitial voids, and creating larger channels through the lattice. This is evident with the thallium salts which have a greater surface area, micropore volume, and mean micropore radius, than those found for the analogous silver salts and the cesium salts having the largest surface area, micropore volume, and mean micropore radii of the three cations examined. The increase of the surface area and micropore volume, as the thallium content in the mixed salts of $\text{Ag}_{3-x}\text{Tl}_x\text{PW}_{12}\text{O}_{40}$ and $\text{Ag}_{4-x}\text{Tl}_x\text{SiW}_{12}\text{O}_{40}$ is increased, also reflects the correlation between cation diameter and the resulting micropore structure.

As noted in Table 2.3, the relative intensities for the indexed peaks of [110] and [222] ($I[110]/I[222]$) are smaller where a microporous structure is present. It has also been noted that an inverse relationship exists with the micropore volume (V_{MP}) and the

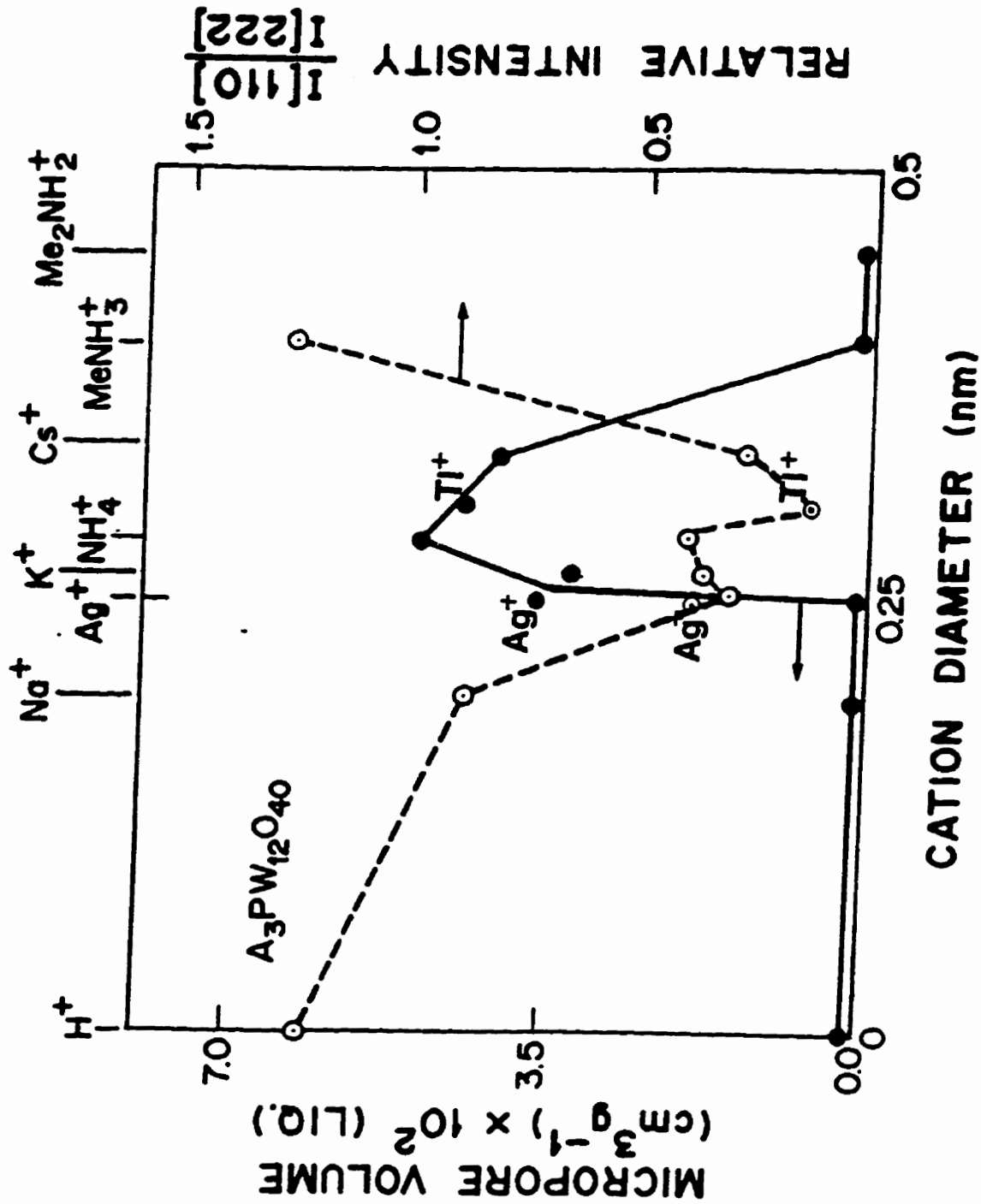


Figure 2.10 - Micropore volumes and XRD $I[110]/I[222]$ ratios for stoichiometric silver and thallium salts of HPW together with values reported earlier for other cations.^{4,5}

relative intensity, $I[110]/I[222]$, for microporous salts.⁵ As illustrated in Figure 2.10, the data for the silver(I) and thallium(I) salts are in good agreement with other salts containing monovalent cations. The inverse relationship between the micropore volume and $I[110]/I[222]$ is quite apparent, confirming the presence of a microporous structure for these salts.

The direct relationship of the cation diameter with the surface area of the salt produced has been previously noted for salts synthesized with other monovalent cations.^{4(a),(b)} The dependence on the cation diameter is clearly evident in Figure 2.11. The data for the salts containing the silver and thallium cations correlate well with previous data of the salts containing monovalent cations, including cesium, indicating that the larger cations facilitate larger pores, created by rotation and translation of the Keggin anions.

Previous work in the laboratory has proven a direct relationship between the mean micropore radius (r_{MP}) and the value of n , the number of adsorbed monolayers determined by the finite BET equation,^{4(a),(c),(d)} as would be expected where microporous structures are present. When N_2 is the adsorbate, adsorption layer thickening will ultimately cause all of the micropores present in a solid to be filled completely. For a given anion, the value of n increases with the increase in cation diameter. The present results for silver and thallium salts are also consistent with this correlation. (Figure 2.12)

The unexpected high surface area of the AgPW in comparison to previous literature reports^{4(a),25(c)} may, at least in part, be attributed to the separation of the precipitate by filtration, in contrast to the somewhat higher temperatures as previously employed where the liquid phase was removed by evaporation. However, characterization of the AgPW salt isolated by evaporation indicated no evidence of the degradation of the Keggin anion structure as found with AgPMo, possibly reflecting the higher thermal stability of the tungsten-containing anion. Although low microporosity and low surface area were noted, unexpectedly a low $I[110]/I[222]$ ratio was present in the powder XRD pattern.^{4(b)} It was concluded that the anion orientation is favourable for micropore formation, but the width of such pores is not sufficiently large to allow penetration by nitrogen molecules at 77 K,^{4(b)} thus resulting in the low surface area measured. Further

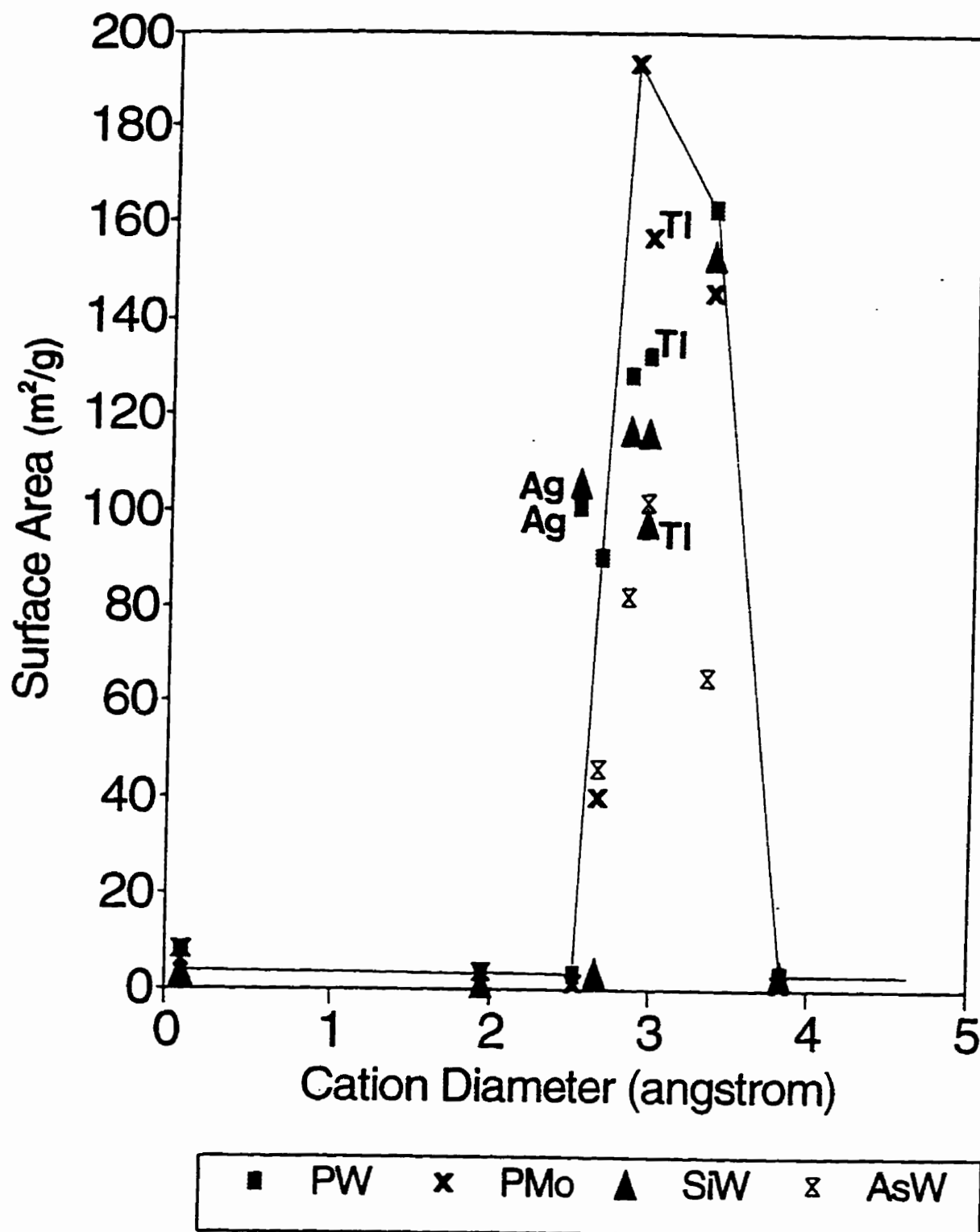


Figure 2.11 - Surface areas and cation diameters for the silver and thallium salts of the three heteropoly acids. Values obtained previously are included for comparison.^{4,5}

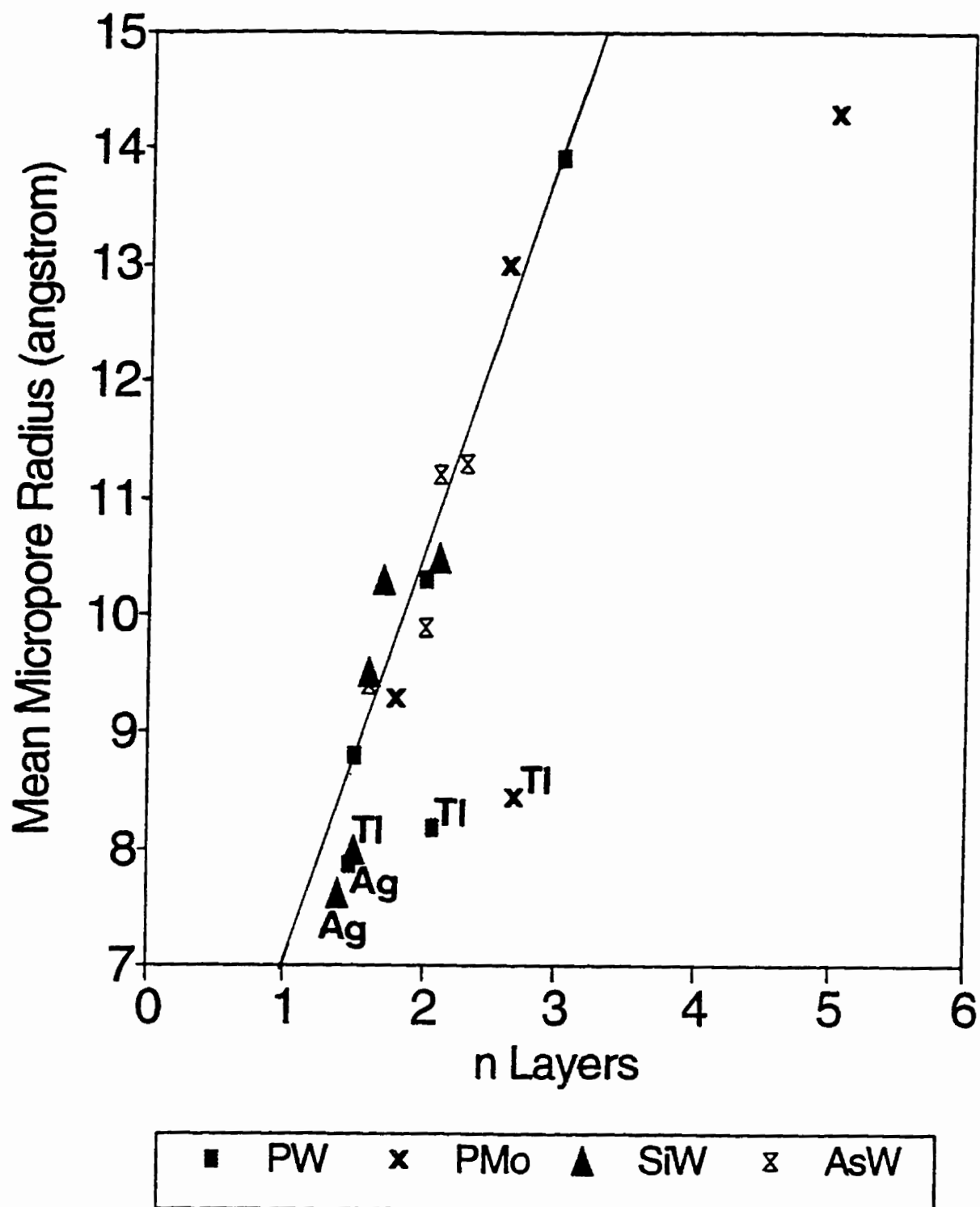


Figure 2.12 - Mean micropore radii versus number of layers (n) from finite layer BET equation for silver and thallium salts of the three acids with comparison to earlier values.^{4,5}

investigations concluded that the AgPW salt is sensitive to the temperature at which it is synthesized, and that the evaporation method enhances the trapping of impurities in the isolated solid, thus blocking the channels created by the microporous structure. The TIPW salt is not affected by temperature to the same extent.

A significant decrease in the surface area was previously observed for the ammonium salts synthesized with a stoichiometric deficiency of the cation and which were isolated by evaporation.⁴¹ However in the present work, the salts isolated by filtration show a less pronounced shift in the surface area. While it is tentatively concluded that filtration, in contrast to evaporation, may minimize the concentration of peripheral impurities on the solid, the differences in microporosity are difficult to rationalize on this basis.

A study of various monovalent salts of 12-molybdophosphoric acid, by x-ray phase analysis (XPA) and x-ray photoelectron spectroscopy (XPS), revealed that in some cases a two-phase solid resulted when isolating the salt by evaporation.⁴⁶ The potassium (K^+), cesium (Cs^+) and ammonium (NH_4^+) salts of 12-molybdophosphoric acid are not soluble in water, and upon an addition of the cation, in a 67% deficit of the cation to acid ratio, a precipitate of the trisubstituted salt forms. When drying the mixture by evaporation, the unreacted acid, left in solution, is adsorbed onto the insoluble salt particles, forming a second layer. This outer layer of the pure 12-molybdophosphoric acid contributes to the low surface area obtained for these salts. In the present work filtration is believed to minimize the formation of an outer layer on the trisubstituted salt. This may explain the larger surface area characterized for AgPW isolated by filtration, in comparison to that separated by evaporation. However, as has been pointed out in earlier work^{4,5,41} precipitation in the presence of either a deficit or excess of the cation would presumably trap the residual protons, in the former system, or the excess cations, in the latter, within the crystallographic structure during precipitation and consequently lead to a blocking of the micropores and hence a decrease in surface areas. This phenomenon could be perceived as the formation of a solid solution rather than that of two phases.

Although surface areas and mean micropore radii show little or no dependence on the relative quantities of the preparative reagents, the mean micropore volumes for a given

salt are generally at a maximum where stoichiometric quantities of the preparative reagents have been employed. Where the cations are present in deficit, residual protons may block the channels whereas with excess cations these produce the same effect. Both the results of TPD experiments and ^1H MAS NMR spectra indicate that residual protons are present in the solids.

The ^1H MAS NMR spectra of the TIPW and TIPMo show only one chemical environment for residual protons in the lattice framework while the other salts were noted as having two different environments. The latter may result from two different stoichiometries of the salt coprecipitating simultaneously due to similar solubility limits in water. With changes in the amount of cation used in the synthesis, one stoichiometry may be preferentially formed over the other. Alternatively, only one stoichiometry of the salt may be formed but the residual protons are capable of residing in more than one site in the expanded form of the lattice framework, depicted in Figure 1.3. These sites, within the lattice structure, may differ slightly in chemical environment depending upon the number of cations substituted into neighbouring sites. With an increase in the ratio of cation to acid used in the synthesis, one site may become preferred over the other by the residual protons, accounting for the change of peak intensities and drifting chemical shifts recorded. The latter rationalization can account for both the drifts of the chemical shifts, especially when only one peak is present in the spectrum (as with TIPW and TIPMo), and the change of peak intensities in the spectrum with the variation of the cation to acid ratio used in the synthesis. If two different stoichiometries of the salt were being formed, the resulting spectra for the powder XRD patterns would be expected to indicate the amorphous nature of the isolated solid.

As noted earlier, 12-tungstophosphoric acid has a chemical shift of 9.6 ppm⁴³ while 12-tungstosilicic and 12-molybdophosphoric acids have chemical shifts of 10.9 ppm⁴³ and 7.4 ppm⁴⁴, respectively. All of the salts examined have smaller chemical shifts, indicating that replacement of the protons by the monovalent cations is affecting the environment of the protons remaining in the structure and their acidity. Although quantitative details have yet to be clarified, it is currently believed that increases in the protonium chemical shift correspond to increases in Bronsted acid strength.^{47,48} A number of arguments have been

presented in support of the suggestion that the chemical shift can serve as a measure for acid strength.⁴⁹ This was initially observed in zeolites where the acidic strength of the OH group correlated strongly with the chemical shift of their protons in ¹H MAS NMR.⁴⁸ Hence, the smaller proton chemical shifts observed in the present work can, at least tentatively, be interpreted as indicative of decreased acidic strengths of the residual protons in the cesium, silver and thallium salts. Although the source of this effect is unclear and will be examined in more detail in Chapters Five and Six, two possibilities can be advanced. The heavier cations may have a direct effect on the hydrogen atoms by their occupation of sites neighbouring the protons in the lattice or, alternatively, an indirect effect through perturbation of the electron densities of the terminal oxygen atoms in the Keggin anion, with which the hydrogen atoms are associated and, consequently, a retardation of the mobility of the protons.

2.5 References

1. G.M. Brown; M.-R. Noe-Spirlet; W.R. Busing; H.A. Levy. *Acta Cryst.*, **B33**, 1038 (1977).
2. G.B. McGarvey; N.J. Taylor; J.B. Moffat. *J. Mol. Catal.*, **80**, 59 (1993).
3. J.C. Clark and D. Hall. *Acta Crystallogr.*, **B32**, 1545 (1976).
4. (a) J.B. McMonagle and J.B. Moffat. *J. Colloid Interface Sci.*, **101**, 479 (1984).
(b) D.B. Taylor; J.B. McMonagle; J.B. Moffat. *J. Colloid Interface Sci.*, **108**, 278 (1985).
(c) G.B. McGarvey and J.B. Moffat. *J. Colloid Interface Sci.*, **125**, 51 (1988).
(d) G.B. McGarvey and J.B. Moffat. *J. Catal.*, **130**, 483 (1991).
(e) J.B. Moffat. *Polyhedron*, **5**, 261 (1986).
5. J.B. Moffat. *J. Mol. Catal.*, **52**, 169 (1989).
6. C. Tourneux and C. Devin. *Acad. Sci. Compt. Rend.*, **232**, 2430 (1951).
7. C. Tourneux and C. Devin. *Acad. Sci. Compt. Rend.*, **233**, 43 (1951).
8. S.J. Gregg and R. Stock. *J. Chem. Soc. Faraday Trans.*, **53**, 1355 (1957).
9. S. Brunauer; L.S. Demming; W.E. Demming; E. Teller. *J. Amer. Chem. Soc.*, **62**, 1723 (1940).
10. K.S.W. Sing in "Characterization of Catalysts." (J.M. Thomas and R.M. Lambert, Eds.) J. Wiley and Sons: New York, 1980, p.12.
11. S.J. Gregg and M.M. Tayyab. *J. Chem. Soc. Faraday. Trans. I*, **74**, 348 (1978).
12. M. Misono and Y. Yoneda. *Chem. Lett.*, 709 (1978).
13. (a) M. Misono. *Catal. Rev. Sci. Eng.*, **29**, 269 (1987).
(b) M. Misono. *Catal. Rev. Sci. Eng.*, **30**, 339 (1988).
14. J.L. Bonardet; J. Fraissard; G.B. McGarvey; J.B. Moffat. *J. Catal.*, **151**, 147 (1995).
15. J.A. Santos. *Proc. Roy. Soc.*, **A 150**, 309 (1935).
16. J.C.A. Boeyens; G.J McDougall; J. Van R. Smit. *J. Solid State Chem.* **18**, 91 (1976).

17. M. Akimoto; T. Tsuchida; K. Sato; E. Echigoya. *J. Catal.*, **72**, 83 (1981).
18. H. Hayashi and J.B. Moffat. *J. Catal.*, **81**, 61 (1983).
19. T. Baba; H. Watanabe; Y. Ono. *J. Phys. Chem.*, **87**, 2406 (1983).
20. Y. Saito and H. Niiyama. *J. Catal.*, **106**, 329 (1987).
21. T. Matsuda; M. Sato; T. Kanno; H. Muira; K. Sugiyama. *J. Chem. Soc. Faraday Trans. I*, **77**, 3107 (1981).
22. G.B. McGarvey and J.B. Moffat. *Catal. Lett.*, **16**, 173 (1992).
23. A. Kasai; T. Okuhara; M. Misono; Y. Yoneda. *Chem. Lett.*, 449 (1981).
24. (a) Y. Ono; T. Baba; J. Sakai; T. Keii. *J. Chem. Soc. Chem. Commun.*, 400 (1981).
(b) T. Baba; J. Sakai; Y. Ono. *Bull. Chem. Soc. Jpn.*, **55**, 2657 (1982).
(c) G. Öhlmann; H. Ehwald; V.S. Musykantov. *React. Kinet. Catal. Lett.*, **35**, 173 (1987).
25. (a) M. Ai. *Appl. Catal.*, **4**, 245 (1982).
(b) T. Baba; H. Watanabe; Y. Ono. *J. Phys. Chem.*, **87**, 2406 (1983).
(c) A. Anwar and A.A. Abdel-Ghaffar. *J. Chim. Phys.*, **89**, 681 (1991).
26. T. Baba; M. Nomura; Y. Ono; Y. Kansaki. *J. Chem. Soc. Faraday Trans.*, **88**, 71 (1992).
27. (a) M. Ai. *J. Catal.*, **67**, 110 (1981).
(b) M. Ai. *J. Catal.*, **71**, 88 (1981).
28. K. Eguchi; I. Aso; N. Yamazoe; T. Seiyama. *Chem. Lett.*, 1345 (1979).
29. I.V. Kozhevnikov; A. Sinnema; H. van Bekkum. *Catal. Lett.*, **34**, 213 (1995).
30. (a) W.P. Thistlethwaite and H. Buchwald. *J. Inorg. Nucl. Chem.*, **7**, 292 (1958).
(b) W.P. Thistlethwaite and H. Buchwald. *J. Inorg. Nucl. Chem.*, **5**, 341 (1958).
(c) W.P. Thistlethwaite and W.T. Watson. *J. Inorg. Nucl. Chem.*, **24**, 1559 (1962).
31. (a) C. Rocchiccioli-Deltcheff; R. Thouvenot; R. Frank. *Spectrochimica Acta*, **32A**, 587 (1976).
(b) C. Rocchiccioli-Deltcheff; M. Fournier; R. Frank; R. Thouvenot. *Inorg. Chem.*, **22**, 207 (1983).
32. C. Rocchiccioli-Deltcheff and R. Thouvenot. *J. Chem. Research (S)*, 46 (1977).

33. S. Brunauer; P.H. Emmett; E. Teller. *J. Am. Chem. Soc.*, **60**, 309 (1938).
34. S.J. Gregg and K.S.W. Sing. "Adsorption, Surface Area and Porosity." Academic Press Inc. (London) Ltd.: London, 1982.
35. A. Lecloux and J.P. Pirard. *J. Colloid Interface Sci.*, **70**, 265 (1979).
36. R.Sh. Mikhail; S. Brunauer; E.E. Bodor. *J. Colloid Interface Sci.*, **26**, 45 (1968).
37. R.Sh. Mikhail; S. Brunauer; E.E. Bodor. *J. Colloid Interface Sci.*, **24**, 451 (1967).
38. G. Tsigdinos. *Ind. Eng. Chem., Prod. Res. Devel.*, **13**, 267 (1974).
39. D.C. Harris. "Quantitative Chemical Analysis."; 2 ed., W.H. Freeman and Co.: New York, 1987, pp.48-55.
40. M. Akimoto; K. Shima; H. Ikeda; E. Echigoya. *J. Catal.*, **86**, 173 (1984).
41. D. Lapham and J.B. Moffat. *Langmuir*, **7**, 2273 (1991).
42. B.K. Hodnett and J.B. Moffat. *J. Catal.*, **88**, 253 (1984).
43. L.C. Jozefowicz; H.G. Karge; E. Vasilyeva; J.B. Moffat. *Microporous Materials*, **1**, 313 (1993).
44. V.M. Matikhin; S.M. Kulikov; A.V. Nosov; I.V. Kozhevnikov; I.L. Mudrakovsky; M.N. Timofeeva. *J. Mol. Catal.*, **60**, 65 (1990).
45. N. Essayem; G. Coudurier; M. Fournier; J.C. Vedrine. *Catal. Lett.*, **34** 223 (1995).
46. (a) I.N. Staroverova; M. Yu. Kutyrev; L.G. Khvtisiashvili. *Kinet. Catal.*, **27**, 596 (1986).
(b) I.N. Staroverova; M. Yu. Kutyrev; A. Yu. Stakheev. *Kinet. Catal.*, **33**, 101 (1992).
47. H. Pfeifer in "Acidity and Basicity of Solids: Theory, Assessment and Utility." Kluwer: Dordrecht, 1994, p.255.
48. D. Freude; H. Ernst; T. Mildner; H. Pfeifer; I. Wolf. *Stud. Surf. Sci. Catal.*, **90**, 105 (1993).
49. H. Pfeifer; D. Freude; J. Karger. *Stud. Surf. Sci. Catal.*, **65**, 89 (1991).

CHAPTER 3

Synthesis and Characterization of Copper(II) and Copper(I) Salts

3.1 Introduction

As discussed in the preceding two chapters, high surface area, microporous solids have been formed for 12-heteropoly oxometalate salts containing monovalent cations of either alkali metals or ammonium.¹⁻³ The transition metal elements of silver(I) and thallium(I) also successfully form microporous structures in salts containing the Keggin anion, as evident in Chapter Two.⁴ The successful preparation of a microporous solid containing the silver(I) cation suggests that it may be possible to form a salt containing the monovalent copper(I) cation, also of group 1B in the periodic table. If a microporous structure is present in the copper(I) salt, the effect of changing the oxidation state from Cu(I) to Cu(II) on the morphology of the salt could be examined. Of particular interest would be whether or not the microporous structure is retained as the oxidation state of the copper cation is increased.

Characterization of the composition of the copper(II) 12-molybdophosphoric salt ($\text{Cu}_3(\text{PMo}_{12}\text{O}_{40})_2$) was first examined by Thistlethwaite,⁵ who determined that the composition of the metal cation to anion ratio was 2.80 despite being prepared from a solution containing three equivalents of base per mole of acid. This salt was investigated as a catalyst for the oxidation of butadiene⁶ and methacrolein,⁷ dehydration of 2-propanol^{7(b),8} and the oxidative dehydrogenation of isobutyric acid.⁹ It was proposed that the copper(II) ions increased the redox ability of the catalyst by acting as an electron reservoir, providing a route for electron delocalization, and to facilitate the transfer of electrons to the molybdenum ion in a reducing environment.¹⁰ However, in some systems, the copper(II) salt exhibited a decrease in thermal stability in comparison to the parent acid.^{6,7(b)} The copper(II) salt of 12-tungstophosphoric acid was explored as a catalyst in the dehydration of 2-propanol¹¹ and 1-butanol.¹² The isomerization of 1-butene and *cis*-2-butene were examined with the copper(II) salts of 12-tungstophosphoric acid¹¹ and 12-molybdophosphoric acid.¹² Dehydration of methanol was facilitated by the copper(II) salts of 12-tungstophosphoric and 12-tungstosilicic acids,¹³ along with the supported

molybdenum-containing analogues of these salts.¹⁴ Although some of the surface areas of these copper(II) salts have been noted in passing^{7(a),10,11,13,15} and the infrared spectrum of $\text{Cu}_3(\text{PW}_{12}\text{O}_{40})_2$ recorded,¹⁵ little or no characterization of the surface and bulk properties has been carried out in order to explain the differences in the catalytic activity as compared with the parent acids.

The introduction of a divalent cation would be difficult, if not impossible, on both electrical neutrality and geometrical grounds. Investigations of the divalent alkaline earths salts of 12-heteropoly oxometalates proved unsuccessful in the establishment of a microporous structure¹⁶ and single x-ray diffraction studies revealed that the Ba^{2+} cation of the $\text{Ba}_3(\text{PW}_{12}\text{O}_{40})_2$ did not occupy the proton's position and there was no evidence of the divalent cation in the lattice network.¹⁷ McGarvey and Moffat concluded that the solids were mixtures of the 12-heteropoly acids and the divalent cations of the alkaline earth metals.^{16,17} As a result, it is doubtful that the copper(II) cation could be incorporated into the lattice structure with the Keggin anion. However the formation of a salt containing the monovalent copper cation may be possible.

Previously, in this laboratory, ion exchange had been performed with the salts of the 12-heteropoly oxometalates containing monovalent cations of alkali metals and ammonium.¹⁸ These salts were solids, insoluble in water, and the exchange occurred in a solid-liquid phase. Although 100% exchange of the cations could not be achieved, the resulting solid retained a microporous structure and high surface area. The extent of the exchange was dependent upon the relative sizes of the entering and leaving cations, with the maximum degree of exchange decreasing as the radius of the cation in the solid phase increased.¹⁸ Since the copper(I) oxidation state quickly converts to copper(II) in water¹⁹ the synthesis of the copper(I) salt of the 12-tungstophosphoric acid in an aqueous solution appears to be less than straightforward.

Solid-state ion exchange appeared to proceed more readily than the conventional exchange in a suspension system for many zeolites. Karge and Beyer²⁰ have provided a review of cation incorporation into zeolites by solid state reactions. Clearfield *et al.*²¹ were the first to incorporate transition metal cations into partially exchanged sodium zeolites via solid-state reactions while Rabo²² examined similar reactions with proton

containing samples of zeolites and halide salts, with the evolution of HCl(g). The technique involves finely dispersed powders of the zeolite and the salt (preferably a halide or oxide) of the cation being mixed and heated, either in a stream of inert gas or in a high vacuum. The temperature required to achieve the required exchange depends on the nature of both ions.²⁰ Solid state exchange was particularly useful for the incorporation of copper(I) cations into zeolites without significant change of the oxidation state of the copper(I) cation to either Cu(II) or Cu(0). Previously copper(I) zeolites had been prepared by reducing the conventionally ion exchanged copper(II) zeolites with H₂, Co or CO-NH₃,^{23,24} but it was difficult to control the extent of the reduction to maintain the cations in only the copper(I) state or maintain the structure of the zeolite.²³

The objective of this chapter is to prepare a high surface area, microporous solid containing the monovalent copper(I) cation and to monitor the effect of changing the oxidation state of the cation on the micropore structure. A method similar to the solid state ion exchange procedure reported by Spoto *et al.*²⁵ was used to synthesize the copper(I) salt of 12-tungstophosphoric acid. The copper(I) exchange reaction was also carried out with ammonium 12-tungstophosphate, based on the report by Karge *et al.* that the copper(I) cation was successfully exchanged with the ammonium form of zeolite Y.²⁶ Salts of the three heteropoly acids (12-tungstophosphoric acid, 12-tungstosilicic acid, and 12-molybdophosphoric acid) containing the divalent copper(II) cation were also synthesized by the traditional method⁵⁻¹⁴ to provide characterization of the surface and bulk properties of the copper(II) salts for comparison.

3.2 Experimental

3.2.1 Synthesis

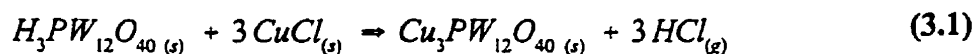
12-Tungstophosphoric acid (H₃PW₁₂O₄₀) and 12-tungstosilicic acid (H₄SiW₁₂O₄₀) were obtained from BDH (Anala R Grade) while 12-molybdophosphoric acid (H₃PMo₁₂O₄₀) was purchased from Aldrich. Copper(II) nitrate (Cu(NO₃)₂·H₂O) was obtained from BDH (Anala R Grade) while copper(II) carbonate (CuCO₃·Cu(OH)₂) and copper(I) chloride (CuCl) were purchased from Aldrich. Ammonium nitrate (NH₄NO₃) was obtained from Mallinckrodt. The salts supplying the cations were used as received

while the acids were recrystallized prior to use. Helium and nitrogen were purchased from Praxair.

The stoichiometric copper(II) salts of the three acids (abbreviated as CuPW, CuSiW and CuPMo, respectively) were synthesized from either copper(II) nitrate or copper(II) carbonate following a procedure similar to the method used to synthesize the silver salts, as discussed in Section 2.2.1. The desired amount of copper(II) nitrate or copper(II) carbonate, dissolved in 2.0 - 4.0 mL of distilled deionized water, was added dropwise to an aqueous solution of the appropriate acid ($\approx 3\text{g}$ or $\approx 1 \times 10^{-3}$ mol), dissolved in 4.0 mL of distilled deionized water. After permitting the solution to stir for ten minutes, at room temperature, a precipitate did not form. The solution was transferred to a crucible with a minimum amount of water (2 x 2.0 mL) and then evaporated to dryness over a hot water bath. The isolated solid was dried overnight under a low vacuum at room temperature.

The stoichiometric ammonium salt of 12-tungstophosphoric acid was made following the identical method as outlined for the synthesis of the silver(I) salts. (Section 2.2.1) Since a precipitate formed with the addition of the ammonium nitrate solution, the salt was isolated by gravimetric filtration and dried overnight under a low vacuum at room temperature.

The stoichiometric ($\text{Cu}_3\text{PW}_{12}\text{O}_{40}$) and deficit ($\text{Cu}_2\text{HPW}_{12}\text{O}_{40}$) copper(I) salts of 12-tungstophosphoric acid were prepared by a procedure based on the method used by Spoto *et al.* for zeolites.²⁵ (Equation 3.1) Approximately 0.5 g of 12-tungstophosphoric acid was placed in a glass flask, similar to the sample holder used for the nitrogen adsorption-desorption isotherms, equipped with a stopcock. The appropriate amount of CuCl(s) was added and the result was evacuated on a vacuum line ($\approx 10^{-4}$ torr). After heating to 300 °C for two hours, while maintaining a vacuum, the flask was cooled to room temperature for a further hour. The sample flask was then transferred immediately to the nitrogen adsorption-desorption apparatus without exposure to air.



This procedure was repeated with the use of the ammonium 12-tungstophosphoric

salt instead of the pure acid and a stoichiometric amount of copper(I) chloride. The final modification to this experiment employed the acid or ammonium salt prepared by outgassing at 10^{-4} torr for two hours at 200 °C. After cooling to room temperature, a stoichiometric amount of copper(I) chloride was added to the flask and the solid mixture was left under vacuum at room temperature for one week.

3.2.2 Characterization Techniques

Infrared spectra were recorded, from either nujol mulls or KBr disks of the salts, for the fingerprint region of the 12-heteropoly anions ($2000 - 400 \text{ cm}^{-1}$) on a Bomem MB-100 FT-IR spectrometer. Powder X-ray diffraction patterns were recorded on a Siemens D500 diffractometer using $\text{CuK}\alpha$ radiation and a graphite monochromator, at 30 mA and 40 kV. The samples were taken directly from the desiccator and the spectrum recorded at room temperature.

Nitrogen adsorption-desorption isotherms were measured on a standard volumetric glass system as depicted in Figure 2.1. The experimental procedure followed to obtain the isotherm is described in Section 2.2.2 except that the pretreatment was not performed on the samples from the solid state ion exchange experiments with copper(I) chloride.

3.3 Results

3.3.1 Characterization of Surface and Bulk Properties of Copper(II) Salts

Contrary to the silver and thallium salts of the three heteropoly acids investigated, the copper(II) salts did not form a precipitate with the addition of the copper(II) solution to the acid solution. Isolation of the salts by evaporation of the aqueous phase resulted in solids heterogeneous in colour. The copper(II) salts of 12-tungstophosphoric and 12-tungstosilicic acids were blue and white in colour while salts of 12-molybdophosphoric acid were green and brown.

In the literature most of the copper(II) salts of 12-heteropoly acids had been prepared using copper(II) carbonate as a source for the copper(II) ions,^{5-7,9-14} since evaporation of the aqueous phase would permit the spectator carbonate ions to be removed in the form of carbon dioxide gas. However, with recent studies indicating that the

integrity of the Keggin anion is dependent upon the pH of the solution,²⁷ there was some concern that the addition of carbonate may cause the solution to become too basic. As a result, the nitrate salt of copper(II) was also investigated. In synthesizing the salts, the copper(II) nitrate salt dissolved readily in water while the copper(II) carbonate formed a suspension. With the addition of the latter to the acid solution, bubbles formed and the solution became clear after several minutes of stirring.

Infrared spectroscopy provides five characteristic bands for the Keggin anion in the region of 2000 to 400 cm^{-1} ,²⁸ two of which are the triply degenerate asymmetric stretch of the central atom-oxygen bond of the central tetrahedron (denoted as $\nu_{\text{as}}(\text{X-O})$) and the asymmetric stretch of the peripheral atom and the terminal oxygen atom bond (denoted as $\nu_{\text{as}}(\text{M-O})$). Completing the set are two bands associated with the peripheral metal-oxygen-peripheral metal bonds, accompanied by some bending character.²⁸ The higher frequency, denoted as $\nu_{\text{as}}(\text{M-O-M})_{\text{inter}}$ involves the peripheral atom-oxygen atom bridge between the octahedra in adjacent M_3O_{13} trimetalate units while the lower frequency, $\nu_{\text{as}}(\text{M-O-M})_{\text{intra}}$, results from the vibration of the metal-oxygen-metal bridge between octahedra which share edges with one another within the same M_3O_{13} unit.

The infrared spectra of the copper(II) salts, prepared as nujol mulls, contained characteristic bands of the Keggin anions in the region of 2000 - 400 cm^{-1} .²⁸ These are summarized in Table 3.1 and indicate that the structure of the Keggin anion is maintained. Figure 3.1 shows the spectra obtained for the copper(II) salts of 12-tungstophosphoric acid, using either copper(II) nitrate or copper(II) carbonate as the source of the copper(II) cation. A slight decrease in the frequencies recorded was noted for the central atom-oxygen bond in the central tetrahedron (denoted as $\nu_{\text{as}}(\text{X-O})$) and the asymmetric stretch of the peripheral atom and the terminal oxygen bond (denoted as $\nu_{\text{as}}(\text{M-O})$). The region containing the intra and inter stretching bands for the peripheral metal-oxygen-peripheral metal bonds, denoted as $\nu_{\text{as}}(\text{M-O-M})$, is very broad with little definition. As a result, only the frequency for the $\nu_{\text{as}}(\text{M-O-M})_{\text{intra}}$ band could be assigned in the spectra. When the spectra were obtained for the same salts prepared as KBr disks, a band characteristic of the $\nu(\text{NO}_2)$ antisymmetric stretch²⁹ for the nitrate ion was present at 1380 cm^{-1} for the salts made from copper(II) nitrate. (Figure 3.1(c)) This band was previously hidden by

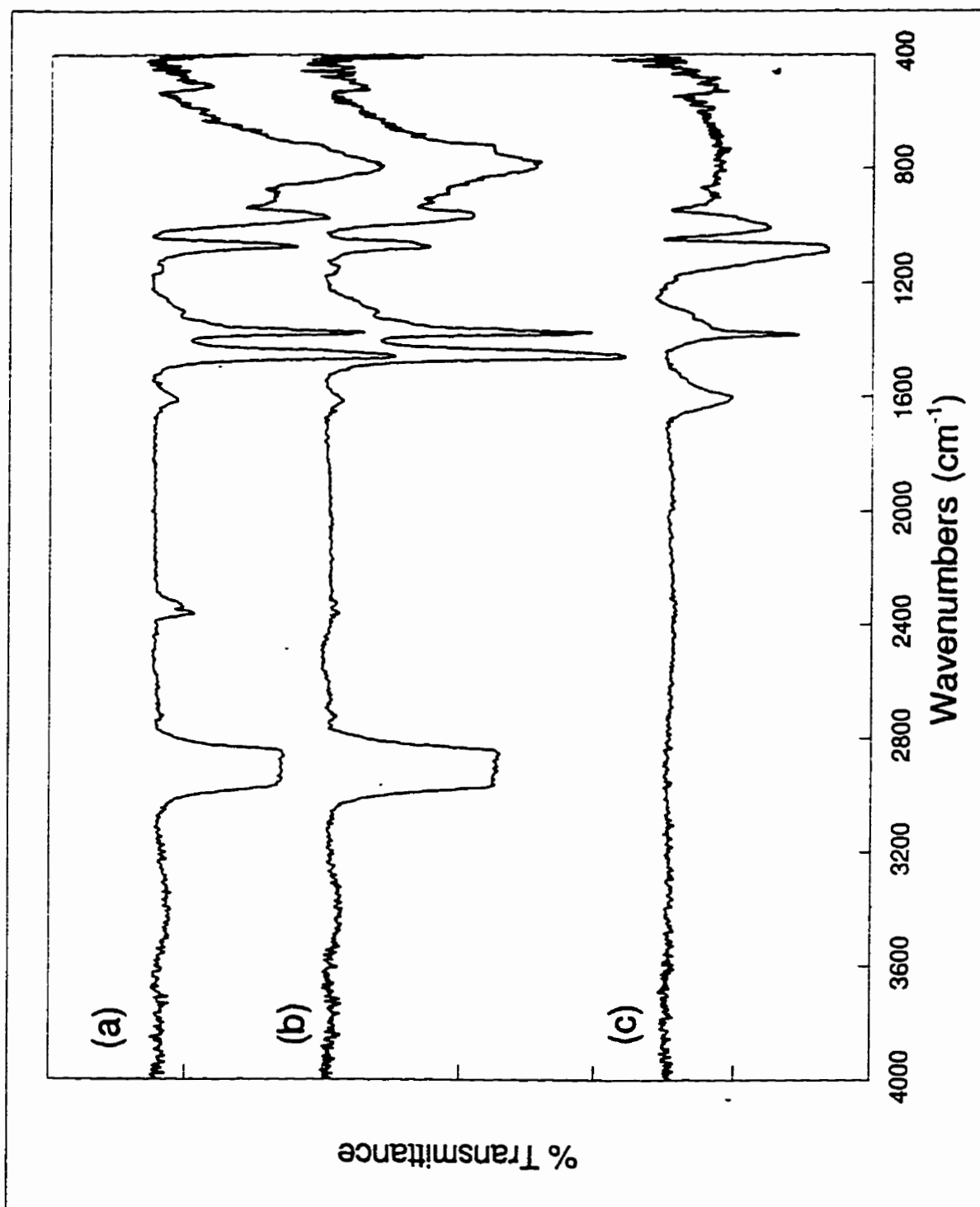


Figure 3.1 - Infrared spectra of copper(II) 12-tungstophosphate.
(a) from copper(II) carbonate (nujol mull); (b) from copper(II) nitrate (nujol mull); (c) from copper(II) nitrate (KBr disk).

Table 3.1 - Characteristic frequencies from infrared spectra of parent acids and copper(II) salts.

| | $\nu(\text{X-O})$ | $\nu_{\text{as}}(\text{M-O})$ | $\nu(\text{M-O-M})$ inter | $\nu(\text{M-O-M})$ intra | $\delta(\text{O-X-O})$ |
|-------------------------------------------------------|-------------------|-------------------------------|------------------------------|------------------------------|------------------------|
| $\text{H}_3\text{PW}_{12}\text{O}_{40}$ ^a | 1080 | 985 | 887 | 807 | 598 |
| HPW + 1.5 $\text{Cu}(\text{NO}_3)_2$ | 1073 | 968 | | 786 | 519 |
| HPW + 1.5 CuCO_3 | 1076 | 974 | | 793 | 624/513 |
| $\text{H}_4\text{SiW}_{12}\text{O}_{40}$ ^a | 1020/930 | 982 | 885 | 792 | 558 |
| HSiW + 2 $\text{Cu}(\text{NO}_3)_2$ | 1019/924 | 980 | | 775 | 537 |
| HSiW + 2 CuCO_3 | 1019/924 | 980 | | 777 | 522 |
| $\text{H}_3\text{PMo}_{12}\text{O}_{40}$ ^a | 1070 | 965 | 870 | 790 | 598 |
| HPMo + 1.5 $\text{Cu}(\text{NO}_3)_2$ | 1065 | 970 | 886 | 793 | 503 |
| HPMo + 1.5 CuCO_3 | 1066 | 968 | 884 | 793 | 500 |

^a Reference 28(a).

the bands associated with nujol. Two other characteristic bands for the nitrate ion are noted to be at 831 cm^{-1} and 720 cm^{-1} ,²⁹ which may have contributed to the broadness and lack of definition associated with the region containing the two $\nu_{\text{as}}(\text{M-O-M})$ bands for the salts made from copper(II) nitrate. The characteristic band for the carbonate ion was not present in the region of $1470\text{-}1420\text{ cm}^{-1}$,²⁹ however additional bands associated with the carbonate ion may explain the broadness present in the region containing the two $\nu_{\text{as}}(\text{M-O-M})$ bands.

The nitrogen adsorption-desorption isotherms were measured for the salts and the surface areas determined by the application of the Brunauer/Emmett/Teller (BET) theory.³⁰ These are summarized in Table 3.2, denoted as S_{BET} . All of the salts maintained a low

Table 3.2 - Summary of surface areas for parent acids and stoichiometric copper(II) salts.

| Sample | Yield (%) | S _{BET} (m ² /g) |
|-------------------------------------------------------------------------------------------------------------|-----------|--------------------------------------|
| H ₃ PW ₁₂ O ₄₀ ^a | | 8.0 |
| H ₃ PMo ₁₂ O ₄₀ ^a | | 8.0 |
| H ₄ SiW ₁₂ O ₄₀ ^a | | 4.0 |
| H ₃ PW ₁₂ O ₄₀ + 1.5 Cu(NO ₃) ₂ ·3H ₂ O | 67.78 | 2.0 |
| H ₃ PW ₁₂ O ₄₀ + 1.5 CuCO ₃ ·Cu(OH) ₂ | 71.56 | 2.3 |
| H ₃ PMo ₁₂ O ₄₀ + 1.5 Cu(NO ₃) ₂ ·3H ₂ O | 77.20 | 9.2 |
| H ₃ PMo ₁₂ O ₄₀ + 1.5 CuCO ₃ ·Cu(OH) ₂ | 79.36 | 6.8 |
| H ₄ SiW ₁₂ O ₄₀ + 2 Cu(NO ₃) ₂ ·3H ₂ O | 78.04 | 1.2 |
| H ₄ SiW ₁₂ O ₄₀ + 2 CuCO ₃ ·Cu(OH) ₂ | 75.67 | 1.5 |

^a Reference 31.

surface area, similar to that observed for the parent acids,³¹ indicating a microporous structure was not present in these salts.

It should be noted that the salts changed colour after the temperature pretreatment of the samples. The copper(II) salts of 12-tungstophosphoric and 12-tungstosilicic acids prepared from copper(II) nitrate turned lime green after heating at 200 °C for two hours in vacuo, while the analogous salts prepared from copper(II) carbonate turned brown. Both salts containing 12-molybdophosphate turned brown. Although no characteristic bands could be assigned in the infrared spectra for the carbonate ion, it should be noted that copper(II) carbonate decomposes on heating in vacuo to form the corresponding copper(I) salt, Cu₂O.¹⁹ This could account for the differences in colour for the salts prepared with copper(II) carbonate in comparison to those prepared with copper(II) nitrate for the same 12-heteropoly acid.

Powder x-ray diffraction patterns were obtained for the six salts and the spectra revealed that an amorphous solid was present in all cases. Indexing of the XRD patterns according to the Pn3m space group proved to be difficult and those which had some

similarities had fewer lines that could be indexed. The lattice parameter was determined for only four of the salts, as denoted in Table 3.3. Although the lattice parameters are slightly smaller than those reported for the pure heteropoly acids,^{2(a),17,32} the degree of hydration has been noted to have an effect on these values.

Table 3.3 - Data from indexed powder XRD patterns for parent acids and stoichiometric copper(II) salts.

| Sample | Lattice Parameter a_0 (Å) | I[110] / I[222] |
|--------------------------------------------------|--------------------------------|-----------------|
| $H_3PW_{12}O_{40} - 6 H_2O$ ^a | 12.5 | 1.22 |
| $H_3PMo_{12}O_{40} - 30 H_2O$ ^b | 23.2 | 0.84 |
| $H_3PW_{12}O_{40} + 1.5 Cu(NO_3)_2 \cdot 3H_2O$ | 10.5 | 0.89 |
| $H_3PW_{12}O_{40} + 1.5 CuCO_3 \cdot Cu(OH)_2$ | 10.5 | 1.11 |
| $H_3PMo_{12}O_{40} + 1.5 Cu(NO_3)_2 \cdot 3H_2O$ | 10.8 | 1.62 |

^a Reference 2(a).

^b References 17, 32.

As discussed in Chapter 2, the ratio of the two peak intensities has been correlated with the presence of a microporous structure.^{2,31} The [110] plane contains the terminal oxygen atoms of the Keggin anions while the [222] plane is the most intense in the spectrum of 12-heteropoly oxometalates. To accommodate the larger cations, substituted for the protons, the Keggin anions must move further apart by rotation and translation. This shifting of the Keggin anions results in fewer terminal oxygen atoms residing in the [110] plane, thus decreasing its peak intensity relative to the [222] peak in the powder XRD spectrum. However, for the copper(II) salts, the values of the I[110]/I[222] ratio are similar to the values obtained for the parent acids and do not show the large decreases as observed with the silver(I) and thallium(I) salts discussed previously in Section 2.3.1. This provides further evidence that a microporous structure was not obtained for the copper(II) salts.

3.3.2 Characterization of Surface and Bulk Properties of Copper(I) Salts

To synthesize the copper(I) salt of 12-tungstophosphoric acid, a method of solid state ion exchange, modified from Spoto *et al.*,²⁵ was used. Copper(I) chloride was mixed with the acid in a stoichiometric amount and heated to 300 °C, under vacuum for two hours. (Equation 3.1) The resulting solid turned brown in colour, similar to the copper(II) salts during their pretreatment for N₂ adsorption isotherms, with lighter coloured flecks present in the sample. When the experiment was repeated with a 33% deficit of the cation, the same discolouration occurred. The reaction carried out at room temperature for one week gave a product light grey in colour; however, the lighter coloured flecks were still present.

After the temperature treatment had been carried out on the solid mixture, the reaction vessel was transferred to the nitrogen adsorption apparatus without exposure to air. Measurements of the surface areas, determined by the application of the BET method to these isotherms,³⁰ were slightly lower than the value reported for the parent acid (Table 3.4), indicating a microporous structure was not created in the preparative experiments.

Table 3.4 - Surface areas and data from indexed powder XRD patterns for copper(I) salts of 12-tungstophosphoric acid.

| Sample | S _{BET} (m ² /g) | Lattice Parameter a ₀ (Å) | I[110] / I[222] |
|--------------------------------------------------------------------|-----------------------------------------|-----------------------------------------|-------------------|
| H ₃ PW ₁₂ O ₄₀ ·6H ₂ O | 8.0 ^a | 12.5 ^b | 1.22 ^b |
| HPW + 2 CuCl @ 300°C | 5.1 | 12.2 | 0.74 |
| HPW + 3 CuCl @ 300°C | 2.9 | 12.2 | 0.63 |
| HPW + 3 CuCl @ 25°C | 1.9 | 12.2 | 0.46 |

^a Reference 31.

^b Reference 2(a).

The powder XRD patterns were measured for all three solids, after measuring the nitrogen adsorption isotherm, and are shown in Figure 3.2. The two reactions carried out at 300 °C show significantly different patterns, with the sample prepared with a

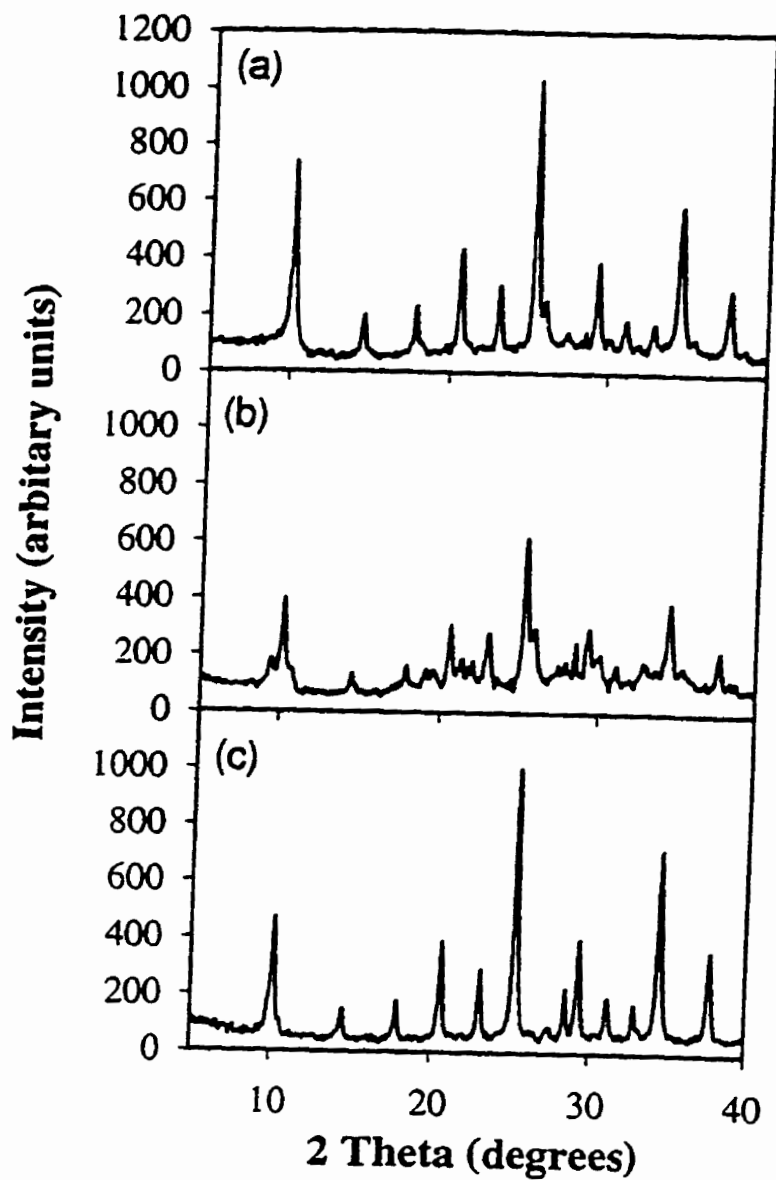


Figure 3.2 - Powder XRD patterns of copper(I) 12-tungstophosphate salts.
(a) HPW + 2CuCl, 300°C (b) HPW + 3CuCl, 300°C (c) HPW + 3CuCl, 25°C.

stoichiometric amount of copper(I) chloride displaying an amorphous pattern, difficult to index and indicating a loss of crystallinity. In contrast, the experiment performed at room temperature was easily indexed in accordance with the $Pn3m$ space group. For all three experiments, the measured lattice parameters (a_0) are similar to the pure acid. (Table 3.4) It is of interest to note that the values for the indexed peak ratio $I[110]/I[222]$ contradict indications by nitrogen adsorption isotherms that a microporous structure was not created, with smaller values recorded in comparison to the parent acid. With the exception of the copper(I) salt, $Cu_3PW_{12}O_{40}$, prepared at room temperature, the peak ratio is not as small as those noted previously for the microporous salts of 12-tungstophosphoric acid containing the silver, thallium and cesium cations. (Chapter 2)

With the success of the suspension ion exchange with the ammonium salts of heteropoly oxometalates¹⁸ and the solid state ion exchange carried out with ammonium zeolite,²⁶ it was thought that the microporous structure already present in the ammonium 12-tungstophosphate salt may encourage the migration of the copper(I) cations into the lattice structure containing the Keggin anions and form the copper(I) salt. The ammonium salt of 12-tungstophosphoric acid contains a micropore structure which has been well characterized and reported in the literature.^{18,33} Although the reported values are for the salt isolated by evaporation, the salt isolated by filtration showed only small differences from these reported values. (Table 3.5)

The solid state ion exchange of the copper(I) chloride with the ammonium salt was carried out under two sets of reaction conditions: 300 °C for 3 hours and 25 °C for one week. In both cases, the resulting solids were grey to beige in colour and appeared homogeneous. Analysis of the N_2 adsorption isotherms, carried out immediately after the temperature treatment without exposure of the solid to air, by the BET method,³⁰ revealed that the surface areas decreased from the value recorded for the pure ammonium salt. (Table 3.5) This decrease was more significant for the reaction at 300 °C. The copper(I) salt prepared at 300 °C had a powder XRD pattern identical to that of the ammonium salt, shown in Figure 3.3, with similar values for the lattice parameter and the $I[110]/I[222]$ ratio. The analogous salt prepared at 25 °C was found to have a smaller decrease in surface area and despite a similar peak ratio of $I[110]/I[222]$, the peak indexed as [222]

Table 3.5 - Surface areas and data from indexed powder XRD patterns for copper (I) salts of ammonium 12-tungstophosphate.

| Sample | S_{BET} (m^2/g) | S_t (m^2/g) | V_{MP} (mL/g) | r_{MP} (\AA) | Lattice Parameter a_0 (\AA) | I[110]/ I[222] |
|------------------------------------------------------------------|-----------------------------------------------|------------------------------------|---------------------------------------------|-------------------------------------|------------------------------------------------|-------------------|
| $\text{H}_3\text{PW}_{12}\text{O}_{40}\cdot 6\text{H}_2\text{O}$ | 8.0 ^a | | | | 12.5 ^b | 1.22 ^b |
| $(\text{NH}_4)_3\text{PW}_{12}\text{O}_{40}$ | 148.9 | 152.6 | 0.057 | 8.2 | 11.7 | 0.44 |
| $(\text{NH}_4)_3\text{PW} + 3 \text{CuCl}$ @ 300°C | 51.8 | 49.6 | 0.017 | 8.0 | 11.6 | 0.45 |
| $(\text{NH}_4)_3\text{PW} + 3 \text{CuCl}$ @ 25°C | 103.5 | 105.2 | 0.040 | 8.3 | 11.6 | 0.51 |

^a Reference 31.

^b Reference 2(a).

was no longer the most intense in the spectrum. There was also a slight shift in the characteristic peaks. Neither spectrum indicated that the resulting solid was amorphous in nature.

Since the ammonium salts still maintain some semblance of a micropore structure, the surface areas (S_t) were also calculated from t-plots, using the method of Lecloux and Pirard³⁴ for calibration purposes, and the resulting surface areas are in good agreement with the values obtained by the BET method. (Table 3.5) The MP method³⁵ was employed to generate the micropore size distribution from the data plotted in the t-plots. As mentioned in Section 2.3.1, calculations for the micropore volume and pore size distributions are a function of the hydraulic radius; however, with heteropoly oxometalates, the assumption is made that the pores are cylindrically shaped and the hydraulic radius (r_h) is equal to one half of the cylindrical radius.³⁶ The calculations and construction of the t-plots and pore size distributions reflect this assumption. The volume of the micropores can be estimated from the t-plots by extrapolating from the linear pressure region of $0.4 < P/P_0 < 0.6$ to obtain the y-intercept. The calculated values for V_{MP} and r_{MP} are contained in Table 3.5. The volume of the micropores mimics the pattern

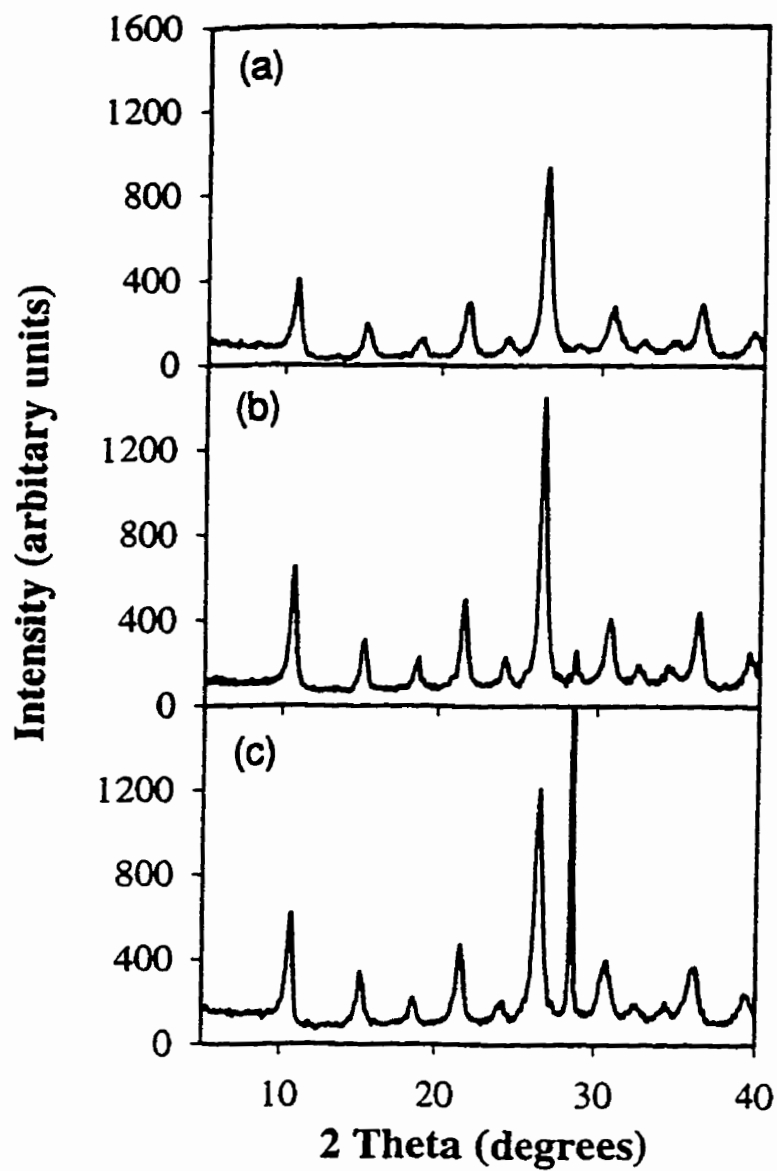


Figure 3.3 - Powder XRD patterns of ammonium and copper(I) tungstophosphate salts. (a) NH_4PW , (b) $\text{NH}_4\text{PW} + 3\text{CuCl}$, 300°C , (c) $\text{NH}_4\text{PW} + 3\text{CuCl}$, 25°C .

observed with the surface areas, although there is only a small variation in the mean micropore radii.

3.4 Discussion

Characterization of the copper(II) salts of the three heteropoly acids failed to provide evidence of a micropore structure and were similar to the results reported previously for the divalent alkaline earth salts,^{16,17} with the surface areas of the copper(II) salts remaining similar to those of the parent acids. Infrared spectroscopy confirmed that the integrity of the Keggin anion was maintained in the isolated solids but the heterogeneous colour of the sample and the amorphous nature of the powder XRD patterns indicated that the divalent cation was present in the mixture with the acid, rather than forming a copper(II) salt. Further evidence was revealed in the infrared spectra of the mixtures prepared from copper(II) nitrate, in which bands characteristic of the nitrate ion were present.

Incorporating the divalent copper cation would cause a cationic lacunar structure due to the substitution of the singly charged protons by the doubly charged copper cation.³⁷ EPR studies of $\text{Cu}_{0.5}\text{H}_3\text{PMo}_{11}\text{VO}_{40}\cdot 13\text{H}_2\text{O}$ and $\text{Cu}_2\text{PMo}_{11}\text{VO}_{40}\cdot 21\text{H}_2\text{O}$ revealed that the copper(II) cations present in these salts formed dimers when heated to 100 °C and 200 °C, respectively, and by 300 °C the dimers and monomers had disappeared for both salts while the formation of clusters and CuO (amorphous) occurred. Aboukais *et al.*³⁸ also noted that with these copper(II) salts supported on silica, the formation of Cu(II) clusters occurred. If in fact the copper cations were incorporated into the lattice structure with the Keggin anions, the charge balance would not be maintained as the dimer and clusters of the copper(II) cations were formed. However, in a heterogeneous mixture, the copper ions could easily move closer to one another to facilitate this. With the pretreatment of the copper(II) solids prior to measuring the N₂ adsorption isotherms, a colour change was noted to occur, which indicated that heating the solid at 200 °C under a vacuum may have facilitated the formation of copper dimers and clusters.

Many factors are required for ion exchange to occur. As noted by McGarvey and Moffat,¹⁸ the exchange capacity in a solid-liquid system containing the 12-heteropoly

oxometalate salts decreased as the radius of the cation in the solid phase was increased with respect to the exchange-in cation in solution. Karge *et al.*²⁰ had noted that the temperatures used in achieving a given degree of solid state ion exchange frequently depended upon the nature of both ions involved. However, in most cases the exchange is fast in the initial period of the solid state reaction and then levels off.

The solid state ion exchange did not appear successful in substituting the copper(I) ion for protons present in 12-tungstophosphoric acid and creating a micropore structure. The presence of the lighter coloured flecks in the sample, after the temperature pretreatment, indicated that the Cu(I) cations may not have been able to migrate into the lattice structure at all and were present as CuCl. The similar colour of the sample in comparison with the solids prepared from copper(II) carbonate, after pretreatment for the N₂ adsorption isotherms, indicated that the Cu₂O oxide may have been formed.¹⁹ Modifications of Spoto's procedure²⁵ may have prevented the ion exchange from occurring. The heteropoly acid did not undergo the same pretreatment as used with the zeolites to remove excess water as there was concern that decomposition of the acid would occur. Karge *et al.*²⁰ had noted, however, that solid state ion exchange with zeolites was not limited by the presence or absence of water. Although the presence of water readily converts Cu(I) to Cu(II) in an aqueous solution, Cu(I) is the preferred oxidation state in the gaseous phase.¹⁹ The authors also used a system which facilitated the removal of any excess CuCl(s) and possible oxides of copper at the end of the reaction,²⁵ but this was not possible with our current system since the same tube was used on the nitrogen adsorption apparatus immediately after the reaction and could not accommodate a wafer form of the heteropoly acid. Previous to Spoto's work, most solid state exchange reactions were carried out as mixed powders.¹⁹

Although the nitrogen adsorption isotherm indicated a microporous structure was not formed in the copper(I) salts of 12-tungstophosphoric, a decrease in the ratio of intensities for the peaks of [110] and [222] in XRD spectra ($I[110]/I[222]$) indicates the orientation of the anions is favourable for the micropore formation. This had previously been noted for the Ag₃PW₁₂O₄₀ salt isolated by evaporation.^{2(a)} It was concluded at that time that the width of such pores had not been sufficiently large to allow penetration by

the nitrogen molecule. A temperature study of the AgPW salt (Section 2.3.3) revealed that the microporous structure of the AgPW salt is sensitive to the temperature at which it is synthesized, and that the evaporation enhances trapping of impurities in the isolated salt, thus blocking the channels created by the microporous structure. Solid state ion exchange is dependent on the ability of the cations to move in and out of the microporous network. In the case of zeolites a microporous structure is already present, but is absent in 12-tungstophosphoric acid. Some exchange may be occurring with the copper(I) cation; however, copper cations entering or protons exiting the lattice network may be trapped and block access to the pores.

Solid state ion exchange was applied with ammonium 12-tungstophosphate since the micropore structure of this salt has been well established.³³ For the reaction carried out at 300 °C with copper(I) chloride, the XRD pattern of the resulting solid is maintained. The solid did not turn as dark in colour as with the reaction of the pure acid. Although there is a large decrease in the surface area of the resulting solid, it is speculated that ion-exchange of the copper(I) ion may have occurred to some extent. It was noted by McGarvey and Moffat that ion exchange occurring in a solid-liquid phase system is limited by the relative sizes of the cations.¹⁸ The extent of the exchange decreased as the radius of the cation in the solid phase increased with respect to the exchange-in cation in solution. Since the diameter of the ammonium cation is larger than that of the copper(I) cation, this may be limiting the exchange. Instead, as CuCl sublimes, the Cu(I) cation may be migrating into the micropore structure of the ammonium salt, blocking access to the pores for the nitrogen molecules during isotherm experiments, thus explaining the retention of the XRD pattern and the significant decrease of the surface area.

With the reaction carried out at room temperature, the change in the surface area is not as significant as the reaction carried out at 300 °C, but the pattern recorded for the powder XRD of the solid indicates that either there has been a significant change in the orientation of the lattice structure, from the Pn3m arrangement, or the sample is a mixture of two crystalline solids. It is possible that the lower temperature would decrease the amount of the copper(I) cations migrating into the pores and the remainder of the CuCl

will remain in the sample holder. The recorded N_2 isotherm and resulting surface area reflects the properties of the two solids being present, as well as the XRD pattern.

This work has provided further information confirming that a microporous structure cannot be formed with the divalent copper cation with any of the three heteropoly acids examined. As has been concluded from investigations with the alkaline earths,^{16,17} the copper(II) cation is present in the isolated solid as either a nitrate or carbonate salt, forming a mixture with the 12-heteropoly acid, rather than forming copper(II) 12-heteropoly oxometalate. Attempts at forming the copper(I) salt of 12-tungstophosphoric acid were unsuccessful in forming a high surface area, microporous solid. Although solid state ion exchange with ammonium 12-tungstophosphate indicated some degree of exchange, or at least migration of the copper(I) cations into the lattice structure, had occurred, this was done at a sacrifice to the micropore structure already present, particularly the high surface area and total micropore volume. Repeating this experiment with a microporous salt containing a cation closer in size to the copper(I) ion may permit the exchange to occur more readily; however it may be difficult to ensure that the outgoing cation would be removed as easily as the ammonium or protium cations with the present reaction conditions.

Although not presently investigated, there has been no indication of the stability of the copper(I) oxidation state once it is established in the lattice structure with the heteropoly anions. The copper (I) cations appear to be stable once incorporated into the zeolite structure but this is not guaranteed to occur with the heteropoly oxometalates.

3.5 References

1. S.J. Gregg and M.M. Tayyab. *J. Chem. Soc. Faraday Trans. I*, **74**, 348 (1978).
2. (a) J.B. McMonagle and J.B. Moffat. *J. Colloid Interface Sci.*, **101**, 479 (1984).
(b) D.B. Taylor; J.B. McMonagle; J.B. Moffat. *J. Colloid Interface Sci.*, **108**, 278 (1985).
(c) G.B. McGarvey and J.B. Moffat. *J. Colloid Interface Sci.*, **125**, 51 (1988).
(d) G.B. McGarvey and J.B. Moffat. *J. Catal.*, **130**, 483 (1991).
3. J.L. Bonardet; J. Fraissard; G.B. McGarvey; J.B. Moffat. *J. Catal.*, **151**, 147 (1995).
4. M.A. Parent and J.B. Moffat. *Langmuir*, **12**, 3733 (1996).
5. W.P. Thistlethwaite. *J. Inorg. Nucl. Chem.*, **29**, 1581 (1967).
6. (a) M. Ai. *J. Catal.*, **67**, 110 (1981).
(b) M. Ai. *J. Catal.*, **71**, 88 (1981).
7. (a) K. Eguchi; I. Aso; N. Yamazoe; T. Seiyama. *Chem. Lett.*, 1345 (1979).
(b) M. Ai. *Appl. Catal.*, **4**, 245 (1982).
8. A.M. El-Awad and K.M. Abd El-Salaam. *Monatshefte für Chemie*, **119**, 1057 (1988).
9. M. Akimoto; K. Shima; H. Ikeda; E. Echigoya. *J. Catal.*, **86**, 173 (1984).
10. (a) H.C. Kim; S.H. Moon; W.Y. Lee. *Chem. Lett.*, 447 (1991).
(b) M. Akimoto; K. Shima; E. Echigoya. *J. Chem. Soc. Faraday Trans. I*, **79**, 2467 (1983).
11. T. Okuhara; T. Hashimoto; T. Hibi; M. Misono. *J. Catal.*, **93**, 224 (1985).
12. (a) T. Matsuda; M. Sato; T. Kanno; H. Muira; K. Sugiyama. *J. Chem. Soc. Faraday Trans. I*, **77**, 3107 (1981).
(b) T. Baba; H. Watanabe; Y. Ono. *J. Phys. Chem.*, **87**, 2406 (1983).
13. (a) Y. Ono; T. Baba; J. Sakai; T. Keii. *J. Chem. Soc. Chem. Commun.*, 400 (1981).
(b) T. Baba; J. Sakai; Y. Ono. *Bull. Chem. Soc. Jpn.*, **55**, 2657 (1982).
(c) T. Baba and Y. Ono. *Appl. Catal.*, **8**, 315 (1983).
14. O.I. Goncharova and T.M. Yur'eva. *Kinet. Catal.*, **28**, 333 (1987).

15. J.S. Vaughan; C.T. O'Conner; J.C.Q. Fletcher. *J. Catal.*, **147**, 441 (1994).
16. G.B. McGarvey and J.B. Moffat. *Catal. Lett.*, **16**, 173 (1992).
17. G.B. McGarvey; N.J. Taylor; J.B. Moffat. *J. Mol. Catal.*, **80**, 59 (1993).
18. (a) G.B. McGarvey and J.B. Moffat. *J. Catal.*, **128**, 69 (1991).
(b) G.B. McGarvey and J.B. Moffat. *J. Catal.*, **130**, 483 (1991).
19. A.G. Massey in "The Chemistry of Copper, Silver and Gold." *Comprehensive Inorganic Chemistry*, **17**, Pergamon Press: Oxford, 1973, Chpt. 27.
20. H.G. Karge and H.K. Beyer. *Stud. Surf. Sci. Catal.*, **69**, 43 (1991).
21. A. Clearfield; C.H. Saldarragar; R.C. Buckley in "Proc. 3rd Int. Conference on Molecular Sieves." (J.B. Uytterhoeven, Ed.) University of Leuven Press: Leuven, Belgium, 1973, pp.241-245.
22. J.A. Rabo in "Zeolite Chemistry and Catalysis." (J.A. Rabo, Ed.) American Chemical Society: Washington, D.C., 1976, p. 332.
23. (a) Y.Y Huang. *J. Am. Chem. Soc.*, **95**, 6636 (1973).
(b) Y.Y Huang. *J. Catal.*, **95**, 6636 (1973).
24. A. Sepuleveda-Escribano; C. Marquez-Alvarez; I. Rodriguez-Ramos; A. Guerrero-Ruiz; J.L.G. Fierro. *Catal. Today*, **17**, 167 (1993).
25. (a) G. Spoto; S. Bordiga; D. Scarano; A. Zecchina. *Catal. Lett.*, **13**, 39 (1992).
(b) G. Spoto; A. Zecchina; S. Bordiga; G. Riccardi; G. Martra. *Appl. Catal. B*, **3**, 151 (1994).
26. H. G. Karge; B. Wichterlova; H.K. Beyer. *J. Chem. Soc.*, **88**, 1345 (1992).
27. G.B. McGarvey and J.B. Moffat. *J. Mol. Catal.*, **69**, 137 (1991).
28. (a) C. Rocchiccioli-Deltcheff; R. Thouvenot; R. Frank. *Spectrochim. Acta*, **32A**, 587 (1976).
(b) C. Rocchiccioli-Deltcheff; M. Fournier; R. Frank; R. Thouvenot. *Inorg. Chem.*, **22**, 207 (1983).
29. K. Nakimoto. "Infrared Spectra of Inorganic and Coordination Compounds" (2 ed.) John Wiley and Sons, Inc.: New York, 1970, pp. 170-173.
30. S. Brunauer; P.H. Emmett; E. Teller. *J. Am. Chem. Soc.*, **60**, 309 (1938).

31. J.B. Moffat. *J. Mol. Catal.*, **52**, 169 (1989).
32. J.C. Clark and D. Hall. *Acta Crystallogr.*, **B32**, 1545 (1976).
33. D. Lapham and J.B. Moffat. *Langmuir*, **7**, 2273 (1991).
34. A. Lecloux and J.P. Pirard. *J. Colloid Interface Sci.*, **70**, 265 (1979).
35. R.Sh. Mikhail; S. Brunauer; E.E. Bodor. *J. Colloid Interface Sci.*, **26**, 45 (1968).
36. R.Sh. Mikhail; S. Brunauer; E.E. Bodor. *J. Colloid Interface Sci.*, **24**, 451 (1967).
37. E. Crusson-Blouet; A. Aboukais; C.F. Aissi; M. Guelton. *Chem. Mater.*, **4**, 1129 (1992).
38. A. Aboukais; D. Ghoussoub; E. Blouet-Crusson; M. Migole; M. Guelton. *Appl. Catal. A*, **111**, 109 (1994).

CHAPTER 4

A Comparison of Methods for the Characterization of the Microporous Structure in Solids.

4.1 Introduction

As discussed in Chapter 1, the characterization of porous solids is of interest to those involved in heterogeneous catalysis and adsorption.¹⁻⁵ In addition to increasing the area of a catalyst available for interaction with the molecules of the reactants, the presence of a pore structure may facilitate shape selectivity; micropores, and large pores may be advantageous for trapping undesirable components contained in the feed stream.^{2,3,6} Information on the pore size distribution is evidently important not only for the characterization of catalysts prior to their use but also for evaluating the morphological changes which such solids display under realistic reaction conditions, as a result of not only specific reaction parameters but also the effects of processes leading to both chemical and physical deactivation. The microporous structures of solids applicable in various adsorption processes are of no less importance. While the morphological properties of a wide variety of these solids have been studied over the years, considerable recent attention has been focused on carbons of various types.^{7,8}

Although a variety of methods are available for the measurement of pore size distributions under special circumstances, the determination and analysis of gaseous adsorption data are undoubtedly the most commonly employed for such purposes.⁹ It is well known that in the adsorption of a one-component gas on a porous solid, two processes may take place. Adsorption layer thickening will occur over the entire range of relative pressures, and where micropores are present, these will fill by this process. In addition, capillary condensation may occur in those solids where mesopores are present, concomitantly with the process of adsorption layer thickening.

Micropores, mesopores, and macropores are typically defined as having pore diameters of less than 2 nm, 2 - 50 nm, and greater than 50 nm, respectively.⁹ Methods for analysis of the adsorption-desorption isotherms of a mesoporous solid usually employ the Kelvin equation to relate the effective pore radius to the relative pressure at which

capillary condensation occurs. Where a microporous structure is present it is generally assumed that these pores fill only by adsorption layer thickening, although some doubts have been raised concerning the validity of this assumption, particularly for the larger micropores.

For microporous solids several methods have been employed for the analysis of the physisorption data in order to generate information on the pore size distribution. The MP method¹⁰ is frequently used for such purposes although other techniques such as the finite layer Brunauer/Emmett/Teller (BET)¹¹ and the Dubinin-Radushkevich (DR)¹² equations have been employed. The MP procedure is based on the conversion of the data for the quantity adsorbed at various adsorption equilibrium pressures into the amount adsorbed as a function of the thickness of the adsorbed layer from which the contribution of pores of different sizes to the volume and surface area can be readily evaluated. Although the relationship between the relative pressure and the thickness of the adsorbed layer would ideally be obtained from a solid of the same nonporous composition as the porous solid of interest, the former is generally not available and the empirical Halsey equation is frequently employed for such purposes. However, a method dependent on the C values from the BET equation has been proposed which may offer advantages not found in the Halsey relation.¹³ The finite layer BET equation is derived similarly to the usual BET relation but with the summations carried out over n layers rather than an infinite number. Although the finite layer equation cannot be placed in a compact linear form, the data from the adsorption isotherm can be computationally fitted to the equation. The calculated values of n , the number of layers, can then be converted to the average radius of the pores. The Dubinin-Radushkevich equation is derived from the exponential dependence of the quantity adsorbed on the adsorption potential and can be employed to generate the micropore volume.

More recently a method for pore size analysis based on the potential between the surface and the adsorbed molecules has been presented by Horvath and Kawazoe (HK) for a carbon surface.¹⁴ The procedure is frequently employed as the software in microprocessors supplied with automatic devices for the measurement of adsorption isotherms. The Horvath and Kawazoe mean-field method has recently been analyzed by

Conner and coworkers.¹⁵ This method has been extended to apply to pores of cylindrical symmetry by Saito and Foley.¹⁶

In Chapter 2 the BET and MP methods were employed to characterize the micropore structure of the prepared salts. As discussed in Section 2.3.2, these results were internally self-consistent, evident by the analyses of replicate trials of the nitrogen adsorption isotherms. The observations of an increase in the micropore volume with the increase in the cation diameter or the amount of cation used in the synthesis appeared to be consistent with those previously reported in the literature (Section 2.4). However, in view of the interest in porous solids and the methods for determination of a pore structure, a comparison of the BET, MP, DR and Horvath-Kawazoe-Saito-Foley (HKSF) methods was performed. These methods were applied to the nitrogen adsorption-desorption isotherms of two nonstoichiometric thallium salts of 12-heteropoly oxometalates, thallium 12-tungstosilicate and 12-molybdophosphate (abbreviated as TlSiW and TlPMo) to compare and contrast the aforementioned methods and the results obtained therefrom.¹⁷ The confirmation of a micropore structure for these two thallium salts was initially reported in Chapter 2.

4.2 Experimental

4.2.1 Experimental

The thallium salts of 12-tungstosilicic and 12-molybdophosphoric acids (abbreviated as TlSiW and TlPMo) were synthesized following the procedure outlined in Section 2.2.1, using an excess of thallium nitrate for a preparative cation:proton ratio of 1.15.

Nitrogen adsorption-desorption isotherms were measured on a standard volumetric glass system fitted with an MKS Baratron type 590HA capacitance manometer, as outlined in Section 2.2.2. The samples were outgassed at 10^{-5} Torr at 473 K for two hours prior to the analysis, carried out at 77 K. Approximately 25 and 10 data points were obtained for the adsorption and desorption parts, respectively, of the isotherm.

4.2.2 Calculations

The calculations employed in the present work to obtain estimates of the surface area are those based on the BET equation,¹¹ the t-plot method,¹⁰ and the Dubinin-Radushkevich equation.¹² The volume of the micropores was estimated by the t-plot method¹⁰ and the Dubinin-Radushkevich equation.¹² The pore size distribution of the samples was obtained from the MP method,¹⁰ the slit model derived by Horvath and Kawazoe¹⁴ and Saito and Foley's line- and area-averaged cylindrical models.¹⁶ These four methods also provided estimates of the average pore radii or diameter for each sample examined.

4.3 Results

The nitrogen adsorption-desorption isotherms for the two salts are depicted in Figure 4.1. The sharp initial rise at the low relative pressures is indicative of the presence of micropores in the solid. As the relative pressure is increased, the amount of nitrogen adsorbed by the sample from each aliquot of gas decreases, although the TIPMo salt does adsorb a large amount of nitrogen gas in the high pressure region.

Based on the Langmuir theory of monomolecular adsorption, the Brunauer/Emmett/Teller (BET) method accounts for the multilayer adsorption of gases on a solid.¹¹ It assumes that each layer can be described by langmuir adsorption with the additional requirement that the heat of adsorption for the first layer may have a unique value while that for each successive layer is equal to the heat of liquefaction. A linear relationship for the BET approach, considering an infinite number of adsorbed layers, can be expressed as

$$\frac{x}{N(1-x)} = \frac{1}{N_m c} + \left(\frac{c-1}{N_m c} \right) x \quad (4.1)$$

so that in the plot of the data the

$$\text{slope} = \frac{C_{BET}-1}{C_{BET}N_m} ; \quad \text{intercept} = \frac{1}{C_{BET}N_m}$$

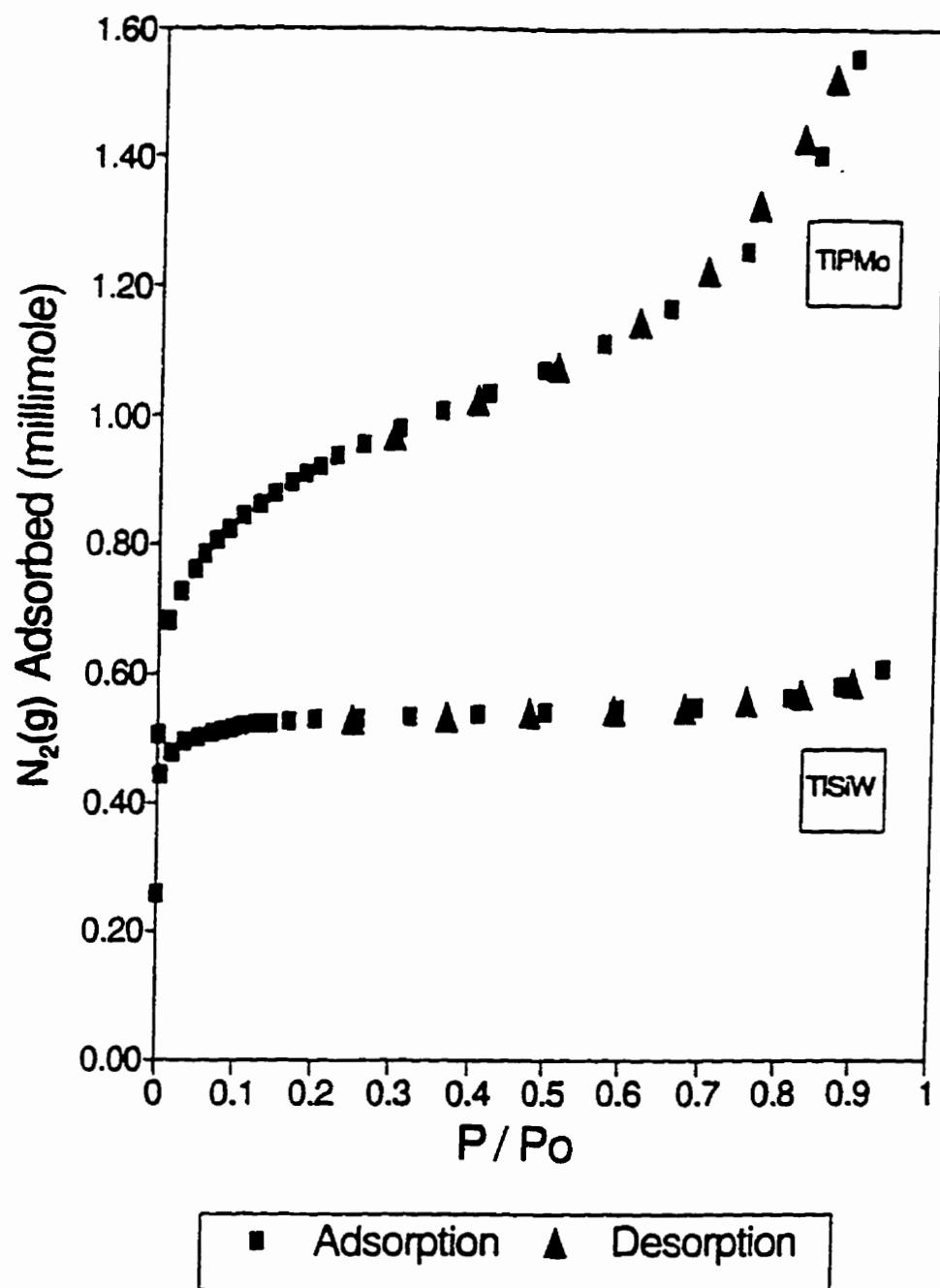


Figure 4.1 - N_2 adsorption-desorption isotherms for $Ti_4SiW_{12}O_{40}$ and $Ti_3PMo_{12}O_{40}$.

where N refers to the moles of nitrogen adsorbed, N_m is the number of moles required to form a monolayer, x is the relative pressure (P/P_0) and c is the BET parameter (also referred to as C_{BET}). The values of N_m and C_{BET} are determined by the following equations

$$N_m = \frac{1}{\text{slope} + \text{intercept}} \quad (4.2)$$

$$C_{BET} = \frac{1}{N_m (\text{intercept})} \quad (4.3)$$

while the surface area (S_{BET}) is calculated by

$$S_{BET} = N_m N_0 (\alpha) \quad (4.4)$$

where N_0 is Avogadro's number and α is the cross-sectional area of the nitrogen molecule ($\alpha = 16.2 \times 10^{-20} \text{ m}^2$).¹⁸

As previously discussed in Chapter 2, the surface areas for these salts were determined initially by the BET method¹¹ and are summarized in Table 4.1, denoted as S_{BET} . The linear region of the BET isotherm has been greatly reduced for both salts from that which is typically observed,¹⁸ with the upper limit of the relative pressure (P/P_0) being 0.07 for TlSiW and 0.17 for TlPMo. The relatively large values for the C_{BET} parameters, summarized in Table 4.1, are also indicative of the presence of micropores.

The finite layer BET relationship of

$$N = \frac{N_m C_{BET} x [1 - (n+1)x^n + nx^{n+1}]}{(1-x)[1 + (C_{BET}-1)x - C_{BET}x^{n+1}]} \quad (4.5)$$

was also applied to each of the two salts. The values of N_m and C_{BET} were determined by the infinite layer relationship (Equations 4.2 and 4.3) while x and N refer to the relative pressure and moles of nitrogen adsorbed, respectively, in the N_2 adsorption isotherm. A

nonlinear regression was performed to determine n , the number of adsorbed monolayers. Values of less than 3, for n , are indicative of the presence of micropores within the solid. As shown in Table 4.1, both salts are consistent with these conclusions. It was noted that of the two constants, N_m and C_{BET} , the value of N_m has the greatest effect on the value of n .

Table 4.1 - Calculated surface areas and C_{BET} constants for the thalious salts, TISiW and TIPMo.

| Sample | P/P _o Range | C_{BET} | S_{BET} (m ² /g) | S_t (m ² /g) | S_{DR} (m ² /g) | n |
|--------|------------------------|-----------|----------------------------------|------------------------------|---------------------------------|-----|
| TISiW | 0.00 - 0.07 | 4700 | 92.7 | 96.2 | 106.2 | 1.4 |
| TIPMo | 0.00 - 0.17 | 920 | 147.2 | 142.0 | 166.3 | 2.8 |

Employing the reference isotherms from Lecloux and Pirard,¹³ plots of the volume of nitrogen adsorbed, V_{ads} , as a function of the thickness of the adsorbed layer, referred to as t-plots, were constructed for each sample. Each experimental P/P_o in the nitrogen adsorption isotherm corresponds to a ratio of the adsorbed volume and the monolayer volume (V/V_m) determined from the reference isotherm. The thickness of the adsorbed

$$t = 3.54(V/V_m) \quad (4.6)$$

layers were then calculated by equation 4.6. The t-plots are linear in the low pressure region and the t-plot surface area (S_t) is calculated using the slope of this section with

$$S_t = 15.47(V_{ads}/t) \quad (4.7)$$

and are in good agreement with those obtained by the BET method. (Table 4.1) Both t-plots are well-behaved in that the extrapolated curves pass through the origin. However, with TIPMo the volume adsorbed did not reach a constant value at the highest value for t . It should be noted that the reference isotherms of Lecloux and Pirard have a lower limit of 0.02 for the range of relative pressure. Extrapolation of the isotherm to zero has led to a discontinuity in the constructed t-plot, and as a result, data points obtained for relative

pressures less than 0.02 have not been included in the t-plots for the salts examined.

Negative deviations occur in the t-plots when narrow pores are filled by multilayer adsorption, indicating that subsequent adsorption does not take place on the entire surface. The volumes of the micropores (V_{MP}) can be estimated for both salts by extrapolating from the linear pressure region of $0.4 < P/P_o < 0.6$ (corresponding to the thickness range of 1.1 - 1.3 nm for the adsorbed layers) to obtain the y-intercept. However, with the deviation from linearity that the TIPMo salt experiences as the thickness of the adsorbed layer increases, a more representative value is expected from the y-intercept of a tangent line taken at $P/P_o = 0.4$ (corresponding to an adsorbed layer of 1.1 nm). This value is denoted in parenthesis in Table 4.2, and is closer to the V_{MP} obtained for the TISiW salt.

The MP method was employed to generate the micropore size distribution from the data on the t-plots.¹⁰ (Figure 4.2) Calculations for the micropore volume and pore size distributions are a function of the hydraulic radius; however, with heteropoly oxometalates, the assumption is made that the pores are cylindrically shaped and the hydraulic radius, r_h , is equal to half of the cylinder radius.¹⁹ The present calculations and construction of the t-plots reflect this assumption. The slope is measured between closely spaced thickness values and the surface area can be determined using equation 4.7. The difference between S_t and that measured for this slope is the surface area of the pores up

$$V = 10^{-4}(S_t - S_l) \left(\frac{t_1 + t_2}{2} \right) \quad (4.8)$$

to that size. The volume of these pores is given by equation 4.8. The procedure is repeated by advancing to the next thickness, measuring the slope, calculating the surface area, and determining the pore volume using equation 4.8 until there is no further measurable change in the slope.

The pore size distributions were constructed by calculating ΔV and Δr values¹⁹ and plotting $\Delta V/\Delta r$ versus r , the mean radius used for determining ΔV . The TISiW salt has a typical distribution observed for the monovalent salts of the 12-heteropoly oxometalates,^{20,21} with a maximum in the 0.7 to 0.8 nm region, while the TIPMo salt has a

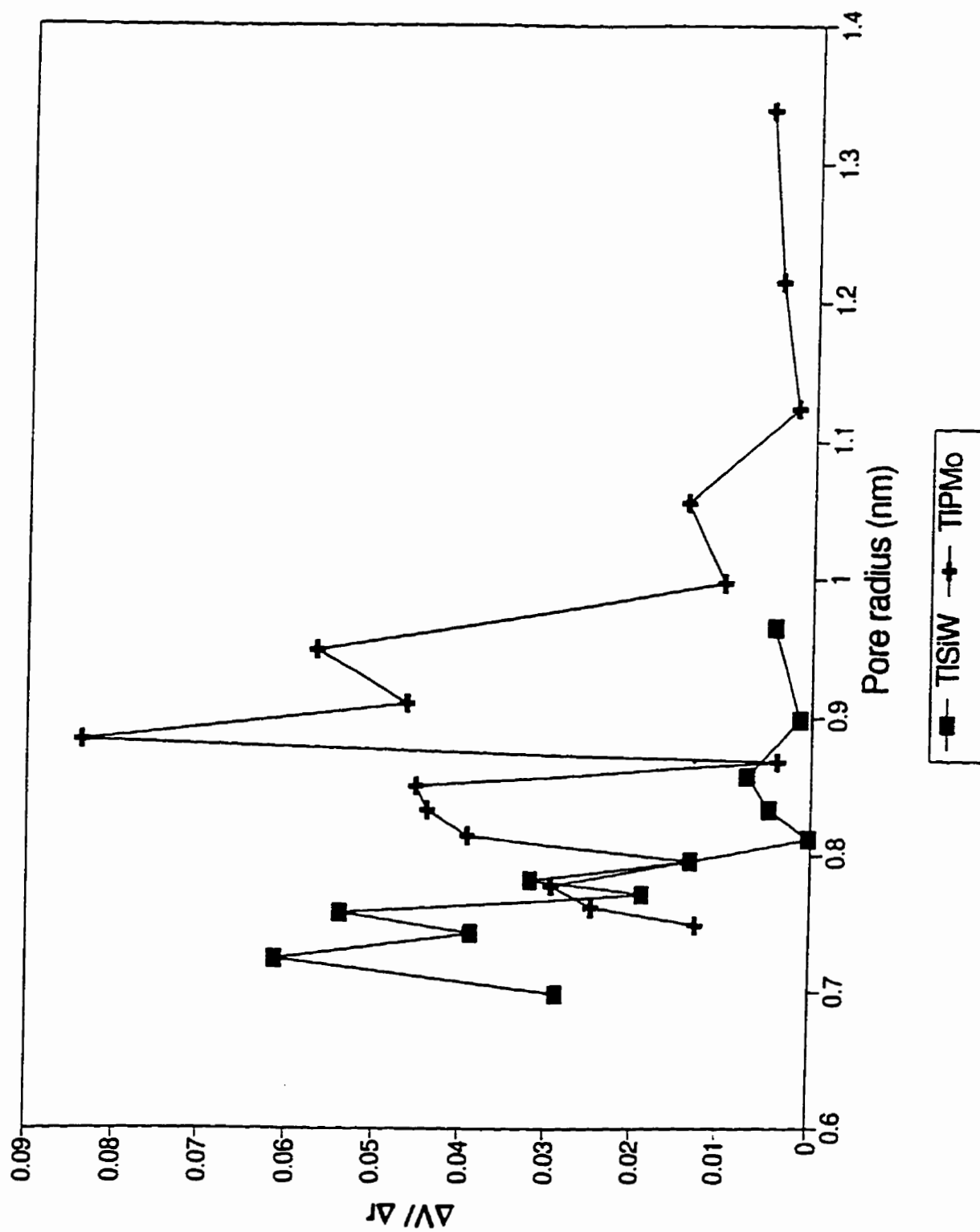


Figure 4.2 - Pore size distribution of $Tl_4SiW_{12}O_{40}$ and $Tl_3PMo_{12}O_{40}$ by the MP method.

wider breadth for its distribution and appears to have three maxima. Both have evidence of pores existing up to 2.0 nm. The mean micropore radius (r_{MP}) for each salt was determined using the equation

$$r_{MP} = \frac{\sum (\Delta V/\Delta r)r}{\sum (\Delta V/\Delta r)} \quad (4.9)$$

and are summarized in Table 4.2. As previously observed in Chapter 2, since both salts contain the same cation, the mean micropore radii are similar in size, with the TIPMo salt being slightly larger, correlating to its larger surface area.

Table 4.2 - Calculated micropore volumes and sizes for the thallosal salts, TISiW and TIPMo.

| Sample | V_{MP} (mL/g) | V_{DR} (mL/g) | r_{MP} (nm) | L_{DR} (nm) |
|--------|---------------------------------------------------------------|----------------------|------------------|------------------|
| TISiW | 3.5×10^{-3} | 3.8×10^{-3} | 0.78 | 1.49 |
| TIPMo | 4.2×10^{-3} (3.7×10^{-3}) ^a | 5.9×10^{-3} | 0.88 | 1.66 |

^a Determined from the tangent.

The use of the Dubinin-Radushkevich (DR) equation¹² to analyze the adsorption isotherm data is based on the volume-filling of the micropores, rather than the assumption of layer-by-layer adsorption on the pore walls that the BET method employs. A linear plot (also referred to as a DR plot) (Figure 4.3) is obtained from the equation

$$\log V = \log V_o - D \log^2 \left(\frac{P}{P_o} \right) \quad (4.10)$$

where D is the slope of $\log V$ versus $\log^2(P/P_o)$. The upward deviation as the saturation pressure is reached is attributed to the multilayer adsorption and capillary condensation in the mesopores.¹⁸ As a result, the volume of the micropores (denoted as V_{DR} in Table 4.2) is obtained by extrapolation from only the low pressure region ($P/P_o < 0.1$) to obtain the y-intercept. These values are larger than the V_{MP} obtained from the t-plots. This is

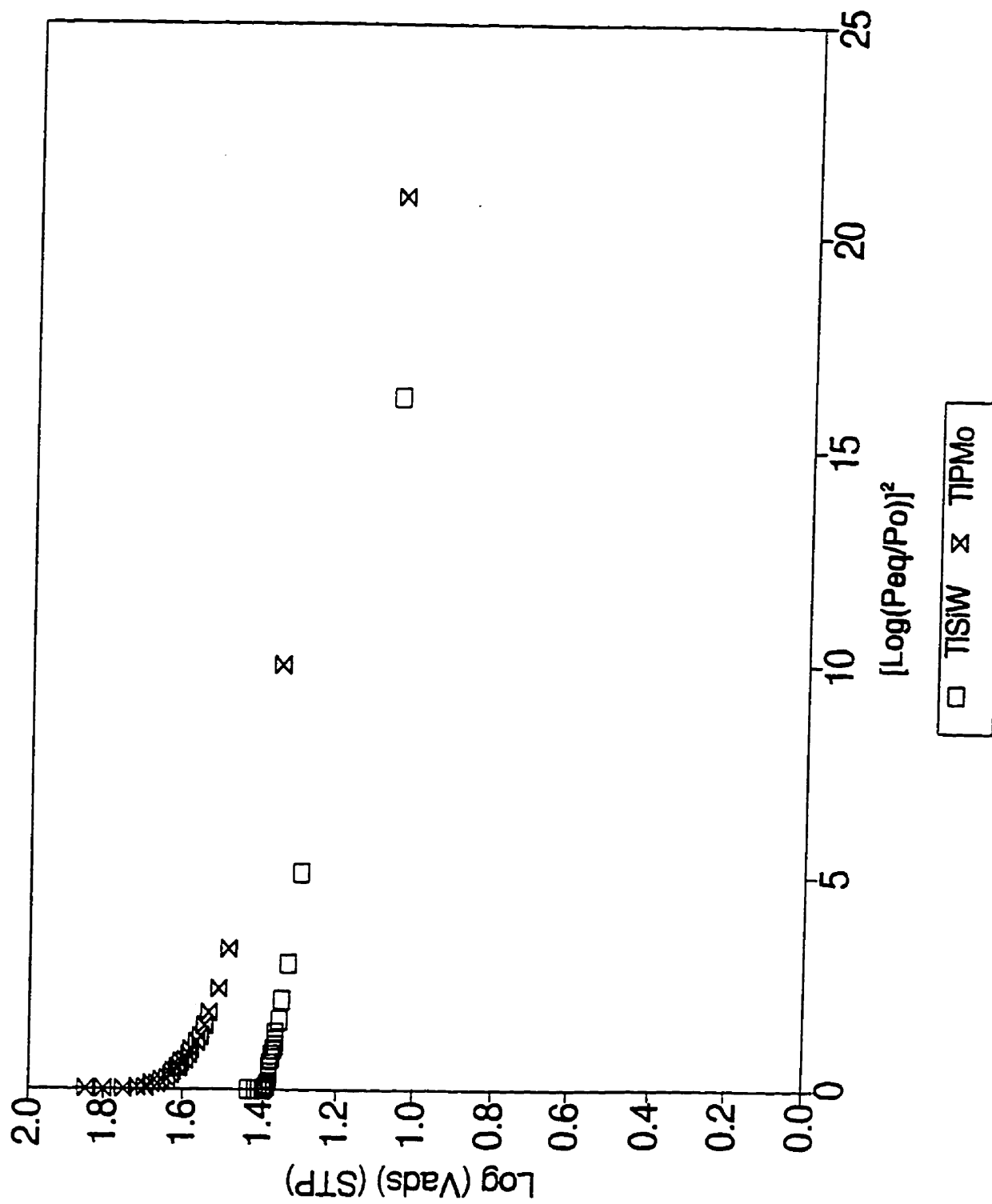


Figure 4.3 - Dubinin-Radushkevich plots for $Tl_4SiW_{12}O_{40}$ and $Tl_3PMo_{12}O_{40}$.

particularly noted with the TIPMo salt, whose upward deviation is significantly greater than that with the TISiW salt in the DR plot. The surface area (denoted as S_{DR} in Table 4.1) can be calculated similarly to that in the BET method^{12(a)} with

$$S_{DR} = (V_{DR})(N_0)(\alpha)/22404 \quad (4.11)$$

where α is the cross-sectional area of the nitrogen molecule and N_0 is Avogadro's number. In comparing the surface areas calculated by the three methods in Table 4.1, those obtained from the DR equation are consistently greater than those by the BET and t-plot methods.

A correction to the DR plots has been illustrated²² to account for the presence and filling of mesopores. The resulting corrected curve is lowered in position with respect to the y axis (the volume of nitrogen), and has a decreased slope, apparent even in the low pressure region. As a result, it appears that extrapolating the V_{DR} value from only the low pressure region ($P/P_0 < 0.1$) does not completely reduce the effect of mesopores present in the system, causing the value obtained for the V_{DR} to be larger than it actually is. This increase is also reflected to the same extent in the calculated surface area (S_{DR}).

The DR method uses the assumption of a Gaussian distribution for the micropore size distribution.¹⁸ With this, the average micropore width (denoted as L_{DR} in Table 4.2) can be calculated by

$$L_{DR} = \left(\frac{\gamma}{T} \right) [(4.45 \times 10^6)(-D)]^{\frac{1}{2}} \quad (4.12)$$

where γ is the molar volume of the adsorbate, relative to a standard ($\gamma = 0.393$ for nitrogen, relative to benzene)^{12(a)}, T is the temperature (77 K) and D is the slope from the plot of $\log V$ versus $\log^2(P/P_0)$. These values of L_{DR} , summarized in Table 4.2, are slightly smaller than twice the value of the mean micropore radius (r_{MP}) for each salt. Despite the problem of the increased slope of the DR plot due to the presence of mesopores, these average micropore sizes correlate well with the data from the MP method. It appears that the presence of mesopores has a greater effect on the intercept of the DR plot than with its slope in the low pressure region.

Horvath and Kawazoe developed a model which takes into account the bulk and surface properties of the adsorbents. On the basis of the calculated potential energy profiles for atoms adsorbed in slit-like pores and the enhancement of the depth of the energy well relative to adsorption on a flat surface,²³ the HK model relates the free energy of adsorption to the average potential inside a slit-like pore.¹⁴ Their initial study involved the adsorption of nitrogen on molecular-sieve carbon, with the generic equation summarized as

$$RT \ln \left(\frac{P}{P_o} \right) = K \frac{N_a A_a + N_A A_A}{\sigma^4 (L-d)} \left[\frac{\sigma^4}{3(L-d/2)^3} - \frac{\sigma^{10}}{9(L-d/2)^9} - \frac{\sigma^4}{3(d/2)^3} + \frac{\sigma^{10}}{9(d/2)^9} \right] \quad (4.13)$$

where N_a is the number of atoms per unit area of adsorbent (a) (atom/cm²),
 N_A is the number of molecules per unit area of adsorbate (A) (molecule/cm²),
 K is Avogadro's number,
 σ is the distance between a gas atom and the nuclei of the surface at zero interaction energy ($\sigma = 0.858 \times d/2$) (nm),
 L is the distance between nuclei of two layers (nm),
and d is the sum of the adsorbate and adsorbent diameters ($d = d_A + d_a$) (nm).

Table 4.3 - Parameters used for the adsorbent and adsorbate components.

| Parameter | Adsorbent Oxide Ion | Adsorbate Nitrogen (N ₂) |
|----------------------------------------------------|------------------------------------|-----------------------------------------|
| Diameter, d (nm) | 0.276 ^a | 0.36 ^c |
| Polarizability, α (cm ³) | 2.5×10^{-24} ^a | 1.74×10^{-24} ^d |
| Magnetic Susceptibility, χ (cm ³) | 1.3×10^{-29} ^a | 2×10^{-29} ^b |
| Density, N (molecules/cm ²) | 1.31×10^{15} ^a | 6.7×10^{14} ^b |

^a Reference 16.

^b Reference 14.

^c Reference 27.

^d D.R. Lide. "Handbook of Chemistry and Physics." 71st ed., CRC Press Inc: USA, 1990, p. 10-199.

Using the data in Table 4.3, the dispersion constant for the adsorbate (A_A) is calculated by the equation

$$A_A = \frac{3}{2}(mc^2\alpha_A\chi_A) \quad (4.14)$$

and the dispersion constant for the adsorbent (A_a) is determined by

$$A_a = \frac{6mc^2\alpha_a\alpha_A}{\left(\frac{\alpha_A}{\chi_A}\right) + \left(\frac{\alpha_a}{\chi_a}\right)} \quad (4.15)$$

where m is the mass of an electron (kg),
 c is the speed of light (m/s),
 α is the polarizability (cm^3),
and χ is the magnetic susceptibility (cm^3).

The model can be extended to other adsorbent-adsorbate systems, and Table 4.3 summarizes the data used for the present system. Incorporating these parameters for the oxide ion¹⁴ as the adsorbent and updating the parameters for nitrogen as the adsorbate, the resulting equation for the slit model is

$$\ln\left(\frac{P}{P_o}\right) = \frac{21.77}{(L-0.636)} \left[\frac{1.847 \times 10^{-3}}{(L-0.318)^3} - \frac{2.540 \times 10^{-7}}{(L-0.318)^9} - 4.981 \times 10^{-2} \right] \quad (4.16)$$

Detailed calculations of equations 4.14 to 4.16 are in Appendix A.

Saito and Foley modified the slit model to accommodate the cylindrical shaped pores of the zeolite microstructure.¹⁶ For the cylindrical model, the line-averaged and area-averaged cases were examined. With substitution of the parameters listed in Table 4.3, the resulting equation for the line-averaged case is

$$\ln\left(\frac{P}{P_o}\right) = 27.85 \sum_{k=0}^{\infty} \left[\frac{1}{2k+1} \left(1 - \frac{0.318}{r_p}\right)^{2k} \left[\frac{21}{32} \alpha_k \left(\frac{0.318}{r_p}\right)^{10} - \beta_k \left(\frac{0.318}{r_p}\right)^4 \right] \right] \quad (4.17)$$

while that for the area-averaged case is

$$\ln\left(\frac{P}{P_o}\right) = 27.85 \sum_{k=0}^{\infty} \left[\frac{1}{k+1} \left(1 - \frac{0.318}{r_p}\right)^{2k} \left[\frac{21}{32} \alpha_k \left(\frac{0.318}{r_p}\right)^{10} - \beta_k \left(\frac{0.318}{r_p}\right)^4 \right] \right] \quad (4.18)$$

with

$$\alpha_k = \left(\frac{-4.5 - k}{k}\right)^2 \alpha_{k-1} \quad \beta_k = \left(\frac{-1.5 - k}{k}\right)^2 \beta_{k-1} ; \alpha_0, \beta_0 = 1 \quad (4.19)$$

Detailed calculations of equations 4.17 and 4.18 are in Appendix A.

Using pressure data from the nitrogen-adsorption isotherms of the two salts, Equations 4.17 to 4.19 were solved by application of the Secant method²⁴ to determine the unknown variable (L for the slit model and r_p for the cylindrical models) at each data point. The resulting effective pore diameter was then calculated from ($L - 0.276$ nm) for the slit model¹⁴ and ($2r_p - 0.276$ nm) for the cylindrical models.¹⁶

The micropore size distributions for the two salts are then plotted similarly to the MP method, with the differential volume adsorbed with respect to the differential pore size vs the pore size (Figures 4.4 and 4.5). These typically result in a Gaussian distribution, with the maxima taken as the average effective pore diameter. (Table 4.4)

Table 4.4 - Summary of effective pore diameter calculated for the thallos salts, TlSiW and TIPMo.

| Sample | Effective Pore Diameter (nm) | | |
|--------|------------------------------|---------------|---------------|
| | Slit | Line-Averaged | Area-Averaged |
| TlSiW | 0.56 | 0.73 | 0.77 |
| TIPMo | 0.54 | 0.61 | 0.62 |

The diameters from the cylindrical models show the reverse of the trend previously observed with the MP and DR methods. The TIPMo salt has a smaller pore diameter than the TlSiW salt, and both salts have values less than the mean micropore radii (r_{MP}) calculated by the MP method and less than half of the average pore width (L_{DR}) calculated by the DR method. Saito and Foley varied each of the parameters listed in Table 4.3 by

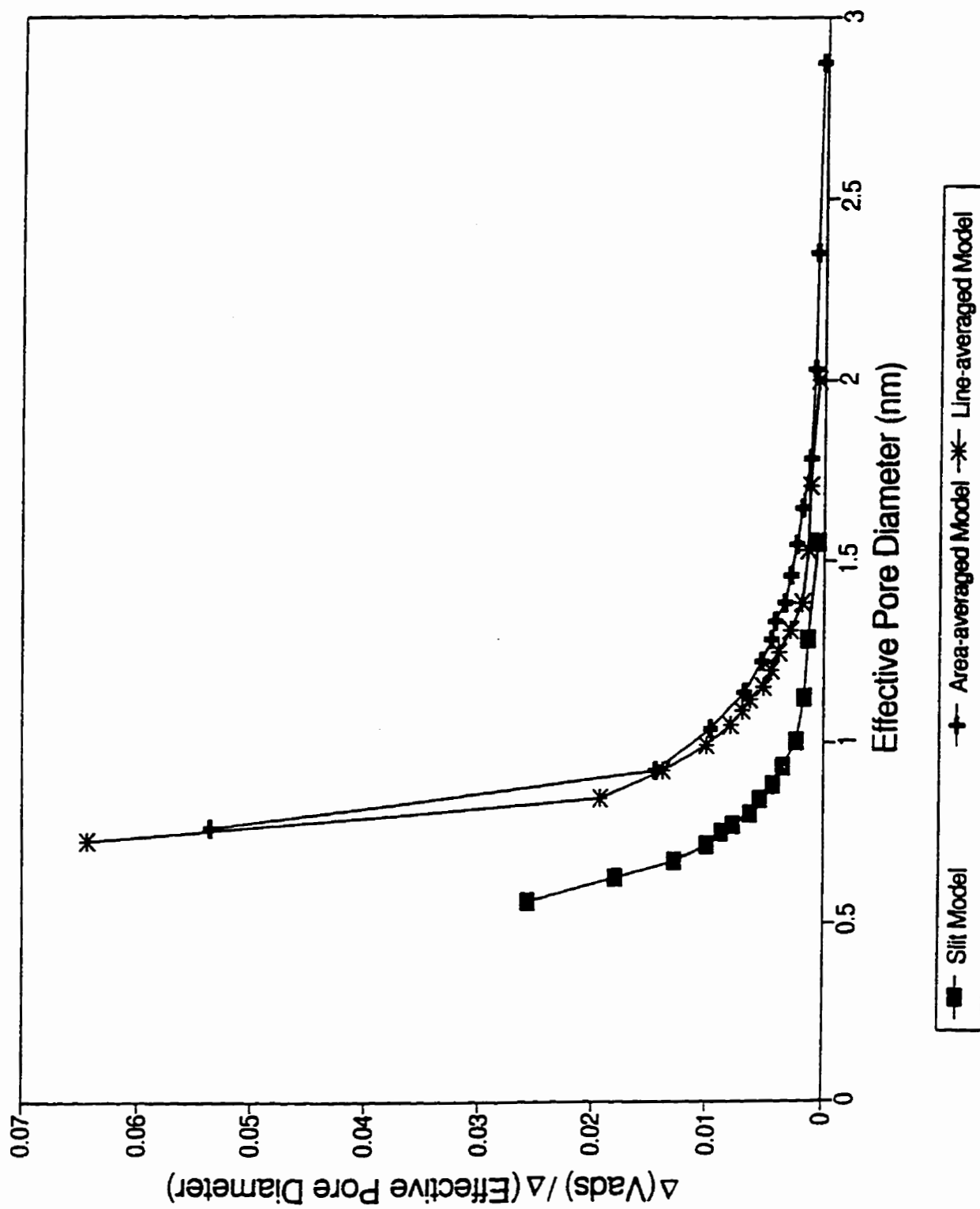


Figure 4.4 - Pore size distribution of $Tl_4SiW_{12}O_{40}$ by HKSF methods.

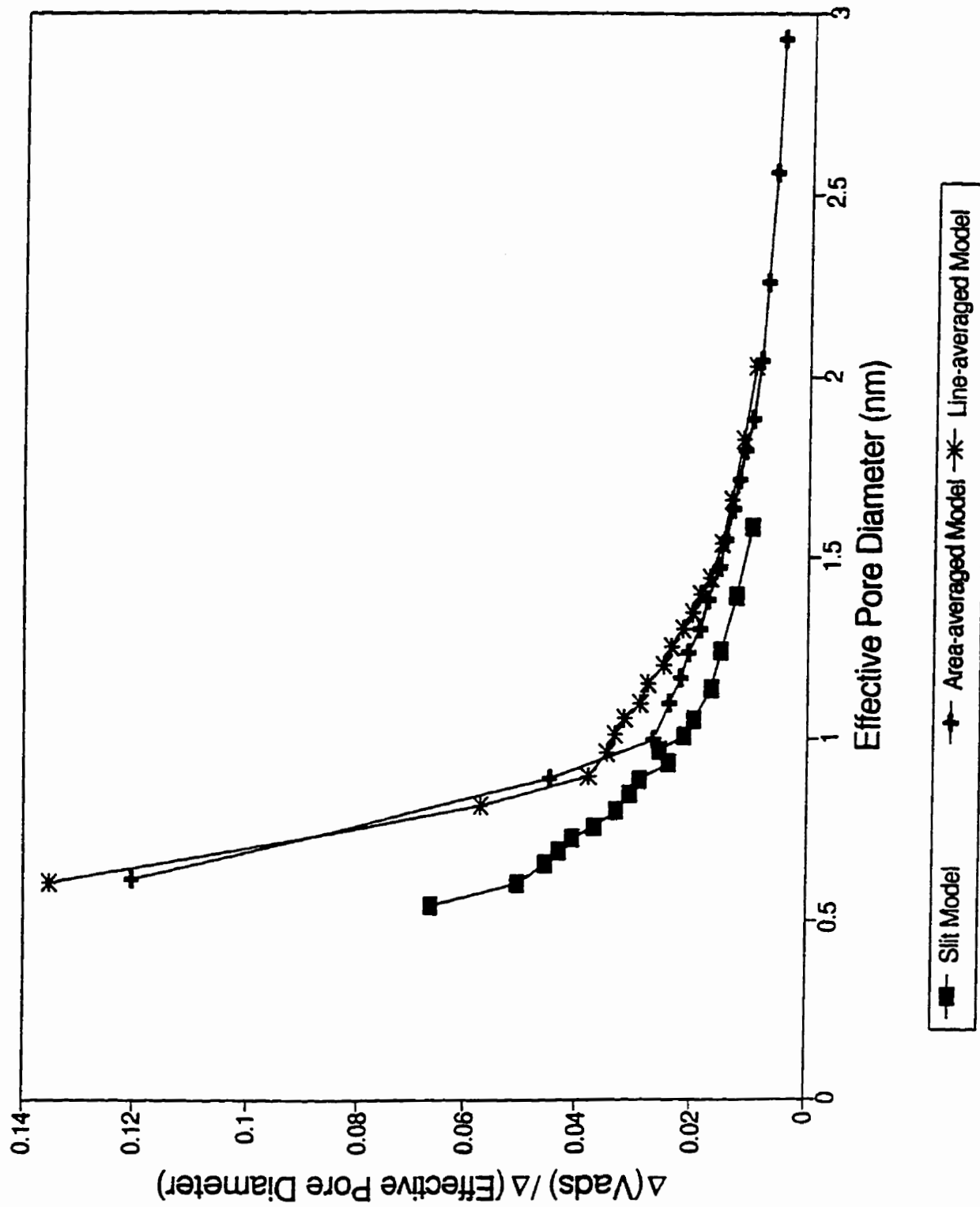


Figure 4.5 - Pore size distribution of $Tl_7PMo_{12}O_{40}$ by HKSF methods.

$\pm 30\%$ and concluded that the diameter of the oxide ion at the surface had the greatest influence on the calculated pore size, while the other parameters only had a moderate to a small effect.¹⁶ In the present work some error may be introduced by the assumption that the diameter of the oxide ion in a zeolite Y system would be comparable to the Keggin anion in the thallos salt.

4.4 Discussion

While no rigorous definition of the surface of a solid is currently available, there is general agreement that the interaction of nonreacting molecules with a solid surface can provide operational definitions of the surface area.⁹ The IUPAC approved method for generating surface area data applies the infinite layer BET theory to the experimentally measured adsorption isotherm. Values falling below the extrapolated linear portion of the experimental data from the BET equation in the very low pressure region have been ascribed to the presence of physisorption sites on the surface with higher energies than the expected BET values for the molecules adsorbing immediately adjacent to the solid surface. Such higher energies may result from the existence of an approximately planar surface which is energetically heterogeneous or from the existence of micropores, which as a result of the close proximity of the adsorbing molecules to a larger fraction of the surface generate enhanced global potential surfaces. With solids containing micropores the reduced range of linearity of the BET plots introduces errors in the determination of both the slopes and the intercepts.

In obtaining morphological information, the finite layer BET and the DR theories suffer from their inability to yield pore size distribution. The HK and HKSF methods, while taking into account the presence of potential surfaces within the pores which are dissimilar from those on the peripheral surfaces, have the disadvantage that either two-body or global potentials for solid surfaces are difficult to construct for real catalytic solids and the simplest adsorbate molecules.

In contrast the MP method avoids any requirements for the calculation of a potential surface but necessitates the availability of relationships between the thickness of the adsorbed layer and the equilibrium relative pressure in the adsorption process.

Although in principle the latter can be obtained from the adsorption isotherm of a nonporous analogue of the porous solid of interest, in practice this is difficult to achieve.

It is clear that the MP and the HK (and HKSF) methods each have their advantages and disadvantages. In the present work the former technique has been employed together with the Lecloux and Pirard procedure for generating t vs P/P_0 data. While the latter has been criticized,^{25,26} comparisons between the results obtained therefrom and those obtained using nonporous solids of similar, but not identical, composition as those of the porous solids of interest provide evidence for the relative validity of the LP procedure.^{20,21} However, the absence of specific reference isotherms for the larger values of C_{BET} imposes a limitation on this approach. The negative deviations from linearity that are evident in the t -plots are a result of the narrow pores being filled by multilayer adsorption so that subsequent adsorption does not occur on the entire surface. The lack of linearity in the pressure region of $0.4 < P/P_0 < 0.6$ contributes to errors in the determination of the micropore volume (V_{MP}).

The DR approach, not unexpectedly, also has its advantages and disadvantages. The existence of linearity in the DR plots is not sufficient to guarantee micropore filling or the validity of V_{DR} .²⁷ This is particularly evident from the observation of linearity at relative pressures approaching unity.¹⁸ In addition the presence of mesopores may, even with relative pressures less than 0.1, result in inflated values for the micropore volume.²² Although a number of techniques have been proposed to correct for the presence of mesopores, none of them is universally applicable.²⁸ Although a consensus has not been achieved²⁹⁻³¹ it has been suggested that the BET and DR equations should provide results in good agreement where the solids have a preponderance of available surfaces located in pores of molecular dimensions.³¹

The approach of Horvath and Kawazoe¹⁴ appears to correct the problems associated with the BET method by taking into account the nature of the adsorbent, with an average potential function determined for the inside of the slit-like pores. However, the determination of a realistic global potential inevitably necessitates the introduction of assumptions and simplifications. However, the application of a global potential accommodates the enhanced adsorption that may occur in micropores and that the BET

and t-plot methods do not explicitly take into account. Saito and Foley confirm that useful information about the micropore structures can be derived from the nitrogen and argon isotherms, in terms of C_{BET} , t-plot, and the DR model.¹⁶ However, as Saito and Foley note these methods do not provide a straightforward relationship between the logarithm of the relative pressure and the pore size¹⁶ such as found in the Kelvin equation. However, the Kelvin equation accounts for capillary condensation, which is not applicable to micropores.³²

The application of the slit and cylindrical models provides a method permitting such a direct relationship and appears to accommodate successfully different trends which may occur in the isotherm. Literature reports of the use of the models developed by Horvath and Kawazoe and Saito and Foley have been successful in describing different systems, correlating well with other methods,^{33,34} although the limitations of each, especially the slit model, have been recognized.¹⁵ In the characterization of other heteropoly oxometalates, Corma *et al.*³⁵ have used the HK method with the microporous ammonium, cesium and potassium salts of 12-tungstophosphoric acid and found these results in good agreement with pore diameters previously determined by ^{129}Xe NMR.³⁶

It is concluded, in view of the deficiencies in each of the presently available methods for the determination of micropore distributions from adsorption-desorption isotherms, that a comparison of the results obtained from the application of a variety of these techniques may be in order to verify results. If only one method is employed to determine the micropore distribution, knowledge of its assumptions and limitations should be considered when reporting conclusions.

4.5 References

1. M.L. Occelli. "Synthesis of Microporous Materials." Van Nostrand-Rienhold: New York, 1992.
2. E.G. Derouane; F. Lemos; C. Naccache; N.R. Ribeiro, Eds. "Zeolite Microporous Solids: Synthesis, Structure and Reactivity." Kluwer: Dordrecht, 1991.
3. D. Barthameuf; E.G. Derouane; W. Hölderich, Eds. "Guidelines for Mastering the Properties of Molecular Sieves." Plenum: New York, 1990.
4. M.L. Occelli. "Zeolite Synthesis." American Chemical Society: Washington, DC, 1989.
5. D.M. Ruthven. "Principles of Adsorption and Adsorption Processes." Wiley: New York, 1984.
6. M. Ternan. *J. Catal.*, **146**, 598 (1994).
7. A.M. Puziy. *Langmuir*, **11**, 543 (1995).
8. C. Moreno-Castilla; F. Carrasco-Marin; M.V. López-Ramón. *Langmuir*, **11**, 247 (1995).
9. J. Rouquerol; D. Avnir; D.H. Everett; C. Fairbridge; M. Haynes; N. Pernicone; J.D.F. Ramsay; K.S.W. Sing; K.K. Unger. In "Characterization of Porous Solids III" (J. Rouquerol; F. Rodriguez-Reinoso; K.S.W. Sing; K.K. Unger, Eds.) *Studies in Surface Science and Catalysis*, **87** Elsevier: Amsterdam, 1994, p.1.
10. R.Sh. Mikhail; S. Brunauer and E.E. Bodor. *J. Colloid Interface Sci.*, **26**, 45 (1968).
11. S. Brunauer, P.H. Emmett and E. Teller. *J. Am. Chem. Soc.*, **60**, 309 (1938).
12. (a) C. A. Leon y Leon. *Altamira Notes*, **September**, 1 (1991).
(b) M.M. Dubinin; E.D. Zaverina and L.V. Radushkevich. *Zh. Fiz. Khim.*, **21**, 51 (1947).
(c) M.M. Dubinin and L.V. Radushkevich. *Proc. Acad. Sci. USSR*, **55**, 331 (1947).
(d) M.M. Dubinin. *Russ. J. Phys. Chem.*, **39**, 697 (1965).
13. A. Lecloux and J.P. Pirard. *J. Colloid Interface Sci.*, **70**, 265 (1979).
14. G. Horvath and K. Kawazoe. *J. Chem. Eng. Japan*, **16**, 470 (1983).

15. R.D. Kaminsky; E. Maglara; W.C. Conner. *Langmuir*, **10**, 1556 (1994).
16. A. Saito and H.C. Foley. *AIChE Journal*, **37**, 429 (1991).
17. M.A. Parent and J.B. Moffat. *Langmuir*, **11**, 4474 (1995).
18. S.J. Gregg and K.S.W. Sing. "Adsorption, Surface Area and Porosity." Academic Press Inc. (London) Ltd.: London, 1982.
19. R.Sh. Mikhail; S. Brunauer; E.E. Bodor. *J. Colloid Interface Sci.*, **24**, 451 (1967).
20. J.B. McMonagle and J.B. Moffat. *J. Colloid Interface Sci.*, **101**, 479 (1984).
21. D.B. Taylor; J.B. McMonagle; J.B. Moffat. *J. Colloid Interface Sci.*, **108**, 278 (1985).
22. M.M. Dubinin in "Chemistry and Physics of Carbon." (P.L. Walker, Ed.) Marcel Dekker Inc.: New York, 1966; **2**, p. 51.
23. D.H. Everett and J.C. Powl. *J. Chem. Soc., Faraday Trans. I*, **72**, 619 (1976).
24. J.B. Riggs. "An Introduction to Numerical Methods for Chemical Engineers." Texas Tech University Press: Texas, 1985; pp. 48-63.
25. G.D. Parfitt; K.S.W. Sing; D.J. Urwin. *J. Colloid Interface Sci.*, **53**, 187 (1975).
26. M.M. Dubinin in "Surface Area Determination." (D.H. Everett and R.H. Ottlewill, Eds.) Butterworth and Co. (Publishers) Ltd.: London, 1970; p 123.
27. P.J.M. Carrott, R.A. Roberts and K.S.W. Sing in "Characterization of Porous Solids." (K.K. Unger, J. Rouguerol, K.S.W. Sing and H. Kral, Eds) *Studies in Surface Science and Catalysis*, **39** Elsevier: Amsterdam, 1988, pp. 89-100.
28. M.M. Dubinin. *Carbon*, **25**, 593 (1987).
29. (a) D.F. Klemplerer in "Surface Area Determination." (D.H. Everett and R.H. Ottlewill, Eds.) Butterworth and Co. (Publishers) Ltd.: London, 1970; pp. 55-57.
(b) B.A. Gottwald in "Surface Area Determination." (D.H. Everett and R.H. Ottlewill, Eds.) Butterworth and Co. (Publishers) Ltd.: London, 1970; pp. 59-61.
30. A. Granville; P.G. Hall; C. J. Hope. *Chem. and Ind.*, 435 (1970).
31. P.L. Walker and R.L. Patel. *Fuel*, **49**, 91 (1970).

32. L.R. Fisher and J.N. Israelachvili. *J. Colloid Interface Sci.*, **80**, 528 (1981).
33. A. Gil and M. Montes. *Langmuir*, **10**, 291 (1994).
34. W.C. Ackerman; D.M. Smith; J.C. Hilling; Y.-M. Kim; J.K. Bailey; C.J. Brinker. *Langmuir*, **9**, 1051 (1993).
35. A. Corma; A. Martínez; C. Martínez. *J. Catal.*, **164**, 422 (1996).
36. J.L. Bonardet; J. Fraissard; G.B. McGarvey; J.B. Moffat. *J. Catal.*, **151**, 147 (1995).

CHAPTER 5

Isomerization of 1-Butene

5.1 Introduction

Isomerization of 1-butene is frequently used as a means of assessing acidic properties of catalysts to compare the conversion, selectivity, and stability of the catalysts. Heterogeneous catalysis of this reaction has been studied for over four decades.¹⁻⁷⁸ Renewed interest in the isomerization of 1-butene has been brought about by the anticipated oversupply of 1-butene coupled with the demand for *iso*-butene as an alkene precursor in the synthesis of methyl *tert*-butylether (MTBE),^{20,21,23,24,29} an octane enhancer replacing tetramethyl lead in reformulated gasoline.⁷⁹ Recent studies have included a wide variety of catalysts, including various oxides,^{2,5,12,12,20,21,23,24} aluminophosphates,^{15,19} and zeolites.^{1,3-7,9,11,13,16,18,25-28} Butler and Nicolaidis²⁹ have also provided a survey of the progress made since the late 1970's in implementing the catalytic skeletal isomerization of linear alkenes. In addition to the interest in industrial applications, skeletal isomerization of 1-butene is of fundamental interest since earlier literature had indicated that the C₄ hydrocarbons should not selectively isomerize to form *iso*-butene, although they can undergo scrambling of carbon atoms over the four positions in the linear molecule.^{66,69}

For catalysts containing Brønsted acid sites, it is generally proposed that isomerization of 1-butene proceeds via the carbenium ion mechanism.^{61,62} Protonation of 1-butene will form either the primary or secondary butyl carbenium ion.⁷⁰ While formation of the secondary butyl carbenium ion is energetically more favourable than the primary butyl carbenium ion,⁶⁹ it is not possible to preclude the direct formation of the latter. From the secondary butyl carbenium ion, double bond isomerization will form the *cis* and *trans* isomers of 2-butene while skeletal isomerization will form *iso*-butene.

(Figure 5.1) Skeletal isomerization is a reaction of moderate difficulty, requiring sites of relatively higher acid strength to catalyze the formation of the thermodynamically less stable primary butyl carbenium ion in contrast to the double bond isomerization of 1-butene which is considered a facile reaction.²⁹ Choudhary provided a review of the kinetics and mechanism of this reaction, as well as the thermodynamics and physical

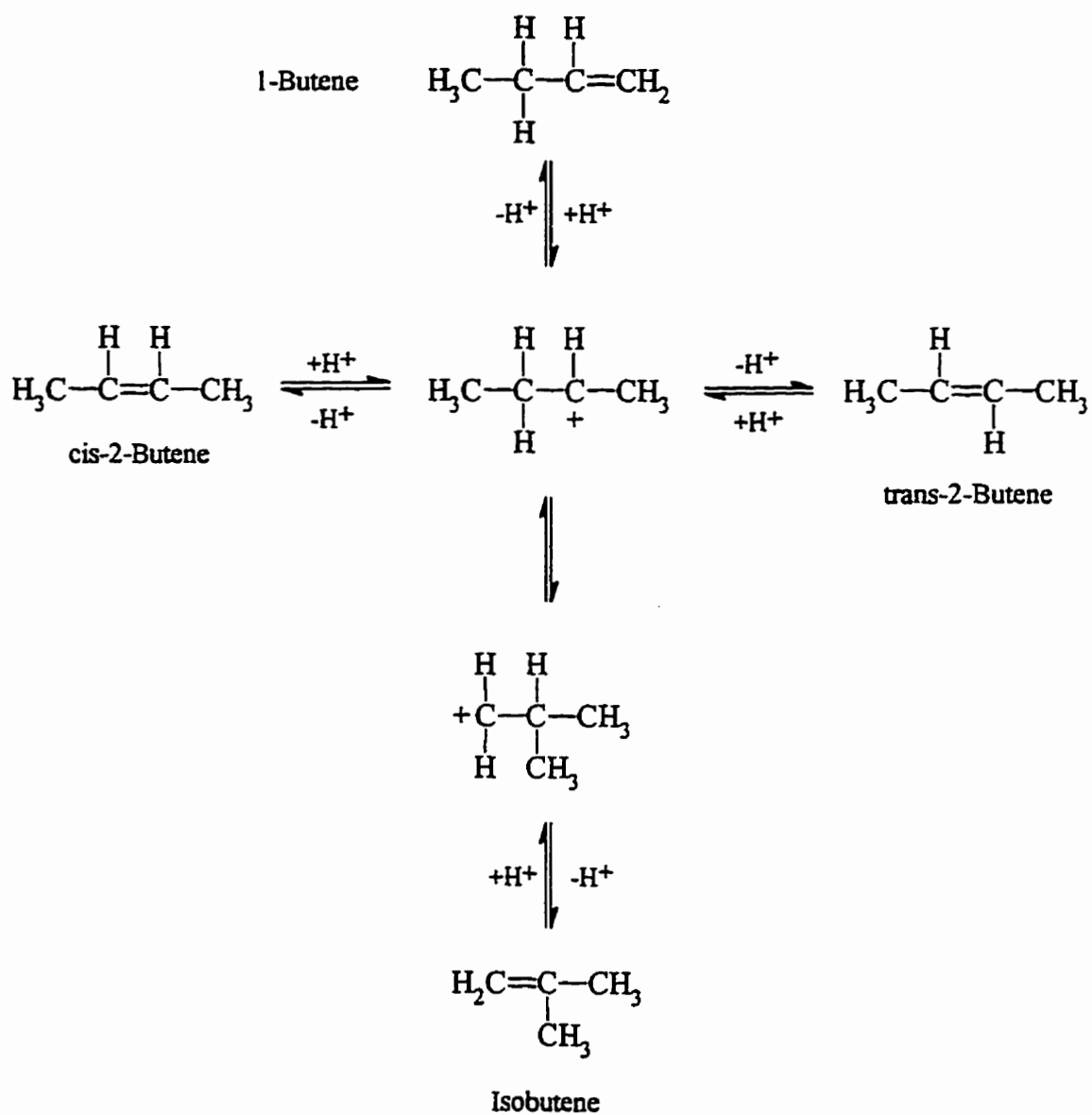


Figure 5.1 - Mechanistic scheme for the isomerization of 1-butene.

properties of the four butenes and the thermodynamics of the reaction system.⁶²

Although the carbenium ion mechanism has frequently been cited for the mechanism for the isomerization of 1-butene,²⁹⁻³¹ debate that a bimolecular mechanism may be operative continues.^{24,26,28} The bimolecular mechanism proposes the dimerization of 1-butene to octene(s) which then skeletally isomerize. *Iso*-butene is formed by the subsequent cracking of the octene(s). Cheng *et al.*^{20,21} have found evidence for the bimolecular mechanism but with the concomitant formation of products such as those containing three and five carbon atoms. It was concluded that the monomolecular mechanism is dominant with the series of oxides, supported and unsupported, investigated, although the bimolecular mechanism is possible in principle.

More recent work has continued to conclude that the skeletal isomerization of 1-butene is monomolecular.^{5,6,8,14,15} Gielgens *et al.*¹⁴ questioned why only byproducts containing three and five carbon atoms (C₃ and C₅) were formed, with no occurrence of C₂ or C₆. Dimerization of 1-butene, as proposed by the bimolecular mechanism, could form intermediates such as 3-monomethylheptene and 3,4-dimethylhexene. Subsequent cracking of these intermediates would include C₂ and C₆ products. In addition, propene and pentene fragments could not be formed from 3,4-dimethylhexene. Dimerization of *iso*-butene should produce trimethylpentene as the intermediate, of which C₃ and C₅ would follow from cracking. It was concluded that the bimolecular mechanism was in fact only involved in the formation of byproducts from *iso*-butene.^{5,6,14}

As summarized in Chapter 2, microporous structures were found for the silver(I) and thallium(I) 12-heteropoly oxometalate salts, indicating that such structures are not restricted to salts prepared from the alkali metals, such as cesium(I). The larger cation diameter results in an increase of the surface area, micropore volume, and mean micropore radius. This is a result of the Keggin anions shifting and rotating in the lattice framework, in order to accommodate the larger cations, and thus removing barriers between the interstitial voids, creating channels throughout the structure. For a given salt, the surface area increases as the preparative cation to proton ratio is increased, but these changes are smaller than observed for salts previously isolated by evaporation.⁸⁰ As discussed in Chapter Two, the difference may be attributed to the removal of a portion of

unreacted reagents during filtration, in particular those on the surface of the precipitated particles.

PAS FTIR studies have indicated that the protons remain in the precipitated heteropoly oxometalate salts, indicating that the substitution of the protons was incomplete despite the use of a stoichiometric amount of the cation.⁸¹ ¹H MAS NMR spectra in Chapter Two of the currently prepared 12-heteropoly oxometalate salts have provided evidence that the creation of a microporous structure has an effect on the chemical environment in which the residual protons reside.⁸² Variations in the preparative cation:proton ratio alter the number of protons remaining in the salt. As a result, the modification of acidity may have an effect on the catalytic properties of the salt.

The objective of this chapter is to provide information on the catalytic properties of the cesium(I), silver(I) and thallium(I) salts of the three heteropoly acids: 12-tungstophosphoric acid, 12-tungstosilicic acid and 12-molybdophosphoric acid. Temperature programmed desorption (TPD) of ammonia and ¹H MAS NMR measurements were used to assess the number of acid sites available within a specific salt and the distribution of acid strengths. Isomerization reactions with 1-butene were performed with the silver(I) and thallium(I) salts to determine the dependence of their catalytic properties, specifically the conversion and product distribution, on the nature of the cation, the stoichiometry and morphology of the salt. This will provide information regarding changes in the acidic strength of the salt when nonprotonic cations are introduced.

5.2 Experimental

5.2.1 Materials

Helium and 1-butene were purchased from Praxair.

The cesium, silver and thallium salts of 12-tungstophosphoric, 12-tungstosilicic and 12-molybdophosphoric acids were prepared as outlined in Section 2.2.1. For the isomerization reactions of 1-butene, the cation:proton ratios of 0.50, 1.00 and 1.50 were examined for the silver and thallium salts of 12-tungstophosphoric acid (denoted as AgPW and TlPW, respectively, hereafter) whereas the 0.85, 1.00 and 1.15 ratios were examined

for the analogous salts of 12-tungstosilicic acid (denoted as AgSiW and TlSiW, respectively, hereafter) and thallium 12-molybdophosphate (denoted as TIPMo).

Since the 12-heteropoly oxometalate salts precipitated spontaneously as microcrystalline materials, the particle size distribution of each salt was determined. After grinding with a pestle and mortar, each salt was passed through a series of mesh sieves (80 mesh, 100 mesh, 150 mesh and 200 mesh) by shaking manually. For all of the salts examined, with exception of the AgPW salts, the largest portion of particles consisted of a diameter less than 75 μm (<200 mesh). This was determined to be greater than 35% of the total mass of the sample for the TlSiW salts, > 40% for the TIPMo salts, > 50% for TIPW salts and > 95% for the AgSiW salts. In contrast the AgPW salts had the largest portion of particles in the diameter range of 106 to 150 μm (100 to 150 mesh) while the pure acids were greater than 180 μm . Variation in the cation to proton ratio used in the synthesis of the salt did not have an effect on the particle size distribution.

The samples of catalyst used in the isomerization of 1-butene consisted of particles < 75 μm (< 200 mesh) in diameter with the exception of the AgPW salts. These salts were sticky in nature and a larger particle size was required to maintain a consistent residence time and avoid a build-up of backpressure in the reactor system. As a result, particles of 106 to 150 μm were used for reactions with AgPW. No difference in activity was noted for HPW with a change in particle size. The particle size of a catalyst can have an effect on the conversion⁸³ and selectivity⁸⁴ observed. However, intrinsic kinetic data have not been determined in the present study so these effects were not considered.

5.2.2 Characterization Techniques

¹H MAS NMR spectra were obtained with a Bruker AMX-500, with an external reference of benzene, at room temperature and the spinning rate of 7 kHz. Prior to the ¹H MAS NMR measurements the salts were heated to 120 °C for 1.5 hours, allowed to cool to room temperature for 1.5 hours, all under a weak vacuum, and stored in a desiccator. The mass of the sample placed in the zirconia holder was recorded prior to each measurement.

For temperature programmed desorption of ammonia the sample was heated to 150

°C over a 20 minute period with a 20 mL/min flow of helium, after which an aliquot of gaseous ammonia (20 mL) was injected. After one minute, the system was cooled to 30 °C over 30 minutes. The ammonia was desorbed with a temperature ramp of 10 °C/min from 30 °C to 650 °C, under a flow of helium (20 mL/min), and monitored by a HP5890 gas chromatograph equipped with a HP5970 series mass selective detector.

5.2.3 Apparatus and Procedure

The catalytic reaction for the isomerization of 1-butene was carried out in a small flow system, constructed from 1/8" stainless steel tubing (0.02" wall thickness), unions, connectors and valves, as depicted in Figure 5.2. A glass tube reactor, constructed from Pyrex, was attached using 1/4"-1/8" reducing unions. The reactor tube (6 mm o.d., 4 mm i.d.) of 21 cm in length had a small bubble (15 mm in length, 10 mm o.d.) placed in its centre, in which the sample of catalyst (150 mg) was supported between two plugs of quartz wool. A thermocouple was placed such that it was located 6.5 cm from the exit side of the tube. A furnace with an inner quartz sleeve surrounded the glass reactor tube and the heating was controlled by a Digi Sense proportional temperature controller equipped with a Type K thermocouple sensor. Temperatures could be set and maintained to ± 0.2 °C. The stainless steel tubing leading from the exit of the glass reactor to the entrance of the gas chromatograph was heated with heating tape to prevent condensation of products in the lines. The reactant mixture could be directed through either the reactor or the bypass section.

The catalyst was pretreated *in situ* in a flow of helium (20 mL/min) at the reaction temperature for 1 hour prior to exposure to a mixture of 17% 1-butene : 83% helium, at the same flow rate. The flow of the gases was regulated using needle valves and monitored using rotameters. The reactant and products were analyzed with a HP 5880A gas chromatograph equipped with a TCD and a Carboxen 101 column (2 meter x 1/8" OD) with the oven temperature set at 50 °C. Reaction temperatures were 100, 200, and 300 °C and initial activities were measured at 10 minutes after the introduction of the reactant mixture, with further sampling at 70 and 130 minutes. The sample loop was injected to the GC by opening a four-way valve for 30 seconds and all exits were vented to the

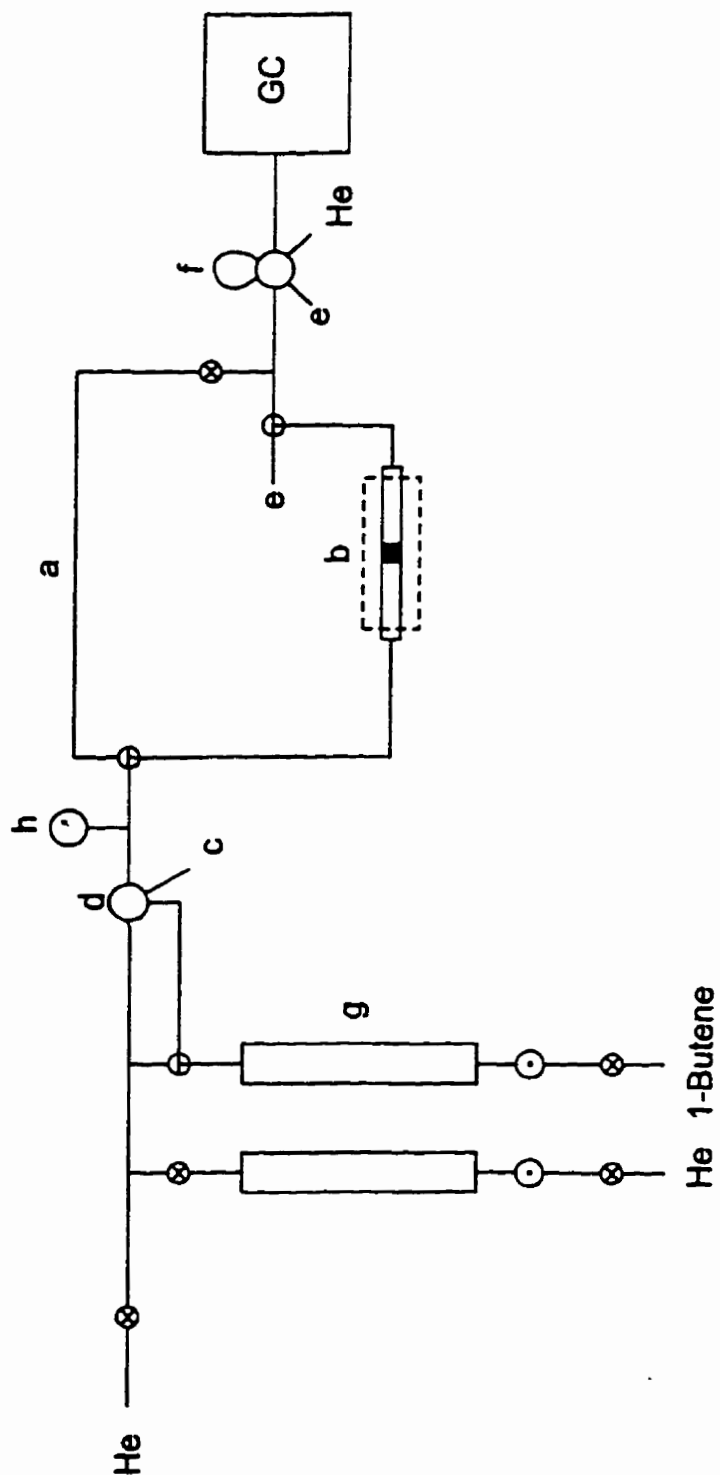


Figure 5.2 - Catalytic reactor system. (a) reactor bypass section; (b) reactor tube and furnace; (c) reactant flow vent; (d) 4-way valve; (e) product flow vent; (f) 6-port valve; (g) rotameters; (h) pressure gauge.

fume hood. No conversion of 1-butene was observed with an empty reactor in the range of temperatures employed in the present work.

5.2.4 Definitions

Cis- and *trans*-2-butene were the only products from the isomerization of 1-butene. The % conversion was based on only the reactants and products monitored by the GC, so that

$$\% \text{Conv} = 100 \left[\frac{\text{total moles of products}}{\text{total moles of products} + \text{moles of unreacted 1-butene}} \right] \quad (5.1)$$

The selectivity of the products was expressed as a ratio of the two isomers of 2-butene.

$$\text{Selectivity} = \left[\frac{\text{moles of cis-2-butene}}{\text{moles of trans-2-butene}} \right] \quad (5.2)$$

5.3 Results

5.3.1 Distribution of Acid Sites and Strengths.

¹H MAS NMR spectra had been obtained for the cesium, silver, and thallium salts of 12-tungstophosphoric and 12-tungstosilicic acids, along with thallium 12-molybdophosphate. These spectra have previously been discussed in Chapter 2 (Sections 2.3.3 and 2.3.5) with the characterization of the micropore structures present in these salts. As a brief summary, the spectrum for TIPW salts consists of a single resonance and as the cation-to-proton ratio increases, the relative peak area attributed to the residual protons decreases. The chemical shift for protons in HPW has been reported as $\delta = 9.6$ ppm.⁸⁵ With an increase in the relative amounts of cation used in the synthesis of the salt, the resonance for the residual protons in the TIPW shifts upfield, reflecting a change in the chemical environment of the residual protons. (Table 5.1) In contrast to the TIPW salts, two resonances are present for the residual protons in the AgPW salts. The larger, more

intense peak mimics the TIPW salts and shifts upfield with the increase in the cation:proton ratio while a smaller weak resonance moves slightly downfield. (Table 5.1) The ^1H MAS NMR spectra for the CsPW salts are similar to those observed for the TIPW salts, with a single resonance moving upfield as the cation:proton ratio is increased. The exception to this is found with the 0.85 salt which exhibits a shoulder on the downfield side of its peak, indicating a portion of the residual protons reside in a second, slightly different environment. This shoulder disappears with those preparations which employ a stoichiometric or excess amount of the cation to synthesize the salt. (Table 5.1) It should be noted that all the peaks observed were overlapped with a very broad peak attributed to the presence of water.

TABLE 5.1 - Chemical shifts (ppm) of residual protons for the stoichiometric and nonstoichiometric salts.

| Salt | 0.85 | 1.00 | 1.15 |
|-------------------------------------------|------------------|------------------|------------------|
| $\text{Ag}_3\text{PW}_{12}\text{O}_{40}$ | 6.4 ^a | 6.0 ^a | 5.7 ^a |
| $\text{Tl}_3\text{PW}_{12}\text{O}_{40}$ | 7.3 | 6.2 | 5.2 |
| $\text{Cs}_3\text{PW}_{12}\text{O}_{40}$ | 7.2 ^b | 6.5 | 5.4 |
| $\text{Ag}_4\text{SiW}_{12}\text{O}_{40}$ | 5.6 ^c | 4.2 | 4.2 |
| $\text{Tl}_4\text{SiW}_{12}\text{O}_{40}$ | 7.2 | 6.8 ^d | 5.6 ^e |
| $\text{Cs}_4\text{SiW}_{12}\text{O}_{40}$ | 6.1 ^f | 6.6 ^f | 7.2 |
| $\text{Tl}_3\text{PMo}_{12}\text{O}_{40}$ | 6.9 | 6.0 | 5.3 |

^a A peak of weak intensity was also observed at 4.3 ppm.

^b A shoulder was observed at 8.1 ppm.

^c A shoulder was observed at 4.3 ppm.

^d A shoulder was observed at 6.1 ppm.

^e A shoulder was observed at 6.2 ppm.

^f A shoulder was observed at 8.4 ppm.

For each of the three 12-tungstosilicate based salts examined, CsSiW, AgSiW and TlSiW, the resulting ^1H MAS NMR spectra each consisted of two peaks located upfield of the pure acid resonance, noted in the literature as $\delta = 10.9$ ppm.⁸⁵ (Table 5.1) The

intensities of the two peaks observed for the silver and thallium salts exchange as the amount of the cation is increased for the salt synthesis although the second resonance appears as a shoulder for the AgSiW salts. However, this does not appear to be the case for the analogous cesium salt, CsSiW, as the cesium content of the salt increases. The spectra for the three cation:proton ratios of the TIPMo salts mimics the trend observed for the TIPW salts. A single resonance is present in the ^1H MAS NMR spectrum, which shifts upfield with the increase in the cation to proton ratio. (Table 5.1) All three cation:proton ratios depict resonances upfield of those reported for the protons in HPMo, $\delta = 7.4$ ppm.⁸⁶

It should be noted at this point that the resonances recorded for the silver salts, AgPW and AgSiW, displayed anisotropy, indicated by spinning sidebands present in the ^1H MAS NMR spectra (not evident in the narrow region depicted in the spectra in Chapter 2). For the AgPW salts this only occurred for the weaker resonance, located furthest upfield. Anisotropy occurs when a proton, whose resonance is being observed, is in close proximity to other protons so that dipolar coupling is experienced. Dipolar coupling can be described as a direct, through space interaction of two nuclear magnetic moments. The spinning rate of the samples could not be increased higher than 7 kHz to remove these spinning sidebands and minimize the anisotropy. The ^1H MAS NMR recorded for the pure acids, HPW and HSiW, also displayed spinning side bands while neither of the thallium or cesium based salts contained resonances which were anisotropic.

The absolute integrals were measured for each of the ^1H MAS NMR spectra. The values obtained for HPW and HPMo, accounting for the amount of the sample measured, were set to be equivalent to three moles of protons per mole of Keggin anion, while the value for HSiW was set to be equivalent to four moles of protons per mole of Keggin anion. The absolute integrals of the salts were then normalized with the value of the parent acid, taking into account the mass of each sample measured. The resulting values are summarized in Tables 5.2 and 5.3 and confirm previous indications that the relative amounts of residual protons decrease with the increase in the relative amounts of cation used in the synthesis. The silver salts for the two acids examined contain a larger portion of protons in comparison to the analogous salts containing either thallium or cesium

Table 5.2 - Composition of 12-tungstophosphate salts containing residual protons.

| Salt | Cation:Proton Ratio ^a | H ⁺ / Keggin Anion ^b |
|--------------------------------------------------|----------------------------------|--------------------------------------------|
| H ₃ PW ₁₂ O ₄₀ | | 3.0 ^c |
| Ag ₃ PW ₁₂ O ₄₀ | 0.50 | 0.94 |
| | 0.85 | 1.78 |
| | 1.00 | 1.27 |
| | 1.15 | 1.26 |
| | 1.50 | 1.14 |
| Tl ₃ PW ₁₂ O ₄₀ | 0.50 | 0.46 |
| | 0.85 | 0.41 |
| | 1.00 | 0.26 |
| | 1.15 | 0.15 |
| | 1.50 | 0.16 |
| Cs ₃ PW ₁₂ O ₄₀ | 0.85 | 0.36 |
| | 1.00 | 0.20 |
| | 1.15 | 0.07 |

^a Preparative ratio.

^b Calculated from absolute integrals in ¹H MAS NMR data. (moles/moles)

^c Assumed for calibration purposes.

cations, which are similar to one another. This difference may be attributed to the solubility limits characteristic of each salt. The significantly larger number of protons present in the silver salts, in comparison to those containing either cesium or thallium, may explain the anisotropic nature of the resonances present in the ¹H MAS NMR spectra of the former. Although expected to have the largest number of protons per mole of Keggin anion present in the series, the 0.50 AgPW salt contains the smallest number of these. This anomaly may be related to the anisotropic resonance. The portion of the absolute integral for the anisotropic peak in the ¹H MAS NMR spectra, including the area contributed by the spinning sidebands, recorded for the 0.85, 1.00 and 1.15 silver salts is

Table 5.3 - Composition of 12-tungstosilicate and 12-molybdophosphate salts containing residual protons.

| Salt | Cation:Proton Ratio ^a | H ⁺ / Keggin Anion ^b |
|---------------------------------------------------|----------------------------------|--------------------------------------------|
| H ₄ SiW ₁₂ O ₄₀ | | 4.0 ^c |
| H ₃ PMo ₁₂ O ₄₀ | | 3.0 ^c |
| Ag ₄ SiW ₁₂ O ₄₀ | 0.85 | 2.08 |
| | 1.00 | 1.06 |
| | 1.15 | 0.84 |
| Tl ₄ SiW ₁₂ O ₄₀ | 0.85 | 1.14 |
| | 1.00 | 0.49 |
| | 1.15 | 0.35 |
| Cs ₄ SiW ₁₂ O ₄₀ | 0.85 | 0.70 |
| | 1.00 | 0.53 |
| | 1.15 | 0.42 |
| Tl ₃ PMo ₁₂ O ₄₀ | 0.85 | 0.30 |
| | 1.00 | 0.14 |
| | 1.15 | 0.08 |

^a Preparative ratio.

^b Calculated from absolute integrals in ¹H MAS NMR data. (moles/moles)

^c Assumed for calibration purposes.

approximately 45 to 48%. In contrast to these three salts, the 0.50 AgPW salt has the upfield peak as the most intense in the spectrum and accounts for a significantly larger portion of the total area. The presence of spinning sidebands, resulting from anisotropy, contributes to the error associated with the absolute integral measured.

Temperature programmed desorption (TPD) of ammonia was carried out on each salt for the three cation-to-proton ratios (0.85, 1.00 and 1.15). Three distinct temperature ranges at which ammonia desorbed were present in the patterns observed for the AgPW salts (Figure 5.3) and are labelled as weak (100 - 300 °C), intermediate (300 - 500 °C)

Table 5.4 - Distribution of acid strengths and total acidity^a of 12-tungstophosphate salts.

| Salt | Cation:Proton Ratio | Acid Strength Distribution ^b (% of total area) | | | Total Specific Acidity ^{c,d} |
|--------------------------------------------------|------------------------|--------------------------------------------------------------|--------------|--------|---------------------------------------------|
| | | Weak | Intermediate | Strong | |
| Ag ₃ PW ₁₂ O ₄₀ | 0.85 | 37 | 48 | 15 | 51.9 |
| | 1.00 | 37 | 48 | 15 | 34.6 |
| | 1.15 | 42 | 46 | 12 | 51.7 |
| Tl ₃ PW ₁₂ O ₄₀ | 0.85 | 33 | 29 | 38 | 6.0 |
| | 1.00 | 15 | 43 | 42 | 1.2 |
| | 1.15 | 58 | 31 | 11 | 4.7 |
| Cs ₃ PW ₁₂ O ₄₀ | 0.85 | 16 | 26 | 58 | 2.1 |
| | 1.00 | 20 | 37 | 43 | 1.2 |
| | 1.15 | 30 | 42 | 27 | 0.8 |

^a Calculated from temperature-programmed desorption of ammonia.

^b Temperature ranges used for acid strength:
weak (100 °C - 300 °C); intermediate (300 °C - 500 °C); strong (> 500 °C)

^c Total Specific Acidity = Total Area Count / (S_{BET} × mass of sample)

^d Values multiplied by (× 10⁸).

and strong (> 500 °C) acid sites. The three stoichiometries of the silver salts appear almost identical, with three peak maxima appearing at similar temperatures and similar distributions between the three ranges of acid strengths. (Table 5.4) The total specific acidity for each salt was determined by normalizing the total area recorded for the TPD pattern by the surface area (S_{BET}) and mass of the sample.

In contrast, the amount of ammonia adsorbed by the CsPW and TIPW salts is at least an order of magnitude less than observed for the silver salts, which is consistent with the decreased number of residual protons calculated from the ¹H MAS NMR spectra. Three peaks are present in the TPD pattern for the 0.85 TIPW salt, with the largest peak appearing at approximately 580 °C. (Figure 5.4c) The pattern for the stoichiometric TIPW salt (Figure 5.4b) shows a very weak peak at approximately the same temperature, but

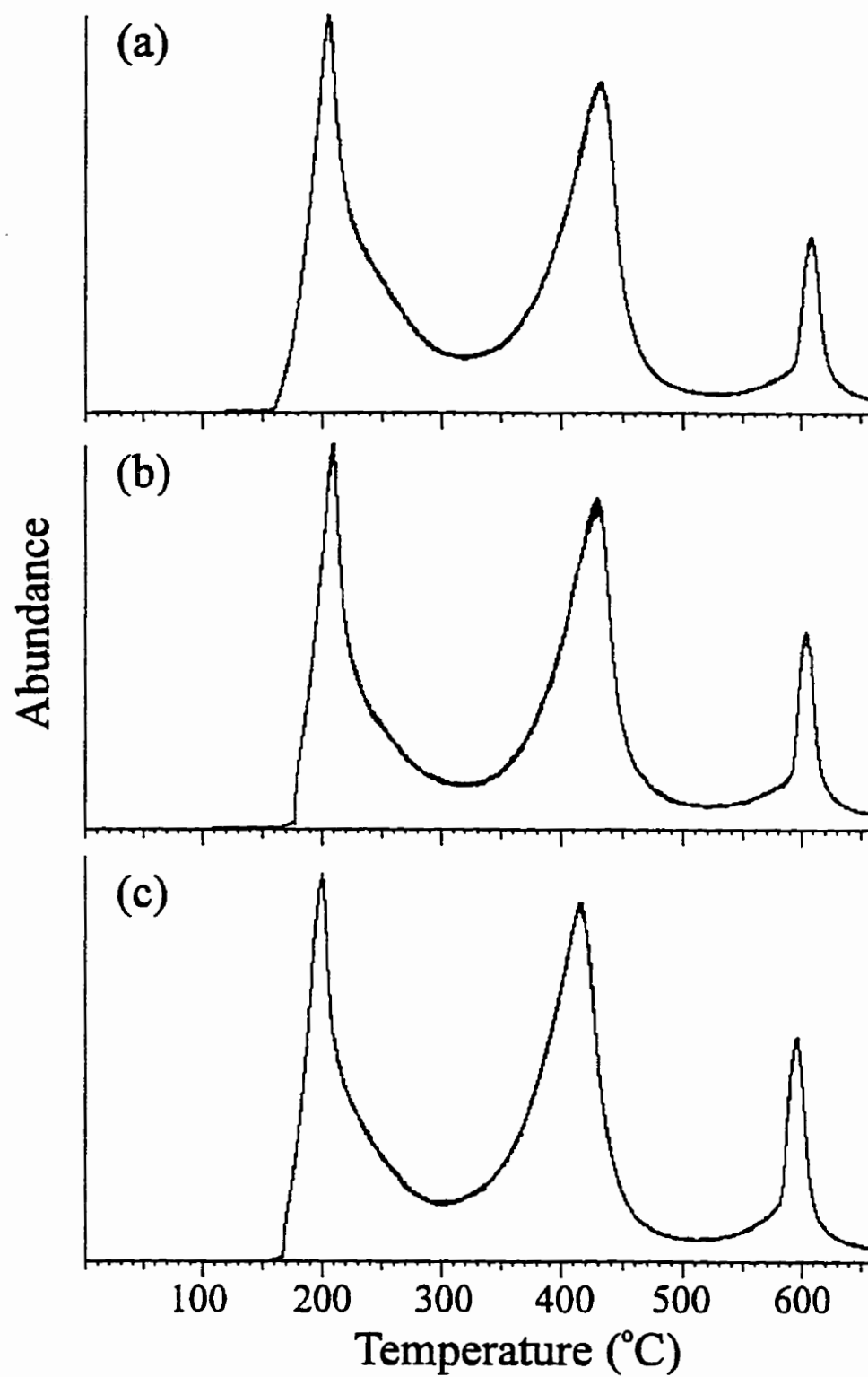


Figure 5.3 - TPD of ammonia with $\text{Ag}_3\text{PW}_{12}\text{O}_{40}$. Cation:proton ratios of (a) 1.15; (b) 1.00; (c) 0.85.

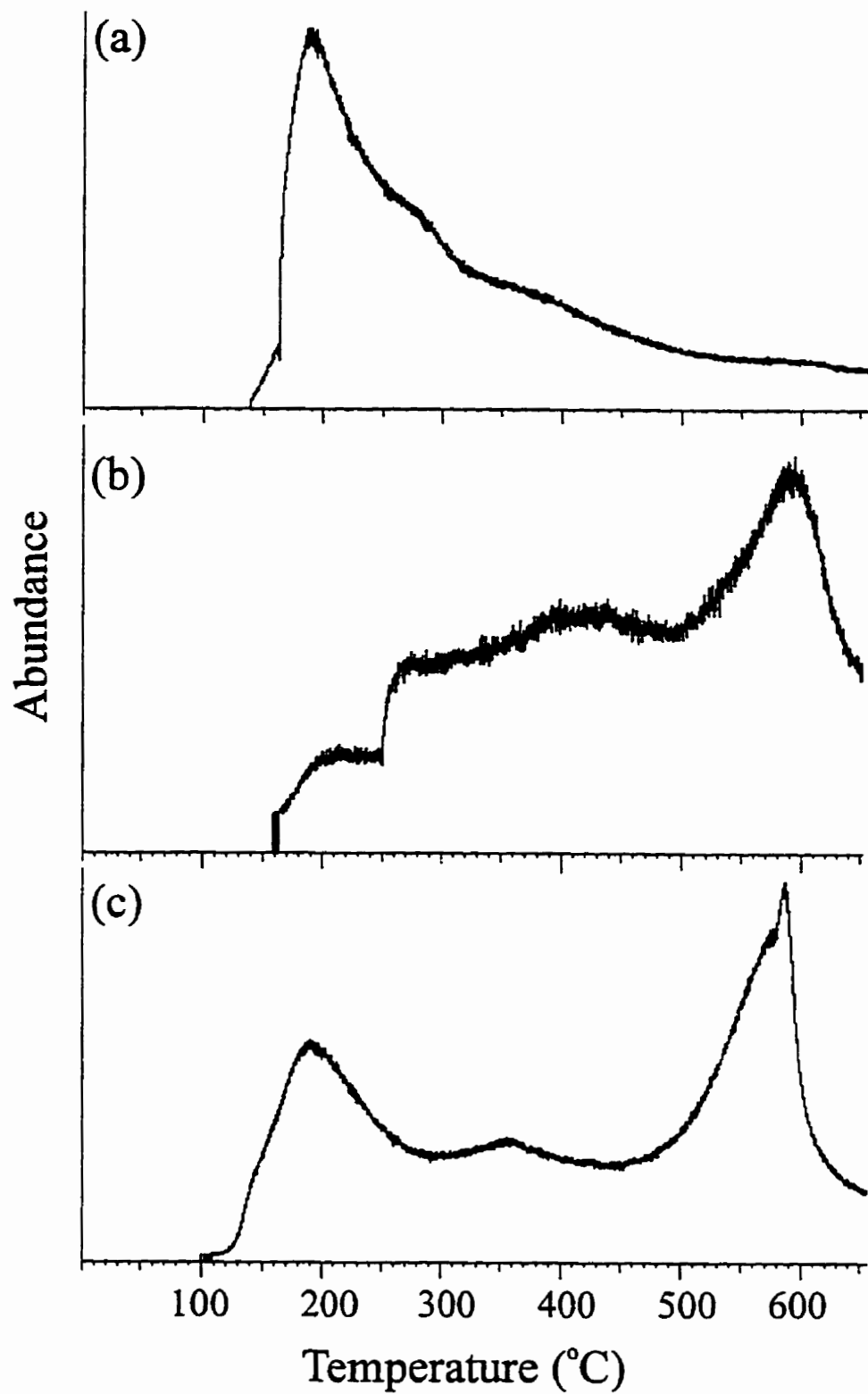


Figure 5.4 - TPD of ammonia with $Tl_3PW_{12}O_{40}$. Cation:proton ratios of (a) 1.15; (b) 1.00; (c) 0.85.

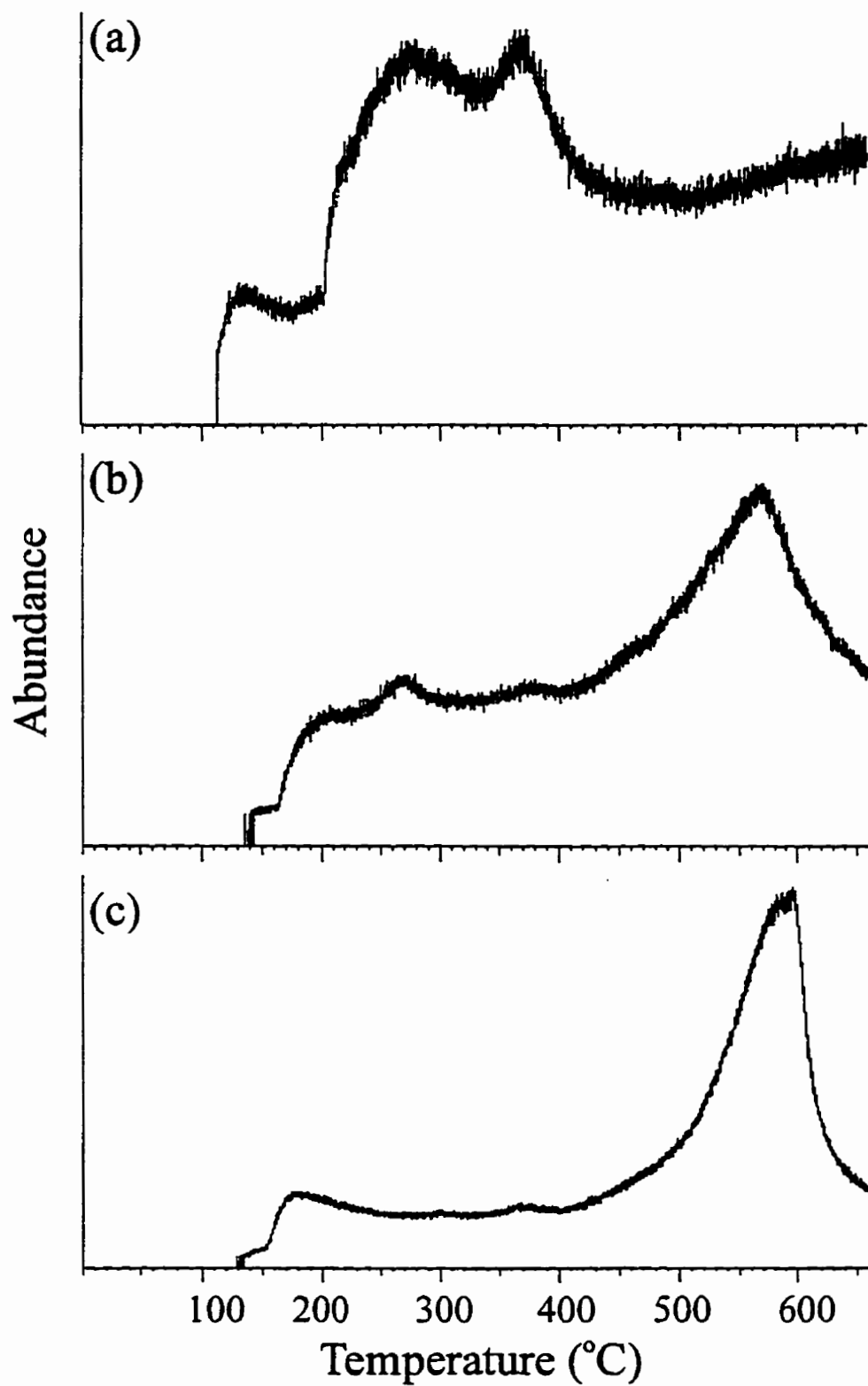


Figure 5.5 - TPD of ammonia with $\text{Cs}_3\text{PW}_{12}\text{O}_{40}$. Cation:proton ratios of (a) 1.15; (b) 1.00; (c) 0.85.

significantly less ammonia is present on this salt than that made with a deficit of the cation. With the TIPW salt having an excess of thallium, a significant difference occurs with the most intense peak at the lowest temperature, as reflected in the distribution in Table 5.4, and a gradual decline in intensity as the temperature increases. (Figure 5.4a) Two shoulders are present on the higher temperature side of the peak, but a peak at greater than 500 °C is now absent. The ammonia TPD for the 0.85 and stoichiometric CsPW salts (Figure 5.5) are similar to those observed for the analogous TIPW salts. The 0.85 CsPW salt has three acidic sites, with the largest peak at approximately 575 °C. Again, the stoichiometric salt has a similar peak at this temperature but significantly less ammonia is present in comparison with the deficit salt. (Table 5.4) For the 1.15 CsPW salt, the most intense peak shifts to a lower temperature, although not quite as low as the analogous TIPW salt.

The three silver salts of 12-tungstosilicate are similar to the AgPW salts, having three distinct temperature ranges at which the ammonia is desorbed and little variation in the distribution of acid strengths as the cation to proton ratio is increased (Figure 5.6 and Table 5.5). A larger portion of the sites are considered weak with the salt from the 12-tungstosilicic acid. Similar to the 12-tungstophosphoric acid series, the amount of ammonia adsorbed by the TlSiW and CsSiW salts is at least an order of magnitude less than observed with the AgSiW salts. The TlSiW and CsSiW salts also lack three well defined regions for the desorption of ammonia. The TPD spectra of TlSiW (Figure 5.7) and CsSiW (Figure 5.8) contain the most intense peak at approximately 300 °C. For the TlSiW salts, the shoulder on the higher temperature side of this peak declines as the cation:proton ratio is increased. With an excess of thallium, the lowest temperature regions accounts for most of the acid sites. (Figure 5.7 and Table 5.5) The CsSiW salts made with a deficit of the cation shows evidence of higher temperature sites at 390 °C, which disappears with the increase in the cation:proton ratio so that an excess of the cesium cation causes a significant increase in the portion of weak acid sites. (Figure 5.8 and Table 5.5)

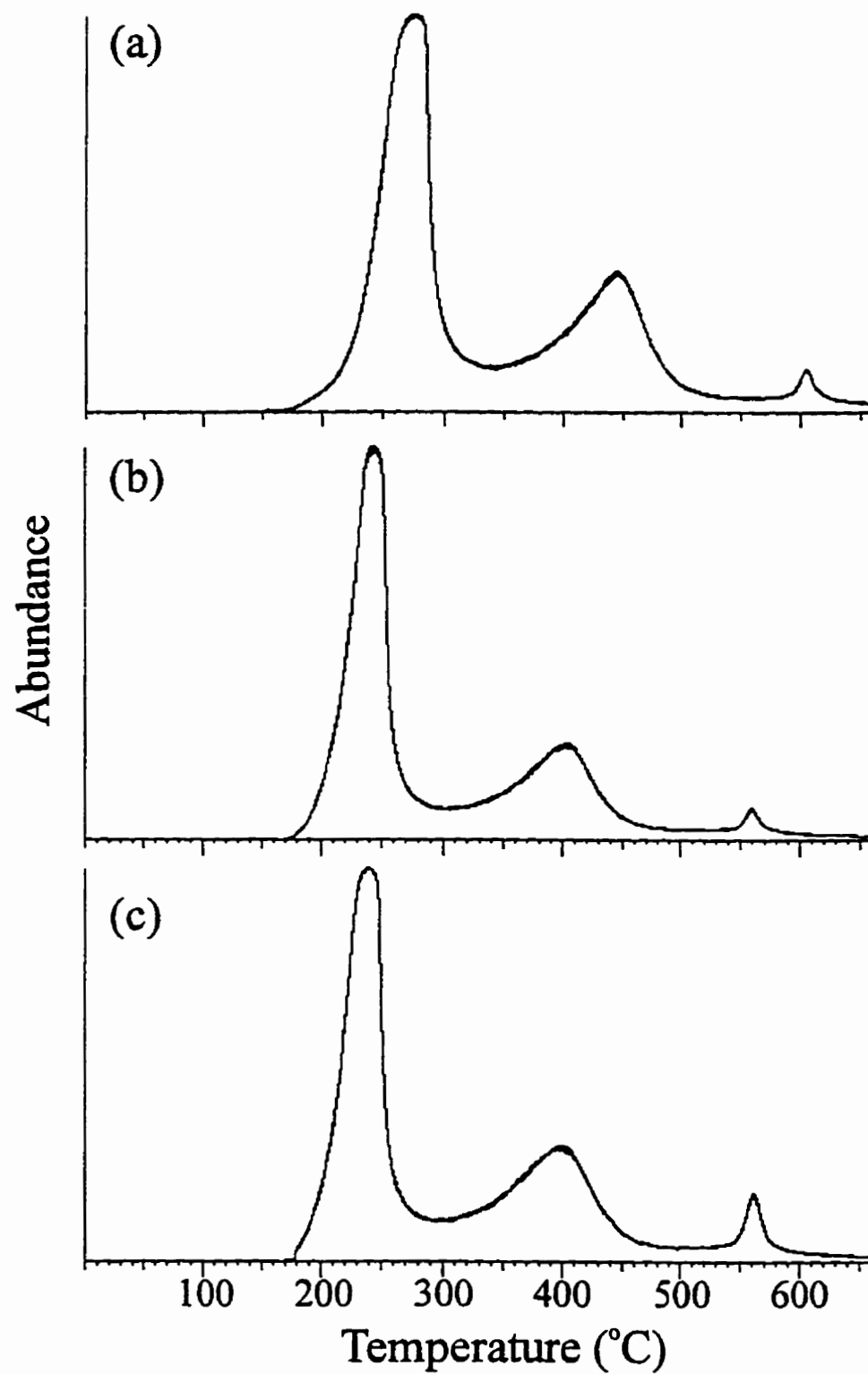


Figure 5.6 - TPD of ammonia with $\text{Ag}_4\text{SiW}_{12}\text{O}_{40}$. Cation:proton ratios of (a) 1.15; (b) 1.00; (c) 0.85.

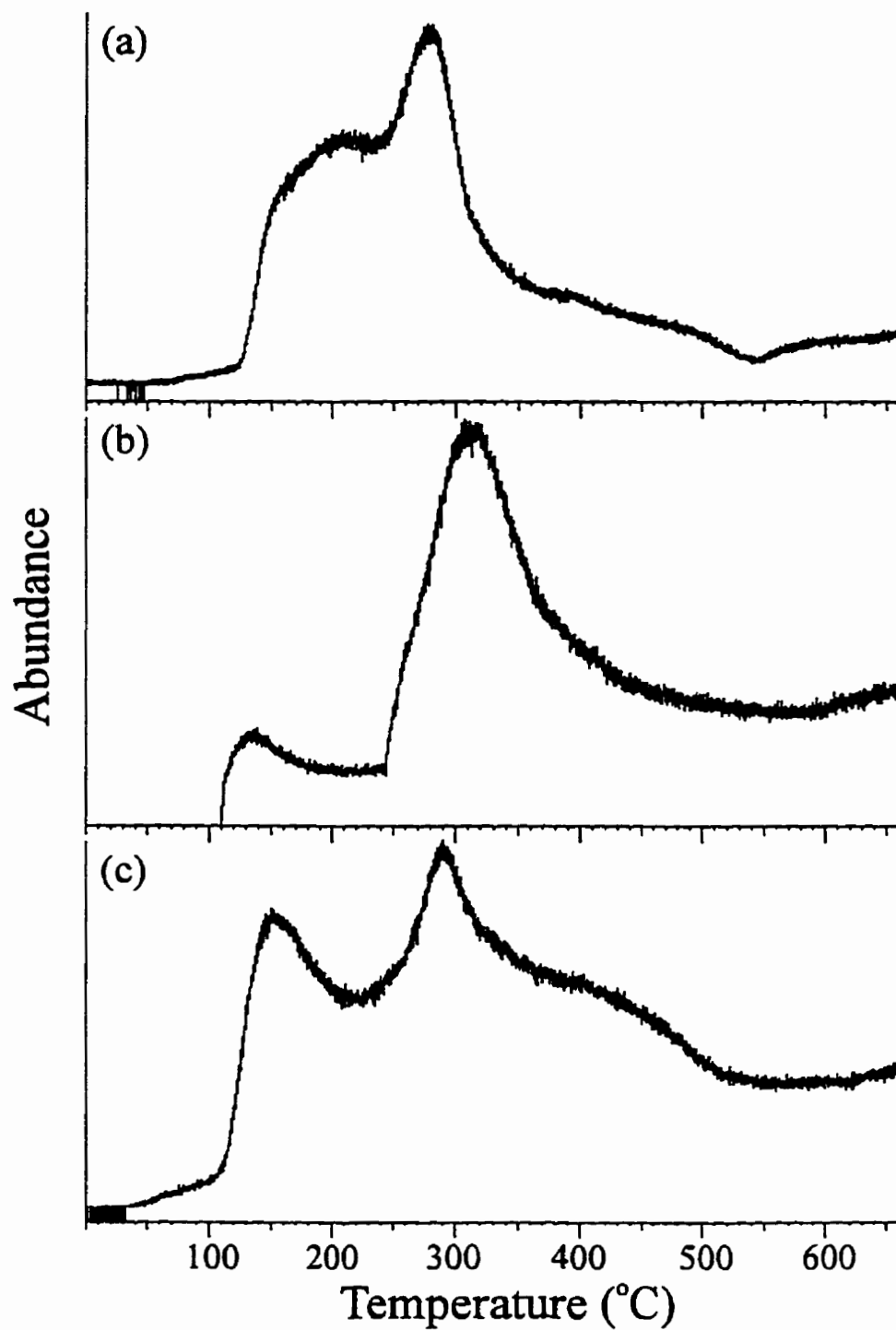


Figure 5.7 - TPD of ammonia with $\text{Tl}_4\text{SiW}_{12}\text{O}_{40}$. Cation:proton ratios of (a) 1.15; (b) 1.00; (c) 0.85.

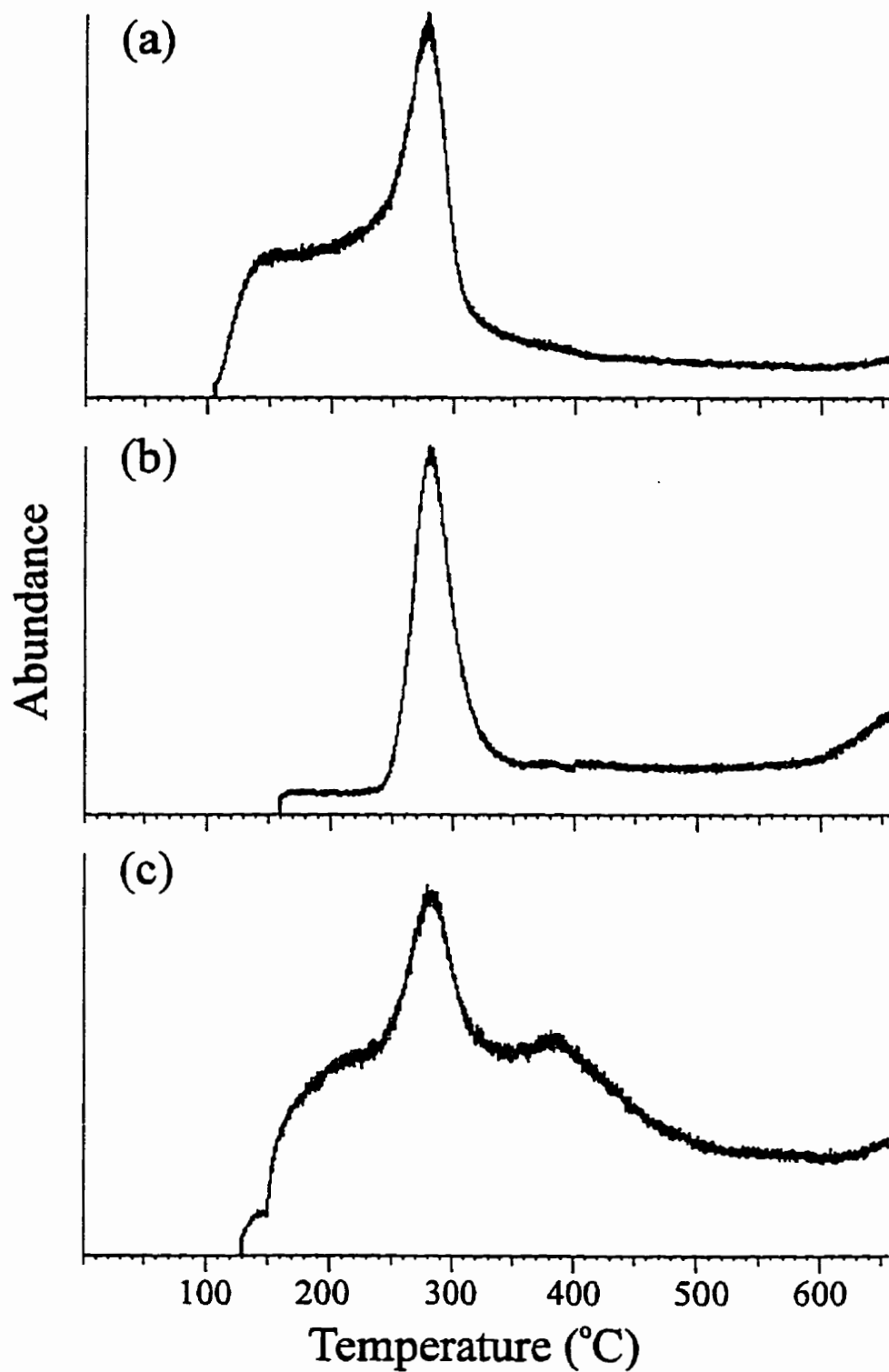


Figure 5.8 - TPD of ammonia with $\text{Cs}_4\text{SiW}_{12}\text{O}_{40}$. Cation:proton ratios of (a) 1.15; (b) 1.00; (c) 0.85.

Table 5.5 - Distribution of acid strengths and total acidity^a for 12-tungstosilicate and 12-molybdophosphate salts.

| Salt | Cation:Proton Ratio | Acid Strength Distribution ^b (% of total area) | | | Total Specific Acidity ^{c,d} |
|---------------------------------------------------|------------------------|--------------------------------------------------------------|--------------|--------|---------------------------------------------|
| | | Weak | Intermediate | Strong | |
| Ag ₄ SiW ₁₂ O ₄₀ | 0.85 | 56 | 36 | 8 | 56.8 |
| | 1.00 | 62 | 33 | 5 | 44.6 |
| | 1.15 | 54 | 38 | 7 | 66.9 |
| Tl ₄ SiW ₁₂ O ₄₀ | 0.85 | 43 | 38 | 18 | 4.7 |
| | 1.00 | 28 | 50 | 22 | 1.2 |
| | 1.15 | 62 | 27 | 11 | 2.9 |
| Cs ₄ SiW ₁₂ O ₄₀ | 0.85 | 40 | 42 | 18 | 1.9 |
| | 1.00 | 42 | 32 | 26 | 0.7 |
| | 1.15 | 70 | 20 | 10 | 1.2 |
| Tl ₃ PMo ₁₂ O ₄₀ | 0.85 | 36 | 55 | 8 | 5.9 |
| | 1.00 | 31 | 55 | 14 | 3.7 |
| | 1.15 | 68 | 23 | 9 | 2.0 |

^a Calculated from temperature-programmed desorption of ammonia.

^b Temperature ranges used for acid strength:

weak (100 °C - 300 °C); intermediate (300 °C - 500 °C); strong (> 500 °C)

^c Total Specific Acidity = Total Area Count / (S_{BET} x mass of sample)

^d (x 10⁸)

The TIPMo salts made with a 15% deficit and stoichiometric amount of thallium have similar TPD patterns with the major peak at approximately 440 °C. (Figure 5.9) This is reflected in the distribution of acid sites. (Table 5.5) With an excess of the cation, a significant shift occurs with the majority of the ammonia desorbed by 300 °C (Figure 5.9a), indicating the loss of the strongest acid sites.

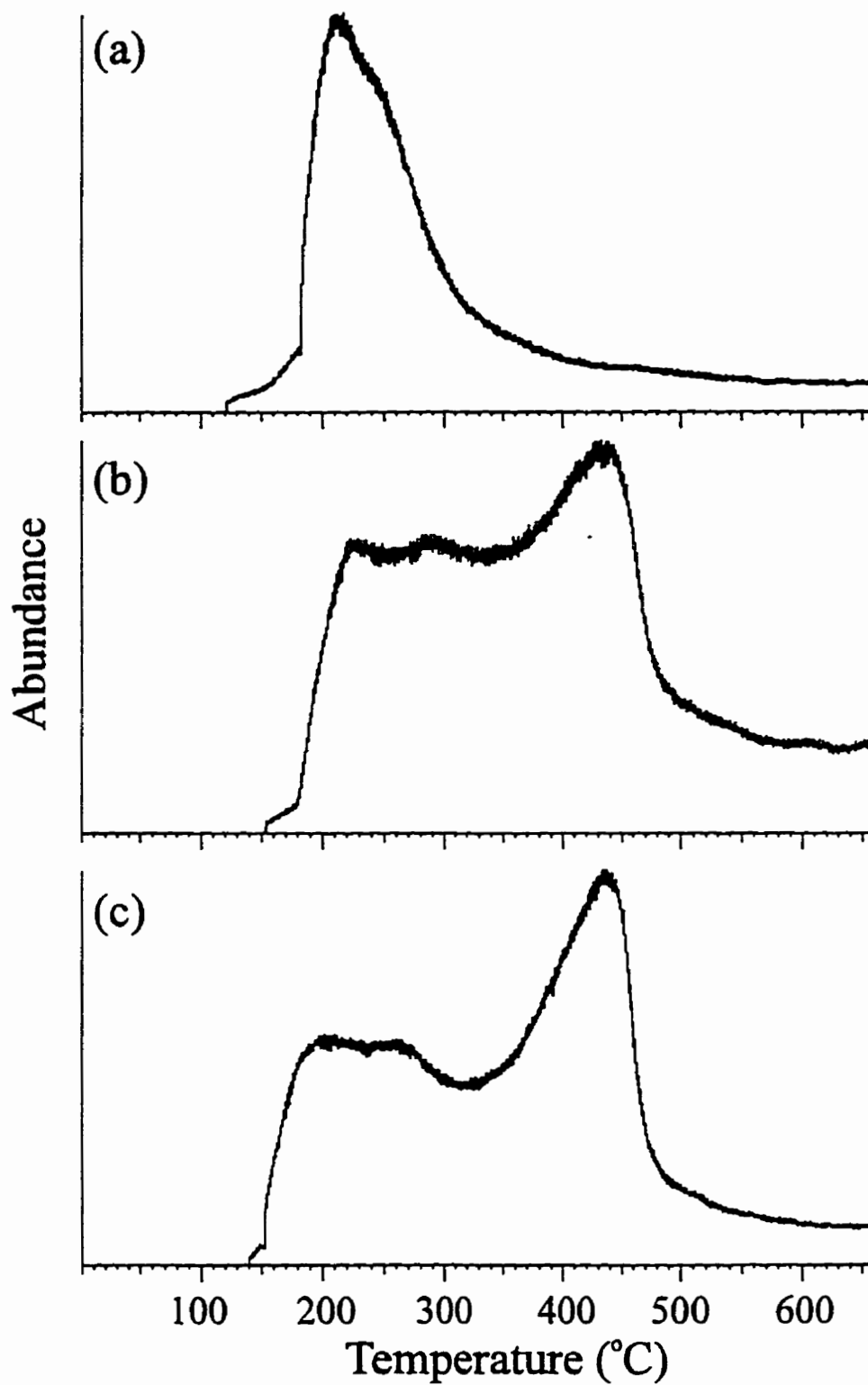


Figure 5.9 - TPD of ammonia with $\text{Tl}_3\text{PMo}_{12}\text{O}_{40}$. Cation:proton ratios of (a) 1.15; (b) 1.00; (c) 0.85.

5.3.2 Isomerization of 1-Butene

Isomerization of 1-butene with the silver and thallium salts of 12-tungstophosphoric acid was carried out at 100 °C, 200 °C, and 300 °C, with the cation:proton ratios of 0.50, 1.00, and 1.50. The activity of the catalyst was measured at 10, 70, and 130 minutes time-on-stream. The only products formed were the *cis*- and *trans*- isomers of 2-butene.

Table 5.6 - Isomerization of 1-butene at 100 °C with salts of $H_3PW_{12}O_{40}$.

| Salt | Preparative Ratio | Conversion (%) | | | Cis/Trans 2-Butene | | |
|------|-------------------|-----------------|----|-----|--------------------|-------|-------|
| | | 10 ^a | 70 | 130 | 10 ^a | 70 | 130 |
| HPW | | 70 | 23 | 18 | 0.361 | 0.363 | 0.358 |
| AgPW | 0.50 | 93 | 92 | 92 | 0.426 | 0.418 | 0.417 |
| | 1.00 | 91 | 81 | 77 | 0.425 | 0.362 | 0.348 |
| | 1.50 | 88 | 41 | 28 | 0.458 | 0.521 | 0.520 |
| TlPW | 0.50 | 88 | 75 | 68 | 0.366 | 0.361 | 0.356 |
| | 1.00 | 25 | 11 | 8 | 1.312 | 1.389 | 1.379 |
| | 1.50 | 0 | 0 | 0 | - | - | - |

^a Time-on-stream (mins).

The conversion at 100 °C is summarized in Table 5.6 and at each of the sampling intervals, all three stoichiometries of the AgPW salts have a higher activity than the pure acid, HPW. Of the three TlPW salts, only the one prepared with a 50% deficit of cation had a higher activity than HPW. A slight decrease in the conversion occurs as the cation-to-proton ratio is increased in the silver salts, at the initial sampling. This trend becomes more pronounced at higher times-on-stream. The decrease in activity is more apparent for the TlPW salt series; particularly the salt with an excess of cation has no activity. The ratio of the two 2-butene isomers produced at 100 °C, *cis/trans*, is shown in Table 5.6. Both the AgPW and TlPW salts have similar *cis/trans* ratios which increase with the cation:proton ratio, although changes are generally small for the AgPW salts. However,

the stoichiometric TIPW salt has a marked increase in the amount of *cis*-2-butene isomer in comparison to the salt made with a deficit of the cation. Increasing the time-on-stream does not appear to alter the product distribution despite the decreased activity.

Table 5.7 - Isomerization of 1-butene at 200 °C with salts of $H_3PW_{12}O_{40}$.

| Salt | Preparative Ratio | Conversion (%) | | | Cis/Trans 2-Butene | | |
|------|-------------------|-----------------|----|-----|--------------------|-------|-------|
| | | 10 ^a | 70 | 130 | 10 ^a | 70 | 130 |
| HPW | | 86 | 78 | 73 | 0.498 | 0.575 | 0.622 |
| AgPW | 0.50 | 87 | 86 | 85 | 0.513 | 0.539 | 0.547 |
| | 1.00 | 87 | 87 | 87 | 0.527 | 0.526 | 0.528 |
| | 1.50 | 87 | 87 | 87 | 0.544 | 0.546 | 0.540 |
| TIPW | 0.50 | 87 | 87 | 87 | 0.545 | 0.537 | 0.519 |
| | 1.00 | 87 | 79 | 70 | 0.575 | 0.689 | 0.789 |
| | 1.50 | 0 | 0 | 0 | - | - | - |

^a Time-on-stream (mins).

Increasing the reaction temperature to 200 °C eliminated any decline in activity as the silver salts for higher times-on-stream or as the cation:proton ratio was increased. (Table 5.7) The AgPW salts have similar activities as HPW, which also shows only a slight deactivation as it remains on-stream. With the increased temperature, the deficit and stoichiometric TIPW salts attain activities similar to those of the silver salts during initial measurements at 10 minutes. The deficit salt maintains this level of conversion with increasing time-on-stream, but the stoichiometric salt shows a decrease similar to that observed with HPW. The 1.50 TIPW salt displays no activity. As with reactions carried out at 100 °C, the *cis/trans* ratios are similar to those of the parent acid and they are maintained with all three stoichiometries of the silver salt, along with the 50% deficit TIPW salt. (Table 5.7) The amount of *cis*-2-butene appears to increase with increasing time-on-stream for the stoichiometric TIPW salt, but is not as significant as at 100 °C.

Table 5.8 contains similar results for the isomerization for 1-butene at 300 °C. At

Table 5.8 - Isomerization of 1-butene at 300 °C with salts of $H_3PW_{12}O_{40}$.

| Salt | Preparative Ratio | Conversion (%) | | | Cis/Trans 2-Butene | | |
|------|-------------------|-----------------|----|-----|--------------------|-------|-------|
| | | 10 ^a | 70 | 130 | 10 ^a | 70 | 130 |
| HPW | | 82 | 81 | 80 | 0.611 | 0.575 | 0.561 |
| AgPW | 0.50 | 81 | 79 | 76 | 0.620 | 0.637 | 0.644 |
| | 1.00 | 82 | 81 | 80 | 0.634 | 0.645 | 0.652 |
| | 1.50 | 82 | 81 | 80 | 0.648 | 0.646 | 0.650 |
| TlPW | 0.50 | 82 | 81 | 81 | 0.654 | 0.641 | 0.641 |
| | 1.00 | 83 | 82 | 81 | 0.655 | 0.653 | 0.653 |
| | 1.50 | 0 | 0 | 0 | - | - | - |

^a Time-on-stream (mins).

all three sampling intervals there appears to be little variation in the conversion between HPW (measured to be $\approx 81\%$, Table 5.8) and the various stoichiometries of silver and thallium salts, with the exception of the thallium salt with a 50% excess of cation. At 300 °C the conversion remains relatively constant with increasing time-on-stream. The *cis* and *trans* isomers of 2-butene were the only products observed and the *cis/trans* ratios for the AgPW and TlPW salts are only slightly larger than those observed with HPW, with little variation occurring as the catalyst remains on-stream. (Table 5.8)

The isomerization of 1-butene was carried out with the 0.85, 1.00 and 1.15 cation:proton ratios of the silver and thallium 12-tungstosilicate salts. The three reaction temperatures and three sampling intervals were identical to those used by the analogous 12-tungstophosphate salts. At 100 °C, the three stoichiometries of the AgSiW and TlSiW salts displayed lower activity than the parent acid, HSiW. (Table 5.9) Most notably, the AgSiW salts displayed only a trace of activity for the three stoichiometries investigated. The 0.85 TlSiW salt was the only salt to display any significant activity at 10 minutes, but this diminished at higher times-on-stream. As with the 12-tungstophosphate salts, the only products formed were the *cis* and *trans* isomers of 2-butene, summarized in Table 5.9.

Table 5.9 - Isomerization of 1-butene at 100 °C with salts of $H_4SiW_{12}O_{40}$.

| Salt | Preparative Ratio | Conversion (%) | | | Cis/Trans 2-Butene | | |
|-------|-------------------|-----------------|----|-----|--------------------|-------|-------|
| | | 10 ^a | 70 | 130 | 10 ^a | 70 | 130 |
| HSiW | | 85 | 60 | 49 | 0.372 | 0.387 | 0.381 |
| AgSiW | 0.85 | 2 | 1 | 1 | 0.659 | 0.576 | 0.540 |
| | 1.00 | 2 | 2 | 2 | 0.701 | 0.662 | 0.795 |
| | 1.15 | 2 | 1 | 1 | 0.712 | 0.502 | 0.475 |
| TlSiW | 0.85 | 34 | 11 | 7 | 1.889 | 2.274 | 2.214 |
| | 1.00 | 2 | 2 | 1 | 1.912 | 1.585 | 0.941 |
| | 1.15 | 0 | 0 | 0 | - | - | - |

^a Time-on-stream (mins).

Small changes in the *cis/trans* ratios are observed for the AgSiW salts as the cation composition of the salt varies or increasing time-on-stream, although these values are slightly higher than 0.4 noted for HSiW. Unlike the deficit TIPW salt, the 0.85 and stoichiometric salts of TlSiW have lower conversions and significantly high values for the *cis/trans* ratio, although this does vary as the reaction proceeds.

Although the reactions with the AgSiW and TlSiW salts at 200 °C have lower conversions than observed for HSiW (Table 5.10), there is a marked increase in conversions in comparison to reactions carried out at 100 °C, most notably with the AgSiW salts. The pattern of a decrease in activity as the cation to proton ratio or time-on-stream are increased remains with the TlSiW salts, but the deficit and stoichiometric salts have similar conversions at sampling intervals of 70 and 130 minutes. The TlSiW salt prepared with an excess of thallium is inactive. At a time-on-stream of 10 minutes, the analogous silver salts do not mimic the observed pattern with the TlSiW salts with the cation composition of the salt. The deficit and stoichiometric salts increase the conversion at 70 minutes, with a smaller range of activities observed for three cation:proton ratios. With increasing time-on-stream to 130 minutes, there is a decrease in activity for the

Table 5.10 - Isomerization of 1-butene at 200 °C with salts of $H_4SiW_{12}O_{40}$.

| Salt | Preparative Ratio | Conversion (%) | | | Cis/Trans 2-Butene | | |
|-------|-------------------|-----------------|----|-----|--------------------|-------|-------|
| | | 10 ^a | 70 | 130 | 10 ^a | 70 | 130 |
| HSiW | | 85 | 72 | 63 | 0.561 | 0.746 | 0.843 |
| AgSiW | 0.85 | 36 | 60 | 45 | 0.760 | 0.746 | 0.841 |
| | 1.00 | 17 | 68 | 55 | 0.838 | 0.729 | 0.820 |
| | 1.15 | 74 | 63 | 50 | 0.662 | 0.813 | 0.915 |
| TlSiW | 0.85 | 67 | 22 | 14 | 0.810 | 1.562 | 1.728 |
| | 1.00 | 32 | 20 | 17 | 1.652 | 1.872 | 1.946 |
| | 1.15 | 0 | 0 | 0 | - | - | - |

^a Time-on-stream (mins).

AgSiW salts. The *cis/trans* ratios monitored for the AgSiW salts (Table 5.10) are larger than values obtained at 100 °C and the parent acid at 200 °C. As observed with the AgPW salts, little variation occurs in the *cis/trans* ratio for the AgSiW salts as the cation composition changes in the salt or contact time with the reactant mixture increases. Similar to TIPW salts at 200 °C, there is an increase in the amount of *cis*-2-butene formed as the thallium content is increased in the salt or with increased time-on-stream.

At 300 °C, a further increase in activity is noted for the 0.85 and 1.00 TlSiW salts for the isomerization of 1-butene, approaching the conversion of the pure acid, HSiW. (Table 5.11) With increasing time-on-stream, the conversion by the stoichiometric TlSiW salt was constant while the deficit salt decreased in activity. The 1.15 TlSiW salt showed no activity. In comparison with reactions carried out at 200 °C, the AgSiW salts have lower conversions at 300 °C, with the greatest activity at 10 minutes. (Table 5.11) With the increased time-on-stream a further decrease occurs while the selectivities remain constant with changes in the cation:proton ratio. As observed with the HPW salts at 300 °C, the 12-tungstosilicate salts have little variation in the product distribution as the time-on-stream increases and the cation:proton ratio increases. (Table 5.11) The value of

Table 5.11 - Isomerization of 1-butene at 300 °C with salts of $H_4SiW_{12}O_{40}$.

| Salt | Preparative Ratio | Conversion (%) | | | Cis/Trans 2-Butene | | |
|-------|-------------------|-----------------|----|-----|--------------------|-------|-------|
| | | 10 ^a | 70 | 130 | 10 ^a | 70 | 130 |
| HSiW | | 81 | 77 | 73 | 0.613 | 0.639 | 0.663 |
| AgSiW | 0.85 | 24 | 11 | 8 | 0.999 | 0.967 | 0.955 |
| | 1.00 | 31 | 14 | 10 | 0.942 | 0.936 | 0.921 |
| | 1.15 | 28 | 10 | 6 | 0.962 | 0.972 | 0.931 |
| TlSiW | 0.85 | 82 | 75 | 60 | 0.656 | 0.773 | 1.089 |
| | 1.00 | 71 | 71 | 70 | 0.891 | 0.898 | 0.921 |
| | 1.15 | 0 | 0 | 0 | - | - | - |

^a Time-on-stream (mins).

approximately 1 is larger than the *cis/trans* ratio of 0.6 noted for the pure acid. However, the 0.85 TlSiW salt produces a ratio similar to that observed with HSiW at 10 minutes time-on-stream and the selectivity for *cis*-2-butene increases with higher time-on-stream.

The thallium 12-molybdophosphate salts with the cation:proton ratios of 0.85, 1.00 and 1.15 were also studied for the isomerization of 1-butene. The parent acid, HPMo, showed low activity at all three reactions temperatures investigated, as expected since HPMo is known preferentially as a redox catalyst rather than acid catalyst. (Table 5.12 to 5.14) At 100 °C the TIPMo salts series shows a decline in conversion as the thallium content or time-on-stream is increased. (Table 5.12) As noted previously with other thallium salts, the 1.15 TIPMo salt was inactive. The product distribution for the two isomers of 2-butene was unchanged with the time-on-stream. However the *cis/trans* ratio increased by a factor of approximately two when the cation:proton ratio was increased from 0.85 to 1.00. (Table 5.12)

The conversion doubled for the TIPMo salts with a temperature increase from 100 °C to 200 °C, and the 1.15 TIPMo salt displayed some activity. (Table 5.13) A decline in the activity of the salt is observed as the preparative quantity of thallium or the time-on-

Table 5.12 - Isomerization of 1-butene at 100 °C with $H_3PMo_{12}O_{40}$ and $Tl_3PMo_{12}O_{40}$.

| Salt | Preparative Ratio | Conversion (%) | | | Cis/Trans 2-Butene | | |
|-------|-------------------|-----------------|----|-----|--------------------|-------|-------|
| | | 10 ^a | 70 | 130 | 10 ^a | 70 | 130 |
| HPMo | | 5 | 2 | 2 | 1.231 | 1.108 | 1.034 |
| TIPMo | 0.85 | 28 | 12 | 9 | 0.965 | 1.007 | 1.000 |
| | 1.00 | 12 | 5 | 3 | 1.856 | 1.835 | 1.751 |
| | 1.15 | 0 | 0 | 0 | - | - | - |

^a Time-on-stream (mins).

Table 5.13 - Isomerization of 1-butene at 200 °C with $H_3PMo_{12}O_{40}$ and $Tl_3PMo_{12}O_{40}$.

| Salt | Preparative Ratio | Conversion (%) | | | Cis/Trans 2-Butene | | |
|-------|-------------------|-----------------|----|-----|--------------------|-------|-------|
| | | 10 ^a | 70 | 130 | 10 ^a | 70 | 130 |
| HPMo | | 9 | 3 | 2 | 1.138 | 1.008 | 0.932 |
| TIPMo | 0.85 | 59 | 34 | 26 | 1.067 | 1.342 | 1.420 |
| | 1.00 | 39 | 23 | 18 | 1.418 | 1.596 | 1.640 |
| | 1.15 | 23 | 10 | 8 | 1.634 | 1.827 | 1.839 |

^a Time-on-stream (mins).

stream are increased. The product distribution tends to favour an increase in the *cis* isomer as the cation:proton ratio is increased (Table 5.13), although this is not as drastic as observed at 100 °C. The increase in temperature now causes the amount of *cis*-2-butene to increase with increasing time-on-stream.

Increasing the reaction temperature to 300 °C does not change the initial activity, monitored at 10 minutes, for the nonstoichiometric salts of TIPMo but the stoichiometric TIPMo approaches a level of conversion of the 0.85 salt. (Table 5.14) Unlike the other two acid-based salts investigated at 300 °C, there is a decrease in conversion as the reaction proceeds, which is more significant than observed at 200 °C. The increase in

Table 5.14 - Isomerization of 1-butene at 300 °C with $H_3PMo_{12}O_{40}$ and $Tl_3PMo_{12}O_{40}$.

| Salt | Preparative Ratio | Conversion (%) | | | Cis/Trans 2-Butene | | |
|-------|-------------------|-----------------|----|-----|--------------------|-------|-------|
| | | 10 ^a | 70 | 130 | 10 ^a | 70 | 130 |
| HPMo | | 4 | 1 | 1 | 0.976 | 0.820 | 0.735 |
| TlPMo | 0.85 | 57 | 22 | 16 | 1.056 | 1.407 | 1.412 |
| | 1.00 | 53 | 17 | 12 | 1.209 | 1.586 | 1.596 |
| | 1.15 | 25 | 9 | 6 | 1.528 | 1.638 | 1.664 |

^a Time-on-stream (mins).

temperature decreases the amount of *cis* isomer formed, relative to *trans*-2-butene, so that although there is an increase in the ratio of products corresponding to the increased time-on-stream and cation:proton ratio, it is not as drastic as observed with reactions at 100 °C and 200 °C.

5.4 Discussion

¹H MAS NMR has provided evidence that residual protons are still present in the isolated salts. Previous photoacoustic (PAS) FTIR studies have shown that the substitution of protons by larger monovalent cations in precipitated salts, prepared as stoichiometric, was incomplete and protons still remained in the isolated solid.⁸¹ For the series of TIPW salts, the protons apparently reside in a single chemical environment with the peak area decreasing as the cation-to-acid ratio is increased. The chemical shift of the pure acid, $H_3PW_{12}O_{40}$, is $\delta = 9.6$ ppm.⁸⁵ With the increase of the cation:proton ratio in the TIPW salts, the resonance shifts upfield to a smaller chemical shift. Two resonances are present in the ¹H MAS NMR spectra for the AgPW series of salts. The larger of the two peaks moves upfield with the increase in the cation:proton ratio while the smaller resonance is displaced slightly downfield, to a larger chemical shift. The ¹H MAS NMR spectra for the CsPW salts are similar to the TIPW salts with a single resonance moving upfield as the cation:proton ratio is increased. A second resonance is present only for the

0.85 CsPW salt, occurring as a shoulder on the larger peak. This disappears for the stoichiometric and 1.15 salts.

As discussed previously in Chapter 2, the two chemical shifts present for the AgPW salts could result from two different stoichiometries of the salt coprecipitating, due to similar solubilities in water. However, the powder x-ray diffraction patterns are not suggestive of an amorphous phase, as would be expected if two different stoichiometries were present in the isolated solid. Alternatively, only one stoichiometry of the salt may be formed but the residual protons may be able to reside in more than one site, differing in the chemical environment as the number of cations substituted into the neighbouring sites varies. This would explain the gradual shift upfield of the resonance as the amount of cation is increased and would account for the second resonance disappearing for the CsPW salts as the cation:proton ratio is increased. The anisotropic nature of only one of the two resonances observed for the AgPW salts supports this assumption.

For the three salts synthesized from 12-tungstosilicic acid, two resonances are present in the ^1H MAS NMR spectra, although in most cases, the second peak appears as a shoulder on a more intense peak, disappearing when an excess of the cation is used in the synthesis of the salt. In contrast, the thallium salts of 12-molybdophosphoric acid have a single resonance. As with the other series of salts, all of the chemical shifts reported for the observed resonances are smaller than those reported for the pure acids, $\delta = 10.9$ ppm and 7.4 ppm for HSiW^{85} and HPMo^{86} , respectively, and are gradually shifted further upfield as the cation-to-acid preparative ratio is increased.

The smaller chemical shift, as compared to the parent acid, and the upfield shift with the increase in the cation-to-acid ratio indicates that both the nature and amount of cations are affecting the chemical environment of the residual protons and, thus, their Brønsted acidity. A number of arguments have been presented in support of the suggestion that the chemical shift can serve as a measure for acid strength⁸⁷ and it is generally believed that an increase in the protium chemical shift is an indication of an increase in the Brønsted acid strength.^{88,89} The intensity of the resolved line in the ^1H MAS NMR spectrum is directly proportional to the concentration of Brønsted acid sites.⁸⁹ From these results it is apparent that the decrease in chemical shift (Table 5.1) and peak

area (Tables 5.2 and 5.3) as the cation:proton ratio increases is indicative of a decrease in both the number and acid strength of the residual protons as compared to 12-heteropoly acids. This is in agreement with previous work with zeolites.⁹⁰ The acid strength of the zeolites decreased on exchange of the protons with metallic cations, with the stronger acid sites exchanging first.

The temperature-programmed desorption of ammonia from the silver salts of HPW and HSiW, synthesized with a 15% deficit or excess of the cation, revealed that the two stoichiometries of the salt have similar numbers of acid sites and distributions of acid strengths. (Table 5.4 and 5.5) This correlated with the chemical shift in the ¹H MAS NMR spectra, differing for the two cation:proton ratios by 0.7 ppm for AgPW. (Table 5.1) In contrast to this, the TIPW and CsPW salts have a 2.0 ppm difference in chemical shift between the salts with a deficit and an excess of the cation. This change in the protium environment is reflected in the ammonia TPD spectra with a decrease in the number of strong acid sites as the cation-to-acid ratio for the TIPW salts is increased. (Figure 5.4 and Table 5.4) A similar trend occurs in the ammonia TPD of the CsPW salts. (Figure 5.5 and Table 5.4) The silver salts of HSiW have a larger difference in the chemical shifts in the ¹H MAS NMR for the nonstoichiometric salts (cation:proton ratios of 0.85 and 1.15) and are notably higher upfield than the AgPW salts. Despite this, the ammonium TPD of these two ratios indicates a similar distribution of acid strength (Figure 5.6), although a larger portion are now considered weak in comparison to the AgPW salts. (Tables 5.4 and 5.5) The difference between chemical shifts recorded for the nonstoichiometric salts for each of the TlSiW and CsSiW series is similar to the AgSiW salts (Table 5.1); however for the ammonia TPD, a change is noted in the protium environment as the cation:proton ratio is increased (Table 5.5), similar to that which is observed with the TIPW and CsPW salt series. It is also of interest that the amount of ammonia adsorbed by the thallium and cesium salts of each acid is approximately an order of magnitude less than that adsorbed by the analogous silver salt, consistent with the higher concentration of residual protons in the silver salts. (Tables 5.2)

Evidently the distribution of acid strength is shifting: the numbers of sites of higher acidity decreases as the relative amounts of the cations are increased. Although

temperature-programmed desorption experiments with ammonia cannot differentiate between Lewis and Brønsted acid sites, previous photoacoustic FTIR studies have shown that the acidity of 12-tungstophosphoric acid can be attributed to Brønsted acid sites with little or no evidence of Lewis acid sites.^{81(a)} It is expected that the derivatives prepared in the present work are similar in this respect.

Isomerization of 1-butene by the salts was initially carried out to gain an understanding of the number and nature of acid sites available in the catalyst by analysis of the conversion levels and product distribution, in comparison to that of the parent acid. As discussed in the introduction, the monomolecular mechanism depicted in Figure 5.1 is followed with the formation of the secondary butyl carbenium ion as the initial step. From this carbenium ion double bond isomerization will form the *cis* and *trans* isomers of 2-butene while skeletal isomerization will form *iso*-butene. Recent experiments in this laboratory¹⁰ have indicated that an equilibrium is established between the secondary carbenium ion, 1-butene, *cis*- and *trans*-2-butenes (as indicated in Figure 5.1) and suggests that the 2-butenes are precursors to *iso*-butene, indicating that the former species are the primary products while *iso*-butene is a secondary product. Stronger Brønsted acid sites and an increase in temperature are required to facilitate the skeletal rearrangement of the secondary butyl carbenium ion to a primary *tert*-butyl carbenium ion required for this product. This is in agreement with Gielgens *et al.*¹⁴ who noted that skeletal isomerization could be suppressed while maintaining activity for the linear isomers, indicating that skeletal isomerization requires a different active site than that involved in linear isomerization. A decrease in *iso*-butene also correlated with a decrease in the byproduct formation, indicating the latter is formed by a consecutive reaction.¹⁴ Szabo *et al.*³⁰ calculated rate constants for the three successive reaction stages: fast double bond migration; skeletal isomerization; and formation of side products. The rate constant for double bond isomerization was higher than that for skeletal isomerization, as expected for a carbenium ion mechanism.

Semiempirical quantum mechanical (Extended Hückel) calculations have predicted that solid heteropoly acids with anions containing tungsten should have higher acid

strengths than those with molybdenum.⁹¹ Isomerization of 1-butene with various 12-heteropoly acids revealed that the level of activity for the acid was not affected by changing the central atom in the Keggin anion in contrast with the observations where the peripheral metal element was changed.⁹² This is consistent with the results observed for the three 12-heteropoly acids investigated in this work. (Tables 5.6 to 5.14) HPW and HSiW had similar conversions at each of the three reaction temperatures studied, although HPW deactivated quicker than HSiW at 100 °C. In contrast, little or no activity was observed for HPMo, even at temperatures as high as 300 °C. This pattern was not maintained after the partial substitution of protons by the monovalent cations of silver and thallium.

The decrease in activity for the salts of HPW at 100 °C as the cation:proton ratio increases indicates the number of acid sites strong enough to facilitate the reaction decreases, although this is more apparent for the TIPW salt series. Despite this, all three stoichiometries of the AgPW salt display higher activity than HPW at each of the three sampling intervals. With the increase of the reaction temperature to 200 °C, all of the AgPW salts now maintain similar conversion levels, slightly higher than HPW, while the stoichiometric TIPW salt decreases in activity as the reaction progresses. At 300 °C all of the salts, with the exception of 1.50 TIPW (which is inactive), have identical activities and selectivities, similar to the pure acid.

In comparison, the silver and thallium salts of HSiW are not able to achieve a similar degree of conversion for the isomerization of 1-butene as the parent acid, even at reactions temperatures as high as 300 °C. In contrast to AgPW, the silver salts of AgSiW attain their highest level of activity at 200 °C, rather than at 300 °C, with a greater variation in the conversion as the cation:proton ratio is increased than that which occurs in reactions carried out at either 100 °C or 300 °C. The significantly lower conversion displayed by the AgSiW salts, in comparison to the analogous AgPW salts, are not surprising as the ammonia TPD revealed a greater portion of weak acid sites present in the AgSiW salts and smaller chemical shifts in the ¹H MAS NMR spectra than observed with the AgPW salts. As before, the TlSiW salts display a decrease in activity as the cation:proton ratio and time-on-stream are increased, although increasing the reaction

temperature to 300 °C increases the stability.

For the thallium molybdophosphate salts, the increased reaction temperature does not counteract the decline in activity corresponding to the increase in the cation content in the salts or the time-on-stream, as observed with the previous salts. Unlike the analogous TlSiW and TlPW salts, isomerization reactions performed at 200 °C and 300 °C are sufficient enough to permit some activity of the 1.15 TlPMo salt. In all cases, the thallium salts have a higher activity than observed for the parent acid, HPMo.

For the isomerization of 1-butene there is a noticeable decrease in the catalytic activity, although not necessarily the selectivity to the products, from the initial sample of the fresh catalytic surface at 10 minutes to samples taken 70 and 130 minutes after exposure of the catalyst to the reactant mixture. It is believed that this decrease in conversion results from the relatively slower rate of regeneration of the Brønsted acid sites in comparison with the rate of formation of the olefinic products on a release of a proton. (Figure 5.1) Evidence of the coking of the catalyst has been established by IR studies of supported 12-tungstophosphoric acid.⁹³

In all of the reactions carried out with the silver and thallium salts of HPW, HSiW and HPMo, only the *cis* and *trans* isomers of 2-butene were formed. No evidence of C₃, C₄, C₅,..., C₈ species were present to give an indication of a bimolecular process. None of the catalysts investigated possessed sites of sufficient strength to facilitate the skeletal isomerization required to form *iso*-butene during the isomerization of 1-butene at the reaction temperatures investigated. This is not surprising since both the ¹H MAS NMR and TPD experiments with ammonia revealed that there is a decrease in the Brønsted acidity with the increased substitution of cations in comparison to the pure acid. Although isomerization of 1-butene at 300 °C by 12-tungstophosphoric acid failed to produce *iso*-butene (Table 5.6), supported HPW was capable of forming *iso*-butene during the isomerization of 1-butene at these temperatures.¹⁰ ¹H MAS NMR studies of the supported acid revealed a downfield shift of the proton resonance, to a larger chemical shift, from that reported for the unsupported HPW, indicating an increase in acid strength when the acid is supported.¹⁰ With the supported HPW, there was also evidence of a bimolecular process under the reaction conditions employed, but this may be only for the

formation of the byproducts.¹⁴

Formation of the *cis* and *trans* isomers of 2-butene occurs through the secondary butyl carbenium ion, which is considered to be a metastable species, not equivalent to a transition state.⁷⁰ The equilibrium distribution of 1-butene:*cis*-2-butene:*trans*-2-butene is 9.3 : 29.8 : 60.9 at 150 °C,⁹⁴ giving a *cis/trans* ratio of 0.49, and 18.0 : 32.5 : 49.5 with a *cis/trans* ratio of 0.656 at 300 °C.⁹⁵ Isomerization of 1-butene with HPW and HSiW acids results in *cis/trans* ratios similar to the equilibrium distribution values (Tables 5.6 and 5.7) with reaction at 100 °C slightly lower than the distribution reported for 150 °C. The *cis/trans* ratio resulting from the reaction over HPMo were close to values of 1.0 with little variation with the changes in reaction temperature. (Table 5.8)

The silver salts of AgPW and AgSiW produced the *cis* and *trans* isomers of 2-butene in ratios proportional to equilibrium values. Only minor variations occurred with the increase in the cation:proton ratio used to prepare the salt. This is consistent with the ammonia TPD spectra in which little change in the distribution of acid strengths occurred with the stoichiometry of the salt. There was little variation in the product distribution for the silver salts with the higher times-on-stream. The exception to this was with the AgSiW salts at 300 °C where the ratios of *cis/trans* isomers were close to a value of 1.

The TIPW salt prepared with a 15% deficit of the cation produced the two isomers of 2-butene in ratios similar to the equilibrium values. However, when the cation content was increased for the stoichiometric salt, the proportion of *cis*-2-butene increased to produce a *cis/trans* ratio higher than the equilibrium value. Increasing the time-on-stream for the 1.00 TIPW salt increased the selectivity for *cis*-2-butene, relative to the *trans* isomer while increasing the reaction temperature decreased the selectivity for *cis* isomer so that equilibrium values were attained for the reactions performed at 300 °C.

For the TSiW salts, reactions at 100 °C produced a random pattern with the *cis/trans* greater than 1. The pattern similar to the TIPW salts with the increase in the *cis/trans* ratio with the increased time-on-stream and increased cation:proton ratio, became apparent with the increase of the reaction temperature to 200 °C. Increasing the reaction temperature to 300 °C decreased the fraction of *cis*-2-butene although the resulting

cis/trans ratio was still greater than equilibrium values and increased for the deficit salt with increasing time-on-stream. The TlPMo salts mimic the pattern observed with the other thallium salts, with the fraction of *cis*-2-butene produced increasing as the time-on-stream or thallium content of the salt increased. Reactions at 100 °C show the greatest range in the *cis/trans* ratio, although all ratios are greater than 1, higher than observed for the pure acid.

Isomerization of 1-butene is considered as a "surface-type" reaction with 12-heteropoly oxometalates due to the limited ability of nonpolar molecules, such as 1-butene, to be adsorbed into the bulk of 12-heteropoly acids.^{96,97} In the present heteropoly oxometalate salts, the creation of a micropore structure now permits freer access of nonpolar molecules into the bulk. Investigating the isomerization of 1-butene with zeolites, Xu *et al.*⁹⁸ attributed the preferential formation of the *cis*-2-butene to the strong steric interaction between the pore wall and methyl groups of the secondary carbenium ion. As noted in Chapter 2, the mean micropore radii (r_{MP}) observed in the present salts is larger than the radius of the 1-butene molecule. In addition, variations in the cation:proton ratios have little or no influence on the mean micropore radius and the maximum micropore volumes occur for salts prepared with a stoichiometric quantity of preparative reagents so this explanation cannot account for the increase in the *cis/trans* ratio as the cation to proton ratio is increased.

With the isomerization reactions carried out with the pure 12-heteropoly acids it was concluded that the formation of the *cis* isomer is favourable for catalysts which are weakly acidic.⁹² This had previously been noted with other catalysts^{2,96} although numerical values reported for the *cis/trans* ratio are largely dependent upon the nature of the acid sites (Lewis or Brønsted) and the resulting mechanism for isomerization. This is consistent with the observations for the ammonia TPD, in which a greater portion of acid sites are classified as weak with the increase in the cation:proton ratio for all the three series of thallium salts examined. At reaction temperatures of 300 °C the *cis/trans* ratio remains unaltered on changes in the preparative ratio of the salt.

As evident from the nitrogen adsorption-desorption isotherms, ¹H MAS NMR and

ammonia TPD, partial substitution of the protons by monovalent cations of cesium, silver, and thallium affects three characteristics of the salts: a microporous structure is created, the number of Brønsted acid sites is decreased, and the distribution of acid sites is shifted. As noted earlier, variations in the cation:proton ratios have significant effects on the pore volumes but little or no influence on the mean micropore radius, as would be expected from the hypothesis of the source of the pore structure advanced earlier.⁹⁹ Not surprisingly, however, the number of residual protons and the chemical environment in which they reside are altered by changes in this ratio. With respect to the isomerization of 1-butene, the change in the distribution of acid sites for the thallium salts is reflected in the product distribution of the two isomers of 2-butene formed. A significantly larger number of protons present in the silver salts in combination with a consistent distribution of acid strengths, despite variations in the cation:proton ratio, contributes to consistent levels of conversion and selectivities despite the stoichiometry of the salt or the duration for which it is left in contact with the reactant mixture. An increase in activity, in comparison to the parent acids, is only observed for the AgPW salts, by a marginal amount, and the TIPMo salts.

It can be concluded that four characteristics of the salts have an effect on the conversions observed in the isomerization of 1-butene: (1) the nature of the cation, (2) the morphological properties of the catalysts, (3) the number of protons, and (4) the distribution of acid strengths. For a given cation, the preparative cation:proton ratio determines the last three. To elucidate the effect of the cations on the residual protons the conversions were divided by the appropriate surface areas and number of protons. (Table 5.15 and 5.16) These values of $\text{conversion}/[\text{m}^2][\text{H}^+]$ should minimize or eliminate the influence of the numbers of protons and morphological differences among the catalysts on the observed conversions.

For the salts displaying activity, the thallium-containing salts generally had higher conversions in the isomerization of 1-butene than the analogous silver salts of the same heteropoly acid, at each of the three reaction temperatures. These findings are consistent with the larger separations between the ^1H chemical shift for the silver(I) salts and that observed for the parent acid in comparison with the analogous thallium salts and the

Table 5.15 - Conversion of 1-butene at 10 minutes with salts of $H_3PW_{12}O_{40}$ and $Tl_3PMo_{12}O_{40}$.

| Salt | Preparative Ratio | Conversion ^{ab} / [(m ²)(H ⁺)] | | |
|-------|-------------------|-----------------------------------------------------------------|-----|-----|
| | | 100 ^c | 200 | 300 |
| AgPW | 0.50 | 3.4 | 3.7 | 3.2 |
| | 1.00 | 1.8 | 2.9 | 2.0 |
| | 1.50 | 1.9 | 0.2 | 1.6 |
| TIPW | 0.50 | 8.9 | 7.4 | 5.9 |
| | 1.00 | 9.0 | 3.6 | 1.4 |
| | 1.50 | 0.0 | 0.0 | 0.0 |
| TIPMo | 0.85 | 0.8 | 1.3 | 1.4 |
| | 1.00 | 0.6 | 2.3 | 2.9 |
| | 1.15 | 0.0 | 3.0 | 3.6 |

^a For measurements taken at 10 minutes.

^b Moles of products multiplied by (1×10^{26}) .

^c Reaction temperature (°C).

smaller number of strong acid sites present in the former.

Semiempirical calculations have predicted the sequence of acidic strengths for the 12-heteropoly acids to be $H_3PW_{12}O_{40} > H_4SiW_{12}O_{40} \gg H_3PMo_{12}O_{40}$.⁹¹ Consistent with this prediction, the HPW salts had higher conversions of 1-butene than observed with the HSiW salts. The increased stability of the TIPMo salts is reflected in the higher conversion for these salts when compared with TlSiW salts, although the values of the former are smaller than TIPW salts. As the cation:proton ratio or reaction temperature increases, the HPW derived salts produce lower conversions. In contrast, the HSiW salts and TIPMo salts show an increase in conversion as the preparative cation:proton ratio or reaction temperature is increased.

The semiempirical quantum mechanical calculations which determined the sequence of acidic strengths for the heteropoly acids indicated that the negative charge on

Table 5.16 - Conversion of 1-butene at 10 minutes with salts of $H_4SiW_{12}O_{40}$.

| Salt | Preparative Ratio | Conversion ^{ab} / [(m ²)(H ⁺)] | | |
|-------|-------------------|-----------------------------------------------------------------|------|------|
| | | 100 ^c | 200 | 300 |
| AgSiW | 0.85 | 0.2 | 4.0 | 2.7 |
| | 1.00 | 0.3 | 3.8 | 7.3 |
| | 1.15 | 0.4 | 21.8 | 8.1 |
| TlSiW | 0.85 | 4.7 | 18.8 | 8.4 |
| | 1.00 | 1.2 | 18.3 | 19.1 |
| | 1.15 | 0.0 | 0.0 | 0.0 |

^a For measurements taken at 10 minutes.

^b Moles of products multiplied by (1×10^{27}).

^c Reaction temperature (°C).

the terminal oxygen atoms in the Keggin anions has an effect on the mobility of the protons, and thus the acidity of the heteropoly acid.⁹¹ Changing the peripheral metal atoms from tungsten to molybdenum would increase the coulombic binding of the proton as the charge on the terminal oxygen atoms is increased, while protonic mobility and acidity will decrease. It appears that the introduction of larger cations into the lattice structure with the Keggin anions also reduces the mobility of the protons. The larger size and repulsive interactions of the cations could restrict the physical movement of the protons. In addition, the nonprotonic cations may perturb the electron densities of the anions, altering the magnitude of the charge on the terminal oxygen atoms. The charge density of Ag^+ is greater than Tl^+ , which is in approximate agreement with the trends observed in the NH_3 TPD, 1H MAS NMR and butene conversion results.

It should be noted that while these interpretations are speculative, the influence of the larger nonprotonic cations on the acidic properties of the heteropoly acids as a result of direct and/or indirect interactions of the protons and the cations is evident.

5.5 References

1. J.H. Houzvicka; R. Klik; L. Kubelkova; V. Ponec. *Appl. Catal.*, **A150**, 101 (1997).
2. A. Béres; I. Pálinkó; I. Kiricsi. *React. Kinet. Catal. Lett.*, **59**, 47 (1996).
3. W.-Q. Xu; Y.-G. Yin; S.L. Suib; J.C. Edwards; C.-L. O'Young. *J. Catal.*, **163**, 232 (1996).
4. P. Meriaudeau; R. Bacaud; L. Ngoc Hung; A.T. Vu. *J. Mol. Catal.*, **A110**, L177 (1996).
5. J. Houzvicka and V. Ponec. *Appl. Catal.*, **A145**, 95 (1996).
6. M.A. Aseni; A. Corma; A. Martinez. *J. Catal.*, **158**, 561 (1996).
7. S.B. Hong and Y.S. Uh. *Catal. Lett.*, **36**, 249 (1996).
8. J. Houzvicka; O. Diefenbach; V. Ponec. *J. Catal.*, **164**, 288 (1996).
9. M. Guisnet; P. Andy; N.S. Gnep; E. Benazzi; C. Travers. *J. Catal.*, **158**, 551 (1996).
10. S. Gao and J.B. Moffat. *Catal. Lett.*, **42**, 105 (1996).
11. R.J. Pellet; D.G. Casey; H.-M. Huang; R.V. Kessler; E.J. Kuhlman; C.-L. O'Young; R.A. Sawicki; J.R. Ugolini. *J. Catal.*, **157**, 423 (1995).
12. S. Meijers; L.H. Gielgens; V. Ponec. *J. Catal.*, **156**, 147 (1995).
13. R. Robert; P.R. Rajamohanan; S.G. Hedge; A.J. Chandwadkar; P. Ratnasamy. *J. Catal.*, **155**, 345 (1995).
14. L.H. Gielgens; M.G.H. van Kampen; M.M. Broek; R. van Hardeveld; V. Ponec. *J. Catal.*, **154**, 201 (1995).
15. L.H. Gielgens; I.H.E. Veenstra; V. Ponec; M.J. Haanepen; J.H.C. VanHooff. *Catal. Lett.*, **32**, 195 (1995).
16. C.L. O'Young; R.J. Pellet; D.G. Casey; J.R. Ugolini; R.A. Sawicki. *J. Catal.*, **151**, 467 (1995).
17. F. Garciachoa and A. Santos. *AIChE Journal*, **41**, 286 (1995).

18. (a) W.-Q. Xu; Y.-G. Yin; S.L. Suib; C.-L. O'Young. *J. Phys. Chem.*, **99**, 758 (1995).
(b) W.-Q. Xu; Y.-G. Yin; S.L. Suib; J.C. Edwards; C.-L. O'Young. *J. Phys. Chem.*, **99**, 9443 (1995).
19. S.M. Yang; D.H. Guo; J.S. Lin; G.T. Wang. *Stud. Surf. Sci. Catal.*, **84**, 1677 (1994).
20. (a) Z.X. Cheng and V. Ponec. *J. Catal.*, **148**, 607 (1994).
(b) Z.X. Cheng and V. Ponec. *Appl. Catal.*, **118**, 127 (1994).
21. (a) Z.X. Cheng and V. Ponec. *Catal. Lett.*, **27**, 113 (1994).
(b) Z.X. Cheng and V. Ponec. *Catal. Lett.*, **25**, 337 (1994).
22. (a) G. Shahid and N. Sheppard. *J. Chem. Soc. Faraday Trans.*, **90**, 513 (1994).
(b) G. Shahid and N. Sheppard. *J. Chem. Soc. Faraday Trans.*, **90**, 507 (1994).
23. P. Patrono; A. La Ginestra; G. Ramis; G. Busca. *Appl. Catal.*, **A107**, 249 (1994).
24. P. Beltrame; L. Forni; A. Talamani; G. Zuretti. *Appl. Catal.*, **A110**, 39 (1994).
25. M.W. Simon; S.L. Suib; C. O'Young. *J. Catal.*, **147**, 484 (1994).
26. H.H. Mooiweer; K.P. De Jong; B. Kraushaar-Czarnetzki; W.H.J. Stork. *Stud. Surf. Sci. Catal.*, **84**, 2327 (1994).
27. S.M. Yang; D.H. Guo; J.S. Lin; G.T. Wang. *Stud. Surf. Sci. Catal.*, **84**, 1677 (1994).
28. T.J. Weeks Jr. and A.P. Bolton. *J. Chem. Soc. Faraday I*, **70**, 1676 (1994).
29. A.C. Butler and C.P. Nicolaidis. *Catal. Today*, **18**, 443 (1993).
30. J. Szabo; G. Szabo; J. VanGestel; D. Cornet. *Appl. Catal.*, **A96**, 319 (1993).
31. J. Szabo; J. Perrotey; G. Szabo; J.C. Duchet; D. Cornet. *J. Mol. Catal.*, **67**, 79 (1991).
32. Y. Hong; F.R. Cheng; J.J. Fripiat. *Catal. Lett.*, **17**, 187 (1993).
33. G. Shahid and N. Sheppard. *Can. J. Chem.*, **69**, 1812 (1991).
34. L. Basini; A. Aragno; A. Raffaelli. *J. Phys. Chem.*, **95**, 211 (1991).

35. A.T. Aguayo; J.M. Arandes; M. Olazar; J. Bilbao. *Ind. Eng. Chem. Res.*, **29**, 1172 (1990).
36. A. La Ginestra; P. Patrono; M.L. Berardelli; P. Galli; C. Ferragina; M.A. Massucci. *J. Catal.*, **103**, 346 (1987).
37. M. Stöcker; T. Riis; Hagen. *Acta Chem. Scand.*, **B40**, 200 (1986).
38. J. Engelhardt; J. Goldwasser; W.K. Hall. *J. Catal.*, **76**, 48 (1982).
39. I.C. Hisatsune. *J. Catal.*, **75**, 425 (1982).
40. H. Itoh; A. Tada; H. Hattori. *J. Catal.*, **76**, 253 (1982).
41. V. Mintsá-Eya; L. Hilaire; R. Toroude; F.G. Gault; B. Moraweck; B. Renouprez. *J. Catal.*, **76**, 169 (1982).
42. A.J. Van Roosmalen and J.C. Mol. *J. Catal.*, **78**, 17 (1982).
43. J.B. Nagy; A. Abou-Kais; M. Guelton; J. Harmel; E.G. Derouane. *J. Catal.*, **73**, 1 (1982).
44. J. Goldwasser and W.K. Hall. *J. Catal.*, **71**, 53 (1981).
45. J. Goldwasser; J. Engelhardt; W.K. Hall. *J. Catal.*, **71**, 381 (1981).
46. E. Rodevas; T. Yamaguchi; H. Hattori; K. Tanabe. *J. Catal.*, **69**, 434 (1981).
47. M.P. Rosynek; J.S. Fox; J.L. Jensen. *J. Catal.*, **71**, 64 (1981).
48. I. Suzuki. *J. Catal.*, **68**, 220 (1981).
49. T. Yamaguchi; Y. Tanaka; K. Tanabe. *J. Catal.*, **65**, 442 (1980).
50. J. Goldwasser and W.K. Hall. *J. Catal.*, **63**, 520 (1980).
51. B.E. Langner. *J. Catal.*, **65**, 416 (1980).
52. M.R.S. Manton and J.C. Davitz. *J. Catal.*, **69**, 156 (1979).
53. Y. Nakano; T. Iizuka; H. Hattori; K. Tanabe. *J. Catal.*, **57**, 1 (1979).
54. J.B. Nagy; M. Guelton; E.G. Derouane. *J. Catal.*, **55**, 43 (1978).

55. M.P. Rosynek and J.S. Fox. *J. Catal.*, **49**, 285 (1977).
56. (a) J.-P. Damon; B. Delmon; J.-M. Bonnier. *J. Chem. Soc. Faraday Trans. I*, **73**, 372 (1977).
(b) J.-P. Damon; J.-M. Bonnier; B. Delmon. *J. Colloid Interface Sci.*, **55**, 381 (1976).
57. Y. Sakai and H. Hattori. *J. Catal.*, **42**, 37 (1976).
58. G.E. Martin and L.W. Hill. *J. Catal.*, **42**, 344 (1976).
59. T. Vemarsu; K. Inamura; K. Hirai; H. Hashimoto. *J. Catal.*, **45**, 68 (1976).
60. H. Hoser and S. Krzyanowski. *J. Catal.*, **38**, 366 (1975).
61. V.R. Choudhary. *Ind. Eng. Chem. Prod. Res. Dev.*, **14**, 227 (1975).
62. V.R. Choudhary. *Chem. Ind. Dev.*, **8**, 32 (1974).
63. A. Ghorbel; C. Hoang-Van; S.J. Teichner. *J. Catal.*, **33**, 123 (1974).
64. V. Ragaini. *J. Catal.*, **34**, 1 (1974).
65. T. Vematsu; K. Tsukada; H. Hashimoto. *J. Catal.*, **32**, 369 (1974).
66. D.M. Brouwer and H. Hogeveen. *Prog. Phys. Org. Chem.*, **9**, 179 (1972).
67. J.B. Nagy; M. Guelton; E.G. Derouane. *J. Catal.*, **55**, 43 (1970).
68. K. Tanabe. "Solid Acids and Bases" Academic Press: New York, 1970.
69. (a) D.M. Brouwer and J.M. Oelderik. *Rec. Trav. Chim. Pays Bas.*, **87**, 721 (1968).
(b) D.M. Brouwer. *Rec. Trav. Chim. Pays Bas.*, **87**, 1435 (1968).
70. (a) J.W. Hightower and W.K. Hall. *J. Phys. Chem.*, **71**, 1014 (1967).
(b) J.W. Hightower and W.K. Hall. *Chem. Eng. Prog. Symp. Ser.*, **63**, 122 (1967).
(c) J.W. Hightower and W.K. Hall. *J. Amer. Chem. Soc.*, **89**, 778 (1967).
71. J. W Hightower; H.R. Gerberich; W.K. Hall. *J. Catal.*, **7**, 57 (1967).
72. D.M. Golden; K.W. Egger; S.W. Benson. *J. Am. Chem. Soc.*, **86**, 5416 (1964).
73. J.B. Peri. "Proc. 3rd Intl. Congr. on Catalysis" North Holland: Amsterdam, 1964, p.1100.

74. H.P. Leftin and M.C. Hobson. *Advances in Catalysis*, **14**, 115 (1964).
75. J. Wei and C.D. Prater. *Advances in Catalysis*, **13**, 203 (1962).
76. L.H. Little; H.E. Klauser; C.H. Amberg. *Can. J. Chem.*, **39**, 42 (1961).
77. J.B. Peri. "Proc. 2nd Intl. Congr. on Catalysis" Edition Technip: Paris, 1961.
78. W.O. Haag and H. Pines. *J. Am. Chem. Soc.*, **82**, 387 (1960).
79. G.J. Hutchings; C.P. Nicolaides; M.S. Scurrall. *Catal. Today*, **15**, 23 (1992).
80. D. Lapham and J.B. Moffat. *J. Mol. Catal.*, **52**, 169 (1989).
81. (a) J.G. Highfield and J.B. Moffat. *J. Catal.*, **88**, 177 (1984).
(b) J.G. Highfield and J.B. Moffat. *J. Catal.*, **89**, 185 (1984).
(c) J.G. Highfield and J.B. Moffat. *J. Catal.*, **95**, 108 (1985).
(d) G.B. McGarvey and J.B. Moffat. *J. Catal.*, **128**, 69 (1991).
82. M.A. Parent and J.B. Moffat. *Langmuir*, **12**, 3733 (1996).
83. K.C. Pratt, in "Catalysis: Science and Technology." (J.R. Anderson and M. Boudart, Eds.) Springer-Verlag: Berlin, 1981, p.173.
84. M.C. White. "Heterogeneous Catalysis." Prentice Hall: Englewood Cliffs, N.J., 1990, p.147.
85. L.C. Jozefowicz; H.G. Karge; E. Vasilyeva; J.B. Moffat. *Microporous Materials*, **1**, 313 (1993).
86. V.M. Matikhin; S.M. Kulikov; A.V. Nosov; I.V. Kozhevnikov; I.L. Mudrakovsky; M.N. Timofeeva. *J. Mol. Catal.*, **60**, 65 (1990).
87. H. Pfeifer; D. Freude; J. Karger. *Stud. Surf. Sci. Catal.*, **65**, 89 (1991).
88. H. Pfeifer in "Acidity and Basicity of Solids: Theory, Assessment and Utility." (J. Fraissard and L. Petrakis, Eds.) Kluwer: Dordrecht, 1994 p. 255.
89. D. Freude; H. Ernst; T. Mildner; H. Pfeifer; I. Wolf. *Stud. Surf. Sci. Catal.*, **90**, 105 (1993).
90. H. Barthomeuf. *Stud. Surf. Sci. Catal.*, **65**, 157 (1991).
91. J.B. Moffat. *J. Mol. Catal.*, **26**, 385 (1985).

92. T. Matsuda; M. Sato; T. Kanno; H. Miura; K. Sugiyama. *J. Chem. Soc. Faraday Trans I*, **77**, 3107 (1981).
93. S. Gao and J.B. Moffat. *Colloids and Surfaces A*, **105**, 133 (1995).
94. (a) M.A. Makarova; E.A. Paukshtis; J.M. Thomas; C. Williams; K.I. Zamaraev. *J. Catal.*, **149**, 36 (1994).
(b) K.I. Zamaraev and J.M. Thomas in "Advances in Catalysis", **41**, (D.D. Eley; W.O. Haag; B. Gates, Eds.) Academic Press Inc.: San Diego, California, 1996., p.335.
95. H.H. Voge and N.C. May. *J. Amer. Chem Soc.*, **68**, 550 (1946).
96. J.S. Vaughan; C.T.O. Conner; J.C.Q. Fletcher. *J. Catal.*, **147**, 441 (1994).
97. M. Misono. *Catal. Rev. - Sci. Eng.*, **29**, 269 (1987).
98. W.-Q. Xu; Y.-G. Yin; S.L. Suib; C.L. O'Young. *J. Catal.*, **150**, 34 (1994).
99. (a) J.B. McMonagle and J.B. Moffat. *J. Colloid Interface Sci.*, **101**, 479 (1984).
(b) D.B. Taylor; J.B. McMonagle; J.B. Moffat. *J. Colloid Interface Sci.*, **108**, 278 (1985).
(c) G.B. McGarvey and J.B. Moffat. *J. Colloid Interface Sci.*, **125**, 51 (1988).
(d) G.B. McGarvey and J.B. Moffat. *J. Catal.*, **130**, 483 (1991).

CHAPTER 6

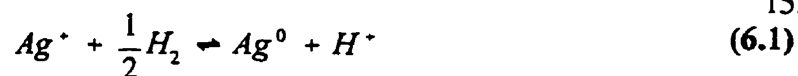
Dehydration of Butyl Alcohols

6.1 Introduction

The conversion of methanol to hydrocarbons gained attention in 1977 with the use of HZSM-5 zeolites as catalysts by Chang and Silvestri.¹ The well defined pore structure and Brønsted acidity characteristic of zeolites promoted an industrial interest in the development of a methanol to gasoline process on ZSM-5 type zeolites.^{2,3} Despite the general acceptance that the dehydration of the alcohol was the initial step of the process,³ there was further debate as to the mechanism involved in the formation of the first carbon-carbon bond. Chang discusses the postulated mechanisms (the carbene, the carbocation, ylide and radical pathways) by which the carbon-carbon bond formation occurs.⁴ The lack of direct evidence to determine the operative mechanism promotes continued work in this field.

In the discussion of the structural aspects of the 12-heteropoly oxometalates in Chapter One, it was mentioned that photoacoustic (PAS) FTIR studies demonstrated that polar molecules such as ammonia, pyridine, and methanol were capable of penetrating from the vapour phase into the bulk structure, where interaction with the protons may occur.⁵ This was of particular interest since the 12-heteropoly acids typically had very small surface areas ($< 10 \text{ m}^2/\text{g}$)⁶ and lacked a microporous structure. In 1982, the catalytic behaviour of 12-tungstophosphoric acid for the conversion of methanol to hydrocarbons was published from work carried out in this laboratory.^{7(a)} During the 1980's further reports of the 12-tungstophosphoric and 12-tungstosilicic acids and several related salts (alkali, alkaline earths, transition metals, and ammonium) studied as heterogeneous catalysts in this reaction continued to be published.⁷⁻¹¹

The first reports by Ono *et al.*^{8(a),(b),(d),(e)} described extensive studies of the silver(I) and copper(II) salts of these acids and revealed that they performed as well as or better than the free acids for the methanol process. They attributed the increased activity to the Brønsted acidity of the salts. They reasoned that these Brønsted acid sites were formed when the metal was reduced by molecular hydrogen, as depicted in Equation 6.1, formed



during the decomposition of methanol. This would generate a proton which would become the operative acidic site in the methanol conversion process. This view was maintained by Misono in review articles discussing the catalytic abilities of the 12-heteropoly salts.¹²

Work in this laboratory has indicated that residual protons are present in the salts after their preparation, apparently contradicting Ono's theory as to the source of Brønsted acid sites. PAS FTIR studies revealed that the precipitation of salts, prepared as stoichiometric, was incomplete and protons remained in the isolated solid.⁵ Further evidence is provided by solid state ¹H NMR studies of the Ag₃PW₁₂O₄₀ and Ag₄SiW₁₂O₄₀ salts, as discussed in Chapter Five (Section 5.3.1); protons are present in the silver salts and the concentration of these acid sites is affected by the preparative cation:proton ratio employed.

Studies by Hayashi and Moffat^{7(a)(c)} concluded that the dehydration of methanol follows a similar dehydration step, as evident with the ZSM-5 catalysts.³ The selectivity of the products was strongly dependent upon the peripheral metal for the acids, with the 12-tungstophosphoric acid forming primarily linear and branched hydrocarbons, consisting predominantly of C₂ to C₅ olefins, while the analogous H₃PMo₁₂O₄₀ acid produced larger amounts of carbon monoxide, although the catalyst was quite active.^{7(a)} Further studies of 12-tungstophosphoric acid revealed that the amount of dimethyl ether produced decreased as the residence time was increased from 50 to 1000 mg·cat min/mL He(g), while the selectivity towards hydrocarbons increased. At the highest residence times, the amount of the longest hydrocarbon produced reached a limiting value or decreased, with the coincidental increase in the production of methane.

PAS FTIR studies^{7(d)(e)} of methanol and intermediates on the adsorbed surface of H₃PW₁₂O₄₀, prior to the carbon-carbon bond formation, indicated that protonation of methanol, forming CH₃OH₂⁺, was the initial step in the production of higher hydrocarbons. The molecular ion is proposed to dissociate to CH₃⁺ and H₂O with the CH₃⁺ subsequently interacting with a terminal oxygen atom of the Keggin anion to form a surface methoxy

intermediate. Further evidence of the formation of the methoxide species was provided by an observed change in the ^{13}C MAS NMR chemical shift of the methylene species, after methanol had been adsorbed by the heteropoly acid.¹³ This species was identified as a methoxide.

Formation of dimethyl ether and regeneration of the protons was proposed to occur by the interaction of the physisorbed methanol molecule and the surface methoxide intermediate.⁷ Although the authors were not able to provide direct evidence for the emergence of a single mechanism for the initial carbon-carbon bond formation, they concluded that the evidence and that found in the literature indicated the onium ylide or carbene mechanism must be operative over HPW.^{7(c)} This was also consistent with the observed production of methane from longer hydrocarbon chains, known to proceed through a carbonium ion intermediate.

The metal salts^{7(b)} and ammonium salt^{7(c)} of 12-tungstophosphoric acid resulted in differences in activity from the parent acid. In particular, the microporous $(\text{NH}_4)_3\text{PW}_{12}\text{O}_{40}$ produced higher conversions of methanol and this increase in activity could not be solely accounted for by the increased surface area of the salt.⁷ Under similar reaction conditions, the product distribution by the ammonium salt consisted mainly of paraffins, rather than olefins as observed with the parent acid, and the selectivity to methane did not increase with the increase in the residence time. The ammonium salt was also noted to have an increased thermal stability and a decrease in the strongest acid sites in the acid strength distribution.^{7(c)} These properties encouraged a more rigorous study of the surface characteristics of the monovalent salts of $\text{H}_3\text{PW}_{12}\text{O}_{40}$, $\text{H}_3\text{PMo}_{12}\text{O}_{40}$, $\text{H}_4\text{SiW}_{12}\text{O}_{40}$ and $\text{H}_4\text{AsW}_{12}\text{O}_{40}$.¹⁴⁻¹⁶ From investigations of the conversion of methanol with the ammonium salt, it was concluded that the surface area, microporosity, and distribution of acid strengths have an effect on the ability of a 12-heteropoly oxometalate salt to perform as a catalyst.

To provide insight into the influence of pore confinement in the zeolite structure and on the nature of the pathways and reaction intermediates involved, an extensive study has been carried out by Thomas and coworkers¹⁷ in the conversion of a series of butyl alcohols (specifically *n*-, *iso*-, *sec*- and *tert*-butanol) with the zeolite HZSM-5. The

dehydration of butyl alcohols has proven to be a useful reaction to characterize acid sites of a catalyst, detecting small changes in their acid strength and concentration and such experiments would complement the work previously carried out with the isomerization of 1-butene, discussed in Chapter 5. 2-Butanol has been used with alumina¹⁸ and mechanical mixtures of oxides.¹⁹ Delmon and coworkers have employed 1-butanol with pure and modified alumina,²⁰ silica aluminas,²¹ and more recently pure and modified alumina phosphate (AlPO₄).²² Others have utilized this alcohol to examine alumina and tungsten oxide,²³ highly dispersed 12-tungstophosphoric acid,²⁴ and alumina on a catalytic membrane.²⁵

As discussed in Chapter Five, partial substitution of the protons in the 12-heteropoly oxometalates by monovalent cations of cesium, silver and thallium affects three characteristics of the salts: a microporous structure is created, the number of Brønsted acid sites is decreased and the distribution of acid strengths is shifted. Variation in the cation:proton ratio alters the number of residual protons and the chemical environment in which they reside. Using these results and interpretations of the previous work with butyl alcohols,¹⁷⁻²⁵ the objective of this chapter is to provide further information on the catalytic properties of the cesium, silver, and thallium salts of the three 12-heteropoly acids by investigating the dehydration of a series of butyl alcohols, specifically *tert*-butanol, 2-butanol, and 1-butanol. These results, in collaboration with the results from ¹H MAS NMR and temperature programmed desorption of ammonia in Chapter Five assessing the number of acid sites available within a specific salt and the distribution of acid strengths, will provide further information on the dependence of catalytic properties of these salts on the nature of the cation, the stoichiometry, and morphology of the salts. This will provide further insight into the perturbation of the acidic strength from introduction of nonprotonic cations.

6.2 Experimental

6.2.1 Materials

Helium was purchased from Praxair, 1-butanol from Fisher (Reagent A.C.S.), 2-butanol from BDH (Anala R Grade) and *tert*-butanol from MCB Reagents. All three alcohols were used as received.

The cesium, silver, and thallium salts of 12-tungstophosphoric, 12-tungstosilicic, and 12-molybdophosphoric acids were prepared as outlined in Section 2.2.1. For the dehydration of butyl alcohols, the preparative cation:proton ratios of 0.85, 1.00, and 1.15 were examined for the cesium, silver, and thallium salts of 12-tungstophosphoric acid (denoted as CsPW, AgPW, and TIPW, respectively), of 12-tungstosilicic acid (denoted as CsSiW, AgSiW, and TISiW, respectively) and thallium 12-molybdophosphate (denoted as TIPMo).

The 12-heteropoly oxometalate salts precipitated spontaneously as microcrystalline materials and the particle size distribution of each salt was discussed in Section 5.2.1. The samples of catalyst used in the dehydration of the butyl alcohols consisted of particles < 75 μm (< 200 mesh) in diameter with the exception of the AgPW salts. These salts were sticky in nature and a larger particle size was required to maintain a consistent residence time and avoid a build-up of backpressure in the reactor system. As a result, particles of 106 to 150 μm in diameter were used for reactions with AgPW. No difference in activity was noted for HPW with a change in particle size. The particle size of a catalyst can have an effect on the conversion²⁶ and selectivity²⁷ observed. However, since intrinsic kinetic data have not been determined in the present study these effects were not considered.

6.2.2 Apparatus and Procedure

The catalytic reaction for the dehydration of butyl alcohols was carried out in a small flow system, constructed from 1/8" stainless steel tubing (0.02" wall thickness), unions, connectors, and valves, as depicted in Figure 6.1. A U-shaped glass tube reactor, constructed from Pyrex, was attached using 1/4"-1/8" reducing unions. The reactor tube (6 mm o.d., 4 mm i.d.) was 22 cm in length and a small constriction was placed 8 cm

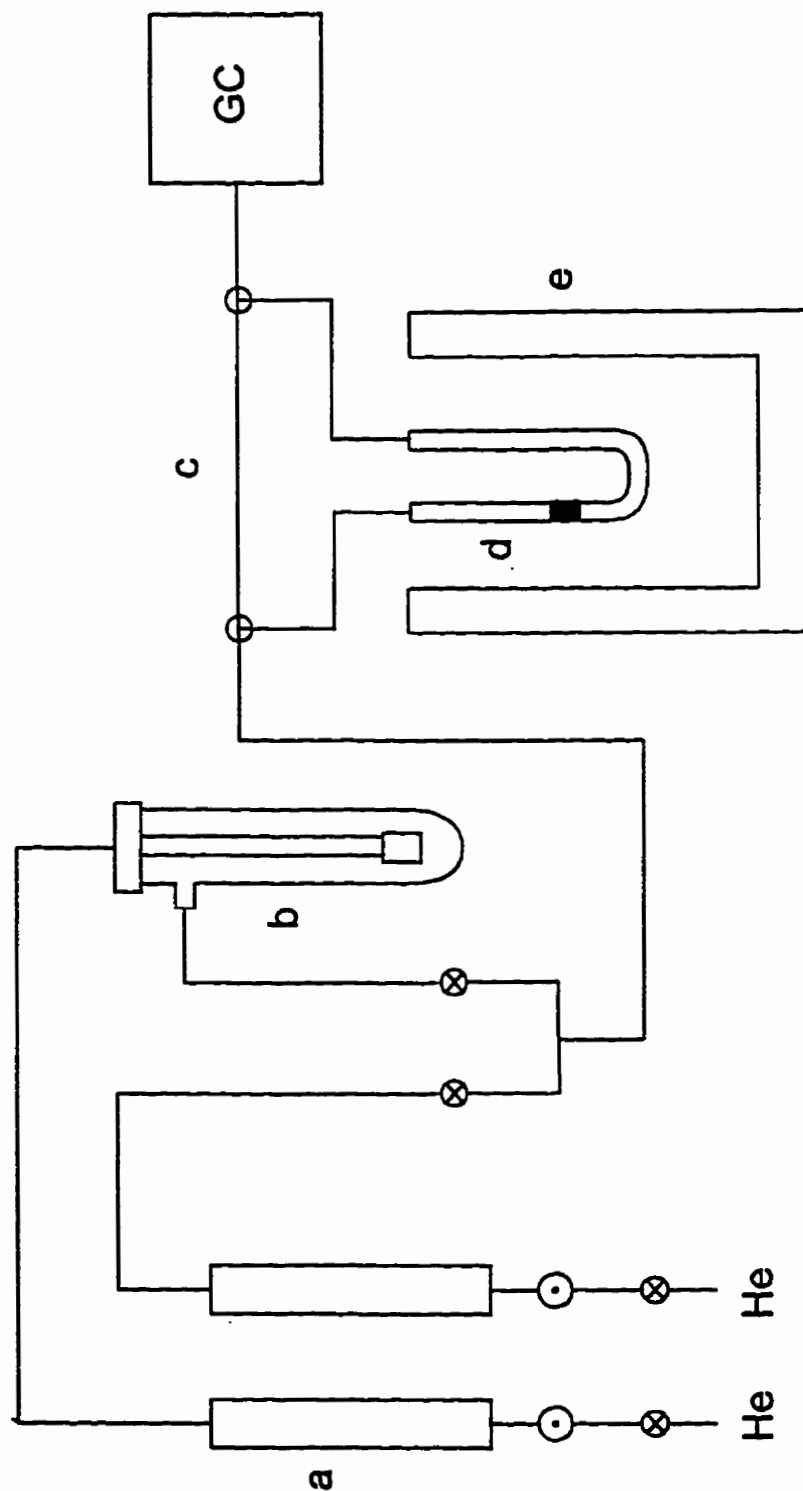


Figure 6.1 - Catalytic reactor system. (a) rotameters; (b) saturator containing alcohol; (c) reactor bypass section; (d) reactor tube; (e) temperature bath.

from the inlet side of the tube at which the sample of catalyst (100 mg) was supported between two plugs of quartz wool. The glass reactor tube was immersed in a Neslab controlled temperature water bath, filled with silicon oil, and temperatures could be set and maintained to ± 0.5 °C. The stainless steel tubing leading from the exit of the glass reactor to the entrance of the gas chromatograph was heated with heating tape to prevent condensation of products in the lines. The reactant mixture could be directed through either the reactor or the bypass section.

The catalyst was pretreated *in situ* at the reaction temperature for 15 minutes for reactions with *tert*-butanol and 20 minutes for the 1- and 2-butanols under a flow of helium (9 mL/min). To introduce the reactant, helium was passed through a saturator containing the alcohol at 25 °C, at 9 mL/min, and then passed through the glass reactor tube containing the catalyst. The flow of the gas was regulated using needle valves and monitored using rotameters. The reactant and products were analyzed with a HP5890 gas chromatograph equipped with a TCD and 1% SP 1000 Carbopack B column (60/80, 8' x 1/8" OD). Initial activity was measured at 5 minutes after the catalyst was in contact with the reactant mixture. Additional measurements were taken every 15 minutes for *tert*-butanol and every 20 minutes for the 1- and 2-butanols for a period up to two hours. The level of activity remained constant after the initial deactivation so that averages were taken of deactivated measurements between 40 and 120 minutes on-stream. Two trials were performed for each experiment and in most cases the average of the two is reported. The dehydration of *tert*-butanol was carried out at 46 °C and the dehydration of 1- and 2-butanol at 108 °C. The sample loop was injected to the GC by the programmed switching of a solenoid six-way valve for 6 sec and all exits were vented to the fumehood. No conversion of the butyl alcohols was observed with an empty reactor in the range of temperatures employed in the present work.

6.2.3 Definitions

Dehydration of *tert*-butanol produced only *iso*-butene. *Cis*- and *trans*-2-butene, 1-butene and small amounts of butane were the only products observed in the dehydration

of 1- and 2-butanols. Mass balances of less than 100% are common in the present work, due to the retention of alcohols and/or their decomposition products on the catalyst. In most cases, the mass balance increased as the reactant time progressed. As a result of this, the % conversion was based on only the reactants and products monitored by the GC, so that

$$\% \text{ Conv} = 100 \left[\frac{\text{total moles of products}}{\text{total moles of products} + \text{moles of unreacted alcohol}} \right] \quad (6.2)$$

The selectivity was calculated on the product basis.

$$\% \text{ Selectivity } (i) = 100 \left[\frac{\text{moles of component } i}{\text{total moles of products}} \right] \quad (6.3)$$

6.3 Results

6.3.1 Dehydration of *tert*-Butanol.

Dehydration of *tert*-butanol at 46 °C produced only *iso*-butene and was a facile reaction for all of the salts investigated. Figure 6.2 shows the conversion for the salts of 12-tungstophosphoric acid examined, measured at 5 minutes and after 120 minutes, while the conversion for the pure acid, HPW, was calculated to be 37% at 5 minutes and 7% at 120 minutes. All three stoichiometries of the AgPW salts displayed higher activities than the pure acid at both sampling intervals. Both the thallium and cesium salts synthesized with a deficit of the cation as well as the stoichiometric TlPW salt produced higher conversions than the pure acid at 5 minutes. A decrease in activity occurred for these salts at higher times-on-stream with the *tert*-butanol, but the stoichiometric and deficit salts maintained higher conversions than found with HPW. For the initial and subsequent measurements, similar activities were noted for the various stoichiometries of the cesium and thallium salts.

A decrease in conversion of *tert*-butanol to *iso*-butene is observed with all of the

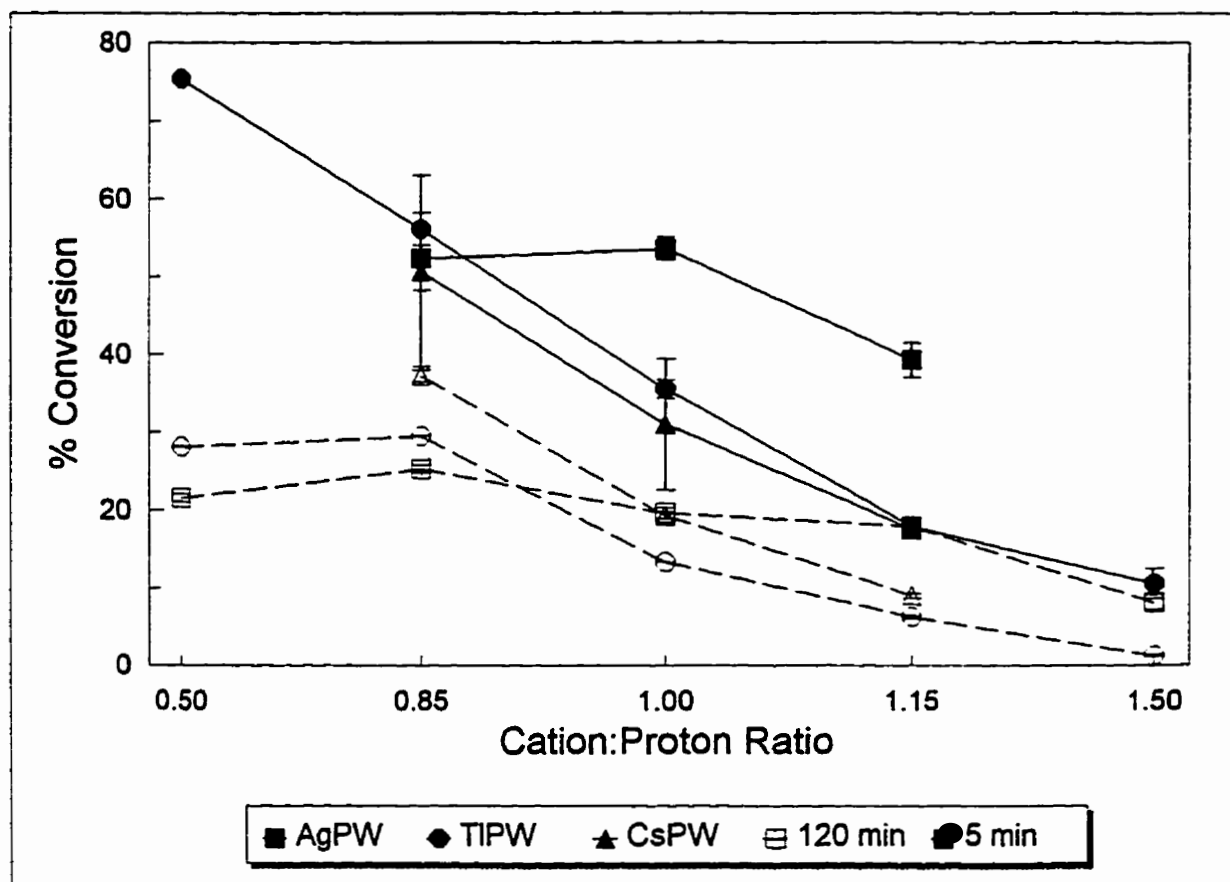


Figure 6.2 - Conversion of *tert*-butanol at 46 °C with salts of $H_3PW_{12}O_{40}$.

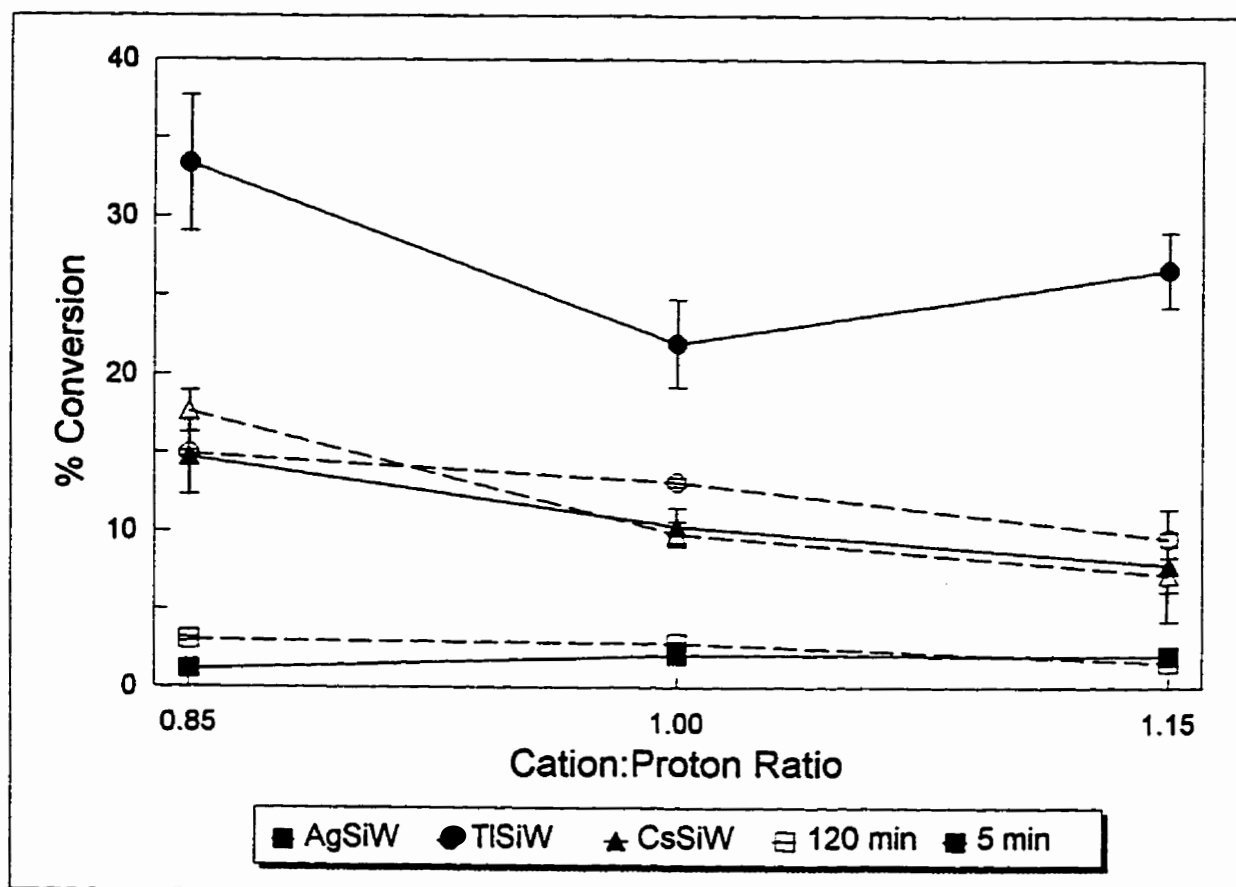


Figure 6.3 - Conversion of *tert*-butanol at 46 °C with salts of $H_4SiW_{12}O_{40}$.

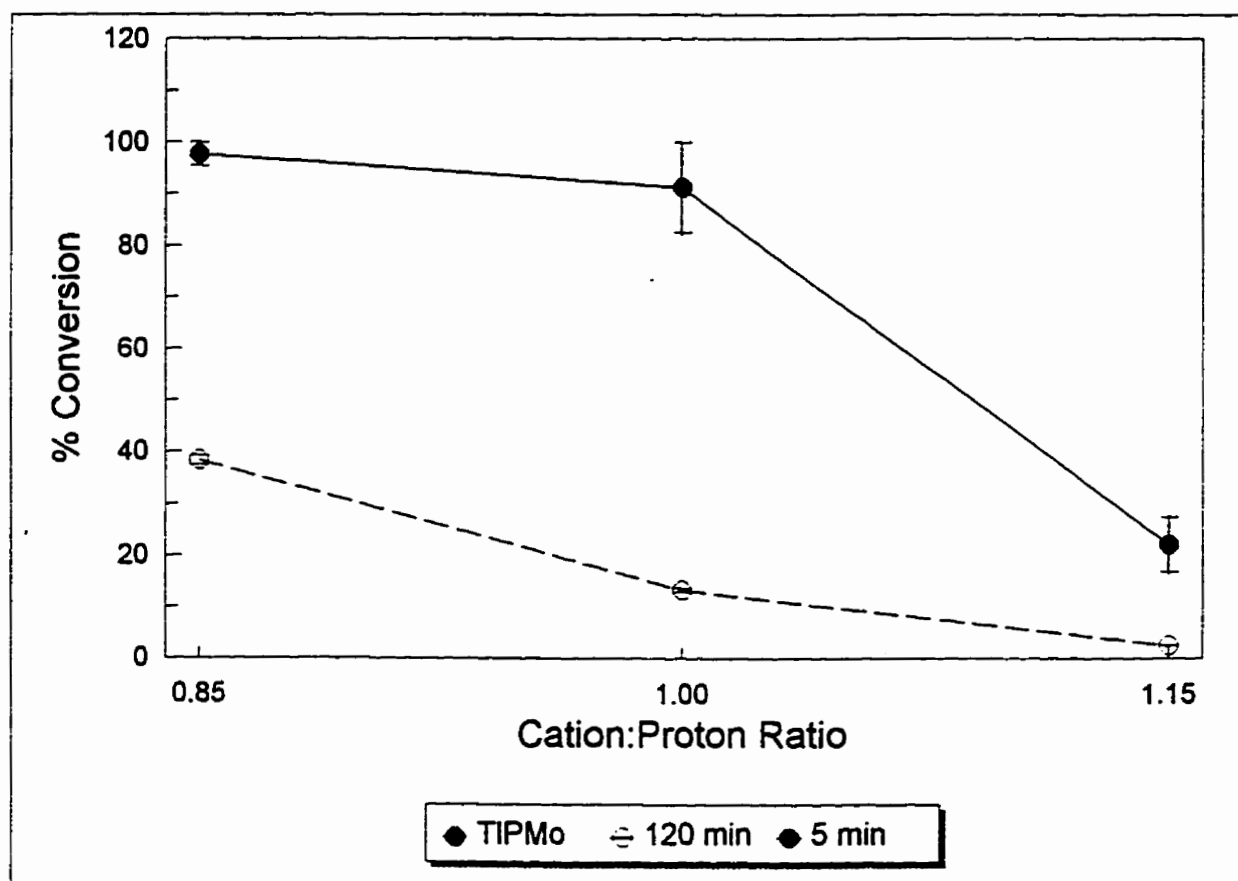


Figure 6.4 - Conversion of *tert*-butanol at 46 °C with $Tl_3PMo_{12}O_{40}$ salts.

salts as the preparative cation:proton ratio is increased, both with the fresh catalyst and after remaining on-stream, although this decline in activity is more pronounced at the 5 minute sampling. The exception to this is the slight increase in activity observed for the 0.50 TIPW and AgPW salts relative to the respective 0.85 salts.

In contrast to 12-tungstophosphoric acid, the HSiW acid increases in activity with increasing time-on-stream. The conversion of *tert*-butanol with HSiW was calculated to be 9% at 5 minutes and 66% at 120 minutes. The thallium and cesium salts displayed higher activities than the pure acid at 5 minutes, while the silver analogues have relatively small activities. (Figure 6.3) A significant decrease in conversion occurs for the TISiW salts with increasing time-on-stream while no significant changes are apparent for the silver and cesium salts. As the preparative cation:proton ratio is increased, there is a slight decline in activity for the three 12-tungstosilicic salts.

In the dehydration of *tert*-butanol by 12-molybdophosphoric acid, initial conversions were approximately 1 to 2%. The pure acid decomposed, forming a dark green liquid in the reactor tube. The thallium salt of 12-molybdophosphoric acid remained stable throughout the reaction and mimicked the trend observed with the salts of HPW. (Figure 6.4) A decrease in conversion occurs as the cation to proton ratio is increased and with increasing time-on-stream. The deactivation as the preparative ratio is increased is more pronounced with measurements taken at 5 minutes.

The deactivation of the salts with *tert*-butanol occurs quickly, within 15 minutes after exposure to the reactant. However, this new level of conversion is maintained with catalysts prepared with a 15% deficit of the cation left on-stream for more than twelve hours.

6.3.2 Dehydration of 2-Butanol.

The dehydration of 2-butanol was carried out at 108 °C, under otherwise identical reaction conditions to *tert*-butanol. The higher temperature was required to facilitate the dehydration of 1- and 2-butanols. It was also observed that a narrower temperature range was present for these two alcohols for the 0% and 100% levels of conversion than

observed for *tert*-butanol.

Figure 6.5 summarizes the conversion for 2-butanol by the 12-tungstophosphate salts. With the fresh catalysts, all three salts synthesized with a deficit or stoichiometric amount of the cation have a conversion similar to that with HPW, which was observed to be 95%. Except for the salt containing silver, a significant decrease occurs for the salts made with an excess of the cation. At this high reaction temperature, little deactivation of HPW is observed with increasing time-on-stream. A similar trend is evident for the silver salts. However, the stoichiometric thallium and cesium salts show a significant decrease in conversion with increasing time-on-stream and 1.15 TIPW and CsPW salts have little or no activity at the higher time-on-stream. (Figure 6.5)

The products produced by the dehydration of 2-butanol were primarily the *cis* and *trans* isomers of 2-butene, together with 1-butene. In some instances, particularly with a fresh surface and a shortage of the cation, trace amounts of butane were present. Tables 6.1 and 6.2 summarize the product distribution observed for the dehydration of 2-butanol by the parent acid and salts. Despite the dependence of the activity on the nature of the cation or the amount of cation used to synthesize the salt, the product distribution remains similar for the AgPW and TIPW salts, regardless of their stoichiometries, with average selectivities of 64, 28 and 8% found for *trans*-2-butene, *cis*-2-butene, and 1-butene, respectively. This pattern is maintained at higher times-on-stream (Table 6.2). The product distribution for the CsPW salts is affected by the cation:proton ratio with an increase in the selectivity to *cis*-2-butene as the relative amount of the cesium cation is increased.

Dehydration of 2-butanol by 12-tungstosilicic acid remains constant at 87%, irrespective of the time-on-stream. Only salts synthesized with a 15% deficit of the cations have similar activities to the pure acid with initial measurements taken at 5 minutes. (Figure 6.6) The conversion decreases as the preparative stoichiometry is increased, although this appears to be more gradual with the silver salts than either of the TlSiW or CsSiW salts. With increasing time-on-stream, unlike the parent acid, deactivation occurs for all three series of salts examined. This is most notable for the

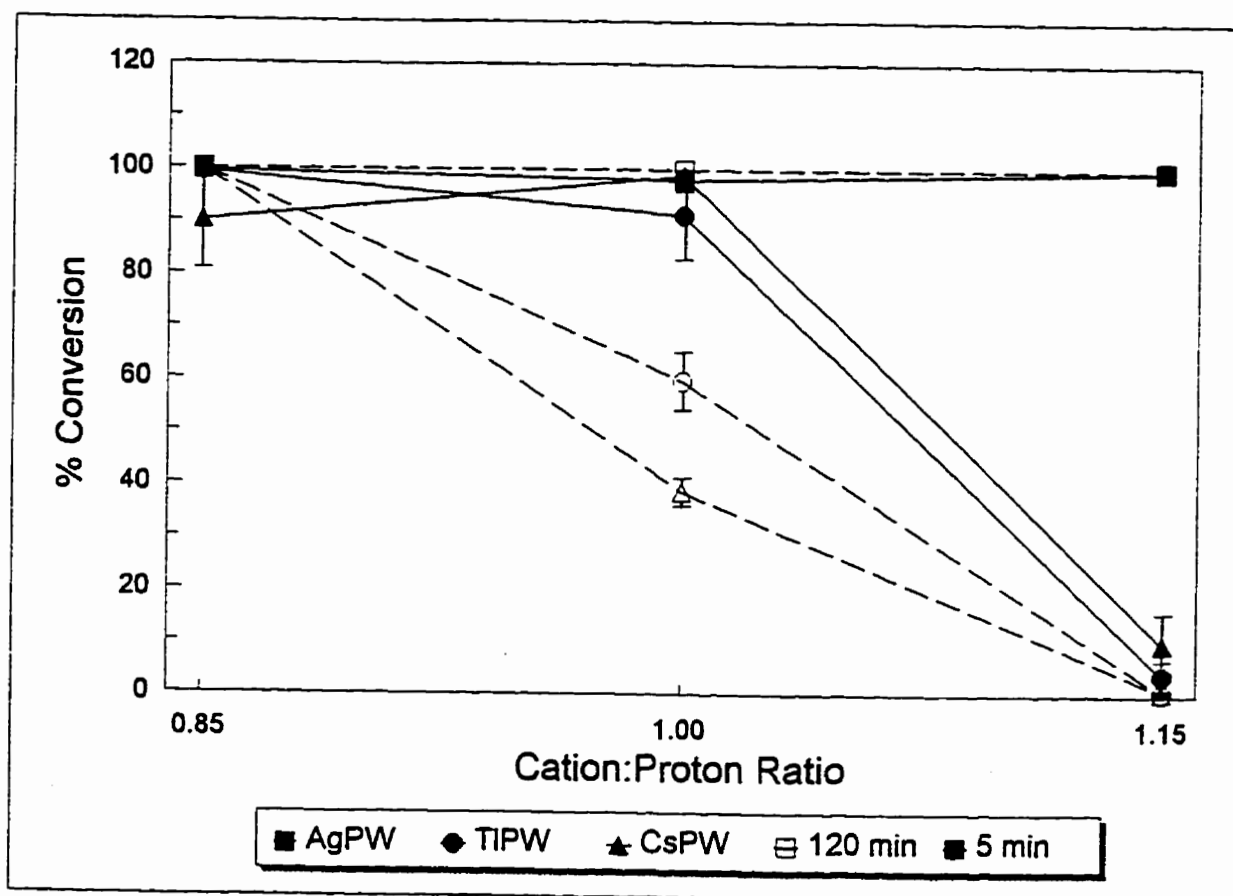


Figure 6.5 - Conversion of 2-butanol at 108 °C with salts of $H_3PW_{12}O_{40}$.

Table 6.1 - Distribution of products in dehydration of 2-butanol with salts of 12-tungstophosphoric acid for initial measurements.^a

| Salt | Preparative Ratio ^b | Selectivity of Products | | | |
|--------------------------------------------------|--------------------------------|-------------------------|----------|----------------------|------------------------|
| | | Butane | 1-Butene | <i>cis</i> -2-Butene | <i>trans</i> -2-Butene |
| H ₃ PW ₁₂ O ₄₀ | | 0 | 7 | 29 | 64 |
| Ag ₃ PW ₁₂ O ₄₀ | 0.85 | 1 | 8 | 28 | 63 |
| | 1.00 | 2 | 8 | 28 | 62 |
| | 1.15 | 0 | 8 | 28 | 64 |
| Tl ₃ PW ₁₂ O ₄₀ | 0.85 | 2 | 9 | 27 | 62 |
| | 1.00 | 0 | 11 | 29 | 60 |
| | 1.15 | 0 | 7 | 40 | 53 |
| Cs ₃ PW ₁₂ O ₄₀ | 0.85 | 2 | 11 | 27 | 60 |
| | 1.00 | 0 | 9 | 32 | 59 |
| | 1.15 | 0 | 12 | 48 | 40 |

^a Time-on-stream of 5 minutes.

^b Cation:Proton ratio.

Table 6.2 - Distribution of products in dehydration of 2-butanol with salts of 12-tungstophosphoric acid at higher time-on-stream.^a

| Salt | Preparative Ratio ^b | Selectivity of Products | | | |
|--------------------------------------------------|--------------------------------|-------------------------|----------|----------------------|------------------------|
| | | Butane | 1-Butene | <i>cis</i> -2-Butene | <i>trans</i> -2-Butene |
| H ₃ PW ₁₂ O ₄₀ | | 0 | 7 | 29 | 64 |
| Ag ₃ PW ₁₂ O ₄₀ | 0.85 | 2 | 8 | 27 | 63 |
| | 1.00 | 0 | 8 | 28 | 64 |
| | 1.15 | 0 | 9 | 28 | 63 |
| Tl ₃ PW ₁₂ O ₄₀ | 0.85 | 1 | 9 | 27 | 63 |
| | 1.00 | 0 | 8 | 41 | 51 |
| | 1.15 | 0 | 0 | 32 | 68 |
| Cs ₃ PW ₁₂ O ₄₀ | 0.85 | 1 | 8 | 28 | 63 |
| | 1.00 | 0 | 8 | 49 | 43 |
| | 1.15 | 0 | 3 | 38 | 59 |

^a Time-on-stream of 120 minutes.

^b Cation:Proton ratio.

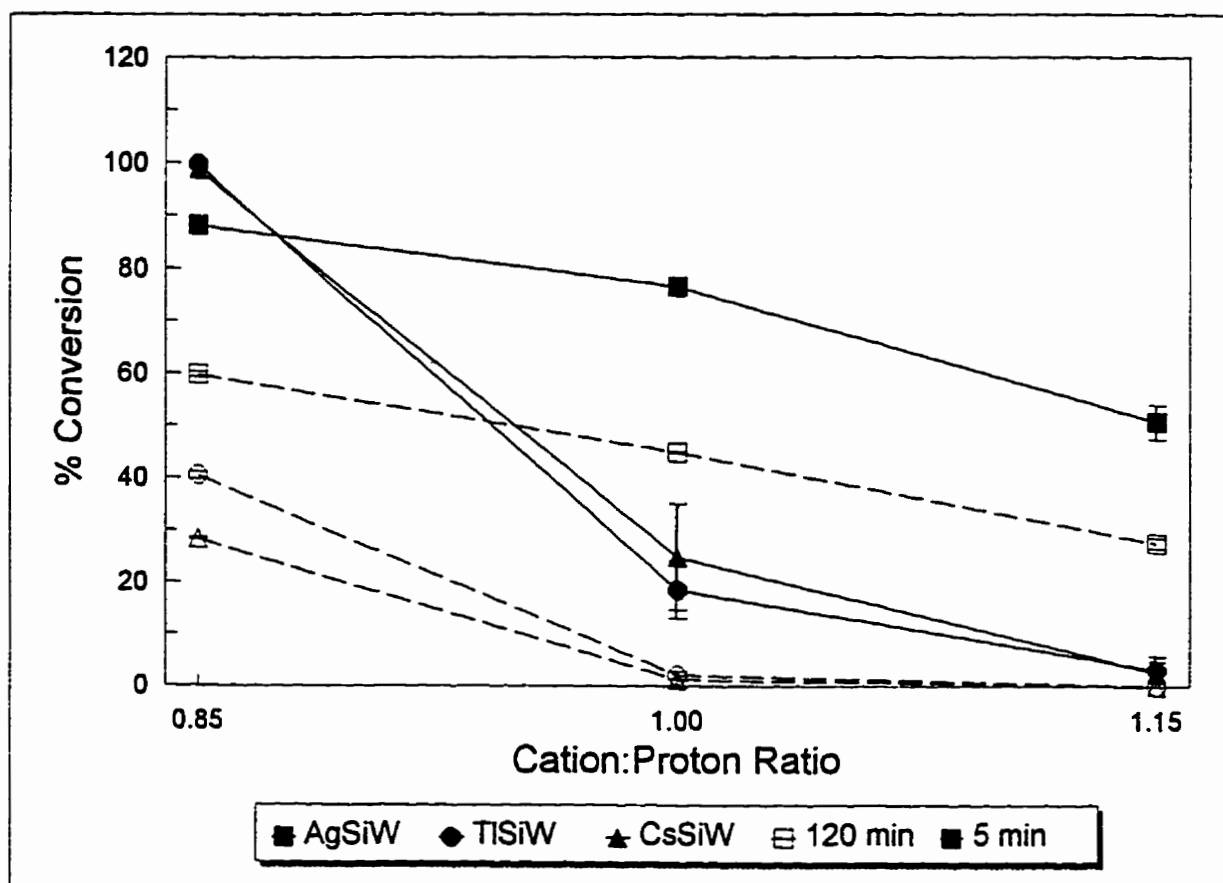


Figure 6.6 - Conversion of 2-butanol at 108 °C with salts of $H_4SiW_{12}O_{40}$.

thallium and cesium salts in which relatively small activities are present for the salts prepared with a stoichiometric amount of the cation and no conversion is evident with those prepared with an excess. (Figure 6.6)

Unlike HPW based salts, no trace of butane was formed with the HSiW salts prepared with a 15% deficit of the cation. (Table 6.3) HSiW has a similar distribution of products that observed for HPW, with 62%, 32%, and 6% for *trans*-2-butene, *cis*-2-butene and 1-butene, respectively. The distribution of products shifts slightly for the three salts of HSiW with a decrease in the amount of *trans*-2-butene as the proportion of 1-butene and the *cis*-2-butene increase, resulting in a product distribution of 11%, 47%, and 42% for the AgSiW salts. The distribution of products is unaffected by the preparative stoichiometry in these salts. (Table 6.3) The TlSiW salts vary slightly from this product distribution with no 1-butene formed for the salt prepared with an excess of thallium while the analogous CsSiW salt, prepared with an excess of the cation, has a distribution similar to that of the parent acid. As with the 12-tungstophosphate salts, no change in the distribution of products with AgSiW is apparent with increasing time-on-stream while the cesium and thallium salts have an increased selectivity to *cis*-2-butene, at the expense of the *trans* isomer. (Table 6.4) The preparative cation:proton ratio used to form the salt appears to have a minimal effect on the product distribution despite changes in the activities of the salts.

The dehydration of 2-butanol with 12-molybdophosphoric acid shows an increase in activity with time-on-stream, with the conversion increasing from 40% at 5 minutes to 92% at 120 minutes. The three stoichiometries of the thallium salt, TIPMo, decrease in activity with higher times-on-stream. (Figure 6.7) The TIPMo salts prepared with either a deficit or stoichiometric amount of the cation result in higher activities than the parent acid for initial measurements at 5 minutes, while only the 0.85 salt maintains a similar level of conversion than the parent acid at higher times-on-stream. The decreased activity with an increase in the preparative cation:proton ratio is consistent with that observed previously with the HPW and HSiW salts in the dehydration of 2-butanol.

The product distribution of the TIPMo salts (Tables 6.5 and 6.6), appears to be

Table 6.3 - Distribution of products in dehydration of 2-butanol with salts of 12-tungstosilicic acid for initial measurements.^a

| Salt | Preparative Ratio ^b | Selectivity of Products | | | |
|---------------------------------------------------|--------------------------------|-------------------------|----------|----------------------|------------------------|
| | | Butane | 1-Butene | <i>cis</i> -2-Butene | <i>trans</i> -2-Butene |
| H ₄ SiW ₁₂ O ₄₀ | | 0 | 6 | 32 | 62 |
| Ag ₄ SiW ₁₂ O ₄₀ | 0.85 | 0 | 11 | 50 | 39 |
| | 1.00 | 0 | 11 | 47 | 42 |
| | 1.15 | 0 | 10 | 48 | 42 |
| Tl ₄ SiW ₁₂ O ₄₀ | 0.85 | 0 | 9 | 38 | 53 |
| | 1.00 | 0 | 11 | 54 | 35 |
| | 1.15 | 0 | 0 | 41 | 59 |
| Cs ₄ SiW ₁₂ O ₄₀ | 0.85 | 0 | 9 | 50 | 41 |
| | 1.00 | 0 | 10 | 54 | 36 |
| | 1.15 | 0 | 12 | 26 | 62 |

^a Time-on-stream of 5 minutes.

^b Cation:Proton ratio.

Table 6.4 - Distribution of products in dehydration of 2-butanol with salts of 12-tungstosilicic acid at higher time-on-stream.^a

| Salt | Preparative Ratio ^b | Selectivity of Products | | | |
|---------------------------------------------------|--------------------------------|-------------------------|----------|----------------------|------------------------|
| | | Butane | 1-Butene | <i>cis</i> -2-Butene | <i>trans</i> -2-Butene |
| H ₄ SiW ₁₂ O ₄₀ | | 0 | 8 | 32 | 60 |
| Ag ₄ SiW ₁₂ O ₄₀ | 0.85 | 0 | 9 | 49 | 42 |
| | 1.00 | 0 | 9 | 47 | 44 |
| | 1.15 | 0 | 8 | 48 | 44 |
| Tl ₄ SiW ₁₂ O ₄₀ | 0.85 | 0 | 10 | 55 | 35 |
| | 1.00 | 0 | 10 | 52 | 38 |
| | 1.15 | 0 | - | - | - |
| Cs ₄ SiW ₁₂ O ₄₀ | 0.85 | 0 | 9 | 56 | 35 |
| | 1.00 | 0 | 10 | 52 | 38 |
| | 1.15 | 0 | - | - | - |

^a Time-on-stream of 120 minutes.

^b Cation:Proton ratio.

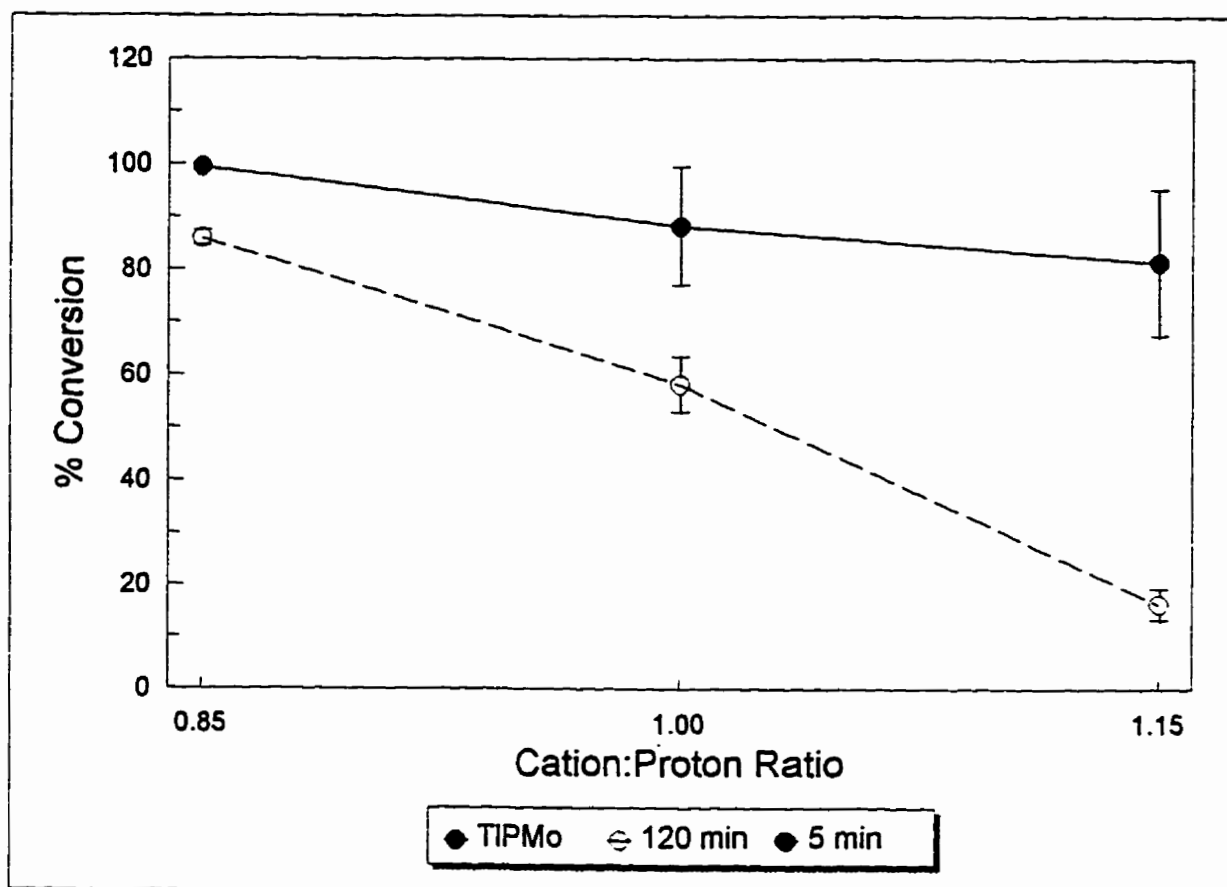


Figure 6.7 - Conversion of 2-butanol at 108 °C with $Tl_3PMo_{12}O_{40}$ salts.

affected by the composition of the salt at a time-on-stream of 5 minutes. As the cation:proton ratio increases, the selectivity to *cis*-2-butene increases, at the expense of the *trans* isomer, while the selectivity to 1-butene remains constant. At higher times-on-stream (Table 6.6), the selectivity for the two 2-butene isomers is approximately equal for the deficit salt. As the preparative stoichiometry is increased, the selectivity to the *cis*-2-butene increases while the 1-butene remains unchanged.

Table 6.5 - Distribution of products in dehydration of 2-butanol with salts of 12-molybdophosphoric acid for initial measurements.^a

| Salt | Preparative Ratio ^b | Selectivity of Products | | | |
|---------------------------------------------------|--------------------------------|-------------------------|----------|----------------------|------------------------|
| | | Butane | 1-Butene | <i>cis</i> -2-Butene | <i>trans</i> -2-Butene |
| H ₃ PMo ₁₂ O ₄₀ | | 0 | 9 | 33 | 58 |
| Tl ₃ PMo ₁₂ O ₄₀ | 0.85 | 0 | 8 | 30 | 62 |
| | 1.00 | 0 | 9 | 35 | 56 |
| | 1.15 | 0 | 9 | 58 | 33 |

^a Time-on-stream of 5 minutes.

^b Cation:Proton ratio.

Table 6.6 - Distribution of products in dehydration of 2-butanol with salts of 12-molybdophosphoric acid at higher time-on-stream.^a

| Salt | Preparative Ratio ^b | Selectivity of Products | | | |
|---------------------------------------------------|--------------------------------|-------------------------|----------|----------------------|------------------------|
| | | Butane | 1-Butene | <i>cis</i> -2-Butene | <i>trans</i> -2-Butene |
| H ₃ PMo ₁₂ O ₄₀ | | 0 | 8 | 36 | 56 |
| Tl ₃ PMo ₁₂ O ₄₀ | 0.85 | 0 | 10 | 46 | 44 |
| | 1.00 | 0 | 9 | 52 | 39 |
| | 1.15 | 0 | 10 | 54 | 36 |

^a Time-on-stream of 120 minutes.

^b Cation:Proton ratio.

6.3.3 Dehydration of 1-Butanol.

Dehydration of 1-butanol was carried out at 108 °C with identical reaction conditions as used with 2-butanol. In comparison to the dehydration of 2-butanol, the level of conversion for 1-butanol with HPW was slightly lower, calculated to be 78% at 5 minutes. For the dehydration of 1-butanol, only the 0.85 AgPW salt had a greater activity than that observed for the parent acid. (Figure 6.8) Both the silver and cesium salts show a decline in activity as the cation-to-proton ratio is increased. Of the three cation:proton ratios examined for the thallium salts, only the salt made with a deficit of the cation shows activity for the dehydration of 1-butanol. With increasing time-on-stream, the conversion with the pure acid decreases by half, to 34%, while the three stoichiometries of the silver salts show little deactivation. (Figure 6.8) The 0.85 TIPW salt maintains a similar level of conversion with increasing time-on-stream. However, the analogous cesium salt displays a decrease in activity, to a level slightly lower than the 0.85 TIPW salt. No activity was present for the stoichiometric and 1.15 TIPW and CsPW salts at higher times-on-stream.

Initial measurements at 5 minutes revealed that approximately equal amounts of the *cis* and *trans* isomers of 2-butene were produced by the acid as well as some butane, resulting in a product distribution of 46%, 47%, 4% and 3% for *trans*-2-butene, *cis*-2-butene, 1-butene and butane, respectively. (Table 6.7) The only other salt to produce butane was the 0.85 CsPW salt. The AgPW salts retained a similar product distribution as was apparent for the 2-butanol dehydration reactions, with little variation as the amount of the cation used to synthesize the salts was altered or time-on-stream increased. (Table 6.8) The 0.85 TIPW salt produced slightly more 1-butene at the expense of the *trans*-2-butene. The product distribution for the dehydration of the 1- and 2-butyl alcohols is more variable with the cation-to-proton ratio of the CsPW salts. It is of interest to note that the selectivity to 1-butene increases with the increase of the cation to proton ratio with the fresh catalyst for both alcohols, although it is more pronounced with 1-butanol (Table 6.7). The 0.85 CsPW salt no longer produces butane at higher times-on-stream. (Table 6.8)

The dehydration of 1-butanol by HSiW was lower than that of HPW, with

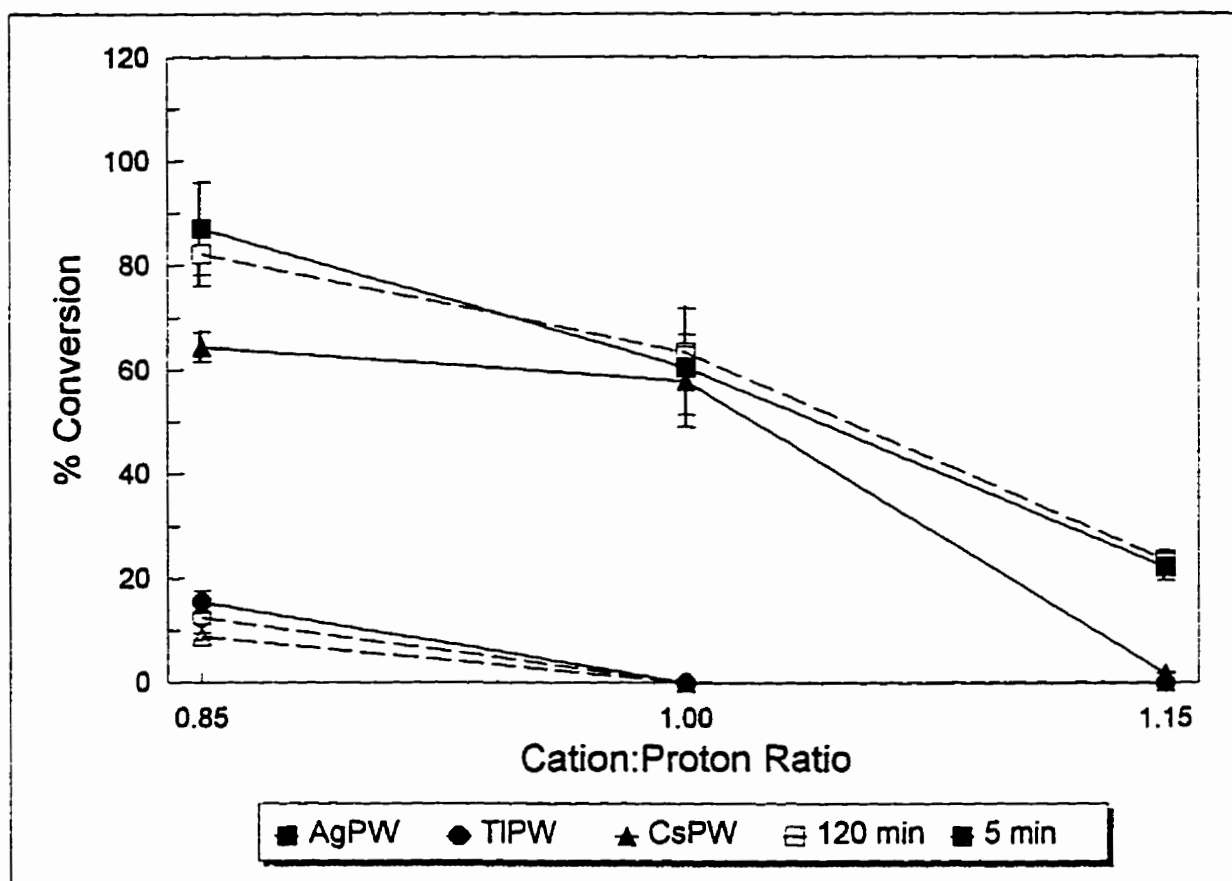


Figure 6.8 - Conversion of 1-butanol at 108 °C with salts of $H_3PW_{12}O_{40}$.

Table 6.7 - Distribution of products in dehydration of 1-butanol with salts of 12-tungstophosphoric acid for initial measurements.^a

| Salt | Preparative Ratio ^b | Selectivity of Products | | | |
|--------------------------------------------------|--------------------------------|-------------------------|----------|----------------------|------------------------|
| | | Butane | 1-Butene | <i>cis</i> -2-Butene | <i>trans</i> -2-Butene |
| H ₃ PW ₁₂ O ₄₀ | | 3 | 4 | 47 | 46 |
| Ag ₃ PW ₁₂ O ₄₀ | 0.85 | 0 | 8 | 28 | 64 |
| | 1.00 | 0 | 8 | 27 | 65 |
| | 1.15 | 0 | 10 | 26 | 64 |
| Tl ₃ PW ₁₂ O ₄₀ | 0.85 | 0 | 15 | 30 | 55 |
| | 1.00 | - | - | - | - |
| | 1.15 | - | - | - | - |
| Cs ₃ PW ₁₂ O ₄₀ | 0.85 | 6 | 33 | 25 | 36 |
| | 1.00 | 0 | 22 | 25 | 53 |
| | 1.15 | 0 | 100 | 0 | 0 |

^a Time-on-stream of 5 minutes.

^b Cation:Proton ratio.

Table 6.8 - Distribution of products in dehydration of 1-butanol with salts of 12-tungstophosphoric acid at higher time-on-stream.^a

| Salt | Preparative Ratio ^b | Selectivity of Products | | | |
|--------------------------------------------------|--------------------------------|-------------------------|----------|----------------------|------------------------|
| | | Butane | 1-Butene | <i>cis</i> -2-Butene | <i>trans</i> -2-Butene |
| H ₃ PW ₁₂ O ₄₀ | | 1 | 7 | 30 | 62 |
| Ag ₃ PW ₁₂ O ₄₀ | 0.85 | 0 | 8 | 28 | 64 |
| | 1.00 | 0 | 8 | 27 | 65 |
| | 1.15 | 0 | 10 | 26 | 64 |
| Tl ₃ PW ₁₂ O ₄₀ | 0.85 | 0 | 15 | 29 | 56 |
| | 1.00 | - | - | - | - |
| | 1.15 | - | - | - | - |
| Cs ₃ PW ₁₂ O ₄₀ | 0.85 | 0 | 19 | 33 | 48 |
| | 1.00 | - | - | - | - |
| | 1.15 | - | - | - | - |

^a Time-on-stream of 120 minutes.

^b Cation:Proton ratio.

activities of 34% and 46% at 5 and 120 minutes, respectively, for the former acid. All of the salts synthesized from HSiW had lower activities than the pure acid (Figure 6.9), and of all the salts examined, only the stoichiometric and excess CsSiW salts displayed any activities similar to the acid at 5 minutes. For the CsSiW salts, the conversion increases as the preparative ratio was increased, however this is short lived with only a relatively small amount of activity present at higher times-on-stream. The conversion by AgSiW and TlSiW showed little variation with changes in the preparative ratio.

HSiW maintains a distribution similar to that observed in previous reactions carried out with 2-butanol, with little change at higher times-on-stream. Tables 6.9 and 6.10 indicate that the salts of HSiW produce a larger fraction of 1-butene in comparison with that observed for the analogous HPW salts. 1-Butene appears to be the primary product at very low conversions. With increase in the preparative cation:proton ratio for the AgSiW salts, an increase in the selectivity to 1-butene is observed.

12-Molybdophosphoric acid has an initial level of conversion of 35% for 1-butanol. However, this dramatically decreases to 3% with increasing time-on-stream. As observed with 2-butanol reactions, the level of conversion decreases for the TIPMo salts as the cation:proton ratio is increased. (Figure 6.10) Similar to the pure acid, the level of activity drops dramatically with increasing time-on-stream, so that only the 0.85 salt displays any activity at 120 minutes. Tables 6.11 and 6.12 summarize the distribution of products for the thallium 12-molybdophosphate salts and HPMo. As observed with the HSiW salts, 1-butene is the primary product, although the selectivity decreases slightly with increasing time-on-stream.

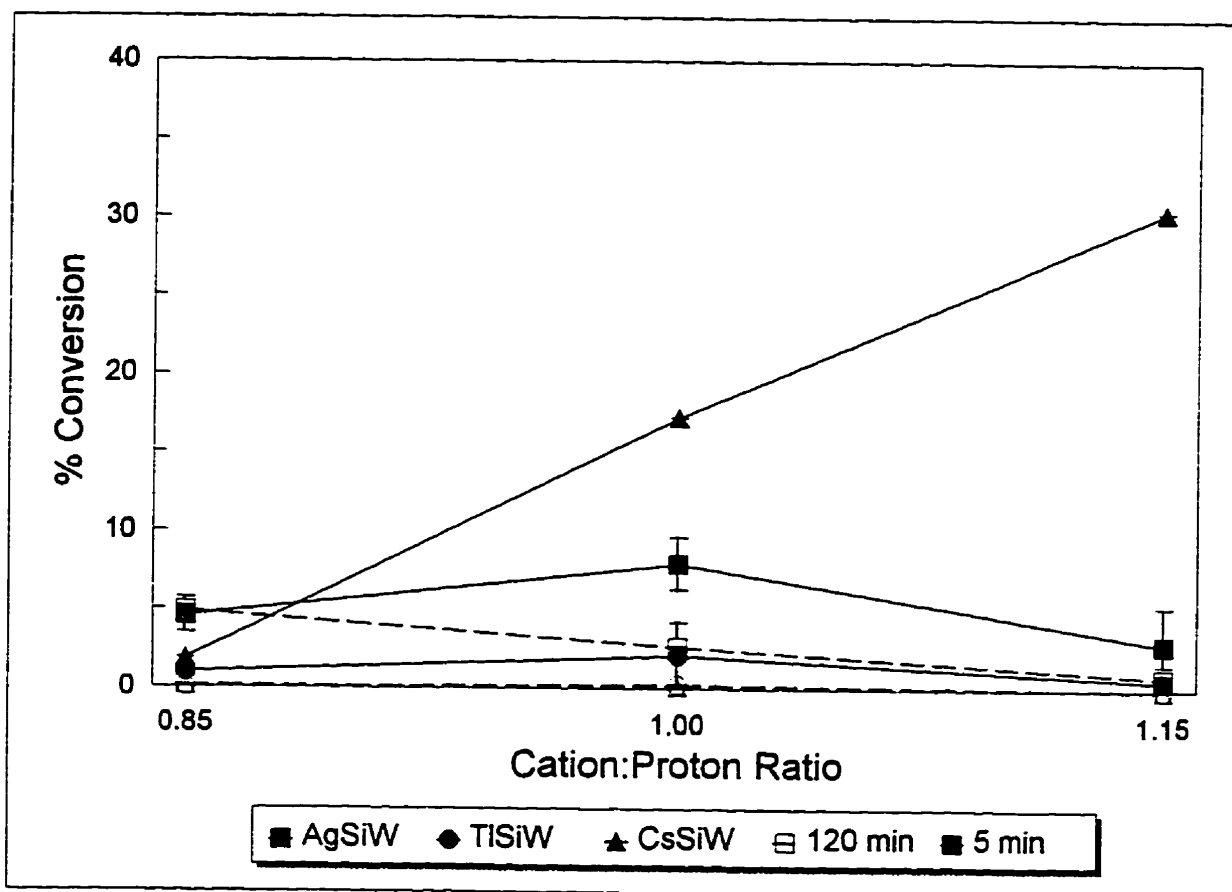


Figure 6.9 - Conversion of 1-butanol at 108 °C with salts of $H_4SiW_{12}O_{40}$.

Table 6.9 - Distribution of products in dehydration of 1-butanol with salts of 12-tungstosilicic acid for initial measurements.^a

| Salt | Preparative Ratio ^b | Selectivity of Products | | | |
|---------------------------------------------------|--------------------------------|-------------------------|----------|----------------------|------------------------|
| | | Butane | 1-Butene | <i>cis</i> -2-Butene | <i>trans</i> -2-Butene |
| H ₄ SiW ₁₂ O ₄₀ | | 2 | 8 | 28 | 62 |
| Ag ₄ SiW ₁₂ O ₄₀ | 0.85 | 0 | 18 | 32 | 50 |
| | 1.00 | 8 | 57 | 11 | 24 |
| | 1.15 | 0 | 94 | 2 | 4 |
| Tl ₄ SiW ₁₂ O ₄₀ | 0.85 | 0 | 100 | 0 | 0 |
| | 1.00 | 0 | 100 | 0 | 0 |
| | 1.15 | 0 | 100 | 0 | 0 |
| Cs ₄ SiW ₁₂ O ₄₀ | 0.85 | 0 | 100 | 0 | 0 |
| | 1.00 | 7 | 93 | 0 | 0 |
| | 1.15 | 46 | 14 | 0 | 40 |

^a Time-on-stream of 5 minutes.

^b Cation:Proton ratio.

Table 6.10 - Distribution of products in dehydration of 1-butanol with salts of 12-tungstosilicic acid at higher time-on-stream.^a

| Salt | Preparative Ratio ^b | Selectivity of Products | | | |
|---------------------------------------------------|--------------------------------|-------------------------|----------|----------------------|------------------------|
| | | Butane | 1-Butene | <i>cis</i> -2-Butene | <i>trans</i> -2-Butene |
| H ₄ SiW ₁₂ O ₄₀ | | 0 | 7 | 26 | 67 |
| Ag ₄ SiW ₁₂ O ₄₀ | 0.85 | 0 | 20 | 33 | 47 |
| | 1.00 | 20 | 16 | 25 | 39 |
| | 1.15 | 17 | 31 | 17 | 35 |
| Tl ₄ SiW ₁₂ O ₄₀ | 0.85 | 0 | 100 | 0 | 0 |
| | 1.00 | 0 | 100 | 0 | 0 |
| | 1.15 | 0 | 100 | 0 | 0 |
| Cs ₄ SiW ₁₂ O ₄₀ | 0.85 | 0 | 100 | 0 | 0 |
| | 1.00 | 0 | 100 | 0 | 0 |
| | 1.15 | 0 | - | - | - |

^a Time-on-stream of 120 minutes.

^b Cation:Proton ratio.

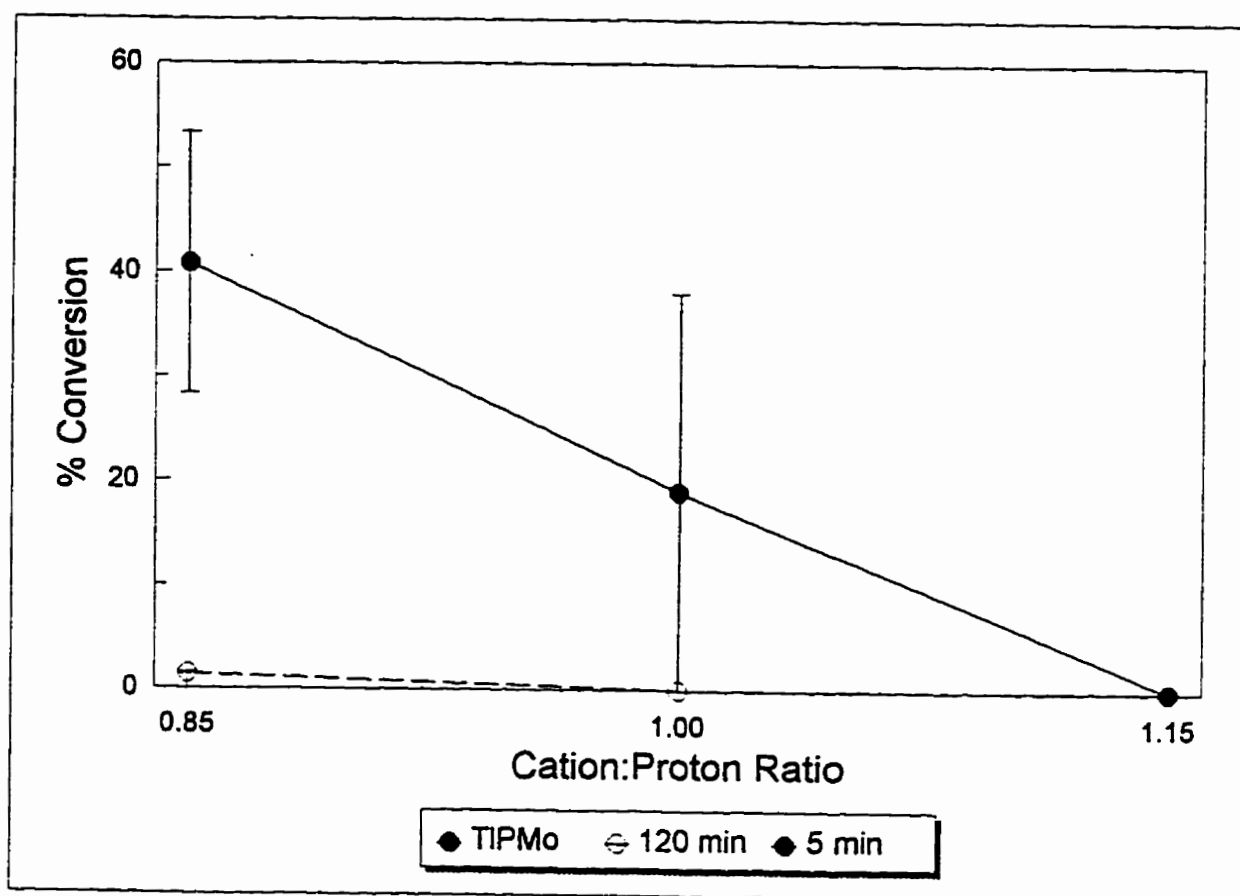


Figure 6.10 - Conversion of 1-butanol at 108 °C with $Tl_3PMo_{12}O_{40}$ salts.

Table 6.11 - Distribution of products in dehydration of 1-butanol with salts of 12-molybdophosphoric acid for initial measurements.^a

| Salt | Preparative Ratio ^b | Selectivity of Products | | | |
|---------------------------------------------------|--------------------------------|-------------------------|----------|----------------------|------------------------|
| | | Butane | 1-Butene | <i>cis</i> -2-Butene | <i>trans</i> -2-Butene |
| H ₃ PMo ₁₂ O ₄₀ | | 0 | 31 | 26 | 43 |
| Tl ₃ PMo ₁₂ O ₄₀ | 0.85 | 0 | 48 | 20 | 32 |
| | 1.00 | 0 | 36 | 12 | 52 |
| | 1.15 | - | - | - | - |

^a Time-on-stream of 5 minutes.^b Cation:Proton ratio.**Table 6.12** - Distribution of products in dehydration of 1-butanol with salts of 12-molybdophosphoric acid at higher time-on-stream.^a

| Salt | Preparative Ratio ^b | Selectivity of Products | | | |
|---------------------------------------------------|--------------------------------|-------------------------|----------|----------------------|------------------------|
| | | Butane | 1-Butene | <i>cis</i> -2-Butene | <i>trans</i> -2-Butene |
| H ₃ PMo ₁₂ O ₄₀ | | 0 | 20 | 19 | 61 |
| Tl ₃ PMo ₁₂ O ₄₀ | 0.85 | 0 | 35 | 15 | 50 |
| | 1.00 | - | - | - | - |
| | 1.15 | - | - | - | - |

^a Time-on-stream of 120 minutes.^b Cation:Proton ratio.

6.4 Discussion

As mentioned in the introduction to this chapter, Section 5.3.1 discussed the experimental results characterizing the acidity of the salts synthesized with the cesium, silver and thallium cations. ¹H MAS NMR provided the first indication that weaker acidity was present in the salts: the chemical shift of the residual protons in the salt is located further upfield of those reported for the parent acid. (Table 5.1) This resonance

continues to move upfield as the preparative cation:proton ratio is increased. A number of arguments have been presented in support of the suggestion that the chemical shift can serve as a measure for acid strength²⁸ and it is generally believed that an increase in the proton chemical shift is an indication of the increase in the Brønsted acid strength.^{29,30} The intensity of the resolved line in the ¹H MAS NMR spectrum is directly proportional to the concentration of the Brønsted acid sites.³⁰ From these results, it is apparent that the decrease in the peak area and chemical shift as the cation:proton ratio increases is indicative of a decrease in both the number and acid strength of the residual protons as compared to the 12-heteropoly acids. The absolute integration of the peaks provided relative amounts of protons residing in the salt. (Tables 5.2 and 5.3)

Temperature programmed desorption of ammonia provided a distribution of acid strengths present in each of the salts examined. (Tables 5.4 and 5.5) For the silver salts of HPW and HSiW, those synthesized with a 15% deficit or excess of the cation have similar distributions in acid strengths. It was also of interest to note that the quantity of ammonia adsorbed by the thallium and cesium salts is approximately an order of magnitude less than that adsorbed by the silver salts. This is consistent with the greater number of protons present in the silver salts than either of the cesium or thallium salts of the same acid. For the remaining thallium and cesium salts, the distribution of acid strength shifts with the number of sites of higher acidity decreasing as the relative amounts of the cations are increased. Although TPD experiments with ammonia cannot differentiate between Lewis and Brønsted acid sites, previous photoacoustic FTIR experiments have shown that the acidity of 12-tungstophosphoric acid can be attributed to Brønsted acid sites with little or no evidence of Lewis acid sites.^{5(a)} It is expected that the derivatives prepared in this work are similar in this respect.

The dehydration of *tert*-butanol, 2-butanol and 1-butanol is expected to form the tertiary, secondary, and primary butyl carbenium ions, respectively. Since the stability of these carbocations decreases in the order tertiary > secondary > primary, the strength of the acid sites required to dehydrate the alcohols should increase for the same series. The dehydration of butyl alcohols can occur through monomolecular and/or bimolecular mechanisms. However, for a bimolecular process, the formation of dibutyl ether is

expected.¹⁷ Studies by Shi and Davis with alumina catalysts revealed that the formation of ethers from secondary alcohols is dependent on the reaction conditions.¹⁸ In extensive studies of the dehydration of butyl alcohols with the HZSM-5 zeolite, Kamaraev¹⁷⁽ⁱ⁾ determined that the formation of butene and ether products takes place via one intermediate, which is a highly reactive surface alkoxide species, similar to that formed during the conversion of methanol to hydrocarbons. The formation of ether depends on the concentration of the alcohol in the surrounding neighbourhood of the alkoxide. In the dehydration of the three alcohols with the cesium(I), silver(I) and thallium(I) 12-heteropoly salts only C₄ products were formed with no evidence for the formation of dibutyl ether or a variation on the chain length of the hydrocarbons. This suggests that the process is monomolecular at least under the conditions employed in the present work.

Dehydration of *tert*-butanol was a facile process for all of the salts investigated. The only product formed was *iso*-butene, with the % conversion decreasing as the cation-to-acid ratio increased. (Figures 6.2 to 6.4) This correlates well with the ¹H MAS NMR data which show that the total number of acid sites available for the reaction is decreasing with the increased substitution by the cation. However, with only a single product formed, there is no indication as to the variation of acid strengths as the amount of cation is increased. The salts of HSiW generally had lower activities than the analogous HPW salts, consistent with the sequence of acidic strengths for the parent acids (HPW > HSiW >> HPMo) determined by Extended Hückel calculations.³¹ 12-Molybdophosphoric acid also remained consistent with this ordering, with only a minimal level of activity present. However, substitution of the protons by thallium greatly enhanced the capability of the salt so that the deficit and stoichiometric TIPMo salts achieved the highest conversions of all of the salts examined.

Similar to observations with *tert*-butanol, a decrease in activity with increasing cation content in the salt or increasing time-on-stream was observed for the dehydration of 2-butanol. The only exception to this is the relatively stable level of conversion maintained by the AgPW salts. For these reactions, HPW and HSiW display little deactivation with higher times-on-stream. With the exception of the initial measurement of the 0.85 salts, the HSiW salts generally possessed a lower level of conversion than

noted for the analogous HPW salts. At higher times-on-stream, the stoichiometric cesium and thallium salts had relatively small levels of conversion while no activity was observed for the 1.15 salts. The TIPMo salts displayed comparable levels of activity to the AgPW salts during initial measurements.

The dehydration of 1- and 2-butanol required a higher temperature than that used for the dehydration of *tert*-butanol. The formation of the products is believed to follow the mechanism, depicted in Figure 6.11, similar to that postulated for the isomerization of 1-butene.³² (Figure 5.1) However, the dehydration of 1-butanol would be expected to form the primary butyl carbenium ion, which would readily convert to the more stable secondary butyl carbenium ion. The secondary butyl carbenium ion would result from the dehydration of 2-butanol. As a result, the dehydration of 1-butanol should require stronger acid sites to form the primary carbocation, so a decrease in the conversion is expected when compared to the dehydration of 2-butanol carried out at an identical reaction temperature. While it is possible for the dehydration of either or both 1- and 2-butanol to follow a mechanism dissimilar from that discussed above, it is assumed the carbenium ion mechanism is followed in the present system. The stoichiometric and 1.15 TIPW salts lack sites strong enough to facilitate the dehydration of 1-butanol and the analogous cesium salts are deactivated after the initial sampling at 5 minutes. This is consistent with the decrease in the proportion of strong Brønsted acid sites for the thallium and cesium salts as the preparative cation:proton ratio is increased. In contrast, all three AgPW salts are capable of dehydrating 1-butanol. The observation that the stoichiometric TIPW salt had little or no activity in the dehydration of 1-butanol at 108 °C but was capable of dehydrating 2-butanol under the same conditions is consistent with the expectation that stronger acid sites are required to form the primary butyl carbenium ion.

Although the HSiW salts consistently displayed lower levels of conversion than the analogous HPW salts in the dehydration of each of the three alcohols, only the 1.15 CsSiW salt does not have the capability to dehydrate 1-butanol. Granted, the conversions for all of the salts were less than 10%, with the exception of the initial measurements of the stoichiometric and excess CsSiW salts. The 1.15 TIPMo salt was also unable to dehydrate 1-butanol, while this salt was active with 2-butanol. At higher times-on-stream,

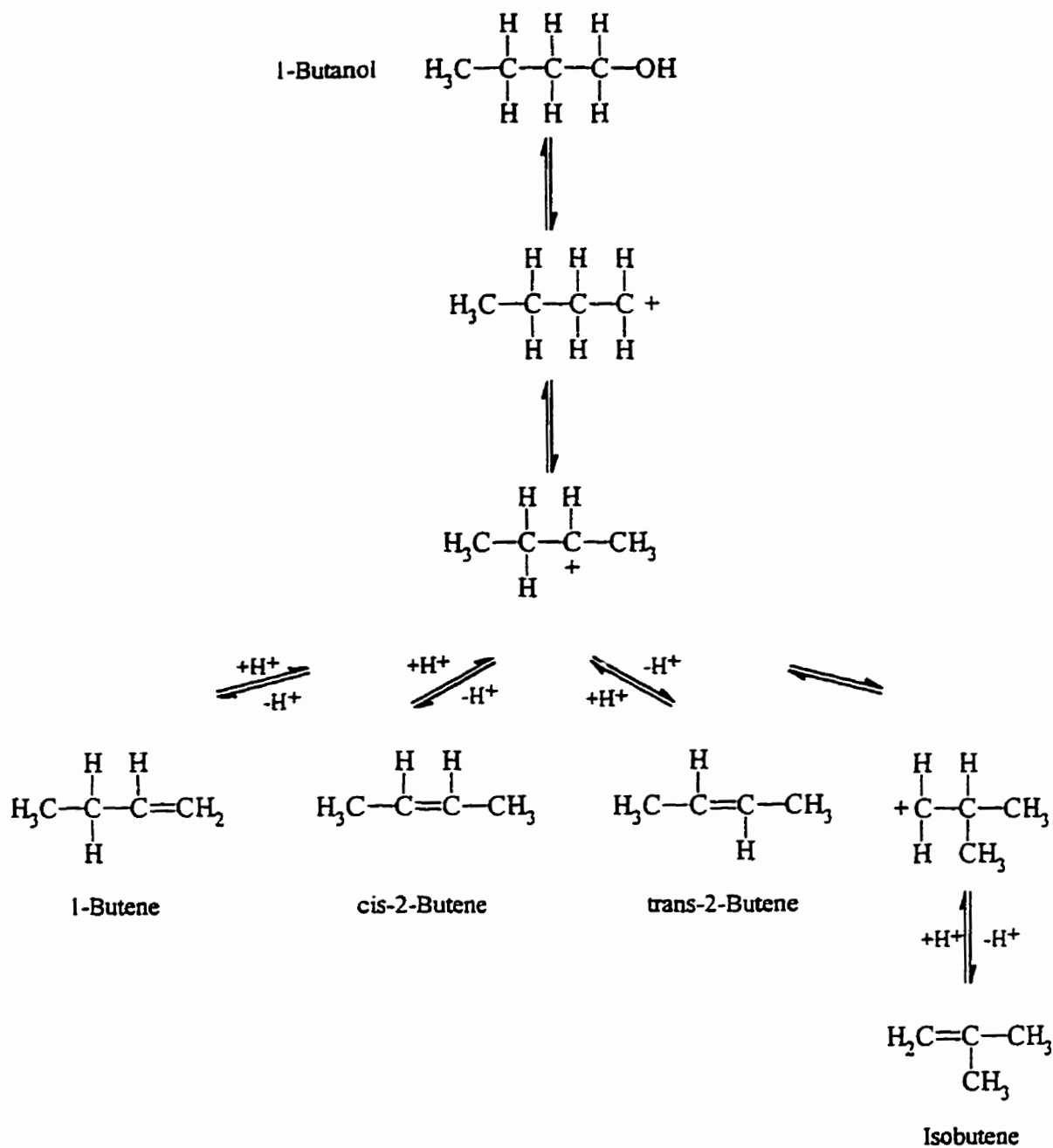


Figure 6.11 - Mechanistic scheme for the dehydration of 1-butanol.

little or no conversion of 1-butanol occurred on the three TiPMo salts examined.

None of the catalysts investigated possessed sites of sufficient strength to facilitate the skeletal isomerization required to form *iso*-butene during the dehydration of the primary and secondary butyl alcohols. This is not surprising since both the ^1H MAS NMR and TPD experiments with ammonia (Section 5.3.1) revealed that there is a decrease in the proportion of strong Brønsted acid sites with the increased substitution of cations in comparison to the pure acid. Although the dehydration of 1-butanol at 250 °C by 12-tungstophosphoric acid³³ failed to produce *iso*-butene, supported HPW was capable of forming *iso*-butene during the isomerization of 1-butene at these temperatures.³² ^1H MAS NMR studies of the supported acid revealed a downfield shift of the proton resonance, to a larger chemical shift, from that reported for the unsupported HPW, indicating an increase in acid strength when the acid is supported.³² It has also been reported that the pore structure of the H-ZSM-5 zeolites kinetically favours the formation of linear rather than branched C_4 carbenium ions when dehydrating butanols.¹⁷⁽ⁱ⁾ The micropore structure of the 12-heteropoly oxometalate salts may play a similar role.

With the supported HPW, there was also evidence of a bimolecular process in the isomerization of 1-butene under the reaction conditions employed.³² To facilitate a bimolecular process in the dehydration of 1- or 2-butanol, two molecules of the alcohol must be adsorbed onto neighbouring sites. For this to be possible, a minimal partial pressure of the butyl alcohol would be required to ensure significant coverage of the catalyst surface.^{18,20(b)} It is possible that under the current reaction conditions (saturation of the helium gas stream at 25 °C) the partial pressure of the alcohol may be below this threshold, promoting the monomolecular mechanism and absence of dibutyl ether.

The equilibrium distribution of 1-butene:*cis*-2-butene:*trans*-2-butene is 9.3 : 29.8 : 60.9 at 150 °C.^{17(g),(i)} The dehydration of 2-butanol at 108 °C by HPW and HSiW achieve similar distributions of products with slightly less 1-butene formed ($\leq 8\%$), while HPMo has an increased selectivity to *cis*-2-butene, at the expense of the *trans* isomer. (Tables 6.7 to 6.9) Trace amounts of butane are produced in the dehydration of 1-butanol by HPW and HSiW with the three butene products having distributions similar to that at

equilibrium. In contrast, HPMo produces significantly more 1-butene (> 20%). (Tables 6.10 to 6.12) These distributions did not appear to be altered with increasing time-on-stream. Dehydration of 1- and 2-butanols by cesium, silver and thallium 12-heteropoly salts increases the selectivity to 1-butene. Although this increase is relatively small for the dehydration reactions with 2-butanol, the difference becomes more significant for 1-butanol, where in some cases, 1-butene is the only product at very low levels of conversion. Generally, the dehydration of an alcohol requires weaker acidic sites than those required for double bond isomerization of an olefin.²⁵ On deactivation of relatively strong acid centres in an alumina membrane the overall conversion of 1-butanol was partially reduced but the selectivity to 1-butene was significantly increased.

As discussed with the isomerization of 1-butene (Section 5.4), formation of the *cis* and *trans* isomers of 2-butene occurs through the secondary butyl carbocation which is considered to be a metastable species, not equivalent to a transition state.³³ A ratio of 1 is expected for the *cis:trans* isomers from this carbocation since the activation energy to form either is identical, although the *trans* isomer is slightly more thermodynamically stable. For 1-butene isomerization, this ratio is expected when the reaction is kinetically limited and the intermediate secondary butyl carbenium ion is considered to be "free".³⁴ However, as demonstrated in the equilibrium distribution at 150 °C, the *trans* isomer is preferentially formed. The AgPW salts, HSiW and HPW exhibit similar product distributions for the dehydration of the primary and secondary butyl alcohols to that which is observed for the isomerization of 1-butene at 100 °C. (Section 5.3.2) The stoichiometric and excess salts of CsPW, TIPMo, and all of the HSiW salts tend to approach a *cis/trans* ratio of 1 for the 2-butanol reactions and the 1.15 TIPW salt did not produce 1-butene. In isomerization reactions carried out with the pure heteropoly acids, it was concluded that the formation of the *cis* isomer is favourable for catalysts which are weakly acidic.³⁶ This had previously been noted with other catalysts,³⁷ although numerical values associated with the *cis:trans* ratio are largely dependent upon the nature of the acid sites (Lewis or Brønsted) and the resulting mechanism. As mentioned earlier, the distribution of products by salts other than AgPW for the 1-butanol reactions differed

from equilibrium values with the tendency to increase in the selectivity towards 1-butene at a cost of *trans*-2-butene. This was observed with CsPW as the cation:proton ratio is increased and with the TlSiW salts forming only 1-butene.

For the dehydration of the butyl alcohols, there is a notable decrease in the catalytic activity, although not necessarily the selectivity to the products, from the initial sample of the fresh catalytic surface to the deactivated catalyst in as little as 15 minutes after exposure of the catalyst to the reactant mixture. It is believed that this decrease in conversion results from the relatively slower rate of regeneration of the Brønsted acid sites in comparison with the rate of formation of the olefinic products on a release of a proton. It should also be noted that mass balances of less than 100% are common in the present work, due to the retention of the alcohols and/or their decomposition products on the catalyst.

As evident from the nitrogen adsorption-desorption isotherms, ¹H MAS NMR and ammonia TPD, partial substitution of the protons by monovalent cations of cesium, silver and thallium affects three characteristics of the salts: a microporous structure is created, the number of Brønsted acid sites is decreased, and the distribution of acid strengths is shifted. As noted in Chapter 2, variations in the cation:proton ratios have significant effects on the pore volumes but little or no influence on the mean micropore radius, as would be expected from the hypothesis of the source of the pore structure advanced.^{14-16,35} Not surprisingly, however, the number of residual protons and the chemical environment in which they reside are altered by changes in this ratio. In examining the catalytic properties of the salt synthesized, it is important to determine which of these variables has the most significant effect in the dehydration of butyl alcohols.

It can be concluded that four characteristics of the salts have an effect on the conversions of butanols: (1) the nature of the cation, (2) the morphological properties of the catalysts, (3) the number of protons, and (4) the distribution of acid strengths. For a given cation, the preparative cation:proton ratio determines the last three. To elucidate the effect of the cations on the residual protons the conversions were divided by the appropriate surface areas and number of protons. (Tables 6.13 and 6.14) These values of conversions/[m²][H⁺] should minimize or eliminate the influence of the numbers of

Table 6.13 - Conversions of the 1-, 2- and *tert*-butanols with salts of $H_3PW_{12}O_{40}$.

| Salt | Preparative Stoichiometry | Conversion ^{ab} / [(m ²)(H ⁺)] | | |
|--------------------------------------------------|---------------------------|-----------------------------------------------------------------|------------------------|-----------------------------------|
| | | 1-Butanol ^c | 2-Butanol ^c | <i>tert</i> -Butanol ^d |
| Ag ₃ PW ₁₂ O ₄₀ | 0.85 | 2.1 | 8.7 | 10.8 |
| | 1.00 | 2.1 | 8.4 | 12.6 |
| | 1.15 | 0.9 | 11.6 | 10.0 |
| Tl ₃ PW ₁₂ O ₄₀ | 0.85 | 1.4 | 21.1 | 25.8 |
| | 1.00 | 0 | 42.2 | 28.1 |
| | 1.15 | 0 | 1.4 | 31.9 |
| Cs ₃ PW ₁₂ O ₄₀ | 0.85 | 4.2 | 28.9 | 33.2 |
| | 1.00 | 0.8 | 38.2 | 35.5 |
| | 1.15 | 0.6 | 11.6 | 51.9 |

^a For measurements taken at 5 minutes.

^b Moles of products multiplied by (1 x 10²⁸).

^c Reaction temperature of 108 °C.

^d Reaction temperature of 46 °C.

protons and morphological differences among the catalysts on the observed conversions.

As would be expected, assuming a carbocation mechanism, the conversions of *tert*-butanol with the HPW derived salts (Table 6.13) are generally higher than those for 2-butanol and, in turn, those for the latter are higher than for 1-butanol for each cation and stoichiometry, although the reaction temperature for *tert*-butanol is lower than that employed with the remaining alcohols. This trend is generally maintained for the HSiW derived salts and TIPMo, although AgSiW is a notable exception. (Table 6.14) Further, the conversions of a given alcohol decrease, in general, with the cation in the order Ag < Tl < Cs, although both TIPW and TlSiW are notable exceptions. Finally, significant changes are observed, for a given cation, as the preparative stoichiometry is altered. Since the acidic strength required to generate the carbocations increase in the order *tert*-

Table 6.14 - Conversions of the 1-, 2- and *tert*-butanols with salts of $\text{H}_4\text{SiW}_{12}\text{O}_{40}$ and $\text{Tl}_3\text{PMo}_{12}\text{O}_{40}$ salts.

| Salt | Preparative Stoichiometry | Conversion ^{ab} / $[(\text{m}^2)(\text{H}^+)]$ | | |
|-------------------------------------------|---------------------------|---------------------------------------------------------|------------------------|-----------------------------------|
| | | 1-Butanol ^c | 2-Butanol ^c | <i>tert</i> -Butanol ^d |
| $\text{Ag}_4\text{SiW}_{12}\text{O}_{40}$ | 0.85 | 0.2 | 5.9 | 0.2 |
| | 1.00 | 0.3 | 8.5 | 0.8 |
| | 1.15 | 0.3 | 7.1 | 1.0 |
| $\text{Tl}_4\text{SiW}_{12}\text{O}_{40}$ | 0.85 | 0.04 | 11.1 | 11.0 |
| | 1.00 | 0.08 | 4.5 | 19.0 |
| | 1.15 | 0.1 | 0.3 | 31.2 |
| $\text{Cs}_4\text{SiW}_{12}\text{O}_{40}$ | 0.85 | 0.08 | 7.0 | 6.2 |
| | 1.00 | 0.3 | 1.3 | 4.9 |
| | 1.15 | 2.3 | 0.2 | 3.6 |
| $\text{Tl}_3\text{PMo}_{12}\text{O}_{40}$ | 0.85 | 0.6 | 15.8 | 36.0 |
| | 1.00 | 0.3 | 53.7 | 39.1 |
| | 1.15 | 0 | 34.7 | 32.8 |

^a For measurements taken at 5 minutes.

^b Moles of products multiplied by (1×10^{28}) .

^c Reaction temperature of 108 °C.

^d Reaction temperature of 46 °C.

2-, 1-butanol it would be expected that the most significant differences in the conversions/ $[\text{m}^2][\text{H}^+]$ would be found with 1-butanol. However, in general for the HPW and HSiW salts, the conversion decreases, for a given cation and alcohol, as the preparative stoichiometry increases, although some exceptions are evident. Cesium is the largest cation examined. The decreased activity for the stoichiometric and excess CsSiW salts may be attributed to the crowding of the structure with four cations required to balance the charge of the $\text{SiW}_{12}\text{O}_{40}^{4-}$ anion, which may result in limiting the mobility of residual protons present in the solid. It should be noted that the powder XRD patterns

could be indexed according to the $Pn3m$ space group for all three stoichiometries of the CsSiW salts. Comparison of the TIPMo salts with the analogous TIPW salts reveals that the molybdenum-containing salts have a higher level of conversion although the HPMo acid is usually considered weaker than HPW. However, as seen with *tert*-butanol, thallium appears to stabilize the Keggin anion and TIPMo also has a larger fraction of intermediate strength acid sites than the analogous TIPW salts, indicated by the ammonia TPD.

Since the separation between the ^1H chemical shift in AgPW and that in HPW is larger than those with the remaining cations and the concentration of strong acid sites is the smallest in the former it would be anticipated that the conversions would generally be the smallest with AgPW regardless of the alcohol. Further, in view of the relatively large number of residual protons in the silver salts, regardless of the stoichiometry, the perturbation effect of cations on the protons would be expected to be diminished.

It is clear that the nature of the cation and anion as well as the preparative stoichiometry have a profound effect on the resulting salts, in particular both the morphological and the acid-based catalytic properties, the latter as evidenced from the results of ^1H MAS NMR, NH_3 TPD, and butanol conversion measurements. For a given cation, changes in the preparative stoichiometry alter the relative numbers of cations and protons with consequent perturbations of the distribution of acidic strengths and catalytic activities in the reactions of butanols while similar effects also result from changes in the nature of the cations.

The acidic strengths of the heteropoly acids are related to the mobility of the protons which is dependent, at least in part, upon the magnitude of the negative charge of the adjacent terminal oxygen atoms of the heteropoly anion. Earlier calculations³¹ have suggested that the coulombic binding of the proton will increase with the charge on these oxygen atoms and concomitantly the protonic mobility and the acidity will decrease. The introduction of cations larger than protons apparently reduces the mobility of the remaining protons. This effect may result from a number of factors. The larger cations may perturb the electron densities of the anions and in doing so alter the magnitude of the charge on the terminal oxygen atoms. It also may be speculated that the large cations

actually impede the movement of the protons as a result of their size and repulsive interactions. In this regard it is noteworthy that the charge densities increase in the order $\text{Cs}^+ < \text{Tl}^+ < \text{Ag}^+$ which is in approximate agreement with the trends seen for the NH_3 TPD, ^1H MAS NMR, and butanol conversion results. While such comments are evidently speculative, direct evidence of the influence of the larger cations on the acidic properties of the heteropoly acids has been provided and hence direct and/or indirect interactions between the protons and larger cations have been shown to exist.

6.5 References

1. C.D. Chang and A.J. Silvestri. *J. Catal.*, **47**, 249 (1977).
2. S.M. Csicsery. *Pure Appl. Chem.*, **58**, 841 (1986).
3. C.D. Chang. *Catal. Rev.-Sci. Eng.*, **25**, 1 (1983).
4. C.D. Chang in, "Perspectives in Molecular Sieve Science." (W.H. Frank and T.E. Whyte Jr., Eds) ACS Press: Washington, DC, 1988, p. 596.
5. (a) J.G. Highfield and J.B. Moffat. *J. Catal.*, **88**, 177 (1984).
(b) J.G. Highfield and J.B. Moffat. *J. Catal.*, **89**, 185 (1984).
(c) J.G. Highfield and J.B. Moffat. *J. Catal.*, **95**, 108 (1984).
6. J.B. Moffat. *J. Mol. Catal.*, **52**, 169 (1989).
7. (a) H. Hayashi and J.B. Moffat. *J. Catal.*, **77**, 473 (1982).
(b) H. Hayashi and J.B. Moffat. *J. Catal.*, **81**, 61 (1983).
(c) H. Hayashi and J.B. Moffat. *J. Catal.*, **83**, 192 (1983).
(d) J.G. Highfield and J.B. Moffat. *J. Catal.*, **95**, 108 (1985).
(e) J.G. Highfield and J.B. Moffat. *J. Catal.*, **98**, 245 (1986).
(f) J.B. Moffat. *Rev. Chem. Intermed.*, **8**, 1 (1987).
8. (a) Y. Ono; T. Baba; J. Sakai; T. Keii. *J. Chem. Soc. Chem. Commun.*, 400 (1981).
(b) Y. Ono and T. Mori. *J. Chem. Soc. Faraday Trans. I*, **77**, 2209 (1981).
(c) T. Baba; J. Sakai; Y. Ono. *Bull. Chem. Soc. Jpn.*, **55**, 2633 (1982).
(d) T. Baba; H. Watanabe; Y. Ono. *J. Phys. Chem.*, **87**, 2406 (1983).
(e) T. Baba and Y. Ono. *Appl. Catal.* **8**, 315 (1983).
9. A. Kasai; T. Okuhara; M. Misono; Y. Yoneda. *Chem. Lett.*, 449 (1981).
10. (a) H. Ehwald; W. Fiebig; H.-G. Jerschke; G. Lischke; B. Parlitz; E. Schreier; G. Öhlmann. *Appl. Catal.*, **34**, 13 (1987).
(b) H. Ehwald; W. Fiebig; H.-G. Jerschke; G. Lischke; B. Parlitz; P. Reich; G. Öhlmann. *Appl. Catal.*, **34**, 23 (1987).
11. Z. Qinwei and D. Jingfa. *J. Catal.*, **116**, 298 (1989).
12. (a) M. Misono. *Catal. Rev. - Sci. Eng.*, **29**, 269 (1987).
(b) M. Misono. *Catal. Rev. - Sci. Eng.*, **30**, 339 (1988).
13. W.E Farneth; R.H. Stanley; P.J. Domaille; R.D. Farlee. *J. Amer. Chem. Soc.*, **109**, 4018 (1987).

14. J.B. McMonagle and J.B. Moffat. *J. Colloid Interface Sci.*, **101**, 479 (1984).
15. D.B. Taylor; J.B. McMonagle; J.B. Moffat. *J. Colloid Interface Sci.*, **108**, 278 (1985).
16. G.B. McGarvey and J.B. Moffat. *J. Colloid Interface Sci.*, **125**, 51 (1988).
17. (a) M.A. Makarova; C. Williams; J.M. Thomas; K.I. Zamaraev. *Catal. Lett.*, **4**, 261 (1990).
(b) M.A. Makarova; C. Williams; V.N. Romannikov; K.I. Zamaraev; J.M. Thomas. *J. Chem. Soc. Faraday Trans.*, **86**, 581 (1990).
(c) C. Williams; M.A. Makarova; L.V. Malysheva; E.A. Paukshtis; J.M. Thomas; K.I. Zamaraev. *J. Chem. Soc. Faraday Trans.*, **86**, 3473 (1990).
(d) C. Williams; M.A. Makarova; L.V. Malysheva; E.A. Paukshtis; E.P. Talsi; J.M. Thomas; K.I. Zamaraev. *J. Catal.*, **127**, 377 (1991).
(e) A.G. Stepanov; V.N. Romannikov; K.I. Zamaraev. *Catal. Lett.*, **13**, 395 (1992).
(f) A.G. Stepanov; V.N. Romannikov; K.I. Zamaraev. *Catal. Lett.*, **13**, 407 (1992).
(g) A.G. Stepanov; A.G. Maryasov; V.N. Romannikov; K.I. Zamaraev. *Magn. Res. Chem.*, **32**, 16 (1994).
(h) M.A. Makarova; C. Williams; K.I. Zamaraev; J.M. Thomas. *J. Chem. Soc. Faraday Trans.*, **90**, 2147 (1994).
(i) M.A. Makarova; E.A. Paukshtis; J.M. Thomas; C. Williams; K.I. Zamaraev. *J. Catal.*, **149**, 36 (1994).
(j) K.I. Zamaraev and J.M. Thomas, in "Advances in Catalysis" (D.D Eley; W.O. Haag; B. Gates, Eds.) Academic Press Inc.: San Diego, California, 1996, Vol 41 p.335.
18. B. Shi and B.H. Davis. *J. Catal.*, **157**, 359 (1995).
19. E.M. Gaigneaux; P.E. Tsiakaras; D. Herla; L. Ghene; P. Ruiz; B. Delmon. *Catal. Today*, **33**, 151 (1997).
20. (a) P. Berteau; S. Ceckiewicz; B. Delmon. *Appl. Catal.*, **31**, 1 (1987).
(b) P. Berteau and B. Delmon. *Catal. Today*, **5**, 121 (1989).
21. P. Berteau; B. Delmon; J.-L. Dallons; A. Van Gysel. *Appl. Catal.*, **70**, 307 (1991).
22. F.M. Bautista and B. Delmon. *Appl. Catal.*, **A130**, 47 (1995).
23. Z.X. Cheng and V. Ponc. *Catal. Lett.*, **27**, 113 (1994).
24. K. Hashimoto; Y. Matsumura; M. Fukuchi; Y. Kera. *Catal. Lett.*, **19**, 375 (1993).

25. M. Lu; G. Xiong; H. Zhao; W. Cui; J. Gu; H. Bauser. *Catal. Today*, **25**, 339 (1995).
26. K.C. Pratt, in "Catalysis: Science and Technology"; J.R. Anderson and M. Boudart, Eds.; Springer-Verlag: Berlin, 1981, p.173.
27. M.C. White. "Heterogeneous Catalysis." Prentice Hall: Englewood Cliffs, N.J., 1990, p.147.
28. H. Pfeifer; D. Freude; J. Karger. *Stud. Surf. Sci. Catal.*, **65**, 89 (1991).
29. H. Pfeifer in "Acidity and Basicity of Solids: Theory, Assessment and Utility." (J. Fraissard and L. Petrakis, Eds.) Kluwer: Dordrecht, 1994 p. 255.
30. D. Freude; H. Ernst; T. Mildner; H. Pfeifer; I. Wolf. *Stud. Surf. Sci. Catal.*, **90**, 105 (1993).
31. J.B. Moffat. *J. Mol. Catal.*, **26**, 385 (1986).
32. S. Gao and J.B. Moffat. *Colloids and Surfaces A*, **105**, 133 (1995).
33. (a) J.W. Hightower and W.K. Hall. *J. Phys. Chem.*, **71**, 1014 (1967).
(b) J.W. Hightower and W.K. Hall. *Chem. Eng. Prog. Symp. Ser.*, **63**, 122 (1967).
34. P. Patrono; A. La Ginestra; G. Ramis; G. Busca. *Appl. Catal.*, **A107**, 249 (1994).
35. G.B. McGarvey and J.B. Moffat. *J. Catal.*, **130**, 483 (1991).
36. T. Matsuda; M. Sato; T. Kanno; H. Miura; K. Sugiyama. *J. Chem. Soc. Faraday Trans I*, **77**, 3107 (1981).
37. J.S. Vaughan; C.T.O. Conner; J.C.Q. Fletcher. *J. Catal.*, **147**, 441 (1994).

CHAPTER 7

Conclusions

7.1 Summary

The present study has been concerned with establishing the existence of a microporous structure in salts of 12-heteropoly oxometalates which contain representative cations of Groups 1B and 3B in the periodic table. The effect of the nature of the cation and anion, and the preparative stoichiometry and morphological and catalytic properties of the salt were examined. As part of the characterization studies of the salts, a critical comparative study of the methods available for the measurements of surface area and pore size distribution was carried out. In addition, the perturbations of acid strength in these salts as a result of the introduction of nonprotonic cations was investigated in the acid catalyzed processes of 1-butene isomerization and dehydration of butyl alcohols.

In Chapter Two, the silver(I) and thallium(I) salts of 12-tungstophosphoric and 12-tungstosilicic acids and thallium(I) 12-molybdophosphate were shown to have a microporous structure. The silver(I) salt of 12-molybdophosphoric acid showed no evidence of microporosity. These results indicate that such structures are not restricted to salts prepared from the alkali metals, and the generally larger size of thallium and silver cations, in comparison to the alkali metals, is not a limiting factor.

IR spectroscopy confirmed that the structure of the Keggin anion is retained while powder XRD patterns indicated that the transition metal cations occupy the positions previously held by the protons in the lattice structure. A microporous structure is created by the transition and rotation of the Keggin anions to accommodate the larger cations, which remove, at least partially, the barriers separating the interstitial voids from one another. The larger cation diameter results in an increase in the surface area, micropore volume, and mean micropore radius. Variations in the ratio of cation to proton used in the preparation of the various salts had a less pronounced effect on the surface area and micropore volume than previously observed and the mean micropore radius remained unaltered. This is believed to be a result of the method used in isolating the resulting

precipitate. Filtration appears to isolate a purer form of the desired salt than evaporation.

^1H MAS NMR studies of the silver(I), thallium(I) and cesium(I) 12-heteropoly salts demonstrated that residual protons are still present in the salts and both the number of acid sites and the environment in which they reside are affected by variation in the preparative stoichiometry. The chemical shifts observed for the residual protons in the prepared salts are upfield of those reported for the pure heteropoly acids, indicating a decrease in acid strength, in comparison to that observed with the acids. In combination with NH_3 TPD studies, it was observed that the number of acid sites present in the silver salts of $\text{Ag}_3\text{PW}_{12}\text{O}_{40}$ and $\text{Ag}_4\text{SiW}_{12}\text{O}_{40}$ decreased with the increase in the cation-to-proton ratio, however the distribution of acidic strengths appeared to be unaltered. In contrast, the thallium(I) and cesium(I) cations have a greater effect on both the number of acid sites and the distribution of acid strengths, with the disappearance of the strongest Brønsted acid sites as the cation:proton ratio is increased.

Although microporous structures apparently generally result with salts prepared from monovalent cations it is not clear whether such microporosity would be retained on an *in-situ* increase of the oxidation state of the cation. Unfortunately, the lower oxidation state of the chosen cation pair Cu(I)/Cu(II) is relatively unstable and consequently preparation and retention of the copper(I) salt is not straightforward. Although solid state ion exchange with the ammonium 12-tungstophosphate salt and a source of Cu(I) produced a solid with a surface area higher than the parent acid but lower than that of the prepared ammonium salt, use of the parent acid and the copper(I) salt did not yield a high surface area, microporous solid. Characterization of the copper(II) salts indicated that a mixture of the copper(II) cation and heteropoly acid was present, rather than a salt.

In Chapter Four, two of the microporous salts, thallium 12-tungstosilicate and thallium 12-molybdophosphate, were employed to compare the use of the Brunauer/Emmett/Teller (BET), MP, Dubinin-Radushkevich (DR) and Horvath-Kawazoe-Satio-Foley (HKSF) methods for the analysis of nitrogen adsorption isotherms in order to characterize the micropore structure present in the salts. Information on the surface areas, pore volumes, and pore size distributions were obtained by these methods. Similar surface areas were obtained by the BET, t-plot and DR methods, while the volume of

micropores determined by the DR method were slightly larger than those calculated by the MP method. Both the BET and DR theories are unable to yield a pore size distribution and although useful information about the micropore structures can be derived from the nitrogen isotherm, these methods do not provide a straightforward relationship between the logarithm of the relative pressure and the pore size distribution. The application of the slit and cylindrical models of the HKSF method permits such a direct relationship and accounts for the physical properties of the adsorbate and adsorbent couple, in addition to the increase in the adsorption energy in the small micropores. This results in the micropore radii calculated by the HKSF methods being less than half of the value calculated by the MP method. It is apparent in this study that knowledge of the assumptions and limitations of each method should be considered when they are applied to an isotherm.

Chapters Five and Six described the catalytic activity of these microporous materials in the acid catalyzed processes of 1-butene isomerization and the dehydration of 1-, 2- and *tert*-butanol. It is clear that the nature of the cation and anion as well as the preparative stoichiometry have a profound effect on the resulting salts and in particular both the morphology and acid-based catalytic properties. The presence of a microporous structure, residual protons, and the distribution of acid strengths were found to be important factors in the catalytic testing studies. In the isomerization and dehydration reactions, the product distribution indicated that a monomolecular mechanism was involved, although this could be a result of the conditions under which the experiments were performed.

With the isomerization of 1-butene, only products resulting from double bond migration were observed, consistent with the results from the ^1H MAS NMR and TPD studies, which indicated the salts would lack acid sites of sufficient strength to facilitate the skeletal isomerization of 1-butene to produce *iso*-butene. The consistent levels of conversion and selectivities for the stoichiometric and nonstoichiometric silver salts was attributed to the larger number of protons present in combination with similar distributions of acid strengths, unaffected by the cation:proton ratio. The shift in the distribution of acid strengths for the thallium salts, with the decrease in the proportion of stronger acid

sites as the preparative ratio is increased, was reflected in the decreased activity and the increased selectivity for *cis*-2-butene as the thallium content in the salt increased. The $\text{Tl}_3\text{PW}_{12}\text{O}_{40}$ and $\text{Tl}_4\text{SiW}_{12}\text{O}_{40}$ salts prepared with an excess of the cation were unable to isomerize 1-butene. An increase in the activity, in comparison to that of the pure heteropoly acid, was only observed for the $\text{Ag}_3\text{PW}_{12}\text{O}_{40}$ salts and marginally with $\text{Tl}_3\text{PMo}_{12}\text{O}_{40}$.

The dehydration of *tert*-, 2-, and 1-butanol is expected to form the tertiary, secondary, and primary butyl carbonium ions, respectively. Since the stability of these carbocations decreases in the order of tertiary > secondary > primary, the strength of the acid sites required should increase for the same series. In the dehydration of the butyl alcohols, the salts of $\text{H}_4\text{SiW}_{12}\text{O}_{40}$ generally had lower activities than the $\text{H}_3\text{PW}_{12}\text{O}_{40}$ salts, which is in agreement with the sequencing of acid strengths for the pure acids, previously observed. In contrast, the thallium salt of $\text{H}_3\text{PMo}_{12}\text{O}_{40}$ had an increased stability over that observed for the parent acid.

The conversion of butyl alcohols decreased with the increased cation content in the salts. The $\text{Ag}_3\text{PW}_{12}\text{O}_{40}$ salts, $\text{H}_3\text{PW}_{12}\text{O}_{40}$, and $\text{H}_4\text{SiW}_{12}\text{O}_{40}$ maintained consistent distributions of products, similar to equilibrium values, unaltered by the time-on-stream or the preparative stoichiometry of the silver salt. Reflecting changes in the distribution of acid strengths, the stoichiometric and excess $\text{Cs}_3\text{PW}_{12}\text{O}_{40}$, $\text{Tl}_3\text{PMo}_{12}\text{O}_{40}$, and all of the $\text{H}_4\text{SiW}_{12}\text{O}_{40}$ salts had a product distribution in which the *cis/trans* ratio approached 1 in the dehydration of 2-butanol. The excess thallium and cesium salts lacked sites of sufficient strength to dehydrate the 1- and 2-butanols. An increase in the selectivity of 1-butene occurred when very low levels of conversion were observed in the dehydration of 1-butanol.

Accounting for the differences in the surface areas and number of residual protons in the salts, the conversion for a given butyl alcohol generally increased with the cation order of $\text{Ag} < \text{Tl} < \text{Cs}$. Since the charge densities increase in the order of $\text{Cs}^+ < \text{Tl}^+ < \text{Ag}^+$, the differences in conversion could be related to the reduced mobility of the residual protons by the introduction of the nonprotonic cations. The larger cations may perturb the electron density of the anions and, in doing so, alter the magnitude of the charge on the

terminal oxygen atom the protons are affiliated with or they may actually physically impede the movement of the protons by their increased size and repulsive interactions.

7.2 Future Work

The present study of the cesium(I), silver(I) and thallium(I) 12-heteropoly salts could be expanded with investigations into other acid-catalyzed systems, such as the dehydration of propanol or the conversion of methanol to hydrocarbons, to provide further information regarding the acidic properties of these catalysts. It would be of interest to examine an oxidation process, such as the partial oxidation of methane to methanol, with the thallium 12-molybdophosphate salt due to the apparent increased stability of this salt in comparison with the pure acid in the acid-catalyzed processes. Generally, $\text{H}_3\text{PMo}_{12}\text{O}_{40}$ is considered to be more effective in redox reactions than the analogous tungsten-containing acids. In addition, the use of temperature programmed hydrogen-deuterium exchange experiments (TPE) may be able to shed more light onto the mobility of the residual protons in the cesium, silver, and thallium salts.

With the successful creation of microporous 12-heteropoly salts containing monovalent cations of silver and thallium, heteropoly salts containing other transition metal cations should be examined as other possible microporous solids. Future work with the copper(I) cation could include a detailed temperature study to determine the optimal temperature at which to perform the solid state ion exchange, modification of the apparatus to permit removal of the excess CuCl and possible copper oxides formed, and the use of a wafer for the heteropoly oxometalate. Use of a microporous salt containing a cation which is closer in diameter to the copper(II) cation may promote the exchange to occur more readily. Although not explored at the present time, possible methods of converting the oxidation state of copper(I) to copper(II) must also be investigated in addition to determining the stability of the copper(I) oxidation state in the solid form.

APPENDIX A

Sample Calculations for the HKSF Methods

As discussed in Chapter Four, Horvath and Kawazoe developed a model which takes into account the bulk and surface properties of the adsorbents. On the basis of the calculated potential energy profiles for atoms adsorbed in slit-like pores and the enhancement of the depth of the energy well relative to adsorption on a flat surface,¹ the HK model relates the free energy of adsorption to the average potential inside a slit-like pore.² Their initial study involved the adsorption of nitrogen on molecular-sieve carbon, with the generic equation summarized as

$$RT \ln \left(\frac{P}{P_o} \right) = K \frac{N_a A_a + N_A A_A}{\sigma^4 (L-d)} \left[\frac{\sigma^4}{3(L-d/2)^3} - \frac{\sigma^{10}}{9(L-d/2)^9} - \frac{\sigma^4}{3(d/2)^3} + \frac{\sigma^{10}}{9(d/2)^9} \right] \quad (\text{A.1})$$

where R is the gas constant (J/(mol·K)),

T is the temperature (K),

N_a is the number of atoms per unit area of adsorbent (a) (atom/cm²),

N_A is the number of molecules per unit area of adsorbate (A) (molecule/cm²),

A is the dispersion constant (J/molecule),

K is Avogadro's number,

σ is the distance between a gas atom and the nuclei of the surface at zero interaction energy ($\sigma = 0.858 \times d/2$) (nm),

L is the distance between nuclei of two layers (nm),

and d is the sum of the adsorbate and adsorbent diameters ($d = d_a + d_s$) (nm).

The dispersion constants for the adsorbate (A_A) and the adsorbent (A_a) are calculated by the following equations.

$$A_A = \frac{3}{2} (m c^2 \alpha_A \chi_A) \quad (\text{A.2})$$

$$A_a = \frac{6mc^2\alpha_a\alpha_A}{\left(\frac{\alpha_A}{\chi_A}\right) + \left(\frac{\alpha_a}{\chi_a}\right)} \quad (\text{A.3})$$

where m is the mass of an electron (kg),
 c is the speed of light (m/s),
 α is the polarizability (cm^3),
and χ is the magnetic susceptibility (cm^3).

The parameters for the oxide ion² as the adsorbent and nitrogen as the adsorbate, listed in Table 4.3, were substituted into equations A.2 and A.3 to obtain the following dispersion constants.

$$A_A = \frac{3}{2}(9.109 \times 10^{-31} \text{ kg})(2.998 \times 10^8 \text{ ms}^{-1})^2(1.74 \times 10^{-24} \text{ cm}^3)(2.0 \times 10^{-24} \text{ cm}^3)$$

$$A_A = 4.273 \times 10^{-66} \text{ Jcm}^6$$

$$A_a = \frac{6(9.109 \times 10^{-31} \text{ kg})(2.998 \times 10^8 \text{ ms}^{-1})^2(2.5 \times 10^{-24} \text{ cm}^3)(1.74 \times 10^{-24} \text{ cm}^3)}{\left(\frac{1.74 \times 10^{-24} \text{ cm}^3}{2 \times 10^{-29} \text{ cm}^3}\right) + \left(\frac{2.5 \times 10^{-24} \text{ cm}^3}{1.3 \times 10^{-29} \text{ cm}^3}\right)}$$

$$A_a = 6.758 \times 10^{-66} \text{ Jcm}^6$$

Using the values of A_A and A_a , the first part of equation A.1 was calculated as

$$\frac{K \frac{N_a A_a + N_A A_A}{RT\sigma^4(L-d)}}{= 6.022 \times 10^{23} \text{ mol}^{-1} \frac{(1.31 \times 10^{15} \text{ cm}^{-2})(6.578 \times 10^{-66} \text{ Jcm}^6) + (6.7 \times 10^{14} \text{ cm}^{-2})(4.273 \times 10^{-66} \text{ Jcm}^6)}{(8.314 \text{ Jmol}^{-1} \text{ K}^{-1})(77 \text{ K})(0.273 \times 10^{-7} \text{ cm})^4(L - 0.636 \text{ nm})}}$$

$$= \frac{21.77}{(L - 0.636 \text{ nm})}$$

while the second part of equation A.1 was calculated as

$$\begin{aligned}
 & \left[\frac{\sigma^4}{3(L-d/2)^3} - \frac{\sigma^{10}}{9(L-d/2)^9} - \frac{\sigma^4}{3(d/2)^3} + \frac{\sigma^{10}}{9(d/2)^9} \right] \\
 = & \left[\frac{(0.273 \text{ nm})^4}{3(L-0.318 \text{ nm})^3} - \frac{(0.273 \text{ nm})^{10}}{9(L-0.318 \text{ nm})^9} - \frac{(0.273 \text{ nm})^4}{3(0.318 \text{ nm})^3} + \frac{(0.273 \text{ nm})^{10}}{9(0.318 \text{ nm})^9} \right] \\
 = & \left[\frac{1.847 \times 10^{-3} \text{ nm}}{(L-0.318)^3} - \frac{2.540 \times 10^{-7} \text{ nm}}{(L-0.318)^9} - 4.981 \times 10^{-2} \text{ nm} \right]
 \end{aligned}$$

The final form of equation A.1 for the HK model is

$$\ln\left(\frac{P}{P_o}\right) = \frac{21.77}{(L-0.636)} \left[\frac{1.847 \times 10^{-3}}{(L-0.318)^3} - \frac{2.540 \times 10^{-7}}{(L-0.318)^9} - 4.981 \times 10^{-2} \right] \quad (\text{A.4})$$

Saito and Foley modified the slit model to accommodate the cylindrical shaped pores of the zeolite microstructure.³ For the cylindrical model, the line-averaged and area-averaged cases were examined. The equation for the line-averaged case is

$$\ln\left(\frac{P}{P_o}\right) = \frac{3\pi K(N_a A_a + N_r A_r)}{4RT(d/2)^4} \sum_{k=0}^{\infty} \left[\frac{1}{2k+1} \left(1 - \frac{d/2}{r_p}\right)^{2k} \left[\frac{21}{32} \alpha_k \left(\frac{d/2}{r_p}\right)^{10} - \beta_k \left(\frac{d/2}{r_p}\right)^4 \right] \right] \quad (\text{A.5})$$

while the equation for the area-averaged case is

$$\ln\left(\frac{P}{P_o}\right) = \frac{3\pi K(N_a A_a + N_r A_r)}{4RT(d/2)^4} \sum_{k=0}^{\infty} \left[\frac{1}{k+1} \left(1 - \frac{d/2}{r_p}\right)^{2k} \left[\frac{21}{32} \alpha_k \left(\frac{d/2}{r_p}\right)^{10} - \beta_k \left(\frac{d/2}{r_p}\right)^4 \right] \right] \quad (\text{A.6})$$

The expansion coefficients, α_k and β_k , in equations A.5 and A.6 are expressed as

$$\alpha_k = \left(\frac{-4.5 - k}{k}\right)^2 \alpha_{k-1} \quad \beta_k = \left(\frac{-1.5 - k}{k}\right)^2 \beta_{k-1} ; \alpha_0, \beta_0 = 1 \quad (\text{A.7})$$

Using the parameters from Table 4.3 and the calculated values of equations A.2 and A.3, the first part of equations A.5 and A.6 was calculated to be

$$\begin{aligned} & \frac{3\pi K(N_a A_a + N_s A_s)}{4RT(d/2)^4} \\ = & \frac{3(3.142)(6.022 \times 10^{23} \text{ mol}^{-1})}{4(8.314 \text{ J mol}^{-1} \text{ K}^{-1})(77 \text{ K})(0.318 \times 10^{-7} \text{ cm})^4} ((1.31 \times 10^{15} \text{ cm}^{-2})(6.578 \times 10^{-66} \text{ J cm}^6) \\ & + (6.7 \times 10^{14} \text{ cm}^{-2})(4.273 \times 10^{-66} \text{ J cm}^6)) \\ & = 27.85 \end{aligned}$$

Substituting 0.636 nm for the variable of d, the final form of equation A.5, the line-averaged case, is

$$\ln\left(\frac{P}{P_o}\right) = 27.85 \sum_{k=0}^{\infty} \left[\frac{1}{2k+1} \left(1 - \frac{0.318}{r_p}\right)^{2k} \left[\frac{21}{32} \alpha_k \left(\frac{0.318}{r_p}\right)^{10} - \beta_k \left(\frac{0.318}{r_p}\right)^4 \right] \right] \quad (\text{A.8})$$

while that for the area-averaged case is

$$\ln\left(\frac{P}{P_o}\right) = 27.85 \sum_{k=0}^{\infty} \left[\frac{1}{k+1} \left(1 - \frac{0.318}{r_p}\right)^{2k} \left[\frac{21}{32} \alpha_k \left(\frac{0.318}{r_p}\right)^{10} - \beta_k \left(\frac{0.318}{r_p}\right)^4 \right] \right] \quad (\text{A.9})$$

with

$$\alpha_k = \left(\frac{-4.5 - k}{k}\right)^2 \alpha_{k-1} \quad \beta_k = \left(\frac{-1.5 - k}{k}\right)^2 \beta_{k-1} ; \alpha_0, \beta_0 = 1 \quad (\text{A.7})$$

Using pressure data from the nitrogen-adsorption isotherms of the two thallium salts discussed in Chapter Four, equations A.4, A.8, and A.9 were solved by application of the Secant method⁴ to determine the unknown variable (L for the slit model and r_p for the cylindrical models) at each data point. The resulting effective pore diameter was then calculated from (L - 0.276 nm) for the slit model² and ($2r_p$ - 0.276 nm) for the cylindrical

models.³ The micropore size distribution and the average effective pore diameter, determined by the HKSF methods, are discussed in detail in Chapter Four.

References

1. D.H. Everett and J.C. Powl. *J. Chem. Soc, Faraday Trans. I*, 72, 619 (1976).
2. G. Horvath and K. Kawazoe. *J. Chem. Eng. Japan*, 16, 470 (1983).
3. A. Saito and H.C. Foley. *AIChE Journal*, 37, 429 (1991).
4. J.B. Riggs. "An Introduction to Numerical Methods for Chemical Engineers." Texas Tech University Press: Texas, 1985; pp. 48-63.